UNIVERSITÀ DEGLI STUDI DI TRIESTE

XXX CICLO DEL DOTTORATO DI RICERCA IN
INGEGNERIA CIVILE

Valutazione Multi-Scala Della Pericolosità Sismica Per l'Egitto

Settore scientifico-disciplinare: GEO/10 e ICAR/09

Dottorando:
Hany Mohammed Hassan ElSayed

Coordinatore:
Prof. Diego Micheli

Supervisore di tesi:
Prof. Fabio Romanelli

Co-Supervisore di tesi:
Prof. Claudio Amadio

Co-Supervisore di tesi:
Prof. Giuliano Panza

ANNO ACCADEMICO 2016/2017

UNIVERSITY OF TRIESTE

XXX PhD PROGRAM IN
CIVIL ENGINEERING

Multi-Scale Seismic Hazard Assessment for Egypt

Scientific sector: GEO/10 and ICAR/09

PhD Student:
Hany Mohammed Hassan ElSayed

PhD Coordinator:
Prof. Diego Micheli

PhD Supervisor:
Prof. Fabio Romanelli

PhD Co-Supervisor:
Prof. Claudio Amadio

PhD Co-Supervisor
Prof. Giuliano Panza

ACADEMIC YEAR 2016/2017

Abstract

Earthquakes are among the most catastrophic natural hazards. Earthquakes can produce significant ground shaking that causes damage to buildings and structures, casualties, economic disruption, and panic among the people. Earthquakes can trigger secondary phenomena e.g., landslides, liquefaction, and generate tsunami not only if the hypocenter is offshore but also if it is inland, close enough to the coast.

Egypt is a country with mainly moderate seismicity; it has witnessed strong earthquake impacts along its long history from far-field sources (e.g., the 365 AD earthquake M_w = 8.5 (Crete, Hellenic arc), 1303 earthquake M_w = 8.0, Rhodes, Hellenic arc) and earthquake impacts from the local sources (e.g., 1969 earthquake M_w = 6.9, Shedwan Island, 1992 earthquake M_w = 5.9, Dahshur, Cairo and 1995 earthquake M_w = 7.2 Gulf of Aqaba). The occurrence of these destructive earthquakes ensures the importance of carrying out a reliable and comprehensive characterization of expected seismic ground shaking, which is essential in order to develop effective seismic mitigation strategies and increase earthquake preparedness for Egypt. So, reliable seismic hazard maps that computed based on correct data and methodology should be prepared for building codes applications; also these maps should be updated when needed.

In the first chapter of this thesis, a review of the existing seismic hazard for Egypt is performed. For the understanding and studying the development of seismic hazard studies for Egypt, we had collected and tested the existing SHA maps, computed at different scales, against the available observations and physical assumptions, data quality, and methodology. Then, we propose some suggestions that could be considered before new seismic hazard maps can be produced and then adopted, for the real benefit of society. In Egypt, the available seismological data is not sufficient for sophisticated testing, but the result of the current testing cannot be overlooked.

In Chapter 2, an update of seismogenic zones and nodes has been performed, which is needed to perform an updated seismic hazard study for Egyptian territory. We think that the incorporation of seismogenic nodes information side by side with the updated seismogenic zones in the seismic hazard computation may improve performance and usefulness of the resulting maps for the studied region, especially for the sites that have been silent in during the earthquake catalog window show no seismic activity in the catalog so far. Also, incorporating such information may overcome the

inadequate performance of the existing maps, which is explained in Chapter 1. Some of the recognized dangerous nodes (D nodes) give more knowledge about seismic risk affecting particular sites, like water power plants and dams, as well as large metropolitan areas. The obtained results provide enough information needed for long-term seismic hazard assessment on the potential earthquake sources in north-east Egypt and will help.

Chapter 3 provides an update for the seismic hazard maps available for Egypt that incorporates recent studies, such as reviewed historical earthquake catalogs, morphostructural zonation data (MZ), revised fault plane solutions and laterally non-varying crustal structure. The neo-deterministic seismic hazard assessment (NDSHA) procedure that may effectively accommodate any reliable new information to adequately compute the earthquake ground motion maps (i.e., PGA, PGV and PGD) is adopted in this work. Also, a sensitivity analysis of different ground motion maps computed adopting different (a) models for the earthquake source process, (b) crustal structure models of the crust and (c) mapmaker's preconceptions (e.g., different seismotectonic models), is provided. The maps of difference and ratio between multiple ground motion maps computed for different variants are shown and discussed in order to explore the influence of using multiple input models. The results provide the potential users with an adequate spectrum of choices and reliably assess and communicate the possible uncertainties.

In Chapter 4, detailed ground motion modeling for the proper characterization of the amplification patterns (site-effects) along three 2D profiles, which are pass-through different directions in historic Cairo area, have been accomplished in the framework of a hybrid approach that combines modal summation and the finite-difference methods computational techniques. The presence of a fill layer of an average thickness of 15m at the top of the soil profile in historic Cairo area, which is capable of greatly amplify the ground shaking and increases the hazard level at the study area. This layer was formed by recurring destruction and rebuilding in the vicinity of Cairo along the history, which piled up to a thickness of a few tens of meters and this layer is geotechnically considered to be weak and capable to produce amplified seismically-induced damage. The expected amplification patterns range between 2 and 5 and occur at a frequency range 1.0 - 7.0Hz based on the location of the site along the profiles, subsurface geometry and the thickness of the sedimentary layer. This chapter represents a fundamental base for the computation of the seismic input (e.g., spectral acceleration, time histories), which is needed for

vulnerability and risk assessment for buildings in historic Cairo in order to protect the cultural heritage structures and save lives.

In Chapter 5, we provided the seismic input (response spectra and time histories) that can be applied for the proper evaluation of the dynamic performance of the minaret of the Madrasa the Princess Tatar al-Higaziya, which by role will help in proposing a seismic conservation strategy for this valuable structure. A detailed numerical model for the minaret was established, accompanied with installing ambient sensors for calibrating the numerical model. Two types of seismic analysis were conducted for the numerical model of the minaret namely, linear-dynamic response spectrum analysis and time history analysis. The response spectrum analysis was selected to replicate the 1992 Cairo earthquake excitation scenario, since no close records of the earthquake near the minaret site were preserved. The numerical model adequately captured the minaret response without producing any signs of cracking or damage, matching with the real behavior of the minaret during the 1992 earthquake. Then, the response spectrum analysis was also adopted for the proposed Conditional MCSI (C-MCSI) spectrum.

The careful assessment of the seismic excitation on the historic minaret through conducting the proposed C-MCSI response spectrum and time history analyses predicts severe damage to the minaret:significant lateral displacements at the minaret top and excessive tensile stress concentration, particularly at the geometric transition zone between the squared base and the hexagon shaft, have been developed. Since the minaret is expected to suffer severe damage against the anticipated scenario of earthquake shaking, a vital protection plan is recommended for the minaret to avoid any future damage or collapse. Stitching the walls with pre-stressed rebar or reinforcement of the inner side of the walls with incorporated steel are wide spread ways for restoring and protecting historic monuments and structures. In addition, skins of reinforced concrete coating or fiber-reinforced plastic (FRP) on the outer side of the walls may be beneficial in enhancing the tensile strength of the walls and hence improve the minaret performance against the anticipated strong earthquake scenario.

Last but not the least, this thesis can be considered as a contribution to be used for the sustainable development, land use, and urban planning in the country that is fast growing. In this work, we provided a reliable estimation of ground motion parameters at different geographical scales (from a national to site-specific scale) to be used in the seismic design and retrofitting of

existing buildings and could be essential for the protection of human life and protection of cultural heritage against the future earthquake threat. Then, we provided the seismic input for a site of cultural heritage structure in historic Cairo, and then we adopted the results in the engineering evaluation of this priceless structure; the same work can be accomplished for any of existing monuments in Egypt if needed. Finally, in the summary and conclusions section, we provide some recommendations to be considered in the future activities.

Acknowledgments

I would like to thank **ALLAH** the omnipotent for standing beside me the whole time to finish this work.

Then, I would like to thank **Dr. Fabio Romanelli**, his great support in both scientific and bureaucratic issues during the Ph.D. program.

I also want to thank **Prof. Claudio Amadio**, for his constructive comments and recommendation in the field of civil engineering.

I also want to express my gratefulness and respect to **Prof. Panza** for his kind care, constructive comments, and suggestions which helped me a lot to develop myself.

My sincere thanks to **Franco Vaccari** and **Andrea Magrin** for their technical support and the helpful discussion we had that help me a lot to improve the usefulness of my results and outcomes.

Special thanks to **Mohamed ElGabry** who was acting as a guide and a consultant whenever I needed. And I will take the stage to thank my colleagues and friends from **NRIAG**.

I would like to thank my engineering advisors **Mohamed Abdel-Monem and Marco Fasan** for their efforts, support and the fruitful discussion that helped a lot in evolving the engineering part of Chapter 5.

Also, I would like to thank **Prof. Hatem Odah, Prof. Hesham Hussein, Prof Alexander Gorshkov, Dr. Antonella Peresan, Dr. Eman Abu El-Nader, Dr. Sawires, Isalm Hamama and Hazem Badr ElDein** for their support.

Moreover, the author is grateful to the PhD coordinator **Prof. Diego Micheli** and the two reviewers i.e., **Dr. Maurizio Indirli** and **Dr. Mohamed ElGabry** for their critical reviews which have greatly helped to improve the thesis.

Also, I would like to deliver special thanks to **my parents** and my wife and "colleague" **Heba ElKosiri** for all kind of support and care that I have received.

Moreover, I would like to express my sincerest thanks to my dear friends at Trieste University for the lovely time we spent together.

Last but not the least important, I would like to thank the **Egyptian Cultural and Mission Sector and the cultural office at the Egyptian embassy in Rome** for the kind care, follow up, and the funds.

Contents **Page**

List of Figures

Fig. No. Page

List of Tables

Chapter 1

Revision of Existing Seismic Hazard Studies for Egypt

1.1 Introduction

The main aim of seismic hazard assessment (SHA) is the reliable quantification of the expected ground shaking and their geographical distribution, and to estimate the associated uncertainty, then to present them in a form useful for practical and effective reduction of seismic risk.

It is clear that the most essential input parameters for seismic hazard estimation process, whatever approach is considered, are: earthquake catalog, seismotectonic sources, the ground motion prediction equation (GMPE) in the case of the Probabilistic Seismic Hazard Analysis (PSHA) or Deterministic Seismic Hazard Analysis (DSHA) and lithosphere structure in the case of Neo-Deterministic Seismic Hazard Analysis (NDSHA). The first two sets of parameters are not easy to define with enough level of accuracy, especially for intraplate regions, where the earthquake generation process is poorly understood, the earthquake catalog is too short and occasionally there is a weak correlation between the observed seismicity and the geologic structures or active faults (e.g., Egypt). Moreover, the identification of the controlling earthquake for the intraplate regions is not a handy way because of the limited seismicity record, very variable length of occurrence time interval, and lack of our understanding about earthquake generating process and different characteristics of the seismotectonic sources. Subsurface active faults “blind faults” in mid-continental regions are an excellent example of the active seismotectonic structure that is capable of producing strong earthquakes, although it is not appropriately characterized (e.g., Western Australia; Cairo-Suez shear zone in Egypt). Therefore, the incorporation of all available information from different multi-disciplines e.g., Morphostructural Zonation (MZ), paleoseismological, geodesy investigations, will be necessary in the proper identification and characterization of active seismic sources, since using the

available instrumental and historical earthquake records alone can incorrectly define or reflect (underestimate) the correct hazard level in the studied area. Moreover, the available strong motion databank for regions of scarce seismicity (e.g., Northeast Africa; Arabian Peninsula) and low occurrence rate for large earthquakes is not sufficient to develop or explore a proper GMPE. Consequently, it is better to resort to scenario-based techniques (e.g., NDSHA) or to use a GMPE that is developed from a reliable source and propagation modeling and then validated using the available ground motion data instead of using imported ones.

In fact, there is the crucial need for a proper formal procedure for collection and rigorous testing of newly developed seismic hazard maps before they can be accepted and then used, so that the society may benefit from such efforts and will not be deceived by the incorrect SHA results like the ones existed (Kossobokov and Nekrasova, 2012; Panza et al., 2012).

This Chapter aims at giving a detailed insight on the seismic hazard studies have been accomplished so far at different geographic scales and for different areas in Egypt, and coming out with some suggestions, comments, and conclusions that could help in improving and enhancing the effectiveness of the future SHA studies. Before we start to shed light on the existing studies for Egypt, we found it is more useful to give a short discussion about the seismic hazard analysis methods and the performance of seismic hazard maps on the global scales. After that, we focus on the existing seismic hazard studies for Egypt, describing the approaches that have been used, the input data and models, the dispersion in the obtained results, the testing of the results against the available macroseismic data and discussing the possible shortcomings. It is relevant to say that in Egypt the available seismological data is not sufficient for sophisticated testing, but the result of the current review cannot be overlooked.

1.2 SHA performance, advances, and shortcomings

After the recent destructive earthquakes, e.g., Sumatra 2004, Wench China 2008, Haiti 2010 and Japan 2011, that took by surprise the existing hazard maps (see Kossobokov and Nekrasova, 2012; Panza et al., 2014), there is an urge to identify the causes of such failures and to improve the procedure of seismic hazard analysis, so that hazard maps possess, at the time they are published, some reliable predictive content and do not need to be revised after each significant earthquakes occurrence, as it often happened till now. Stein et al. (2012) studied the causes of the failure of seismic hazard maps related with the Tohoku 2011 (March 11, $M_w = 9.1$)

event and they identified different overlapping factors that can cause a hazard map to fail: e.g., wrong physics, wrong assumptions, and wrong data. Also, they introduced some suggestions that could help in improving the performance of such SHA map.

Traditional PSHA-based seismic hazard maps (e.g., SHA for Egypt) are: (1) strongly dependent on the length, completeness and the quality of earthquake database being used; (2) do not adequately consider the seismic source process, seismic wave propagation model and local site condition; (3) do not appropriately consider the temporal properties of earthquakes occurrence, since they are based on the assumption of random occurrence of earthquakes, that implies the independent occurrence of earthquakes in both time and space; this means that the probability of occurrence of two events at the same time and space is about zero, contrary to what sometimes observed; (4) do not adequately consider the available information from paleoseismological, morphostructural and geodesy based studies. In fact, for countries like Egypt, the number of records of large earthquakes is too limited to attempt to describe correctly the probability of occurrence and ground motion particularly.

The modern PSHA approach (for the complete description see, e.g.,, Petersen et al., 2008; Atkinson and Goda, 2011) could implement data about active sources and has some improvements relative to the traditional one, as a) the adoption of active fault databases; b) point and finite source modeling can frequently be used in developing a GMPE and generating the time histories from a controlling fault for dynamic structural analysis; c) Morpho-tectonic and paleoseismological studies, as well as GPS and InSAR measurements, are used in the determination of segmentation, attitude, depth, and slip-rates of fault sources; d) to characterize the distribution of earthquake magnitudes, Gutenberg- Richter or magnitude frequency (GR) relationship was commonly used for a relatively large regional sources in PSHA, but for small sources it resort to Characteristic Earthquake (CE) model which refers to the characteristic magnitude occurs more often than predicted by the GR models proposed above; e) weights in a logic tree are commonly determined by a large group of experts instead of "the author's experience and judgment"; f) residuals in GMPEs are decomposed into epistemic uncertainty and aleatory uncertainty. Only aleatory uncertainty was included in the integration for annual rates of exceedance. Epistemic uncertainty is moved to the logic tree; g) Seismotectonics and crustal structures, as well as seismicity, were commonly used in delineating the seismic source zones and focal depth distribution function. Basin depth and Vs_{30} were used in developing the GMPE;

h) Output ground-motion level is not a single value, but a spectrum covering 0 to 10 seconds. PGV, PGD, and Arias intensity may also be included.

According to the Multiscale Seismicity (MS) model (Molchan et al., 1997), the GR relation is valid as a law only for the earthquakes that have a linear dimension of the surface rupture small compared to the dimensions of the analyzed region, i.e., in the point source approximation. When focusing on a relatively small site, the point source approximation may no longer be valid, and therefore GR is not applicable as a law. For example, an event with $M \geq 7$, whose rupture length can be estimated around 50km (Wells and Coppersmith, 1994) can be considered as a point source only if the studied seismogenic zone has linear dimensions more than 500km (Panza et al., 2014). The use of small areas has given rise to the CE model (Schwartz and Coppersmith, 1984).

The endemic lack of adequate strong motion database that makes the development GMPE or even selecting of a proper one a challenging task if not impossible at the moment, it appears urgent to resort to a scenario-based approach to SHA. NDSHA approach is a scenario-based method for seismic hazard analysis, where realistic synthetic seismograms are used to construct earthquake scenarios

The DSHA and NDSHA agree in: a) considering the MCE not necessarily coincident with Maximum Historical Earthquake (MHE); b) accommodating any reliable information from paleoseismological, MZ investigations or similar studies; c) not using the GR relation or CE model. Also, they differ in the step that is common to standard DSHA and PSHA: the use of GMPE, or attenuation relations, in the ground motion estimation.

In fact, from the basic principles of continuum mechanics (e.g., Aki and Richards, 2002), the ground motion generated by a seismic (point) source can be expressed as the tensor product of the seismic moment tensor and the derivative of the Green's function of the medium, the extension to finite-dimension sources being straightforward. Since GMPEs are scalar, they cannot adequately describe this tensor nature of the ground motion.

The performance of any hazard map can be tested against the available observed intensity and/or recorded ground motion values, and this test may help in the adoption of procedures to differentiate between reliable and unreliable hazard assessments. This may lead to the improvement of the physics, data, and knowledge on which seismic hazard maps are based and eventually improve their reliability. Moreover, the validation of the seismic hazard assessment

and clear communication of possible uncertainties associated with SHA to potential end users are two essential elements that could help the different users to decide how much credence to place on this map.

1.3 Seismic hazard studies for Egypt

Although many lessons learned through the time, most of the existing seismic hazard studies for Egypt failed to predict the ground motion parameters for earthquakes had occurred after their publication. The failure is evidenced by merely comparing the expected ground motion parameters by different studies with the macroseismic intensity, which is shown and discussed by this Chapter. The failure may be due to the fact that, to identify the location and characteristics of seismotectonic sources for Egypt, only seismological observations (about 118years) have been considered, while paleoseismological and MZ investigations or similar studies that are suitable to identify seismotectonic sources that may be active over a time scale that is larger (long recurrence) than the instrumental database time span have been not investigated yet or ignored or unappreciated.

The seismic hazard maps computed for Gulf of Aqaba before the occurrence of 1995 M_w = 7.2 represent a striking example of seismic hazard underestimation in Egypt. The PGA estimated for Gulf of Aqaba region was ranging between 30-40gals as computed by Ibrahim and Hattori (1982) with 90% probability of non-exceedance in 50 years and 100-125gals with 90% probability of non-exceedance in 100 years calculated by Sobaih et al. (1992) based on intensity model developed by Maamoun (1979). Also, the assigned maximum intensity for the Gulf of Aqaba in the work of Maamoun et al. (1984) was IV on the Medvedev-Sponheuer-Karník scale (MSK; see Medvedev and Sponheuer, 1969) scale. These values were proven wrong (underestimated) by the occurrence of Aqaba earthquake on November 22, 1995, with M_w = 7.2 when the observed intensity for the Egyptian coast from this event is VIII on the MSK (Medvedev-Sponheuer-Karník) scale which equal to 100-200gal. We think the low observed intensity for this strong event could be due to the very low population density and the location of event offshore of the Gulf if such event would occur again in the future, a higher intensity level is expected due to the increase of developments along the Gulf. Also, the observed PGA values on the vertical component (which is the maximum of the 3 components) for Eilat (EIL) (located on an alluvial fan of about 50m thick overlying granite at about 93 km epicentral distance) and

Shivta (SVT) (which is located on consolidated chalk with almost no site effect at 244.1km epicentral distance) strong motion stations were about 113.6 and 38gals, respectively (Gitterman, March 1999, unpublished report). Therefore, the development of a formal procedure for the reliable identification of the location, configuration (fault geometry and orientation) and the potential (maximum magnitude) of earthquake sources becomes a necessary step for sound seismic hazard and risk mitigation.

Egypt is well defined as a relatively moderate seismicity country, although it has experienced strong earthquake effects through history from far-field (Hellenic arc, Cyprian arc, and the Dead Sea fault system) and near-field (e.g., North Red Sea, Gulf of Aqaba, Gulf of Suez, South-West Cairo (Dahshur Zone), and the continental margin of Egypt) earthquake sources. The reasons behind the strong risk from modest seismic hazard are the high population density, the proximity of some seismic sources to urban cities, profound effect of the path and local site condition, the deterioration of the buildings, absence of maintenance, and the poor design and construction practice. According to the macroseismic data, the 365 Crete, 1303 Rhodes, 1969 Shadwan Island (entrance of the Gulf of Suez), and 1992 Cairo (Dahshur) events are examples of earthquakes that generated the strongest impacts in Egypt. If these earthquakes will occur with similar magnitude shortly, a high seismic risk in Egypt is expected due to the increase of exposure and vulnerability, which are the main elements in the risk concept, so the necessity of reliable seismic hazard assessment to mitigate the possible losses in the future is a due.

The seismic hazard studies for Egypt were started a long time ago aiming to predict the ground motion parameters and to mitigate the possible risk (see Tables 1.1, 1.2, and 1.3). The review of the previous seismic hazard studies in Egypt (e.g., Sawires et al., 2016a) was routinely stimulated by the increase of instrumental earthquake observations rather than by methodological advances or the release of a new data about the active faults and/or strain rates and/or paleoseismology.

The current Chapter aims to give an insight into the development of seismic hazard studies achieved so far in Egypt and to show how the seismic zoning maps have been changing with progress both in seismological theory and observational practice.

Although the importance of the new developments in SHA methodology and practice, it is worth to mention that, most of the available SHA maps for Egypt are based on the traditional approaches and have not implemented the newly proposed improvements in their computations,

so far. Approximately, 80% of all SHA studies conducted until now about Egypt at different geographic scales are based on the traditional PSHA and it is still in use in the construction of newly developed SHA maps at different scales (e.g., EzzElarab et al., 2016; Sawires et al., 2016b) upon which the current Egyptian building code is dangerously based.

It worth mention that, the recently released studies have adopted the traditional PSHA method and mainly focus of the collection, update, and revision of the earthquake catalog rather than to the critical review and improvement of the methodology and other elements that are crucial to reach a reliable, as much as possible, estimate of hazard (Tables 1.1, 1.2, and 1.3). Moreover, a recently released traditional PSHA study for Egypt done by Gaber et al. (2018) has came out to the conclusion that *"the update of the PSHA maps due to the occurrence of few earthquakes of moderate size and without any real advancement in methodology or inclusion or development of a new investigation will not cause any significant changes in the ground motion values and the pattern of the isocontour maps"*.

It worth to mention that, most of the available SHA studies for Egypt (e.g., Ibrahim and Hattori, 1982; Abdel-Fattah, 2005; Mohamed et al., 2012; EzzElarab et al., 2016) have limited the output of the seismic hazard assessment to one or two value(s), i.e., peak ground acceleration (PGA) for the horizontal component and response spectrum (RS) rather than the complete frequency content, effective acceleration, bracketed duration, incremental velocity and damaging potential (e.g., Decanini and Mollaioli, 1998; Bertero and Uang, 1992). Also, they did not pay the due attention, in a sound and physically correct way, to the so-called "site-effects", that may be not persistent when earthquake source changes (Molchan et al., 2011). Actually, the sediments of the Nile Valley and its Delta can have a substantial impact on the polarization (also defined amplification/de-amplification) of seismic waves in the horizontal plane and on ground failure or soil liquefaction (e.g., El-Sayed et al., 2004).

Additionally, most, if not all of the existing PSHA studies in Egypt supply the horizontal component of the ground motion only, basing on the untested assumption that the amplitude of the vertical component of strong-motion can be defined as a fraction of the horizontal one. The vertical component generally could be less than the horizontal components, but this is not necessarily true for high-frequency ground motion in the near-source condition (e.g., Shrestha, 2009). The directivity, propagation effect, and local site condition may combine and produce a dominant vertical component (e.g., Gazli, Uzbeksitan 1976 M6.8; Nahhani, Canada 1985 M6.8;

Chi-Chi, Taiwan 1999 M7.6) and that is why it is essential to reliably estimate the vertical component of the ground motion as well.

In fact, earthquake time histories may be not crucial for the land use and urban planners, but are of a great importance for structural and technical engineers willing to design a new structure and/or evaluate the seismic performance of the existing built environment, and to investigate the non-linear behavior of soil at the site of interest. So, it is crucial to exploit the current methodologies for modeling the generation and propagation of seismic waves, as done with NDSHA, can to provide a comprehensive database of computed seismograms for Egyptian territories that suffer from the lack of useful strong motion databases.

Table 1.1: Available regional-scale seismic hazard assessment (SHA) studies for Egypt, with the related input data, arranged in chronological order.

Study	SHA method	Input parameters			Site definition
		Earthquake Catalog (EC)	Seismotectonic Zones (SZ)	Ground Motion Prediction Eq. (GMPE) (or Structural Model (SM) if specified)	Rock/soil
Sobaih et al. (1992)	PSHA	EC till 1984	Ten SZs	Maamoun et al. (1979)	*
Ahmed et al. (1992)	PSHA	EC from 1900 to 1980s	Five SZs	Maamoun et al. (1979)	*
Riad et al. (2000)	PSHA	EC from 2800 BC to 1996	Sixty-two local and regional SZs	Campbell (1981) and Crouse (1991)	≥800m/s
Sabry et al. (2001)	PSHA	No information about the data sources used, neither about the earthquake catalog nor the time completeness	Thirteen SZs	Aptikaev and Kopnichev (1980), Hu et al. (1996), McGuire (1978), Bolt and Abrahamson (1982) and Riad and Yousef (1999)	*
El-Sayed et al. (2001)	NDSHA	EC from 528 till 1997	Ten SZs	Five SMs of Egypt with regional average properties for the bedrock are used.	≥1000m/s
Abdel-Fattah (2005)	PSHA	EC for the period 1067-2003	Eleven SZs	Deif (1998) and Atkison and Boore (1995, 1997)	≥800m/s
Mohamed et al. (2012)	PSHA	EC with M ≥ 3 updated to 2009	Two SZs models are considered, with weights	Youngs et al. (1997), Zhao et al. (2006), Abrahamson and Silva (1997), Boore et al. (1997), Campbell and Bozorgnia (2003) and Campbell and Bozorgnia (2008)	≥800m/s
Mourabit et al. (2014)	NDSHA	EC updated till 2011 for earthquakes with M ≥ 5	Thirteen SZs	Same as El-Sayed et al. (2001)	≥1000m/s

**no information*

Table 1.2: Available local scale seismic hazard assessment (SHA) studies for Egypt, with the related input data, arranged in chronological order.

Study	Method	Study area	Input parameters			Site definition
			EC	SZ	GMPE	Rock/Soil
El-Hefnawy et al. (2006)	PSHA	**Sinai peninsula**	EC with M ≥ 3 for the period from 184 BC and 2003	Twenty-five SZs	Joyner and Boore (1981)	≥800m/s
Deif et al. (2009b)	PSHA		EC from 112 BC to 2006	Twenty-eight SZs	Ambraseys et al. (1996)	≥750m/s
Fat-Helbary and Ohta (1996)	PSHA	**Aswan area**	About 350 events with M≥ 3.2 recorded between 1981 and 1995	Both Line Source Model (LSM), for the natural sources, and Area Source Model (ASM), for induced seismicity	Fat-Helbary and Ohta (1994b)	≥800m/s
Deif et al. (2009a)	DSHA		Single-event scenarios are used	Three seismotectonic models are considered in this study	Ambraseys and Bommer (1991a), Fat-Helbary and Ohta (1994b), Ambraseys et al. (1996) and Deif and Tealeb (2001).	≥750m/s
Deif et al. (2011)	PSHA		EC with M ≥ 2.5 for the time interval from 1900 to 2009	Ten SZs	Ambraseys et al. (1996), Abrahamson and Silva (1997), and Boore et al. (1997)	≥800m/s
Badawy (1998)	PSHA	**Northern Egypt region**	EC for the time interval from 1960 to 1995	Three SZs	Intensity-based GMPE is developed and used for the northern Egypt region	*
Deif (1998)	PSHA		EC extending from 2200BC to 1997	Twelve SZs	Joyner and Boore (1981)	*
Saleh (2005)	DSHA	**Western Desert**	EC with M_S ≥ 3.5 for the time interval from 1964 to 2003	Eight SZs	Deif and Khalil (2003)	≥800 m/s
El-Adham and El-Hemamy (2006)	PSHA		EC for the time interval from 184 BC to 2004	Fifteen SZs	Deif (1998)	≥800m/s
Kebeasy et al. (1981)	Intensity-based approach	**Alexandria**	EC comprises 130 events for the time interval from 2200 BC till 1978	Two SZs	Gutenberg and Richter (1956)	*

**no information*

Table 1.3: Results of the national and local seismic hazard assessment studies for Egypt, arranged in chronological order. PGA values, in units of g, are rounded to 2 decimal digits, as a rule, to be conservative in the reported results.

Study	SHA method		Gulf of Aqaba	The entrance of the Gulf of Suez	Cairo	Nile Delta	Aswan	Alexandria	Sinai peninsula
Kebeasy et al. (1981)	Gutenberg-Richter (1956)		*	*	*	*	*	0.07	*
Ibrahim and Hattori (1982)	PSHA		0.03-0.04	0.03-0.04	0.08-0.10	0.08-0.10	0.005-0.01	0.03-0.04	0.03-0.04
Sobaih et al. (1992)	PSHA		0.1-0.13	0.10-0.15	0.04-0.06	0.04-0.06	0.06-0.08	0.06-0.08	0.04-0.15
Ahmed et al. (1992)	PSHA		0.15-0.16	0.18-0.20	0.06-0.07	0.07-0.09	0.10-0.16	0.09-0.10	0.05-0.20
Cairo Earthquake, October 12, 1992 M_w = 5.9 and I_{MSK}=VIII. Aqaba Earthquake, November 22, 1995 M_w = 7.2 and I_{MSK}=VIII.									
El-Sayed (1996)	PSHA		0.40	0.35	0.20	0.20	0.15	*	
Fat-Helbary and Ohta (1996)	PSHA		*	*	*	*	0.03-0.05	*	*
Badawy (1998)	Intensity-based PSHA		0.25	0.25	*	*	*	*	*
Deif (1998)	PSHA		0.18-0.22	0.14-0.2	0.06-0.08	0.02-0.06	*	0.04-0.06	0.04-0.22
Riad et al. (2000)	PSHA		0.11-0.22	0.11-0.22	0.11	0.11	*	*	*
Sabry et al. (2001)	PSHA		0.20-0.23	0.17-0.25	0.15-0.17	0.17-0.23	0.10-0.12	0.17-0.20	0.17-0.25
El-Sayed et al. (2001)	NDSHA		0.15-0.33	0.15-0.30	0.15-0.30	0.15-0.30	0.08-0.15	0.15-0.30	*
Abdel-Fattah (2005)	PSHA	a) Deif (1998)	0.13-0.19	0.17-0.21	0.13-0.15	0.13-0.15	0.13-0.17	0.13-0.15	0.11-0.21
		b) Atkinson and Boore (1995)	0.09-0.15	0.11-0.17	0.09-0.11	0.07-0.11	0.11-0.17	0.07-0.09	0.05-0.15
Saleh (2005)	DSHA		0.04-0.08	0.04-0.12	0.04-0.08	0-0.02	0-0.04	0-0.02	0-0.08
El-Hefnawy et al. (2006)	PSHA		0.21-0.27	0.15-0.21	*	*	*	*	0.06 -0.27

El-Adham and El-Hemamy (2006)	PSHA	*	*	*	0.004-01	*	0.1-0.16	*
Deif et al. (2009b)	PSHA	0.1-0.18	0.08-0.1	*	*	*	*	0.020-0.18
Deif et al. (2009a)	DSHA	*	*	*	*	0.15	*	*
Deif et al. (2011)	PSHA	*	*	*	*	0.03-0.15	*	*
Mohamed et al. (2012)	PSHA	0.18-0.23	0.10-0.13	0.08-0.10	0.03-0.08	0.10-0.20	0-0.03	0.05-0.23
Mourabit et al. (2014)	NDSHA	0.15-0.6	0.15-0.6	0.15-0.3	0.02-0.08	0.15-0.3	0.08-0.3	*

**No PGA estimated for the study area.*

-All PGA values from PSHA studies are computed with10% probability of exceedance in 50 years.

It is well known that, the quality of the results obtained by utilizing numerical codes, based on physics modeling, depends on the quality of the input data (Panza et al., 2013). It seems that one of the major problems in the seismic hazard studies carried out for Egypt, is that how much the used earthquake catalogs are representative of the real seismicity of the study area (e.g., Badawy, 1998; Saleh, 2005). So, it is required to use all available information (e.g., geodesy) and to plan new comprehensive investigations where crucially necessary (e.g., paleoseismology) to better identify and characterize the seismic sources for Egypt. The appropriate incorporation of aforementioned information is an essential factor in SHA by whatever approach and may help in improving the performance of the SHA maps, since the use of historical earthquake records alone may not yield a hazard map of appropriate performance. Badawy (1998) has mentioned that before the 1960s the earthquake location accuracy is not adequate for the analysis. The catalog used in this study is too short and insufficient to reliably estimate the seismic hazard, mainly when the assessment is carried out using PSHA methods, which strongly depend on the amount of data available (35 years of seismological observations are useless in the hazard estimation because of the undue extrapolation to large earthquake occurrence rate), see Table 1.2. Also, some of the existing studies do not communicate the characteristics of the earthquake catalog being used (e.g., Sabry et al., 2001).

The second important factor is the GMPE in the case of PSHA or DSHA and the lithosphere structure in the case of NDSHA. In fact, most of the GMPEs used in the estimation of earthquake ground motion parameters for Egypt have been developed for other regions that differ, for instance, in the tectonic setting, faulting style, and crustal structure thus they are "imported GMPEs." The reason behind the adoption of imported GMPEs is insufficient strong motion database, which is not sufficient to construct an empirical relationship for Egypt or to explore and evaluate the suitable GMPE. The limit is due to the few numbers of recorded strong motion events (about eight events till 2016), low magnitude range (4.0-5.5) and low spatial distribution of the accelerometers (about twelve strong motion stations distributed irregularly over the territory at a relatively far distance from the most of active sources), see Fig. 1.1.

Most of the existing SHA studies for Egypt have incorporated many different GMPEs in logic tree framework, which are developed for regions of tectonic setting somehow similar to the present-day tectonic setting of Egypt, but they did not consider at all the profound effects of the propagation path and the possible change in the rupture process that definitely are quite variable

from path to path. There is no consensus on a single or a set of GMPE(s) that should be used. The choice of suitable GMPE(s) always depends on the mapmakers' preference, not on a rigorous evaluation by a large group of experts, and most of the studies have used more than one GMPE each associated with different weighting value in a hope to tackle the possible epistemic uncertainties.

Fig. 1.1: Spatial distribution of strong motion stations (white triangles) and the recorded events (red stars) during the period from 2008 till 2016.

Moreover, the inspection of the existing seismic hazard studies for Egypt has revealed that there is not a clear and proper communication for the characteristics of the GMPEs being used and sometimes is difficult to figure out how those studies have defined a rock site regarding shear velocity. Abdel-Fattah (2005) for example, gives the priority to the results based upon the "imported" GMPE of Atkinson and Boore (1995, 1997) because, from his point of view, there is a proper consistency between the local and regional seismicity and tectonics of the region (i.e., North America), for which the Atkinson and Boore (1995, 1997) GMPE was estimated, and the local and regional seismicity and tectonics of Egypt. No scientific justifications are given to support his choice, but just considerations and opinions (conventional wisdom), not to mention that the scatter between the two sets of estimates, more than 60%, makes it meaningless the

precision of 0.02g, which corresponds to about 2% (Tables 1.1 and 1.3). Moreover, the inclusion of various GMPEs for hazard estimation for Egypt has been done in some studies without particular caution for the possible incompatibility between different equations.

Base on the reasons mentioned above, it is essential to resort to a more reliable solution for modeling the generation and propagation of seismic waves (e.g., the structural models and related computation of realistic broadband signals as done with NDSHA) which is the topic of Chapter 3. In fact, the regional structural models are an important input in SHA computation based on NDSHA and have a profound effect on the resultant ground motion maps, although, all of the existing models for Egypt are too simple, and the revision of the crustal models is needed taking into account all the crustal studies available for different regions of the Egyptian territory, and eventually, to plan new comprehensive studies over a regular grid where crucially necessary.

In some of SHA studies (e.g., Kebeasy et al., 1981; Badawy, 1998, see Table 1. 2), the attenuation relationships which have been developed based upon the decay of macroseismic intensity in Egypt were used to estimate the annual seismic hazard maps in terms of intensity variations with different level of non-exceedance. In fact, because of the subjective nature of intensity determination, the discrete characteristics of the intensity scale and the poor correlation of intensity with specific source characteristics and strong motion data, the intensity-based ground motion estimates are not preferred.

In addition, the ground-motion variability has not been taken into account in most of the existing traditional PSHA studies for Egypt. Incorporating this kind of variability can be done by integrating over the standard deviation reported in GMPEs being used, which significantly affects estimated ground motions, especially at very low probabilities of exceedance. Only a few studies have introduced and considered the ground motion variability in the hazard analysis (e.g., Deif et al., (2009a, b). Ignoring the variability in ground motion could be the reason behind the low PGA values that have been estimated for Egypt. The dropping of sigma (σ) in SHA does not only lead to underestimating the computed ground-motion intensity, but it is also inconsistent with the standard probabilistic approach (Bommer and Abrahamson, 2006).

Most of the estimated ground motion maps for Egypt are not validated against the available observation or the macroseismic data. Also, the uncertainties associated with the computation of ground motion parameters are neither sufficiently assessed nor presented to the different potential users.

1.4 Discussion

We must accept and adopt as reliable, the seismic hazard maps that fit well with what recorded (good performance) and that are based upon correct and tested theory, physics, assumptions, and methodology, with a full understanding of their limitations and their relation to other steps in engineering and risk analysis. Also, we have to try to improve those maps whenever a new data or theoretical developments become available.

In Egypt, many seismic hazard studies have been carried out over different time and geographical scales, as reported in Tables 1.1, 1.2, and 1.3. Most of these studies are based on the traditional probabilistic approach and show that the ground motion acceleration values on the maps are exceeded by earthquakes occurred after their publication (e.g., Figs 1.2, 1.3, and 1.4). The failure of these maps is evidenced by testing the PGA values converted from observed intensity based on the table given by Medvedev and Sponheuer (1969) against the predicted ground motion before the occurrence of an earthquake which cannot be overlooked. The maximum observed intensity (I_{MSK}) is VIII for the 1992 Cairo earthquake corresponding to 100-200gal, VII for the 1981 Aswan earthquake, corresponding to 50-100gal. Moreover, the maximum I_{MSK} for the 1969 earthquake (March 31, 1969 $M_w = 6.9$) is XI and equivalent to about 200-400gal, while for the 1995 earthquake (November 22, 1995, M = 7.2) is more than VIII, corresponding to 100-200gal (Fig. 1.6). Thus, it is more useful to analyze the cause(s) of the failure to understand what went wrong and improve the assessment and therefore, the mitigation process.

The input differences between the existing PSHA studies are the earthquake catalogs, geometry of seismotectonic models (Tables 1.1 and 1.2) and analyst expertise and preconceptions; as a consequence, a large scatter in the ground motion parameters values for the same region, but from different studies (sometimes in the same year, i.e., with the same earthquake catalog) is observed, as reported in Table 1.3 and shown in Figs 1.2, 1.3, and 1.4. Seemingly, one of the main problems of PSHA computation in Egypt is the relatively short time base of seismic observations and the absence of useful information about active faults (Tables 1.1 and 1.2). Saleh (2005) studied the seismic hazard in Egypt using DSHA and the PGA hazard values estimated by his work are the lowest among many other results from NDSHA and PSHA for the Gulf of Aqaba (Fig. 1.2), Cairo (Fig. 1.3), and Alexandria (Fig. 1.4) regions, this is due to

the shortness of the earthquake catalog that covers the time span from 1964 to 2003 on which they study is relied and ignoring the pre-instrumental earthquake catalog, which represents an essential segment of the available seismological information for Egypt.

Considering a set of possible hazard maps for Egypt computed with different input data and adopting different models and assumptions (sensitivity test) can help in adequately defining the uncertainty in the resultant hazard maps (Chapter 3). Sensitivity check of hazard maps for different input data can be quickly done in straightforwardly with NDSHA. Skeptical reviews and testing of published hazard maps and assessments should be regularly done and released to evaluate the state of art of hazard knowledge and to identify possible steps forward and needs.

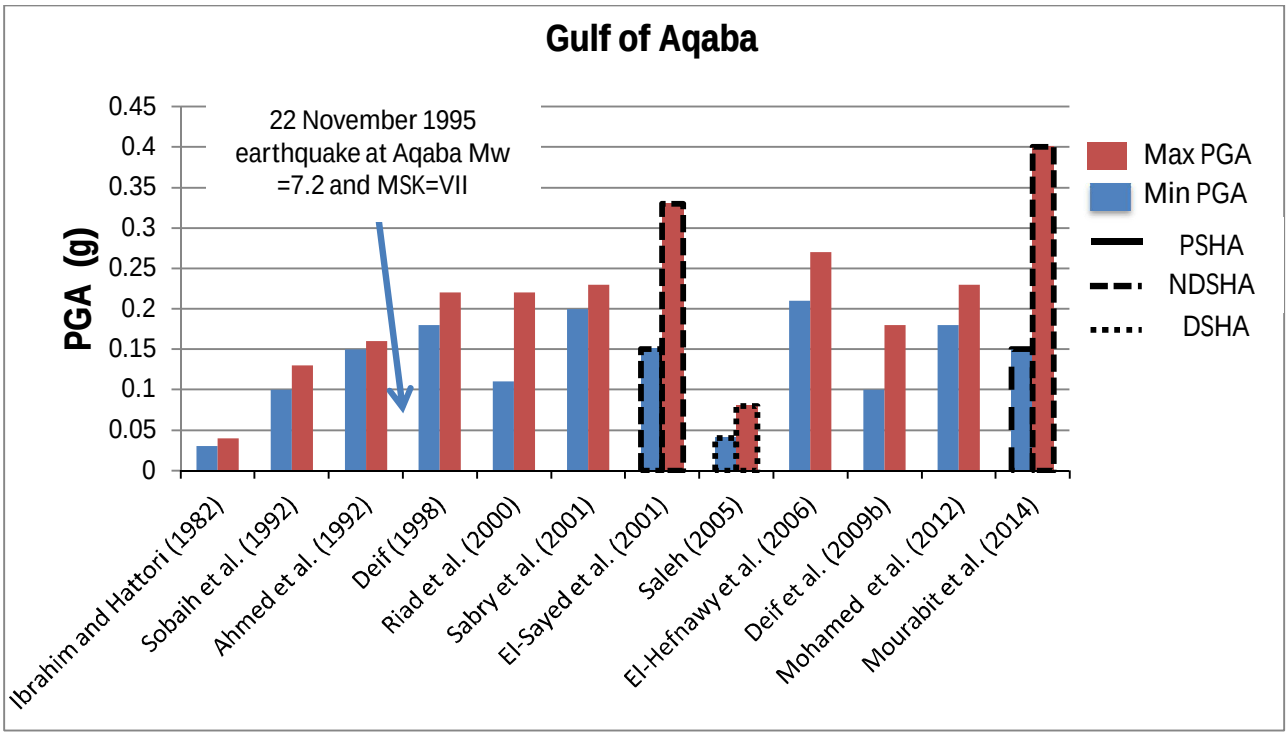

Fig. 1.2: Comparison between the Max and Min PGA values estimated by the different studies for the Gulf of Aqaba region.

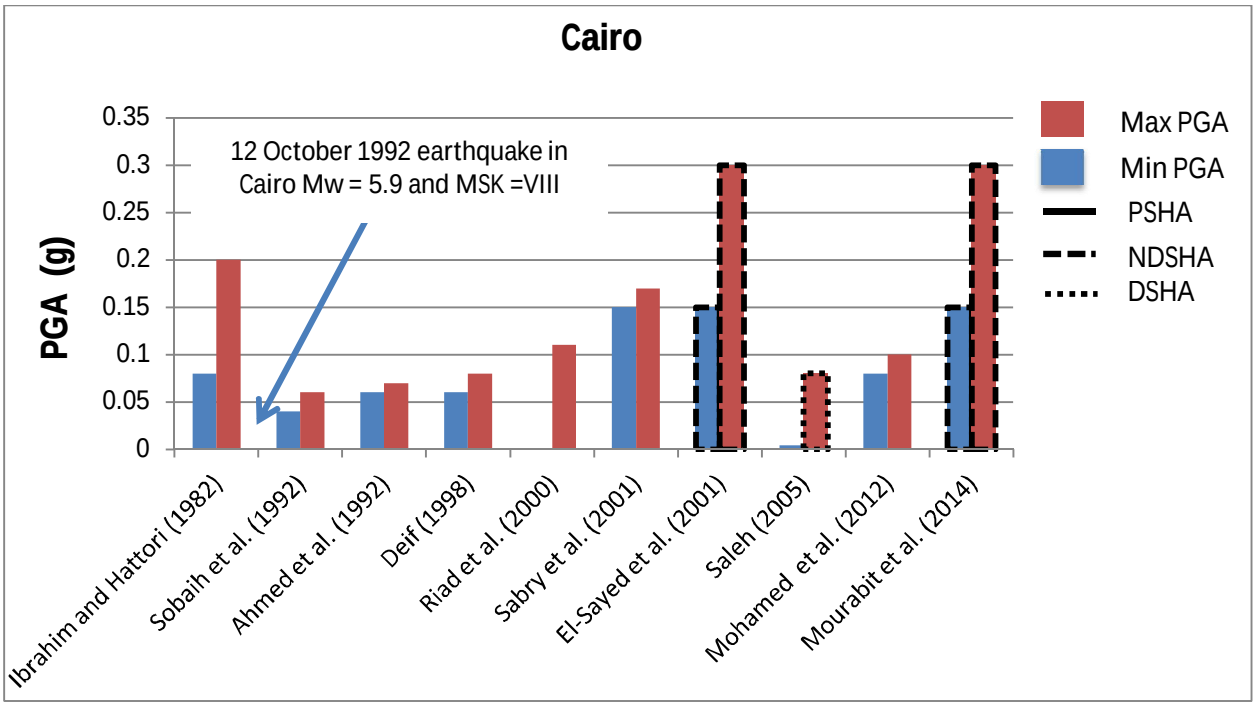

Fig. 1.3: Comparison between the Min and Max PGA values estimated by the different studies for the Cairo region.

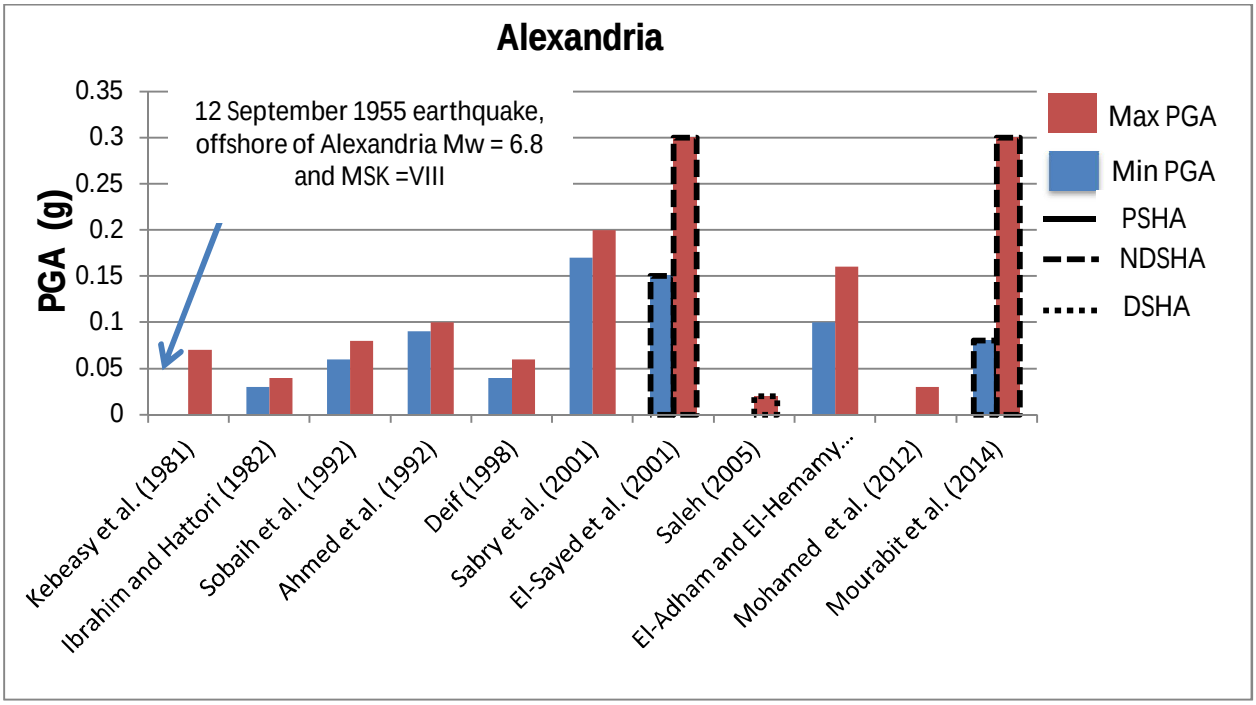

Fig. 1.4: Comparison between the Min and Max PGA values estimated by the different studies for the Alexandria region.

The PGA values estimated using the NDSHA approach represent the upper boundary for the different seismic hazard maps in the different regions in Egypt (Figs 1.2, 1.3 and 1.4); thus, they turn out to be conservative and physically reliable. Also, there is no significant change in PGA values from El-Sayed et al. (2001) and Mourabit et al. (2014), this may be due to the fact that, NDSHA needs only earthquake catalogs with $M \geq 5$ (during the period from 2001 to 2014 occurred just a few events of moderate magnitude). It is worth to mention that, the computation of NDSHA maps available for Egypt is carried out using the earthquake catalog and no information about the control faults or MZ has been used, so far. Although, the fact that the earthquake catalogs for Egypt used in Mourabit et al. (2014), which is an NDSHA based study, and Mohamed et al. (2012) "PSHA studies" are almost the same, the predicted ground motion values obtained from NDSHA are more significant and comparable with the observed intensities.

The comparison among different probabilistic seismic hazard maps (at regional and local scales, Tables 1.1 and 1.2) for the same site reveals that the PGA values are not consistent and considerable differences are found; the local studies can be more detailed, though not necessarily more reliable (e.g., Klügel, 2005). For example, the PGA values for Aswan, reported in Table 1.3, vary in the range from 0.005-0.2g, showing a large scatter in the expected values. So, it could be difficult for the potential users to decide what ground motion value to rely on in the design or retrofitting of the built environment. Furthermore, there are substantial differences between PGA values determined by the same study at the same site, but using different GMPEs (e.g., Abdel-Fattah, 2005), Tables 1.1, 1.2, and 1.3.

It is relevant to mention that the application of weights to each logic tree component (e.g., seismicity parameters, seismotectonic and GMPEs) for the existing PSHA studies for Egypt can lead to artifacts, since the weights are given according to the author's experience and judgment rather than the stringent physical arguments and analysis of a group of experts. Moreover, the use of weights without careful understanding may add a new source of uncertainty, i.e., the author bias; this fact explains why the PGA values which are obtained by different studies in Egypt at the same site, but with the same PSHA algorithm are significantly different. Actually, with weights used in existing PSHA for Egypt, given any set of numbers, any desired average value can be obtained.

Furthermore, a large number of the reviewed studies (e.g., Ibrahim and Hattori, 1982; Badawy 1998; Abdel-Fattah, 2005) supply the PGA maps as the only significant ground motion

parameter. The recently developed studies (e.g., Deif et al., 2009a, b; Mohamed et al., 2012) have provided both PGA and spectral acceleration values at the nodes of a regular grid for Egypt. Different earthquake hazard maps can naturally be appropriate for different purposes. A map showing the variation in predicted ground motion in terms of PGA or intensity scale may be useless to the designer of critical structures and geotechnical engineer who need detailed, and more realistic, seismic inputs consisting of three components seismogram, but at the same time, this map may be of some use to the land use planner who needs a handy way to evaluate the earthquake impacts on mankind and property.

The revision of existing seismic hazard studies in Egypt also indicates that just a few of those studies (e.g., El-Sayed et al., 2001) are tested against the available historical and instrumental seismicity. El-Sayed et al. (2001) examined the predicted ground motion parameters against the observed intensity (in terms of the maximum MSK) for earthquakes of 1955 (Alexandria offshore), 1969 (entrance of Gulf of Suez), 1981 (Aswan) and 1992 (Cairo), with intensity values of VIII, IX, VII and VIII, respectively, and found a good comparison between the observed and converted ones. However, any earthquake hazard map must be tested against real seismic data before any practical estimation of risks can be made. Otherwise, the use of untested seismic hazard maps may and do cause a high level of unpredicted fatalities and economic losses (Wyss et al., 2012).

In spite of, the poor performances and fundamental shortcomings of existing PSHA studies available for Egypt, the seismic design strategy as well as the building code and its update still rely upon the maps from those studies. In order to overcome the limits of design procedures based upon PSHA seismic input (Fasan et al., 2015; Rugarli, 2014), it is necessary to resort to a new seismic design strategy based upon the NDSHA definition of the seismic input in Egypt.

In this study for the insight understanding of the development of seismic hazard studies for Egypt, we have adequately collected and tested the existing SHA maps, computed at different scales, against the available observations and physical assumptions, data quality, and methodology. Finally, we propose some suggestions that could be considered before new seismic hazard maps can be produced and then adopted, for the real benefit of society. The suggested recommendations will be considered in the next Chapters.

From the present review of the seismic hazard studies in Egypt, the following conclusions can be drawn and may be considered in the next seismic hazard maps:

1. It is urgently necessary to review the list of seismic sources and controlling earthquakes that may influence the site of interest. The use of revised earthquake catalog and quality controlled fault solutions for Egypt is required in future studies.

2. It worth mention that, a project that embraces teams of archeologists, architects, engineers, geologists, historians, paleoseismologists, and seismologists needs to be launched in order to enhance the earthquake record for Egypt by detailed and comprehensive examination of the remains of ancient sites and structures that are distributed over wide range of time and space.

3. After the occurrence of every significant earthquake in Egypt, there is ensuing change both in seismotectonic sources and in hazard maps (see the chronological order of seismic hazard studies summarized in Tables 1.1, 1.2 and 1.3); this is an evidence of lack in seismic sources identification and characterization, that results in the underestimation of seismic hazard. Revisions are appropriate, but not each time a strong earthquake occurs.

4. Most of the existing PSHA and DSHA studies in Egypt have restricted the assessment results to the single measure of PGA and RS that, alone, do not express the damaging capability, and ignore other parameters that have a good correlation with the damage observed.

5. The dropping of sigma (σ) "the ground motion variability" in SHA does not only lead to underestimating the computed ground-motion intensity, but it is also inconsistent with the standard probabilistic approach.

6. The structural anelastic models are an essential input in SHA computation using scenario-based approaches and have a profound effect on the resultant ground motion parameters. All of the existing models are too simple, and the need for the revision of the crustal models is obvious, taking into account all the crustal studies available for different regions of the Egyptian territory and eventually, to plan new studies where crucially necessary. An overwhelming simplification is the use of attenuation relations or GMPE, which is not only destroy the tensor nature (intrinsic in continuum mechanics) of earthquake ground motion but also, in the case of Egypt, they are "imported" from distant regions.

7. The use of weights in the logic tree components of PSHA can lead to misleading results, adding the author's bias into the gross uncertainty of the seismic hazard assessment process. This kind of uncertainty can lead to variations in the computed PGA values in the same

region, obtained by different studies even when all other (input) parameters are kept fixed. Thus, this drawback can be reduced but not eliminated, if the adopted weights in a logic tree are determined by a large group of experts rather than by the author's experience and judgment.

8. From the SHA studies in Egypt published so far, it is clear that the instrumental and historical earthquake catalogs may be useful in the description of known past earthquake activity but not for reliably anticipating the expected ground motion parameters.

9. Parametric tests at local scale are an indispensable task (especially after the damage of Onagawa nuclear power plant after the April 2011 aftershock, with M_w = 7.1 of the March 2011 M_w =9.1 main Tohoku earthquake) in the seismic hazard analysis for critical structures in Egypt (Panza et al., 2012); this is a possibility naturally offered by NDSHA, practically at no additional cost. The parametric studies allow us to generate exhaustive ground-shaking scenarios for evaluation of the site-specific seismic hazard. For example, the source depth has a considerable effect on the resulting ground motion. The scenarios computed for different source depths may be readily performed for the new urbanization of areas close to seismogenic zones and the verification (e.g., see: http://www.provincia.trieste.it/opencms/opencms/it/attivita-servizi/cantieri-della-provincia/immobili/Programma_verifiche_sismiche/) of the existing ones.

10. Joint use of all available data from seismology, geodesy (e.g., GPS and InSAR) geophysics, paleoseismology, morphostructural analysis, and tectonics is crucial in the identification and characterization of seismogenic zones where large, yet unobserved earthquakes may occur (discussed intensely in Chapter 2). Such information will significantly increase the knowledge about the seismic sources and thus, enhance the performance of seismic hazard maps in Egypt.

11. It is well recommended for the seismic hazard analysts to understand the needs of the potential users (e.g., public and engineers) in order to be able to enhance the usefulness of their studies. Also, it’s vital to undoubtedly explore, evaluate, and communicate the uncertainties associated with the estimation of seismic hazard map to different users. This could help the potential users in deciding how much credence to place on the estimate itself. Moreover, it would be better if the newly developed seismic hazard map can be tested against the available observations and macroseismic data before they can be accepted and then fruitfully adopted.

Chapter 2

Updating the Definition of Seismic Sources for Egypt: Seismogenic Zones and Seismogenic Nodes

The identification of possible seismic sources affecting the area of study is a substantial component of the seismic hazard assessment process, regardless of the approach being used. To reliably identify and characterize seismic sources, information from different disciplines (e.g., regional and local geology; present-day tectonics; seismicity) is required as discussed in Chapter 1.

Over the last few decades, new evidences on the capability of the seismic source areas adjacent to urban cities in Egypt (e.g., seismological, historical, paleoseismological; crustal deformation studies) to produce medium to strong earthquakes have been discovered by many authors (e.g., Ambraseys et al., 2005; Ambraseys, 2009; Badawy et al., 2010; Seleem and Aboulela, 2011; Mahmoud, 2002). This highlights the importance of the identification and evaluation of the seismogenic sources (i.e., seismogenic zones and nodes) in Egypt as a prerequisite for a reliable estimate of seismic hazard and to reduce the consequent risks on people and their property.

In Egypt, most of the highly populated cities, industrial activities, cultural heritage and archeological sites are concentrated along the Nile Valley and Delta. The local moderate size earthquakes (e.g., the Cairo 1992 earthquake), and larger magnitude events at relatively far distances along the extreme north of the Red Sea and the Gulfs of Suez and Aqaba (e.g., Shedwan 1969 and the 1995 Gulf of Aqaba earthquakes), as well as the northern continental margin of Egypt (e.g., the Alexandria 1955 and the Ras El-Hekma 1998 earthquakes) and eastern Mediterranean region (e.g., the 365 and 1303 earthquakes) are the primary controllers of seismic risk in Egypt. Thus, their evaluation must be taken into account in the planning and development of new and urban cities.

2.1 **Seismogenic zones**

During the last decades several seismotectonic studies have been accomplished in Egypt (e.g., Riad et al., 2000; Abou Elenean and Deif, 2001; Sawires et al., 2015). The proper characterization of active seismic sources requires incorporation of different types of data (e.g., geological, seismicity, GPS, Geophysical). In this Chapter, we utilize all the information available for local and regional geology, satellite images, Digital Elevation Model (DEM), present-day tectonics, geophysical methods (for location and configuration of subsurface sources), updated seismological record, and updated focal mechanism data.

Ideally, with a long, complete, detailed, and accurate earthquake record and/or with an appropriate understanding of earthquake generation process, identification and characterization of seismogenic sources would be an easy and direct task. So far, the adequate level of understanding of earthquake generation process or sufficient amount of data are not available, thus, the seismic hazard analyst has to deal with a short, incomplete, and inhomogeneous (varying level of details) record of earthquakes and with varying levels of understanding of earth physics (Reiter, 1991). The poor understanding and limited amount of available data about the earthquake process could produce different degrees of uncertainties in the hazard assessment. With such kind of uncertainties, it will be difficult to adequately appraise the fault activity, earthquake size or the precise boundaries of seismic sources. The optimal way to reduce the imperfect knowledge and gaps in available seismicity and associated uncertainties is to judiciously incorporate all available, reliable information from different approaches, newly developed techniques, and strategies.

In the NDSHA, the knowledge gaps can be appropriately treated, either by incorporating available data from seismology, paleoseismology, morphostructural, geodetic, and related studies or by performing extensive parametric and sensitivity analysis to better and accurately define and addressing the effect endemic lack of knowledge, analyst preconceptions and insufficient data and uncertainties (see Chapter 3) on the resultant hazard maps. Moreover, using multiple approaches for the accurate earthquake-size estimation (e.g., historical seismicity; paleoseismic studies; source characteristics), techniques, scaling parameters, wide set of data, and study locations (more data) will improve the understanding of a seismotectonic setting and the potential of the seismic source being studied and this coul naturally produce a accurate SHA. The identification of seismic sources can be accomplished by integrating all available data in the form of geospatial layers in GIS tool.

The data compilation for seismic source identification and characterization needs to be complemented by a detailed study of the related scientific pieces of literature.

Before starting to upgrade the seismogenic zones map of Egypt, it is necessary to briefly describe all the available information based on which the work has been done:

Tectonic setting: Egypt is located in the northeastern part of the African continent and surrounded by three main tectonic elements (Fig. 2.1): the African-Eurasian plate margin, the Red Sea rift system and the Gulf of Aqaba-Dead Sea fault system. The present-day tectonic deformation and associated seismicity in Egypt is a manifestation for the interaction and the relative motion along those boundaries and their remote effects inside the Egyptian territory, through stresses transmitted across the plates to weak zones in the lithosphere.

The African or Nubian plate is moving in the northward direction relative to Eurasia plate at a rate of about 10mm/yr (DeMets et al., 1990 and 1994) and subducts underneath the Eurasian plate at Cyprian and Hellenic arcs (ElGabry et al., 2013), while the Arabian plate is moving to the north-northwest relative to Eurasian plate at rate of about 20-25mm/yr (DeMets et al., 1990 and1994; Jestin et al., 1994), causing crustal spreading along the axis of the Red Sea and lateral slip along the Dead Sea transform zone, producing the Gulf of Aqaba at the southern end, Dead Sea and east Anatolian trend at the north (El-Fiky, 2000). The differential motion between the Africa and Arabia plates which is about 10-15mm/yr is thought to be consumed predominantly by a left-lateral motion along the Dead Sea transform fault (McClusky et al., 2000, El-Fiky, 2000).

Seismological data: the available seismological record for Egypt can be temporarily divided into three segments:

1) The geologic record of earthquakes (long time range), can be extended into millions of years of geologic time to reveal the fault activity and it represents the most critical piece of information for seismogenic sources identification needed for seismic hazard analysis. Although the importance of the geologic record, all the existing seismotectonic models for Egypt have been developed without incorporating this vital piece of information, because of the lack of available geological and paleoseismological investigations, the only exception is Aswan area in southern Egypt.

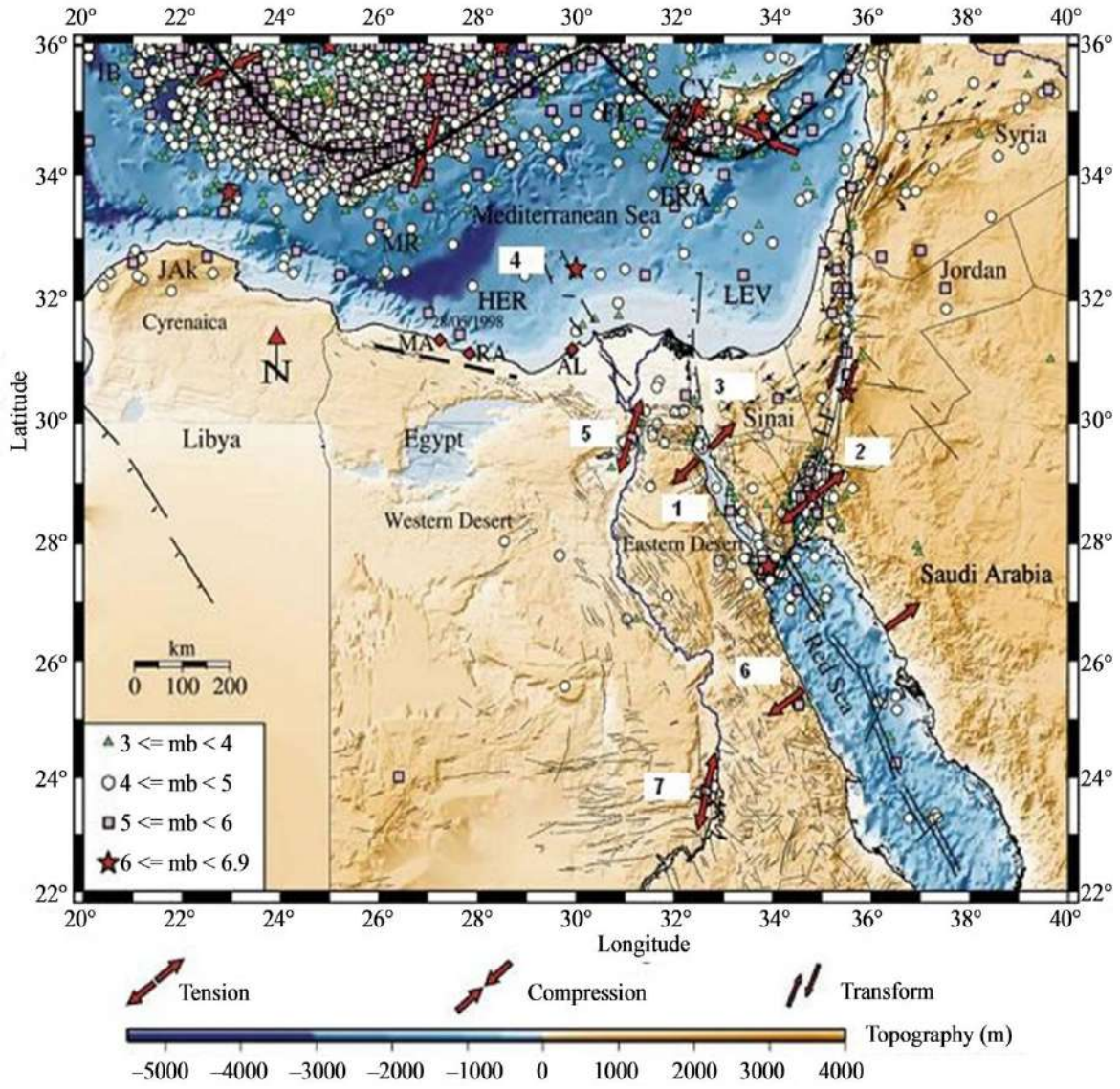

Fig. 2.1: Tectonic boundaries and shallow seismicity pattern (h ≤ 60 km) of the Eastern Mediterranean Region (Abou Elenean and Hussein, 2007).

2) The historical seismicity (intermediate range time) is the seismicity that has written pieces of evidence in the historical record of humankind. The existence, interpretation, and use of the available historical seismicity are of significant interest in seismic hazard analysis, and in most cases, it plays an essential role in defining either the seismic input or seismic design for buildings. Also, historical earthquakes can play a role in forecast and mitigate of the potential earthquake damage and human losses from future ones as they can give valuable information on the earthquake strength, location, and recurrence interval for each region (Ambraseys, 1971).

Moreover, historical data are essential information to construct an isoseismal map and consequently to obtain some information on the attenuation of macroseismic intensity with distance. Additionally, the available historical earthquake catalog needed to be evaluated against bias and awareness of the writer or writers of the history.

Egypt has a long historical seismicity record in the relative sense which goes back in time about four millennia with variable levels of reliability and details. Several authors have studied the historical seismicity of Egypt (e.g., Maamoun et al., 1984; Badawy et al., 2010).

3) The third seismological segment is the shortest in term of time it covers, relative to geological and historical segments, and is named as instrumental seismicity. This segment is essential because it subjects to our direct observations and measurements that can be formally analyzed.

Instrumental earthquake era in Egypt started in 1899; nevertheless, much of the seismic activity along its remote borders was not revealed until the increase of the spatial resolution of the seismic network, deployed by NRIAG, both locally and regionally. After more than 118 years from the installation of the first seismic station, the territory of Egypt is defined as a relatively low to moderate seismic activity region and characterized by the occurrence of small to moderate-size events (intraplate events). Most if not all the more strong events take place infrequently farther east, along the northern Red Sea, the Gulf of Suez entrance or the Gulf of Aqaba, and to the north, the eastern Mediterranean region (interplate events).

The instrumental seismicity provides information about the ongoing tectonic deformation and other details on the earthquake location, depth, magnitude, and source characteristics. The accuracy of earthquake location varies in time and space. Accurate instrumental seismicity is substantial in the identification and characterization of seismotectonic sources or features capable of producing earthquakes of significant size. Due to the relatively short period the instrumental seismicity usually cover relative to the time window of concern, it fails to reflect the actual potential of seismic sources (earthquake-size and earthquake type). So additional seismological record segments or studies are needed. In fact, inaccurate determination of earthquake parameters (e.g., the errors in location and depth may be of a particular importance when attempting to correlate seismicity with active geologic structures) and the possible contamination to the catalog from quarry blasts can lead to erroneous conclusions in seismic hazard analysis, so we have to be careful when we deal with earthquake catalogs.

It worth mention that, a project that embraces teams of archeologists, architects, engineers, geologists, historians, paleoseismologists, and seismologists needs to be launched in order to enhance the earthquake record for Egypt by detailed and comprehensive examination of the remains of ancient sites and structures that are distributed over wide range of time and space.

Upgrading of the seismic catalog is an essential step in the seismic hazard analysis. Here, an updated historical and instrumental catalog for earthquakes in and around Egypt (far and near-source) with $M \geq 5$ compiled from different sources covering the period from 1210 BC till 2016 is used. Usually, strong motion from earthquakes with $M \geq 5$ is of much engineering interest due to the possible earthquake impacts (Panza and Suhadolc, 1987).

The first step in seismotectonic studies is the determination of the type of seismic hazard estimates to be used. The primary goal of the current upgrade of the seismotectonic model for Egypt is to incorporate the new investigations then to be adopted in the computation of updated seismic hazard maps within the framework of NDSHA procedure. For seismogenic sources identification, an updated catalog of earthquakes with $M \leq 5$ is considered based on the idea that significant earthquake deformation in the upper crust may begin at $M_w \geq 4.5$-5.0 (Meghraoui, 2015, personal communication). In the opinion of the author, using earthquake catalog with $M \geq 5$ may naturally help in the reduction of errors related to the estimation of the earthquake location, depth, focal mechanism, and magnitude. Also, utilizing earthquake catalog with magnitude threshold $M \geq 5$ may help in compiling a reliable and uncontaminated earthquake catalog, through the natural screening of the possible non-tectonic seismic events (e.g., blasts, reservoir-induced seismicity). In fact, most if not all of non-tectonic seismic events in Egypt that occur in the areas that show both natural and artificial seismic events (e.g., the northern part of Egypt, Eastern Desert, and Aswan) are of magnitude beyond 4.5. For drawing the seismogenic zone's boundary earthquakes with $M \geq 3$ have been used, but we do not consider a zone as seismogenic if it had no $M \geq 5$. Besides the identification of seismogenic zones, we used MZ and the pattern recognition analysis as a complementary method to the seismotectonic zones model to define the seismogenic nodes not marked by strong earthquakes so far. The local instrumental catalog (for the period from 1900-2016 with magnitude M5+, (see Table 1 in Appendix A) has been compiled using different data sources (e.g., NRIAG catalog; ISC catalog; Abu El-Nader, 2010; Kebeasy et al., 1981) starting from the catalog compiled by Peresan et al. (2009), used in Mourabit et al. (2014) as a reference catalog. In 2010, a team of seismologists from NRIAG have revised the historical

earthquakes catalog, and they qualified each event in the catalog using quality level descriptors (poor, fair, and good) to the existence of the events (Q_e), location (Q_l) and date (Q_d). The revised historical catalog of Badawy et al. (2010) has been considered in this work, after excluding the historical events of poor existence and location quality and with small modifications (adding or removing events) based upon recently published paleoseismological and archeological studies (e.g., Casciati and Borja, 2004).

The remote sensing imagery: it is an advantageous technique for mapping buried faults (either active or inactive) and geologic structures, where the geophysical surveys are costly and difficult to conduct, also where are no available the geological investigations (Elmahdy and Mohamed, 2016). In Egypt, some studies have been done for mapping geological linear structures (lineaments) using digital elevation model data (e.g., Koch and Mather, 1997; Elmahdy and Mohamed, 2014b; Elmahdy and Mohamed, 2016) (Fig. 2. 2). Those maps can be used with other information for the reliable identification of seismic sources.

Geophysical techniques: gravity, magnetic and seismic profiles provide useful information about the location and configuration of geological structures and active faults. Also, the geophysical investigations are robust tools in the identification of buried seismic sources that have not surface expressions or geologic pieces of evidence (Fig. 2.3). To adequately perform the seismic sources delineation, all available geophysical information should be used. Many geophysical studies have been conducted to delineate the geological structures in Egypt (e.g., Said, 1990). In fact, the magnetic survey is a very effective tool in the delineation of buried tectonic trends.

Magnetic anomalies do not occur randomly, but they are aligned along definite and preferred patterns (Said, 1990). According to Said (1990) the results of aeromagnetic surveys in Egypt reveals the following observations: There are tectonic trends that have affected Egypt during the geologic history: north-south (East African Rift trend), north-northeast (Aqaba trend), northwest (the Red Sea and or Gulf of Suez trend), east-west (Tethyan trend), east-northeast (Syrian Arc System trend), west-northwest (Darag trend), and northeast (Aualitic or Tibesti trend). Some tectonic patterns are more characteristic of some parts of the country than others; some trends show more strength in some parts of the country than in others.

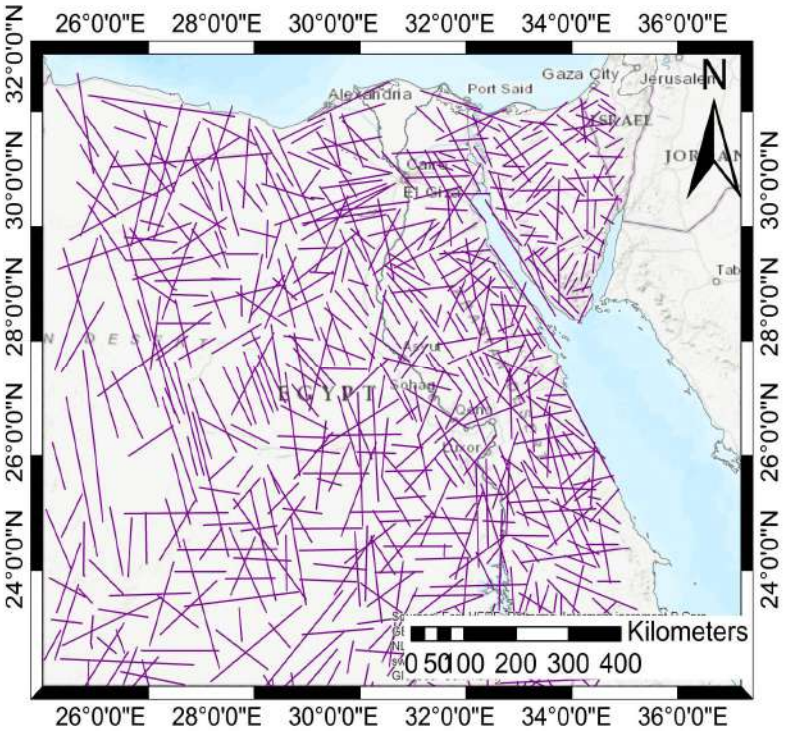

Fig. 2.2: Morpho-tectonic lineaments auto-detected from DEM with Rose diagrams represent trends of auto-detected lineaments in each region of Egypt (Elmahdy and Mohammed, 2016).

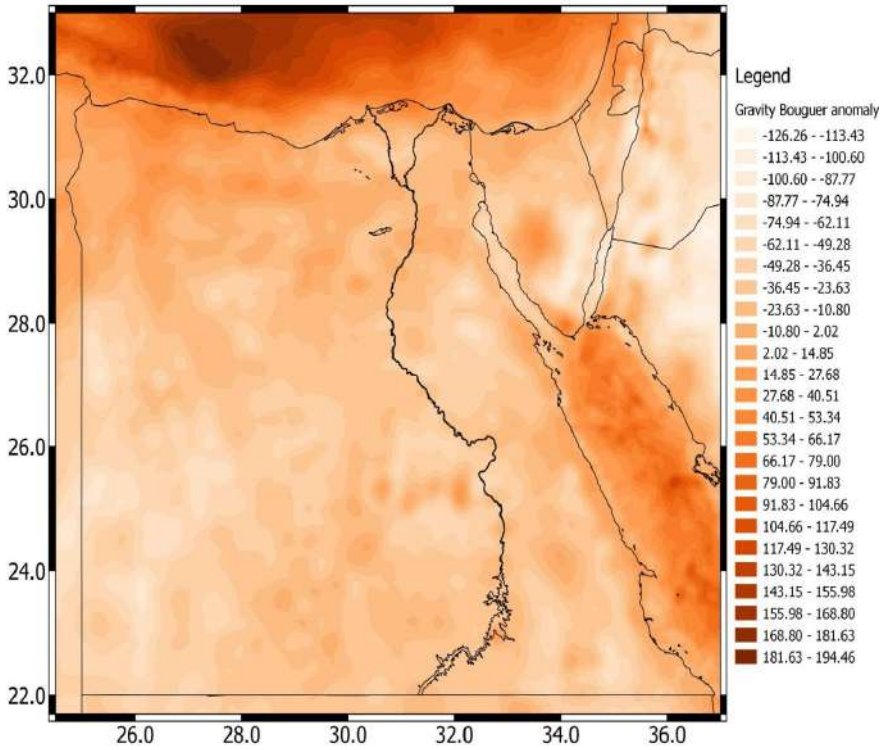

Fig. 2.3: Gravity Bouguer anomaly map of Egypt (obtained from Förste et al., 2015 model, and then contoured).

Geodetic maps: GPS is a technique that has a sufficient accuracy to measure the small motions produced by tectonic movements. By using repeated and accurate measurements of elevation and horizontal displacements, the crustal deformation can be detected then mapped. The monitoring of the crustal deformation in Egypt has been started since 1983, after the occurrence of 14 November 1981 earthquake $M_l = 5.6$ in Aswan, southern Egypt. The present spatial distribution of GPS network in Egypt is distributed among the most active regions (e.g., the Gulf of Suez; the Red Sea; Cairo) as shown in Fig. 2.4. For the update of the seismotectonic model purpose we used all the available crustal deformation studies accomplished at local and regional scales (e.g., El-Fiky 2005; Saleh and Becker, 2015).

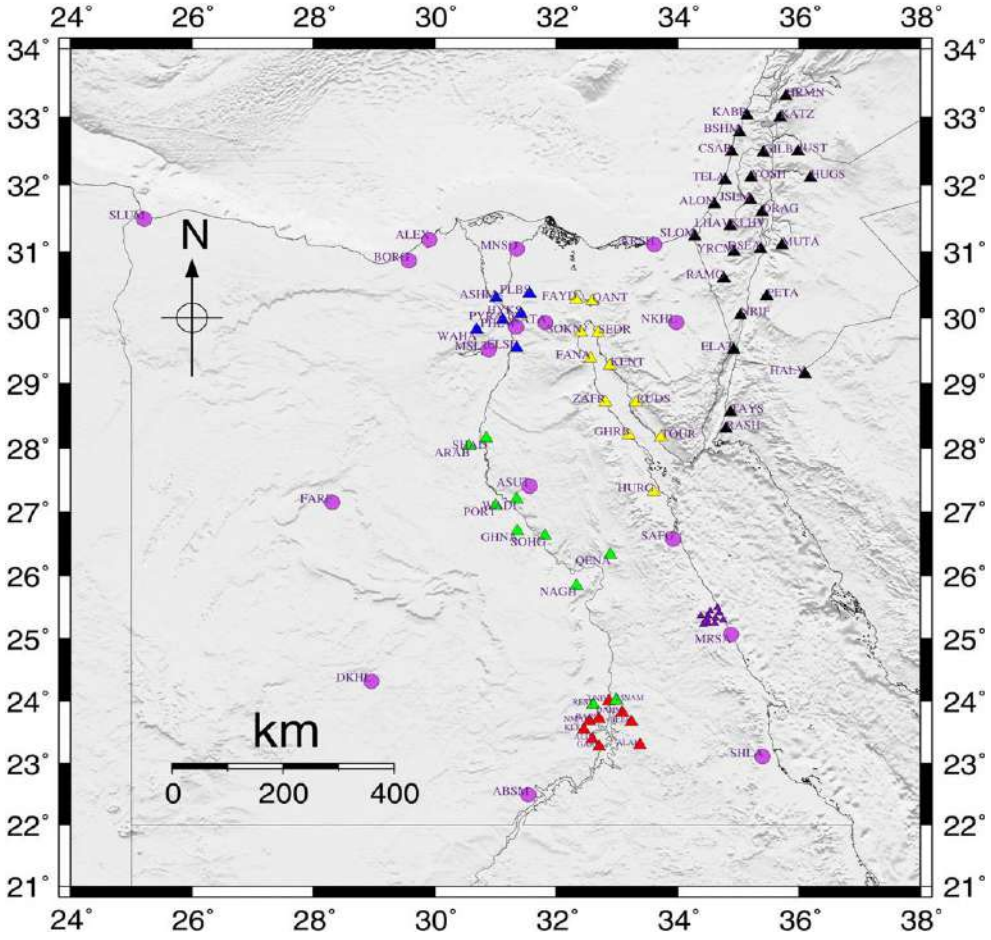

Fig. 2.4: Spatial distribution of the GPS sites in Egypt (after Saleh and Becker, 2015).

Focal mechanism and stress data: the focal mechanism and stress studies are essential for studying the seismotectonic setting of the region of interest, because they can provide information about the directions of tectonic stress at depth. Focal mechanism and stress data are beneficial in

the definition and characterization of seismotectonic sources, which represent the primary input for any seismic hazard analysis. Many focal mechanisms and source inversion studies have been conducted during the last decades to characterize the source configuration (geometry and orientation), focal depth, and moment tensor (e.g., Abdel Fattah, 1999; Abou Elenean 1997; Abou Elenean, 2007; Hussein et al., 2013). A region of a uniform seismogenic process can be delineated based upon the available focal mechanism data. For the period of the 1950s till 2004, the revised and updated focal mechanism catalog of Abu El-Nader (2010), (Fig. 2.5 a ($M \geq 4$) and b ($M \geq 5$)) was used, where the best solutions for focal mechanism have been introduced after applying quality control schemes. For the period from 2004 till 2016, a reliable fault plane solution catalog was compiled from the published pieces of literature in international journals and the Centroid-Moment-Tensor (CMT) solutions (e.g., Abou Elenean and Hussein, 2007; Abu El-Nader et al., 2013).

Geological data: the geological and tectonic maps which can help in the definition of potential seismic sources are useful in the seismotectonic sources delineation. Also, the available maps for the major faults with the tectonic activity during different geologic time are of substantial importance in seismotectonic studies. The first map that shows the distribution of surface tectonic trends (whether they are active or inactive) based upon the geologic survey in the basement rocks outcrops was 1981 geologic map of Egypt (EGSMA, 1981). This map shows the concentration of tectonic trends in the areas where the basement rocks cropping out or the areas of thin sedimentary cover. Moreover, information on active faulting in Egypt is too sparse to be used as source model. The only exceptions are Aswan area in southern Egypt and Wadi Hagoul in the Eastern Desert.

It is well known that the seismic activity represents evidence on the mechanical adjustment to stresses and ongoing tectonic deformations. The present-day tectonic deformation can be deduced from incorporating the geology, tectonics, and seismic activity investigations. Based on the fact that, most of the earthquake activities take place along active faults, plate boundaries and margins (e.g., Sykes, 1967), this information can be used to delineate major active seismotectonic province or major tectonic trends. The integration could help in defining and characterizing different major seismotectonic provinces (active tectonic patterns) within which, small seismic sources can be identified by taking a close look based upon available details (e.g., focal mechanisms, GPS, bathymetry; topography, stress data).

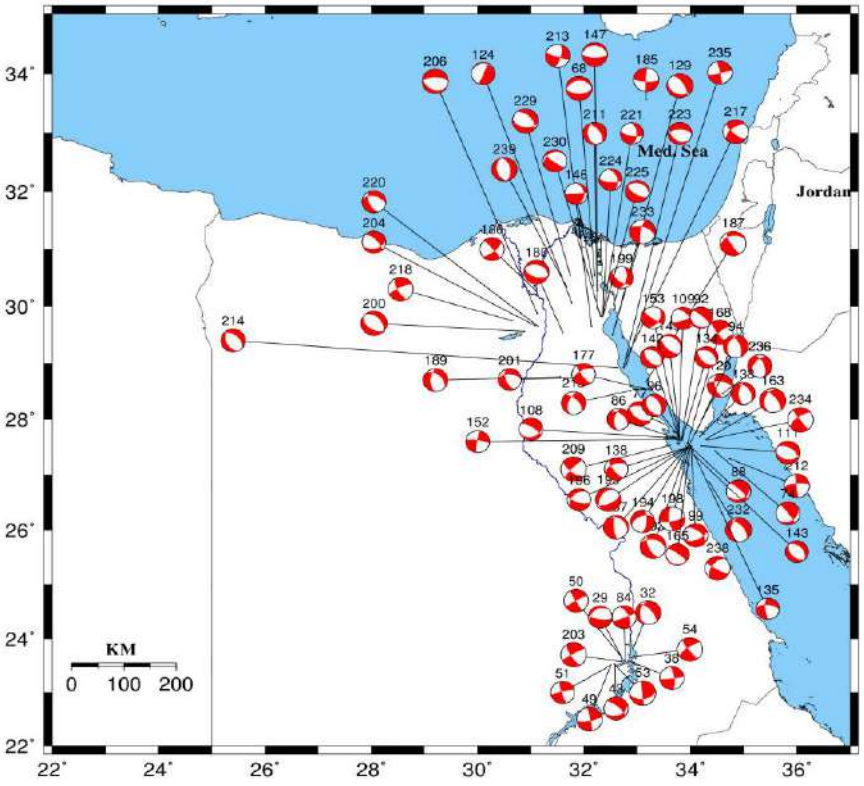

a)

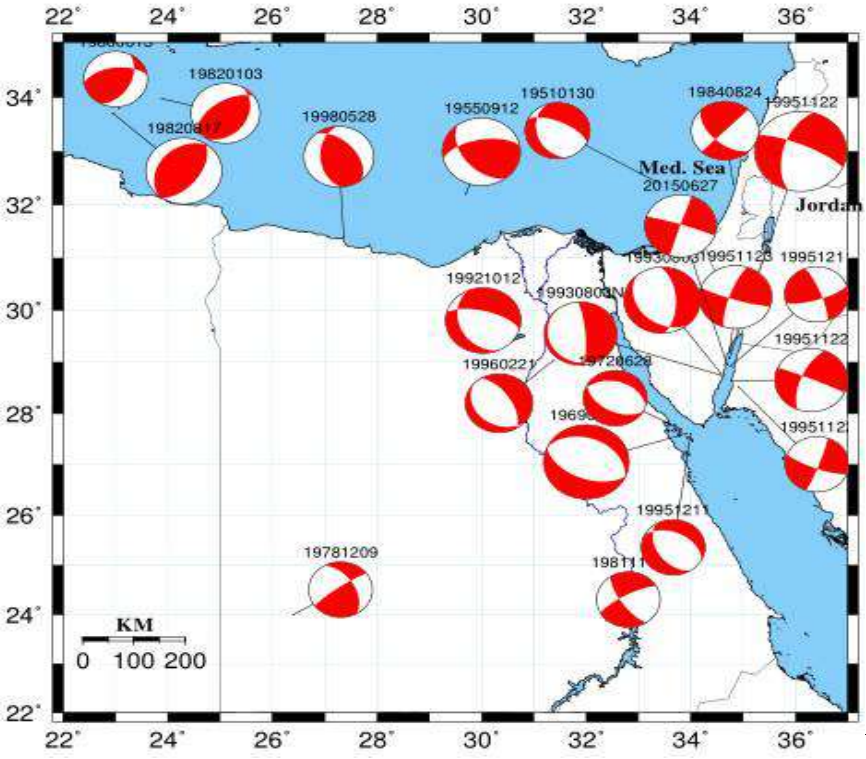

b)

Fig. 2.5: Focal mechanism solutions for earthquakes with M ≥ 4 (a) and M ≥ 5 (b) that occurred during the time interval 1900-2016.

Figs. 2.1 and 2.6 give a general view of seismic activity and main tectonic elements in and around Egypt. It reveals clustering and aligning of the seismic activity along with some specific tectonic trends and individual faults which consist of the previous studies (e.g., Abou Elenean, 1997). Some of these clusters follow the known active trends and/or the intersection of major active faults of the Red Sea, the Gulf of Suez, and the Gulf of Aqaba. Others significant inland active zones are found in the northern part of the Eastern Desert between the Nile Valley, the Gulf of Suez, Cairo-Suez district zone, southwest Cairo (near Dahshur, where the 12 October 1992 earthquake had occurred), Aswan (Kalabsha), and Abu-Dabbab area. Other few activities are observed along the Nile Valley, the north of Idfu, west of Asyut, Gilf El Kebeir, southwest of Bani Suef, and Marsa Alam areas.

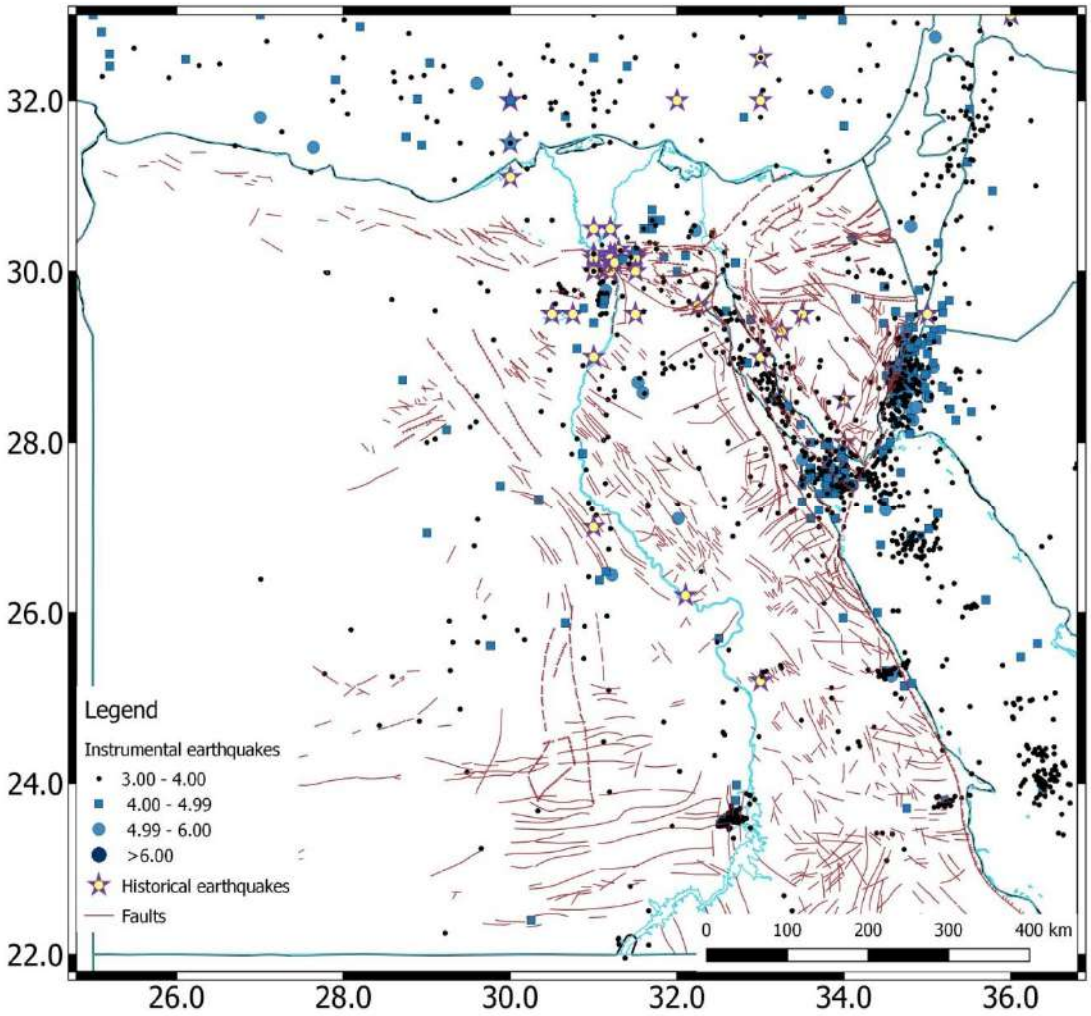

Fig. 2.6: Seismicity of Egypt plotted with faults delineated by EGSMA (1981).

The seismicity map of Egypt mainly confirms the results of existing seismotectonic studies, but they do not clearly show or evidence the existence or spatial continuation of some hypothetical trends; such as the possible extension of the Gulf of Suez trend to the north (towards the Mediterranean Sea) as pinpointed by previous studies Kebeasy (1981), the East Mediterranean-Cairo-Fayum belt shown by Kebeasy in Said (1990) or the concept of Pelusium trend which has not confirmed yet as explained by Neev (1975). This map also indicates that seismic activity decreases and becomes dispersed toward the Nile Delta and the Mediterranean Sea, which agree with the results of Salamon et al. (1996) and Abou Elenean and Hussein (2008).

2.1.1 Gulf of Aqaba-Dead Sea transform fault SSZs

The Gulf of Aqaba represents the eastern branch of the Red Sea, it is about 180 km long and 15-25 km wide (Ben-Avraham et al., 1979), lies in the southernmost segment of the Levant Fault. It differs from the Gulf of Suez in the age of evolution and the tectonic regime, also in the topography of the bottom; it has irregular bottom topography of an average depth of 1,250m (Said, 1990) (Fig. 2.7). The Gulf of Aqaba is bounded in the west by Sinai Mountains (Egypt), which show a sizable inherited systems of faults mostly oriented parallel to the gulf (Eyal et al., 1981) and in the east by Hejaz Mountains (Saudi Arabia), which show a similar regional strike. Abdel-Fattah (2005) has performed detailed seismicity and tectonic study of the 1993 and 1995 Aqaba earthquake swarms and concluded that the Gulf of Aqaba has a complex tectonic regime and can be represented by local extensional stresses and strike-slip stresses, and dominant regional strike-slip stresses.

The Gulf of Aqaba is characterized and formed by the development of a series of four NNE-SSW en-echelon rhomb grabens or pull-apart basins (Garfunkel, 1981). These from north to south, respectively include Eilat, Aragonese, Dakar, and Tiran deeps (Fig. 2.7) and they are connected by en-echelon strike-slip faults striking nearly in N20° as indicated by Ben-Avraham (1985). Generally, most of the gulf is occupied by three elongated faults bounded basins striking NNE. The major faults of the gulf are arranged as en-echelon, with transverse, probably normal faults at basin end and interiors.

Two types of faults are found in the recently active Gulf of Aqaba: strike-slip and dip-slip normal faults (Garfunkel, 1981). The main faults in the Gulf of Aqaba are trending towards N-S and NNE-SSW. These trends are well correlated with the cracks system of different orientations

observed in the rocks on both flanks and as well as within the Gulf, as reported by many authors (e.g., Klinger et al., 1999; Ben-Avraham et al., 1979 and 1985).

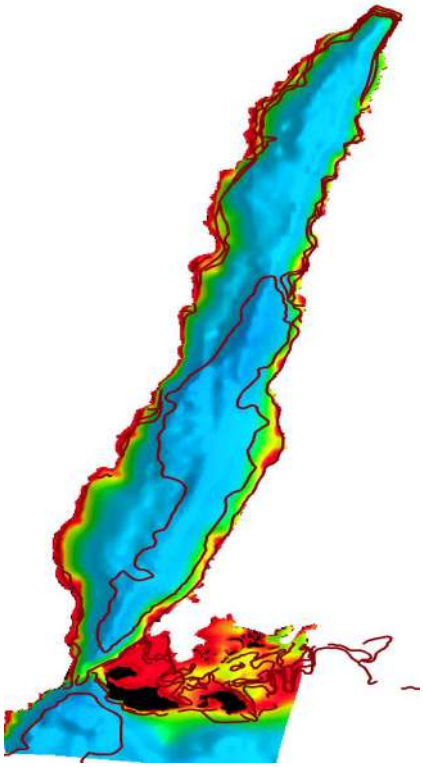

Fig. 2.7: Bathymetry map of the Gulf of Aqaba.

During the last decades, four significant earthquake swarms had struck the Gulf of Aqaba i.e., 21 January, 1983, 3 August 1993, 22 November, 1995, and 27 June, 2015, earthquakes. The 22 November, 1995, Aqaba earthquake, which is located to the south of the 1993 swarm, is the largest instrumentally observed event in Gulf of Aqaba and Egypt as well (M_w = 7.2) during the last century.

The focal mechanism solutions for the Gulf of Aqaba earthquakes show strike-slip and normal faulting types. All these mechanisms exhibit a tension axis trending almost NE-SW to E-W except two events showing a tensional axis in the NNW-SSE and NW-SE direction (Fig. 2.8). From tectonic point of view, the occurrence of these mechanisms may be related to the extensional motion in the Red Sea and the anticlockwise rotation of Arabia with respect to Sinai sub-plate along the Dead Sea transform fault system. The diversity of focal mechanism solutions is consistent with the cracks system of different orientations that were reported by many authors (e.g., Klinger et al., 1999). Also, those mechanisms are consistent also with the GPS observations that followed the 22 November 1995 swarm as concluded by Kimata et al. (1997).

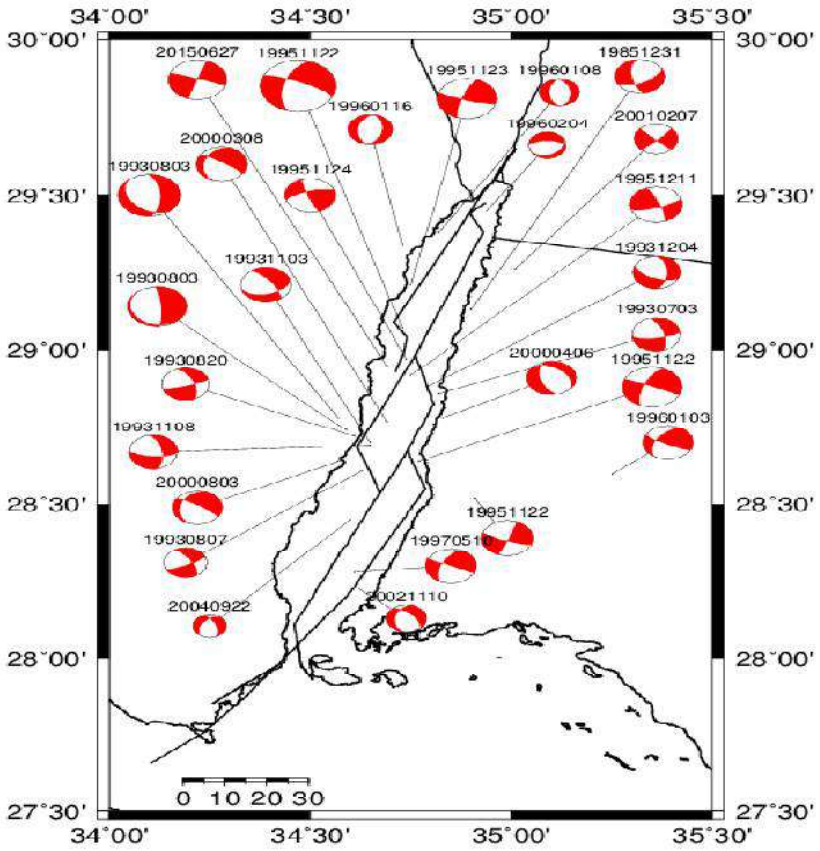

Fig. 2.8: Fault plane solutions in the Gulf of Aqaba updated after Abu El-Nader (2010).

Ben-Avraham (1985) has studied the structural framework of the Gulf of Aqaba using bathymetry, shallow seismic profiles, magnetic, and gravity data. The bathymetric study indicates that three main elongated en-echelon basins occupy the gulf's interior. The northern part is the characterized by a single flat-bottom and relatively shallow depth basin; the central part is the narrowest but the deepest of all the gulf basins, while the southern part is the widest and of intermediate depth relative to the northern and southern part. Ben-Avraham (1985) conclude that, the asymmetry in the central and southern parts of the Gulf of Aqaba suggests that the active strike-slip motion occurs on the western boundary (the Sinai peninsula), while the asymmetry in the northern part is due to the fact that the strike-slip motion is taking place along the eastern border (Saudi Arabia).

The continuous seismic profiles used for studying the shallow structure by Ben-Avraham (1979) and Ben-Avraham (1985) show that faulting structures control the morphology of the

Gulf of Aqaba and the Gulf's basins differ in their shallow structure (shape, geometry, and bathymetry) due to ongoing deformation. Moreover, the northern and southern faults that bound the basins are characterized by a different faulting nature (Ben-Avraham, 1985). The crustal thickness of the north of the gulf is about 35km and 27km in the southern region.

The analysis of different geophysical data (continuous seismic profiles, bathymetry, gravity, heat measurements and magnetic) collected for the Gulf of Aqaba to better understand its structure and seismotectonic setting reveal that the gulf can be separated into three distinctive deeps. The southern part is shallow and similar to the northern Red Sea region, and broader than other parts. The magnetic anomaly map shows, smooth anomaly trending NNE in the same strike direction of the gulf, while the gravity data analysis shows that, the free air anomalies are less negative than the other two parts. Also, the continuous seismic profiles to study the crustal structure in the southern part of the Gulf indicate that the crust thins significantly. Furthermore, the observed heat flow value in the south is the highest in the Gulf (Ben-Avraham, 1985).

The central part is the narrowest and the deepest part of the gulf, showing a relatively high tectonic activity with respect to other parts. Irregular topography characterizes the seafloor of the central part of the Gulf. The Bouguer gravity anomaly map for the gulf shows that the central part is characterized by higher values than the other parts and this may be due to the effect of the ongoing tectonic activity on both shallow and deep crust. The heat flow values in the gulf decrease from south to north ($78mWm^{-2}$, $66mWm^{-2}$ and $54mWm^{-2}$ in the southern, central and the northern part, respectively).

The northern part of the Gulf is characterized by a crustal structure much simpler than other parts (southern and middle) and very similar to the structure of the Dead Sea. The bathymetry data shows a relatively single and flat-bottomed basin. The Bouguer gravity anomaly map shows that the northern anomaly is the larger in the Gulf of Aqaba. Furthermore, the heat flow values are lower than those in the other two parts.

Hussein et al. (2013) divided the Gulf of Aqaba into two zones of uniform stress fields using revised focal mechanism solutions (based on quality control scheme) till 2004. Using all the available information about the Gulf of Aqaba, we propose three seismic sources; northern, central, and southern zones (Fig. 2.9).

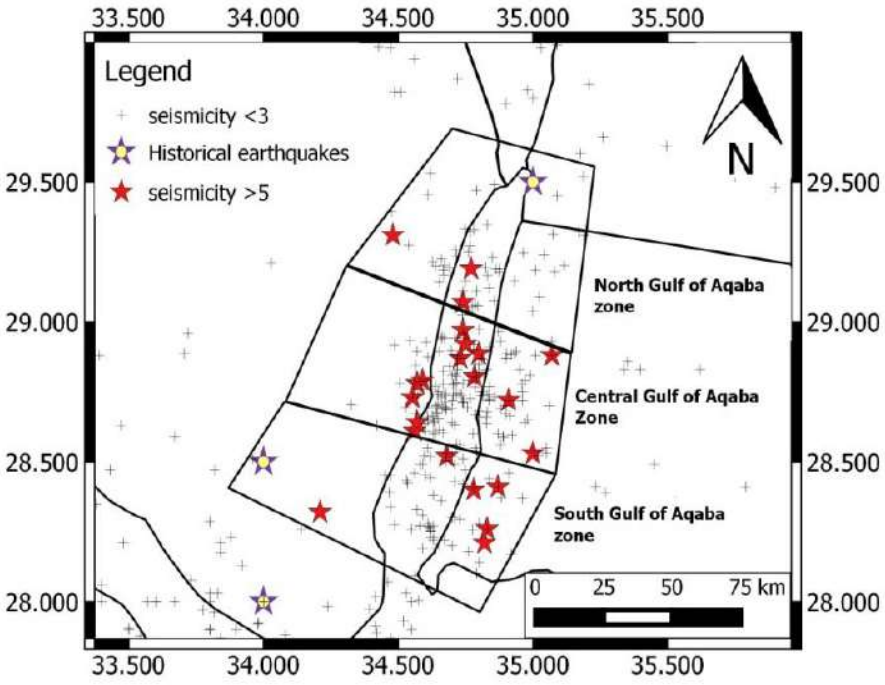

Fig. 2.9: SSZs for the Gulf of Aqaba.

2.1.2 Gulf of Suez SSZs

The Gulf of Suez represents the northern extension of the Red Sea rifting. It represents the northwestern branch of the Sinai triple junction (McKenzie et al., 1970; Le Pichon and Franchateau, 1978; Cochran, 1983) together with the Gulf of Aqaba and the Red Sea. Gulf of Suez is different from the Red Sea and Gulf of Aqaba regarding bathymetry, water chemistry and type of deposits; also, it is flatted-bottom with an average depth ranging between 55-75m (Said 1990). Many evidences reveal that initial rift in the Gulf of Suez and the Red Sea (Late Oligocene-Early Miocene) was synchronous, as indicated by the early Miocene dykes in southern Sinai (Bartov et al., 1980), and has thick marine sediments of Miocene age in the rift which is thicker than regions bordering it to the east, west and south (Garfunkel and Bartov, 1977).

The Gulf of Suez rift is characterized by its structural asymmetry deduced by three half grabens of different tilt directions which were attributed by Moustafa (1976) to three transverse dip provinces, including northern, central, and southern parts of the rift. Those dipping provinces include several rift blocks of consistent dip direction. The dip direction of fault blocks along the rift changes from the southwest in the north to northeast and back to the southwest in the south

defining the three half grabens, respectively (Fig. 2.10). Two accommodation zones exist between those half grabens which extend transversely across the rift (Bosworth, 1985), Gharandal accommodation zone (about 60km wide) in the north (Moustafa 1996a) and Morgan accommodation zone (about 20km wide) in the south (Moustafa, 1976).

The dominating geologic structure in the Gulf of Suez rift is faulting (Colletta et al., 1988). Two major sets of fault patterns have influenced the rifting processes: the main NW Clysmic and the transfer trends. Faults belonging to these trends show a large normal dip-slip component and very small strike-slip components (for more details, see Moustafa, 1993, 2004 and the references therein).

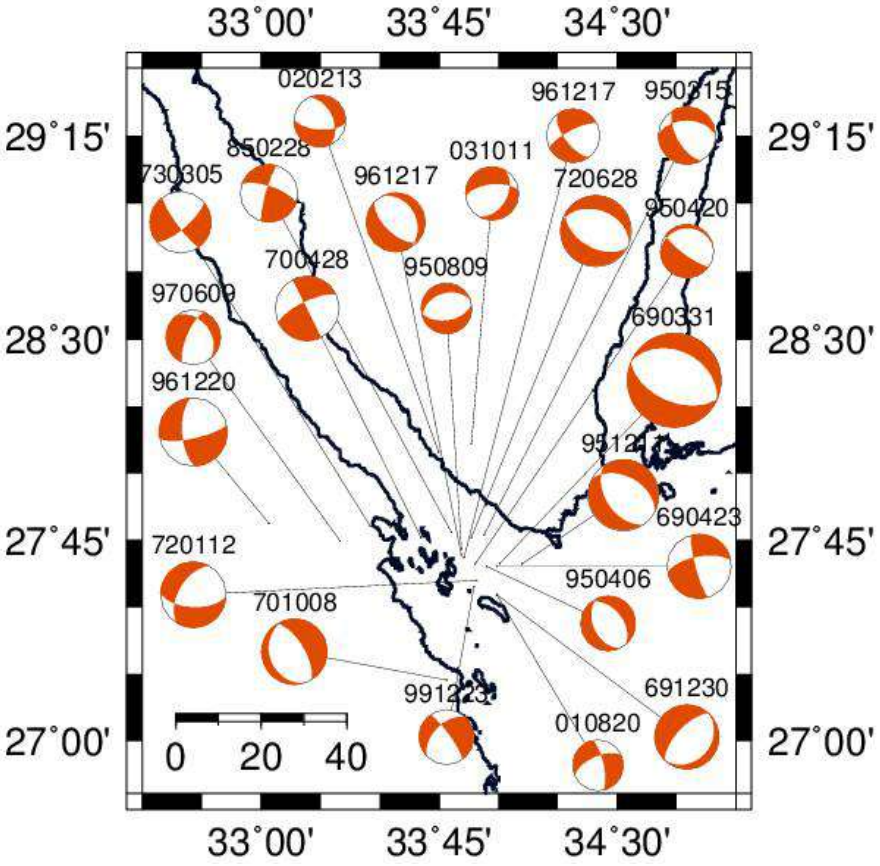

Fig. 2.10: Focal mechanism solutions for the Gulf of Suez (Abu El-Nader 2010).

Moustafa and Abd-Allah (1992) attributed the northern termination of the Suez rift to the northwestward as a transfer of throw from the north part of the rift into the Cairo-Suez district via east-west oriented pre-rift faults. Also, they indicated that the ending of the NNW-SSE faults along western Sinai by the E-W Themed fault. Dixon et al. (1987), Moustafa (1997) and Younes

et al. (1998) have shown that preexisting basement fault zones such as the NW trending shear zones of Najd system in the Arabian plate (Davies, 1984) were reactivated during the late Oligocene-Miocene extension. These Precambrian fault zones have strongly controlled the orientations of the Cenozoic rift faults. The Bouguer gravity anomaly map of the Gulf of Suez reveals three distinctive zones: northern, central and southern zones. The northern and central zones show low gravity anomalies of about -50mgal but they are separated from each other and the surroundings by zones of intensive gravity variation. The southern zone of the Gulf of Suez has the same gravity value, but it differs from the northern and southern zones in the shape of the anomaly.

Abdel-Monem et al. (2011) have studied the crustal deformation along the Gulf of Suez and they concluded that based on the annual rotation rates and the distribution of dilatation and shear strains, the study area could be divided into three main parts. The northern part is characterized by relatively low to moderate dilatation and maximum shear strain values, while the southern part has relatively small amount of dilatation and shear strain. The central part is revealing relatively high amount of dilatation and maximum shear strain.

Low to moderate seismic activity characterizes the north of the Gulf of Suez. Also, its southern part (north of the Red Sea) is characterized by higher seismicity than the northern one. This is evidenced by the high observed heat flow, the presence of nucleation of magmatic activity and disturbance in bottom topography relative to the rest of the gulf (Maamoun et al., 1984; Hussein et al., 2006) (Fig. 2.11). In the southern part, significant events have occurred of relatively moderate magnitudes (4.0-6.9) (e.g., 31 March, 1969, and 28 Jun, 1972, of magnitudes about 5.5 and 6.8Ms, respectively).

The seismic activity in the southern part of the Gulf of Suez reveals scarce clustered type seismicity. Hussein et al. (2006) show that two distinct clusters (seismic sources) can be deduced from the distribution of seismicity and the associated focal mechanisms. The first cluster is located in the south of Ras Mohamed region; at the southern tip of the Sinai Peninsula, while the second is located at Shadwan Island (source of 1969 earthquake), and Gubal Island. Moreover, Hussein et al. (2006) have shown the spatial distribution of seismic activity, and the associated focal mechanisms indicated that the Gubal Island has higher seismic activity than Shadwan Island and Ras Mohamed (Fig. 2.10).

The Gulf of Suez can be divided into two distinct seismic zones based on seismicity, the similarity in focal mechanism solutions, heat flow measurements and the present-day magmatic activity: the northern and southern seismic sources (Fig. 2.11). The southern zone contains the Gubal and Shadwan Islands while the northern one includes the middle and northern parts of the gulf, which is characterized by scattered and small to moderate size seismicity.

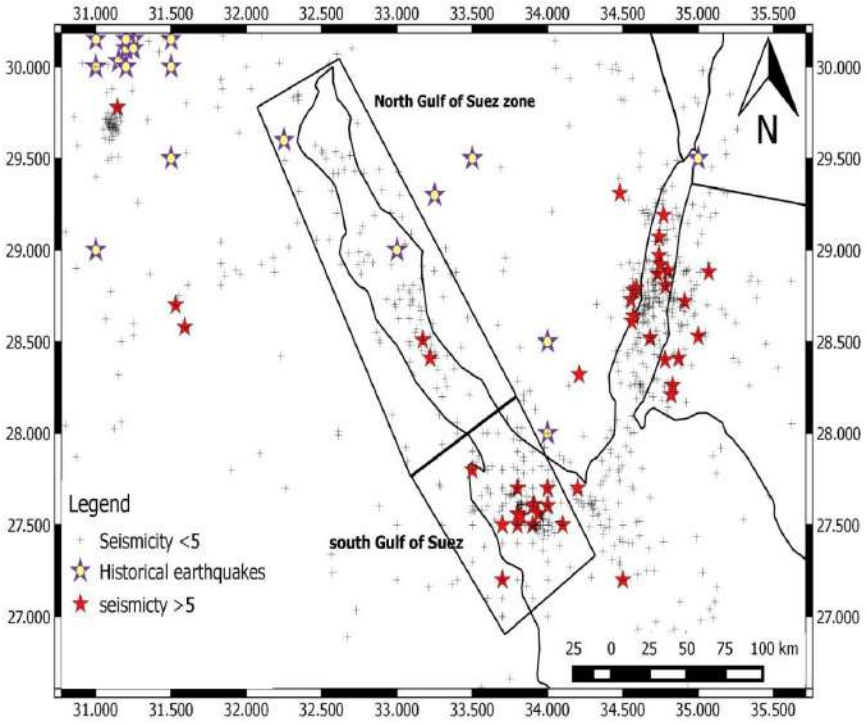

Fig. 2.11: SSZs of Gulf of Suez.

2.1.3 The Red Sea SSZs

The Red Sea rift system is perhaps the best example of recent continental rift and active sea-floor spreading. The rift had been formed due to the relative movements between African and Arabian plates. The rift system was developed by early anticlockwise rotation of the Arabian plate from the African plate. It divides at the northern end into two parts: the Gulf of Suez and the Gulf of Aqaba (sinistral shear). Both stratigraphic and structural studies show that the Red Sea and the Gulf of Suez rifting began in Oligocene time and then developed in the Miocene (Said, 1990).

Gaulier et al. (1988) conducted a seismic survey in the Egyptian half of the northern Red Sea that included 13 expanding spread profiles for crustal structure study purpose. The

interpretation of those profiles shows that the depth to the Moho is at a range of 13-15km on most of the profiles.

The bathymetry of the northern Red Sea rift (of relatively high seismic activity) reveals a series of terraces stepping down to an axial depression at a depth of 1100-1200m (Martinez and Cochran, 1988; Cochran, 2005).

Magnetic anomalies throughout the northern Red Sea have been interpreted as arising from individual volcanoes or intrusions (Cochran et al., 1986; Guennoc et al., 1988; Martinez and Cochran, 1988; Cochran, 2005). Using the available information for the Red Sea part of Egypt, we propose two seismic zones, as shown in Fig. 2.12. The northern zone is occupying the north of the Red Sea and Sinai apex and relatively high seismicity characterizes it.

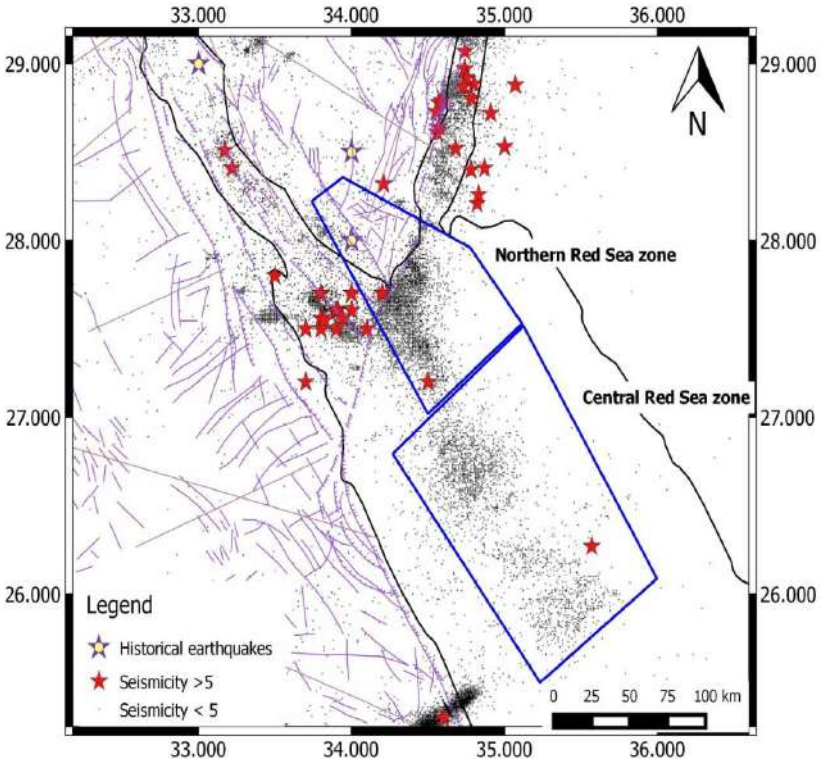

Fig. 2.12: SSZs depicted for the Red Sea.

2.1.4 Passive continental margin SSZs

Over the last decades, a number of moderate to large size earthquakes (e.g., 12 September 1955 earthquake $M_s \sim 6.8$ with a maximum intensity VII on the MSK scale) have occurred along the Egyptian continental margin (Mediterranean coast) causing buildings damage and panic

between population living along the northern coast and in the Nile Delta region. The continental margin of Egypt is located in the southern part of the folded arc forming the Mediterranean ridge, and it is characterized by a narrow continental shelf extending for about 15-20km seaward. The focal mechanism solutions indicate that the present-day NNW compressional stresses related to the movement between the African and Eurasian plates are translated into either reverse mechanism along E-W to ENE-WSW trending faults or normal mechanism along NNW-trending faults (Fig. 2.13) (Abu El-Nader et al., 2013). Four seismogenic sources are delineated along the Egyptian continental margin based on the spatial distribution of earthquakes and focal mechanisms, as well as the previous studies (Fig. 2.14).

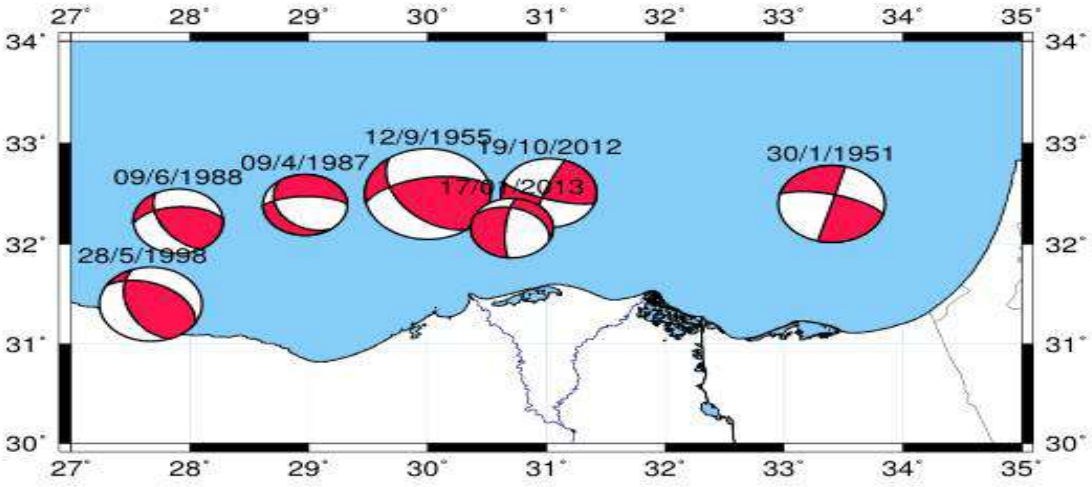

Fig. 2.13: Fault plane solutions for the large instrumentally recorded events along the continental margin.

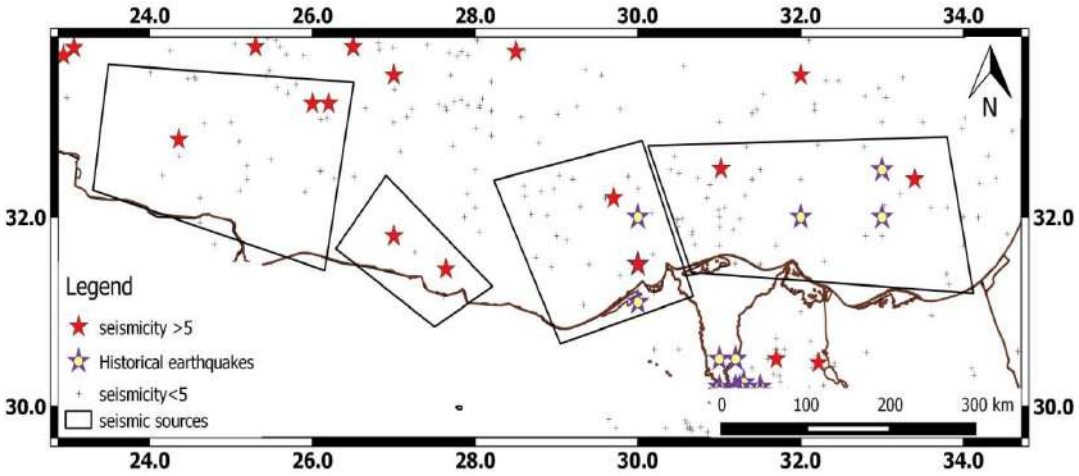

Fig. 2.14: Proposed SSZs for the continental margin.

2.1.5 Eastern Desert SSZs

2.1.5.1 Cairo-Suez district SSZ

This zone is located in the northern part of Eastern Desert of Egypt and covers the area that extends from the northern end of the Suez rift to the Nile Valley. The Cairo-Suez district is affected by the late Oligocene-early Miocene deformation related to the opening of the Gulf of Suez in response to ENE-WSW oriented extension. Meanwhile, it is probable that a part of this deformation is transferred to the land and led to the rejuvenation of the deep-seated preexisting E-W oriented faults by dextral transition (oblique-slip movement) in addition to NW-SE striking faults (Moustafa and Abd Allah, 1992). This produced E-W elongated belts of left stepped en-echelon normal faults (Moustafa et al., 1985), overlie preexisting deep-seated faults of right lateral strike-slip movement (Smith, 1965; Moustafa, 1988). The Cairo-Suez area on this basis is characterized by several E-W elongated belts of E-W to WNW normal faults having left stepped arrangement. Those belts are consistently found throughout the area and act as transfer zones between the NW oriented normal faults (i.e., to transfer the throw from one NW oriented fault to another) (Fig. 2.15).

The Cairo-Suez shear zone represents one of the intraplate seismic active sources in Egypt. This region represents a source of a potential seismic threat as evidenced by GPS surveys (~2mm/year by Mahmoud et al., 2005 and ~5mm/year by Badawy, 2001), the occurrence of moderate size earthquakes and the presence of morphostructural indicators (e.g., fault scarps). The historical and instrumental earthquake catalogs are too short and incomplete to reflect the actual seismic potential (i.e., MCE) of this source zone. From the spatial distribution of seismicity, three clusters can be distinguished: Wadi Hagul, Abu Hammed, and bitter lakes, respectively. The bitter lakes form the eastern extreme of the Cairo-Suez region. The spatial distribution of seismicity in this area is well consistent with the main E-W trend, in particular to the south while in the northern part the seismicity is diffused and it is difficult to attribute it to any of the known active faults or geologic structure.

The majority of this activity is more likely conformable with preexisting NW-SE, E-W, and NNW dominant surface faults. The focal mechanism solutions for this region reveal both pure normal faults and oblique-slip ones with a predominant dip-slip normal component trending in NW-SE and the E-W directions, as shown in Figs. 2.15 and 2.16.

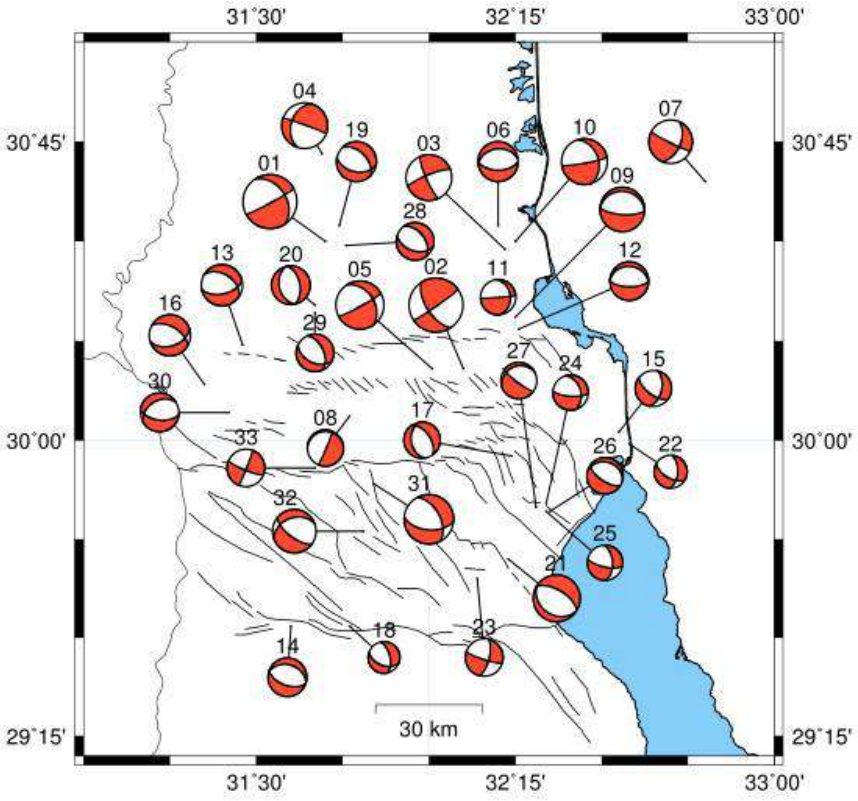

Fig. 2.15: Focal mechanisms for earthquakes occurred in the Cairo-Suez district.

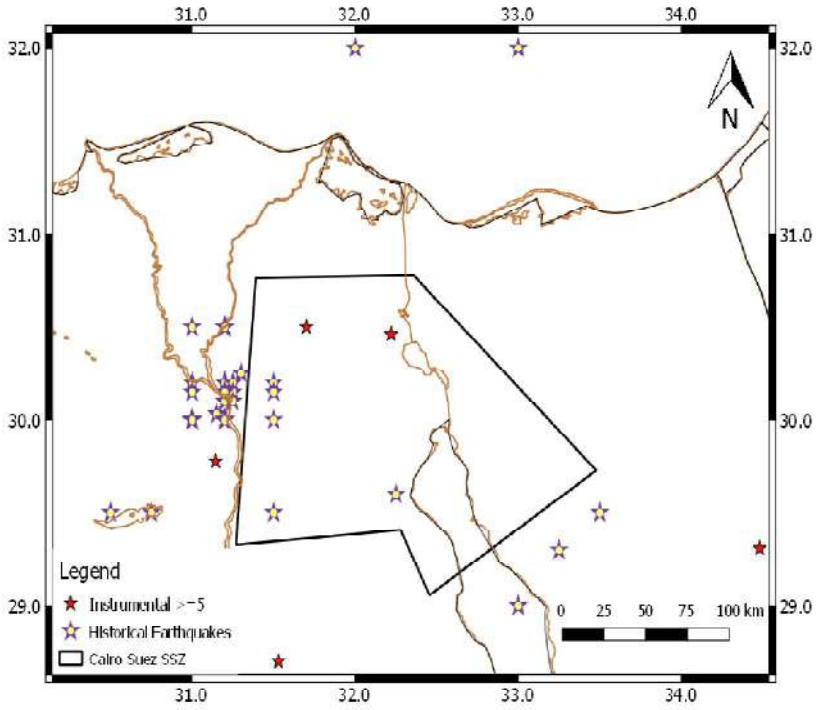

Fig. 2.16: Delineated Cairo-Suez SSZ.

2.1.5.2 Abu-Dabbab SSZ

Abu-Dabbab area is located in the east of the Eastern Desert at the Red Sea coast and is characterized by relatively high seismicity (swarm-type seismicity) and complex tectonic setting (Fig. 2.17). The most significant events that struck the area were the 12 November 1955 (M_l = 5.6) and 2 July 1984 (M_l = 5.1) earthquakes. The spatial distribution of the earthquakes in Abu-Dabbab shows that the seismicity is aligned along the predominant NE-SW trend perpendicular to the Red Sea rift system. Based on both satellite images and geology survey, the area reveals two predominant local trends of major, minor faults, and lineaments: the minor trend has NNW–SSE direction and the major trend is ENE–WSW (Said, 1990). Focal mechanism solutions for Abu-Dabbab earthquakes show different faulting styles, and normal faulting, with a strike-slip component, is the dominant one with ENE-WSW and E-W trend directions. Mohamed et al. (2013) have studied the crustal deformation in Abu-Dabbab area using GPS and seismicity data, and they concluded that the area showed non-uniform distribution in magnitude and direction of horizontal movements and suffered from variable compression and tension during the observation time. Mohamed et al., (2013) interpreted the compressional and tensional stresses to be a result of either the extension related to the magmatic intrusion into the Precambrian-crust of Abu-Dabbab area (local stress) or the shortening (regional stress) due to the opening of the Red Sea rift.

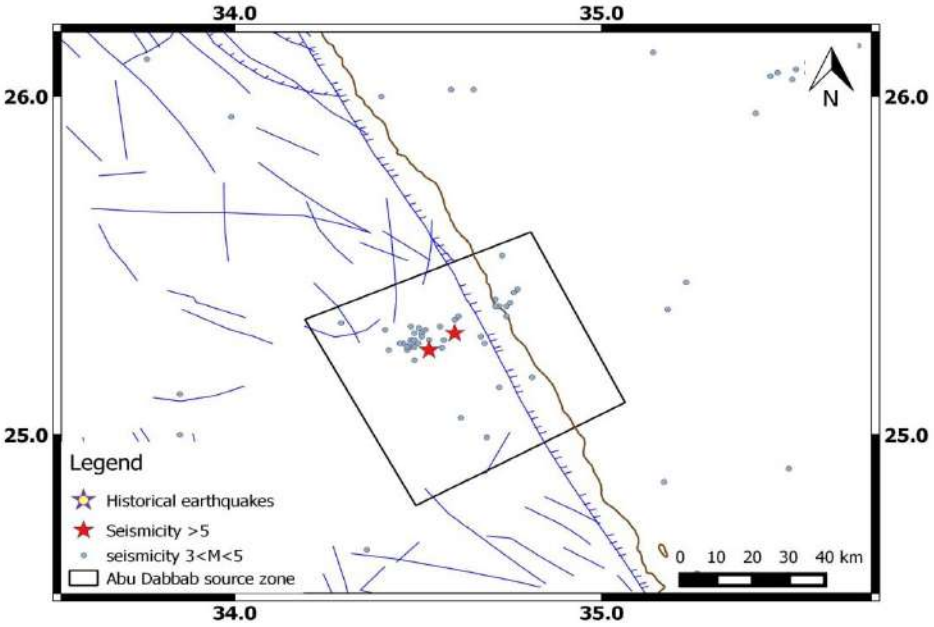

Fig. 2.17: Abu-Dabbab SSZ.

2.1.6 Nile Valley and delta SSZs

2.1.6.1 Sohag - Assyut - Idfu SSZs

This zone comprises three seismic sources Sohag, Asyut, and Idfu sources, and is characterized by low to moderate size seismic activity aligned along the ENE direction, which is inconsistent with Gulf of Aqaba-Dead Sea fault system trend. In 2006, an earthquake with M_l = 4.0 was triggered west of Idfu city. The strongest earthquake occurred in this zone was the 1210 BC with VI intensity on the MSK scale. Focal mechanism solution of the 2006 event shows strike-slip faulting with normal component (Fig. 2.18). There are no available detailed crustal deformation studies for this part of Egypt, so far. The seismicity of this zone is well known to be affected by mining quarries and considering events with a magnitude larger than five will naturally resolve the problem of the catalog being contaminated.

The spatial distribution of earthquakes in Sohag-Assyut source displays a sporadic and scattered distribution of seismicity without preferred trend. The largest earthquake occurred in this zone is the 14 December 1998 M_l = 5.4. (Mohamed, 2007).

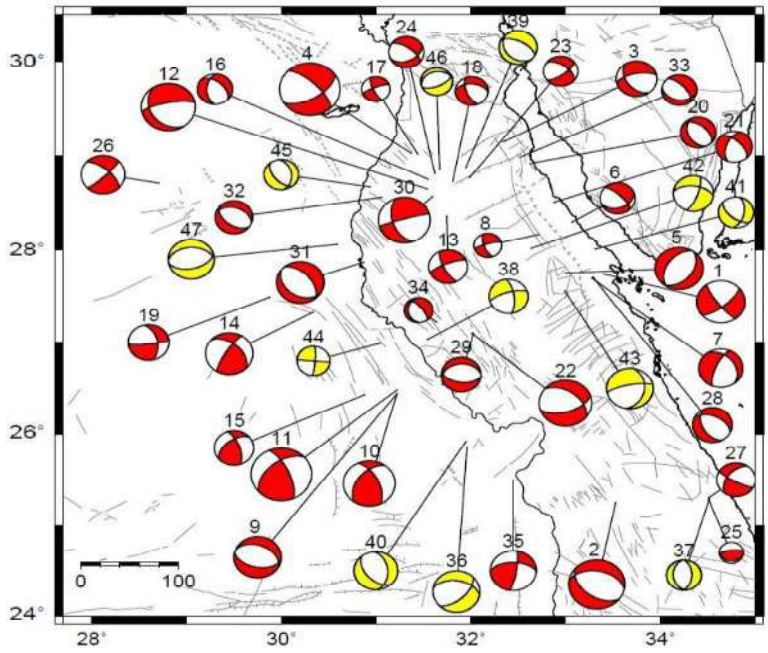

Fig. 2.18: Focal mechanisms of events occurred in the central part of Egypt (Marzouk et al., 2014).

2.1.6.2 Bani-Sueif SSZ

The southwest Bani-Sueif seismic source (Fig. 2.19) is located in the northern part of the Eastern Desert, about 130km southeast of Cairo. The trend analysis of the surface and subsurface

faults deduced from both geological and geophysical investigations in this seismic zone (Abou Elenean and Deif, 2003) reveals two predominant faulting trends, i.e., NE and NW. The dominant fault type is normal fault with NW trend and dipping towards NE and SW, with lengths ranging from 8-10km, as deduced from the geological survey carried out at the area (Hassan et al., 1978). The spatial distribution of earthquakes reveals scattered seismicity without a preferred trend, and the first and largest instrumentally recorded event in this zone is the 11 October 1999 earthquake (M_l = 5 and observed intensity VI on the MMI scale).

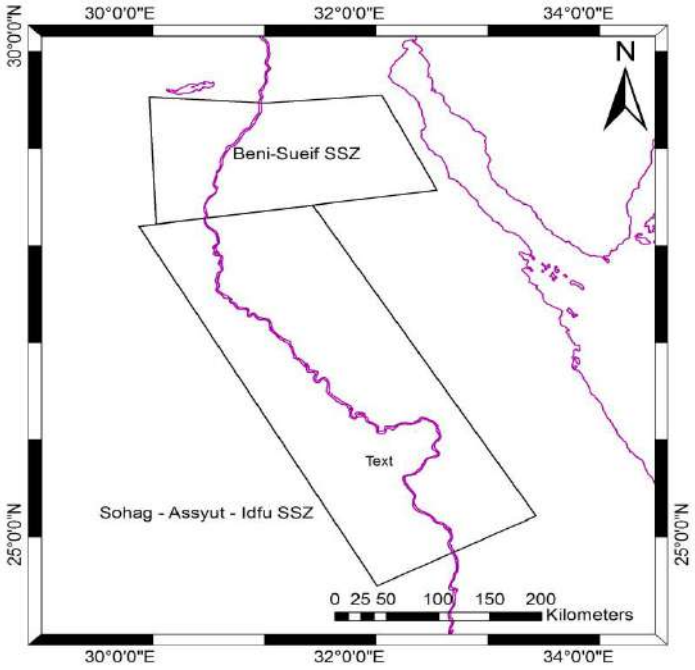

Fig. 2.19: SSZs along the Nile Valley.

2.1.6.3 Aswan seismic source zone

This seismic source is located in southern Egypt, west of the Nile River in which the Aswan high dam is located that reserved Naser Lake behind. Before the occurrence of 14 November, 1981, earthquake. After this event, many workers have shed light on the tectonic, geology and seismicity of this area not only because of possible hazard for humankind and property located downstream, mainly due to the presence of Aswan high dam and the possible secondary effects. In 1985, Woodward-Clyde Consultant (WCC) had introduced the first report about the seismic activity and the stability of that critical structure. After the detailed evaluation of active faults and localizing structures in Aswan region and surroundings, the WCC had

concluded that the area is characterized by the presence of two main sets of fault system: the north-south and east-west fault systems. The E-W fault trends are dominant, longer, and have had more activity as well as longer total slips compared to the N-S faults (e.g., Kalabsha fault). The Kalabsha fault is the major (concerning of length) E-W fault in the area of the normal type. There are some evidences that the E-W faults were reactivated up to recent times, which may support the drainage pattern along the scarp and along Kalabsha fault which has not graded itself to the underlying structures (Fig. 2.20). Most of the available focal mechanism solutions for earthquakes of $M \geq 3$ show right-lateral motion along ENE-WSW to E-W trending plane and left lateral along NNW-SSE to N-S (Abu El-Nader 2010) (Fig. 2.20).

There is a long-standing debate between the geoscientist (e.g., Kebeasy in Said 1990) about the origin of seismic activity in Aswan, whether if its cause is tectonic or reservoir-induced seismicity. On the other hand, the N-S faults (e.g., Gabel El Barqa and Kurkur faults) are of oblique-slip fault type and run at right angle to the strike of the sandstone beds which trends E-W (El-Khashab et al., 1991). WCC (1985) report revealed that the predominant fault displacement in the area is strike-slip, with a small normal component that produced scarps with small displacement along the faulting length. The present-day seismic activity in Aswan evidences that most of these faults (E-W and N-S trends) (e.g., Gabel El Barqa, Dabud, Seiyal, and Kalabsha faults) are active whereas the Khor El-Ramala, Bay and Gazelle faults are considered as inactive.

WCC (1985) demonstrated that the origin of this fault system might be related to secondary perturbations of far and primary active tectonic regimes such as a major Trans-African fracture system, differential movement in the mantle and differential spreading rates along the Red Sea rift. Aswan is characterized by low to moderate size seismicity, and the spatial distribution of earthquake epicenters is aligned along the main active faults and clustered near the intersection points of the E-W and N-S striking set of faults.

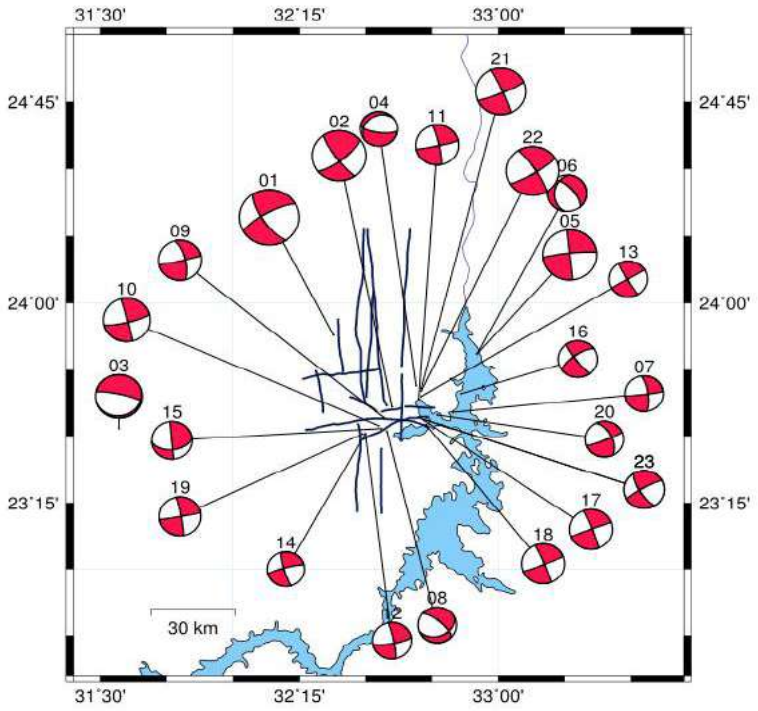

Fig. 2.20: Focal mechanism solutions for the Aswan area (drawn after Abu El-Nader, 2010).

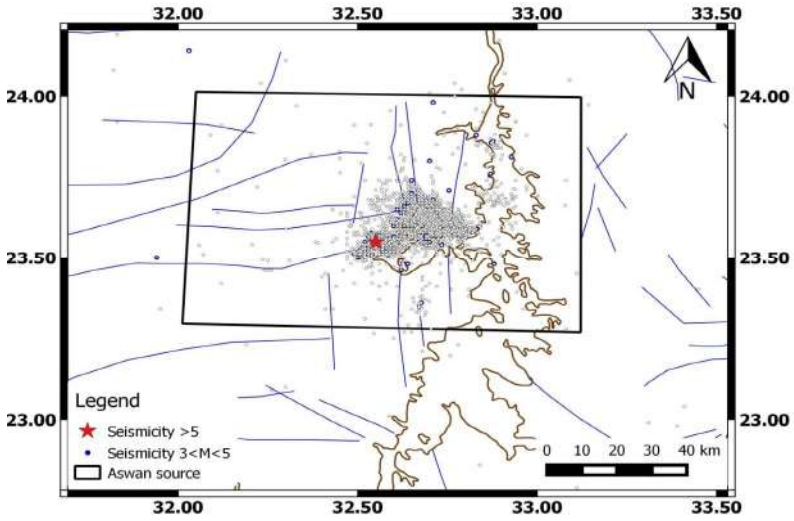

Fig. 2.21: Aswan seismic SSZ.

Mahmoud (2002) has studied the relative horizontal displacements in Aswan region using about three years GPS data and demonstrates that all sites of the Aswan network are moving in the north direction with 10-14mm total displacement, which corresponds to a velocity of 3.3-4.6mm/yr. WWC (1985) concluded that the estimated slip rates by paleoseismological

investigations for east-west and north-south faults were 0.03mm/yr and 0.01-0.02mm/yr, respectively. The comparison between the results of those two studies (i.e., Mahmoud, 2002 and WCC, 1985) reveals significant inconsistency between the slip rate values obtained from GPS and paleoseismological data, which calls for additional studies to assess the reliable ongoing crustal deformation in this area.

2.1.7 The Western Desert SSZs

2.1.7.1 Dahshur-El Fayum SSZ

This source is located in the northern part of the Western Desert, which generally forms a part of the unstable shelf, (Said, 1962), further to the west of the Cairo-Suez shear zone. The predominant structural features of this zone are faults. After the occurrence of the 12 October 1992 earthquake in the Dahshur seismic source zone, many geophysical studies (e.g., gravity and magnetic due to the absence of surface rupture) have been conducted (e.g., Refai et al., 1973; Meshref, 1990; Egyptian Geological Survey, 1993) to reveal the main tectonic trends. These studies showed that the main fault trends are E-W (Mediterranean trend), NE-SW and NW-SE (the East African and Gulf of Suez trends). Abou Elenean et al. (2000) declared that this zone is seismically active as indicated by the occurrence of small to moderate earthquakes; the most significant events originated in this zone are the October, 1920 and 12 October, 1992 earthquakes with an observed magnitude of M_l = 4.9 and M_w = 5.9, respectively. The spatial distribution of earthquakes reveals that the earthquakes epicenters are aligned along the N-S direction. There are many historical earthquakes have been occurred in this zone and they are concentrated within the area of high population, inside the Nile Valley and Delta (area of rare seismicity), which emphasis the possible impact of population density and distribution and soil behavior on the location of historical earthquakes obtained from intensity maps of these events. Abu El-Nader (2010) has studied the focal mechanism solutions for 47 events in this zone and has concluded that the solutions vary from pure dip-slip to pure strike-slip. There are 13 solutions implying pure normal dip-slip with nearly N-S to NE T axes trend, 12 showing pure strike-slip motion with T axes trending NNE to NE and 22 events reveal normal oblique mechanism, with T axes trending NNE to NE (Fig. 2.22). The estimated average horizontal velocity deduced from present-day crustal deformation studies in Dahshur area is about 5.1±1.1mm/yr in NW-SE direction, and the area

suffered from variable tension and compression stresses. The Dahshur source is the nearest and the most hazardous for Cairo metropolitan (Fig. 2.23).

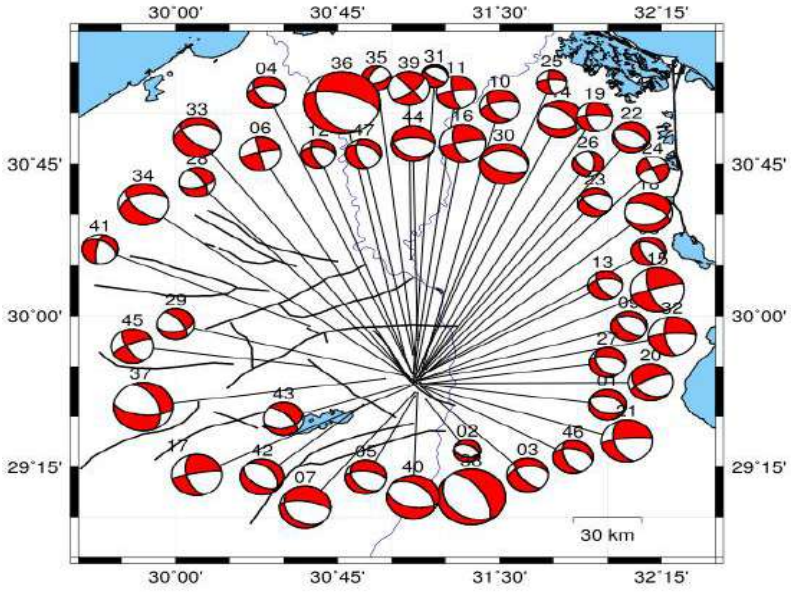

Fig. 2.22: Focal mechanism solutions for earthquakes recorded in the Dahshur-El Fayum SSZ.

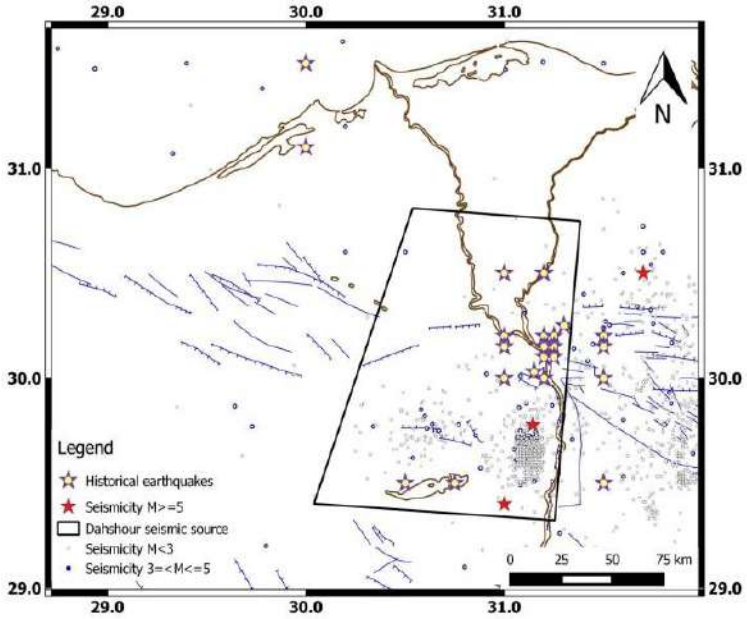

Fig. 2.23: Dahshur-El Fayum SSZ.

2.1.7.2 <u>Gilf El-Kebir SSZ</u>

Gilf El-Kiber plateau is the most prominent topographic feature in the Western Desert with an area of ~12,000km^2 and height of ~1km. Only one earthquake was recorded within this zone on 9

December 1978 with M_w = 5.7 southwestern Egypt. The focal mechanism of this event is not well controlled due to the large azimuth gap and absence of nearby stations, but it reveals a dextral strike-slip fault (strike-slip with reverse motion fault) with NE strike.

2.1.8 Eastern Sinai SSZ

The Sinai Peninsula is surrounded by the most active seismic trends in Egypt, i.e., Gulf of Aqaba (to the east) and Suez (to the west) and Cyprian arc (to the north). Themed fault is a prominent structural feature in Sinai separating the tectonically known unstable part that contains Syrian Arc System from the stable part in central and south Sinai. Hussein and Abd-Allah (2001) suggested that the northern Galala fault that separates the Galala plateau province from the Cairo-Suez province is the westward continuation of Themed fault. They justified their findings based on the similarities in fault configuration and on the age of generation and rejuvenation.

The spatial distribution of present-day seismicity within Sinai shows a scattered pattern and difficulty of relating or correlating the seismicity to any active faults or geologic features. The eastern Sinai source zone (Fig. 2.24) is located along the border between Egypt and Palestine and is characterized by relatively low scattered seismicity. The largest event had recorded in this zone was the 28 October 1999 earthquake, with M_l = 5.

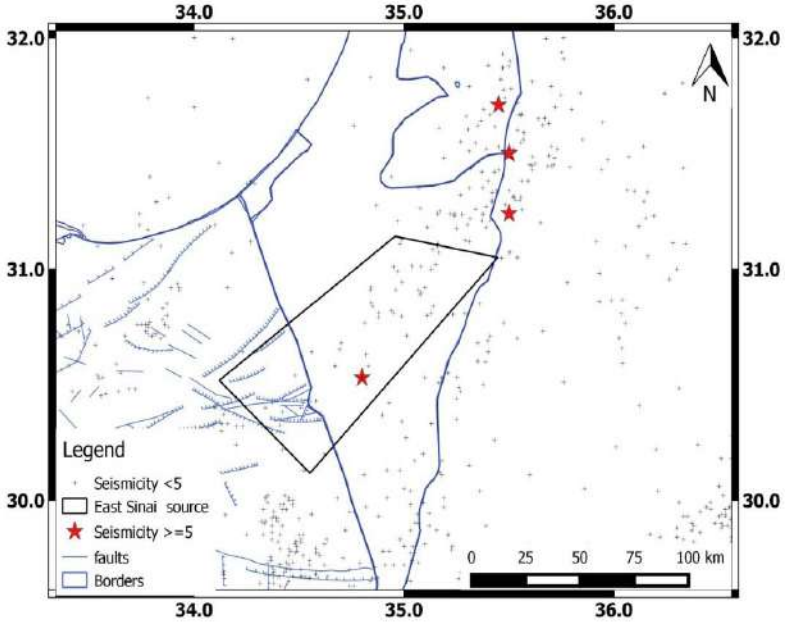

Fig. 2.24: East Sinai SSZ.

The upgrade of the seismotectonic model of Egypt was motivated due to newly released information, and it will be subject to future modification when new data are available. Fig. 2.25 shows 20 seismogenic zones that have been delineated for Egypt using all the available information from different disciplines to be used in NDSHA computation in the next Chapter. Most of the defined zones are bounded along well known and clearly defined active trends and faults, while few of them cover the areas that exhibit sporadic seismic activity. The seismotectonic zones, which are marked by strong earthquake M5+, are identified in this work. This condition could guarantee reliable identification of seismogenic zones not influenced by non-tectonic events (e.g., quarry blasts) which are common in many areas in Egypt. We use magnitude between 3 and 5 to define the zones borders reliably. Then, for areas that did not show earthquake M5+, we have used pattern recognition analysis for the identification of seismogenic nodes (earthquake prone sites), which represents a complementary step. A responsible seismic hazard assessment requires the incorporation of both results (i.e., defined seismogenic zones and nodes).

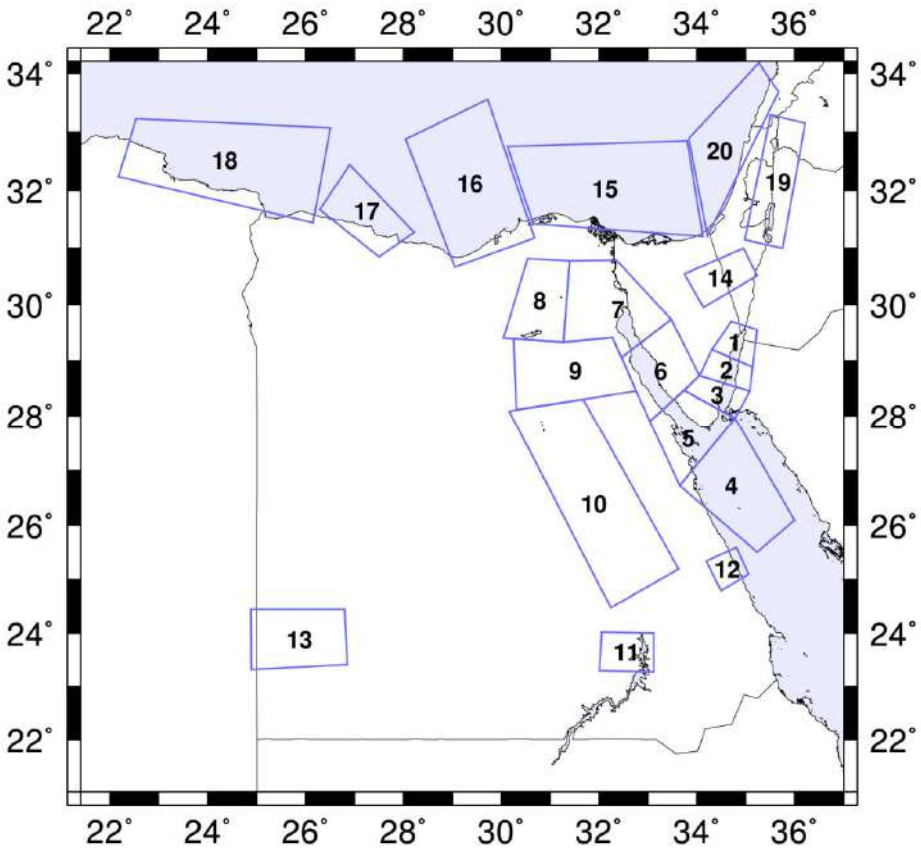

Fig. 2.25: An updated seismotectonic zones model for Egypt.

2.2 Recognition of seismogenic nodes with M ≥ 5 in the northeast part of Egypt.

The too short time span of the available earthquake catalog for Egypt relative to the long recurrence interval of intraplate and mid-plate earthquakes, and/or the poor understanding of earthquake rupture process and the characters of the seismogenic zones, make it difficult to efficiently identify the seismogenic sources and their earthquake potential and related hazard. So, it is rational to suppose that not all the potentially seismogenic sources are marked by strong earthquakes or showed up a significant activity during the time covered by the historical record.

The pattern recognition of morphostructural nodes could provide quantitative and methodological criteria for identifying the areas where large earthquakes may occur, taking into account a broad set of possible tectonic, geologic, topographic maps, gravity data, and satellite images (Gorshkov et al., 2003 and reference therein).

In this section, an earthquake is considered as a strong if it has a size of M5+, the choice of this threshold is based on the seismicity level in the northeast Egypt. The result from this work is significant for knowledgeable seismic hazard assessment for Egypt. The identification of prone areas to M ≥ 5.0 earthquakes in northeastern Egypt has been carried out in this Chapter by applying the morphostructural zoning (MZ) method (Alexeevskaya et al., 1977; Rantsman,1979; Gorshkov et al., 2003), to delineate morphostructural nodes, i.e., specific structures formed at the intersections of fault zones. A pattern recognition algorithm CORA-3 (Gelfand et al., 1976; Gorshkov et al., 2003) has been employed to classify the delineated MZ nodes into seismogenic and non-seismogenic nodes based on some criteria selected by CORA-3 on the basis of topographic, geological, and geophysical parameters characterizing the nodes.

The first evidences on the correlation of strong earthquakes with nodes in the Pamirs - Tien Shan region were reported by Gelfand et al. (1972). The spatial control of seismicity by intersecting faults was also confirmed in some seismic areas of the world (Talwani 1988; Hudnut et al. 1989; Girdler and McConnel 1994). King (1986) proved that initiation and healing of ruptures are conditioned by fault intersections.

During the last four decades earthquake-prone areas for different target magnitudes have been identified in a significant number of seismic regions of the world with the approach being used in this section (Cisternas et al. 1985; Gelfand et al., 1972, 1976; Gorshkov et al., 2000, 2002, 2003, 2004, 2010; Gvishiani et al., 1987, 1988; Peresan et al., 2014). The validity of the methodology was periodically evaluated comparing the location of the target events occurred in

the studied regions after the publication of the results with respect to recognized seismogenic nodes (Gorshkov et al., 2003, 2005; Soloviev et al., 2014). Specifically, Soloviev et al. (2014) have shown that totally 87% of the relevant post-publication earthquakes occurred at the nodes that have been in advance assigned to seismogenic ones. In Egypt, two intermediate earthquakes occurred in areas that have been defined as seismogenic nodes i.e., the Gulf of Aqaba 16 May 2016, $M_l = 5$ and another along the Cairo-Suez district 21 January 2017 $M_l = 4.3$ just after the presentations of this work in two international conferences (Hassan et al., 2016; Gorshkov et al., 2016).

One of the main advantages of MZ is that, it does not need prior knowledge of regional seismicity of the studied region, whereas paleoseismological studies need information about the seismic activity. Also, MZ represents a much cheaper and quicker way to identify the seismogenic sources rather than the expensive and time-consuming paleoseismic investigations.

The results of the recognition represent a step for identifying the seismogenic sites, and it is highly recommended to verify and validate the existence of the sources especial for nodes located near urban areas using detailed paleoseismic studies The identification of seismogenic nodes can be accomplished, by integrating all available data in the form of layers in Geographic Information System.

2.2.1 Geomorphology, tectonic setting, and seismicity of the study region

Geographically, Egypt is located in the northeastern corner of the African continent and the proper understanding of the geomorphological development of Egypt requires the identification of different geographic provinces. According to Said (1990), Egypt can be divided into four major provinces; Western Desert; Eastern Desert; the Sinai Peninsula; Nile Valley and Delta, but here we shed light on the geomorphology of the study area only.

Nile Valley is a narrow valley (average width about 10km) filled with alluvial sediments and bounded by cliffs of different rock units along its length. Near Cairo, the Nile Valley opens out to the Nile Delta by divides into two branches (Rosetta and Damietta branches). The Western desert represents about two-thirds of the whole area of Egypt and extends from the Nile Valley westward to the borders with Libya. This province can be divided into three sub-provinces; Southern, Middle, and Northern sub-provinces. The southern sub-province is covered by Nubian sandstone and the most prominent topographic feature within this region is Gilf Kebir plateau

(more than 1000m height asl). This plateau is dissected by valleys and oases which bounded by high steep walls. Middle limestone plateau sub-province extends along both sides of the Nile Valley, the Farafra, and Bahariya oases are located within this plateau and bounded by steep cliffs. The Northern sub-province is extended from middle plateau northward to the Mediterranean coast characterized by the presence of Qattara depression which is the largest in this sub-province and bounded by cliffy slopes along northern and western sides (for more details, see Said, 1990).

The Eastern Desert extends from Nile Valley eastward to the western coast of the Red Sea and Gulf of Suez (Fig. 2.26). The Eastern Desert consists of the Red Sea mountain groups aligned parallel to the coast and generally composed of crystalline igneous and metamorphic rocks. The north Red Sea Mountains are separated from the limestone plateau by a broad valley (Qena valley) which extend southward to near Qena. This plateau is called Maaza plateau and is in continuation with middle limestone plateau sub-province of thfe Western Desert across the Nile River (Said, 1990). There are significant differences between the Eastern and Western deserts, the Eastern Desert is intensively dissected by lineaments of different orientation and all its drainage patterns are being external (Nile Valley and the Red Sea). Also, the Red Sea Mountains are surrounded in the south by a sandstone plateau extending southward to Sudan (see Said, 1990 and references therein).

The Sinai Peninsula is a triangular with a base extending along the Mediterranean and the apex ending between the Gulfs of Suez and Aqaba, separated from the mainland Egypt by the Gulf of Suez and Suez Canal. The south Sinai represents the core of the peninsula and the highest part in Egypt (the highest peak is Gebel Katherina about 2641m asl) and it is composed of igneous and metamorphic rocks forming a part of the so-called Arabian-Nubian Shield which is a stable tectonic unit. This part is dissected by intensely incised valleys, which are drained towards Gulfs of Suez and Aqaba. The central part of peninsula consists of sub-horizontal Mesozoic and Tertiary sediments, creating the plateau of Gebel El Tih- Egma, separated from east, south and west sides by steep scarps. The northern Sinai is characterized by the presence of folds belonging to Syrian arc system, which are aligned northeast-southwest and this part continue northward to the Mediterranean coast and drained by Wadi Al-Arish (see Said, 1990 and references therein).

Fig. 2.26: Major structures of the study region.

Tectonically Egypt is bounded from east and north directions by three main tectonic elements, the African-Eurasian plate margin in the north and the Red Sea rift system and the Gulf of Aqaba-Dead Sea fault system in the east. The present-day tectonic deformation and related seismicity in Egypt are related to the interaction and the relative motions along these boundaries and their remote effects inside the Egyptian territory. According to Said (1990), the results of aeromagnetic surveys in Egypt reveal the following observations:

There are tectonic trends that have affected Egypt during the geologic history: north-south (East African Rift trend); north-northeast (Aqaba trend), northwest (the Red Sea and or the Gulf of Suez trend); east-west (Tethyan trend); east-northeast (Syrian Arc System trend); west-northwest (Darag trend), and northeast (Aualitic or Tibesti trend) (Saleh et al., (2013). Some tectonic trends are more characteristic of some parts of the country than others; some trends show more strength in some parts of the country than in others.

The present-day tectonic deformation can be deduced from incorporating the geology, tectonics and seismic activity investigations. Based on the fact that, the main earthquake activity takes place along active faults or plate boundaries and margins (e.g., Sykes 1967; Kasahara 1981), it can be used to delineate major active seismotectonic province or major tectonic trends.

Abou Elenean (1997) points out that most of the earthquake activities in Egypt are aligned along the known active trends and/or the intersection (triple-junction) of major active faults of the Red Sea, the Gulf of Suez, and the Gulf of Aqaba (Fig. 2.27). Other significant inland active zones are; one in the northern part of the Eastern Desert between Nile Valley and Gulf of Suez (Cairo-Suez district zone); a second located southwest Cairo near Dahshur, where the 12 October 1992 earthquake occurred, the region of southern Aswan (Kalabsha) and Abu-Dabbab area (the Red Sea mountains). Other small activities are observed along the Nile Valley; to the north of Idfu, west of Asyut, southwest of Bani Suef and Marsa Alam areas.

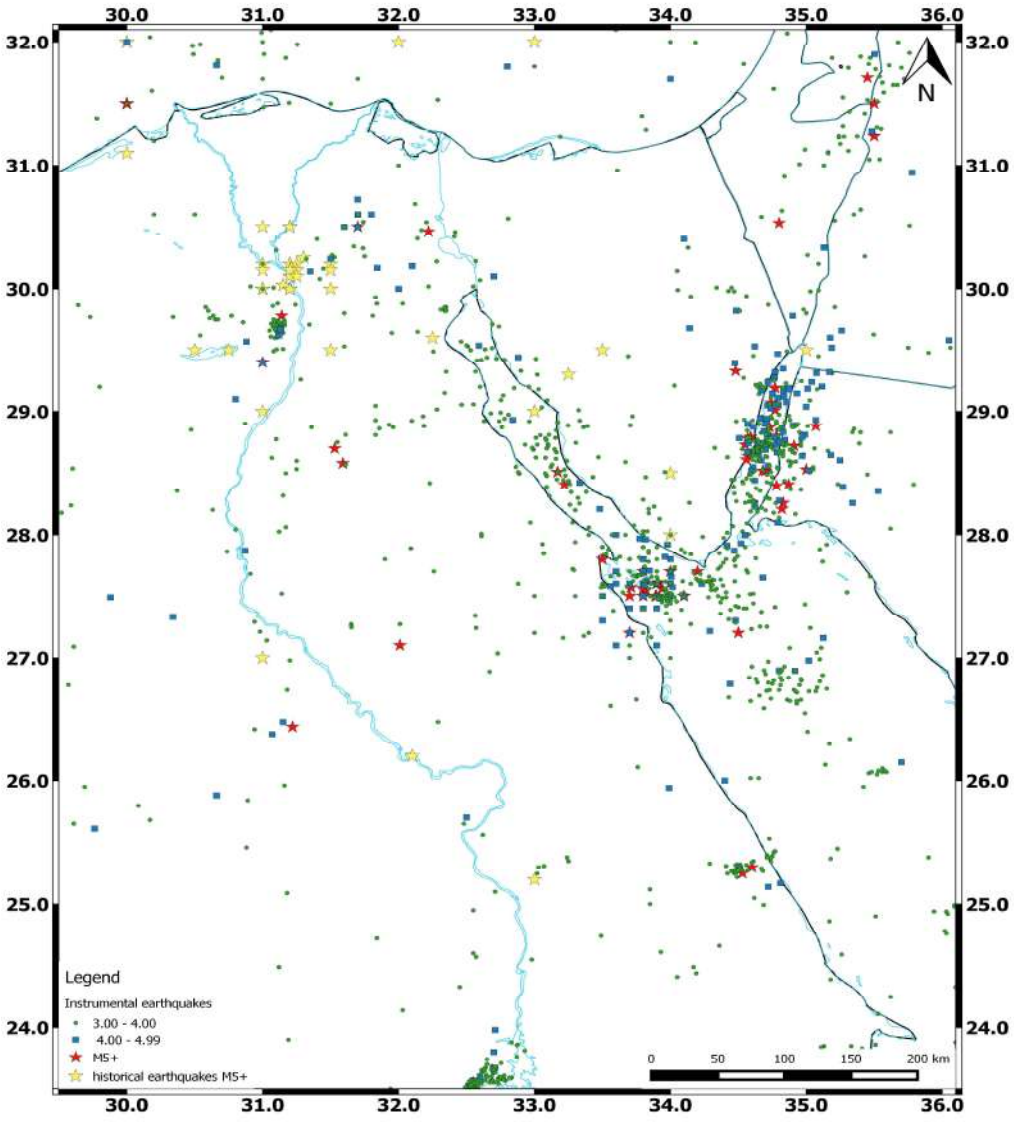

Fig. 2.27: Seismicity of the study region.

The present-day seismicity map of Egypt mainly correlate well with existing seismotectonic studies except for some hypothetical trends, which are not clear; such as the possible extension of the Gulf of Suez trend to the north (towards the Mediterranean Sea) as supposed by previous studies (e.g., Eppelbaum and Katz, 2015), the East Mediterranean-Cairo-Fayum belt shown by Said (1990) or the concept of Pelusium trend which has not confirmed yet (Neev, 1975).

2.2.2 Morphostructural zoning

The study region includes the Sinai Peninsula and the northern part of the Eastern Desert, between the Nile River and the Red Sea. Using the MZ method (Alexeevskaya et al., 1977; Rantsman, 1979; Gorshkov et al., 2003), we have constructed the MZ map displayed in Fig. 2.28. Performing MZ we have analyzed topographic maps of the Egyptian General Survey Authority (EGSMA, 2004), tectonic and geological maps of the Egyptian Geological Survey and Mining Authority (EGSMA, 1981&2009), satellite photos, and publications on geomorphology and geology of the Egypt territory (Said, 1990; Eppelbaum and Katz, 2015; Neev, 1975). During the MZ analysis, the seismicity data (earthquake catalogs) available for Egypt were not used.

The goal of MZ is to outline a system of hierarchically ordered areas (territorial units) presented by the homogeneous present-day topography and tectonic structure. Lineament and blocks structure delineated by MZ (see Table 2.1) consists of the following three elements: *(1)* territorial units (***blocks***) of different rank; *(2)* their boundary zones, ***morphostructural lineaments***; and *(3)* sites where lineaments intersect, ***nodes*** (e.g., Gorshkov et al. 2000; 2003). Unlike the seismotectonic analysis paying the main attention to the fault network, MZ firstly outlines the relatively homogeneous blocks and secondly their boundaries (lineaments).

Large landforms such as ranges, basins, plateaus, and their morphometric indices (height and strike) are the main subject of the analysis in MZ. The spatial variations of the elevations and strike of these landforms allow outlining homogeneous areas with respect to their elevation and strike. In lowland regions, the variation of the drainage pattern is the most informative input data for delineating the homogeneous areas (Peresan et al., 2014).

At the first stage, MZ outlines "mountain countries," the largest 1st rank territorial units. Two 1st rank units – the Sinai Peninsula and the Eastern Desert have been delineated within the study region. These mountain countries are separated from each other and from surrounding large-

scale geotectonic units by the first rank lineaments. The Sinai and the Eastern Desert are separated by the 1st rank lineament traced along the narrow depression of the Suez Canal dominated by the Sinai fault (Eppelbaum and Katz, 2015) and southwards along the Gulf of Suez.

Table 2.1: Basic definitions of the morphostructural zoning (after Gorshkov et al., 2000; 2003; 2010)

MZ unit	Rank of the unit	Definition
"Mountain country"	1st	a single ***mountain country*** is a territory of the same orogenesis and certain appearance of the relief (physiography)
Megablock	2nd	***megablock*** reveals a common trend in lateral variations of elevation and orientation of large landforms
Block	3rd	***block*** is an area where elevations and orientations of large landforms are homogeneous and drainage pattern is uniform within this area
Lineaments	The rank of lineament is also defined as 1st, 2nd, and 3rd, depending on the rank of the MZ unit limited by the lineament.	***Longitudinal*** ones limit large landforms (ranges, basins, plateaus) separating them from each other. ***Transverse*** ones cross large landforms at sites where these forms change their elevation or strike.
Node	Non-ranked unit	***Node*** is an area of some extent centered on the intersection of lineaments.

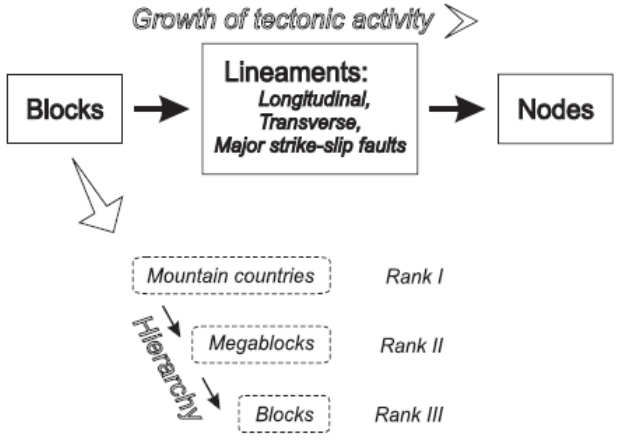

Fig. 2.28: Basic scheme of the morphostructure (after Gorshkov et al., 2003).

In the east, the Sinai is bounded by 1st rank lineament that corresponds to the Dead Sea Transform fault. First rank lineament limiting the Eastern Desert in the west is going along the

Nile Valley that represents in the study region a graben bounded on either side by large normal faults (RIGW, 1997). On the east, the Eastern Desert is bounded by the 1st rank lineament going along the continental slope of the Red Sea. The northern boundary of the Eastern Desert is the 1st rank transverse lineament from 8 to 10 (Fig. 2.29) that separates the Eastern Desert from the alluvium plain developed in the Nile Delta. The northern boundary of the Sinai is 1st rank lineament from 1 to 4 traced along the continental slope of the Mediterranean Sea. Both the Eastern Desert and the Sinai were subdivided into second rank territorial units, megablocks. Table 2.2 presents the distinctive morphological features of megablocks.

Table 2.2: Morphological characteristics of megablocks

Megablock number in Fig. 2.29	**Mean peak altitude of ranges (m)**	**Major strike of ranges**	**Major tectonic orientation**	**Morphology**
Sinai				
I	430	NW-SE	NW-SE	plain and small isolated hills
II	892	nearly E-W	NW-SE	Plateau
III	1300	NW-SE	NW-SE	Plateau
IV	2650	NE-SW	NW-SE	coastal ranges
Eastern Desert				
V	256	E-W	E-W	Plain
VI	1000	E-W	nearly E-W	Plateau
VII	600	NW-SE	NW-SE	Plateau
VIII	2187	NW-SE	NW-SE	extended range dissected by transverse wadis
IX	1090	nearly N-S	NW-SE and N-S	range and plateau

Megablocks have been divided into smallest units of the 3rd rank, blocks. They are limited by 3rd rank lineaments traced at sites where we observed the changes in elevation and/or orientation within a single large landform. Delineated lineaments reveal different orientation within each megablock in accordance with predominant structural and topographic strike. 239 intersections of lineaments have resulted from MZ. We treat each intersection as a single node, although the detailed studies of the nodes by Gvishiani et al. (1988) and by Gorshkov et al. (2009) shown that some of the nodes can include more than two intersections of lineaments.

2.2.2.1 **Nodes and earthquakes M5+**

The map in Fig. 2.29 shows that shallow earthquakes M5+ selected from the historical earthquake catalog of the Badawy et al. (2010) correlate with some of the nodes. The distance between the points of the intersections and epicenters does not exceed 20km. We apply the pattern recognition technique for identifying other nodes in northeast Egypt having the potential for generating earthquakes M5+. In this work, the node is formally defined as a circle of radius R = 20km surrounding each lineament intersection. Such node size is in agreement in the linear extent of earthquakes sources in the interval of magnitudes between 5 and 6 (Wells and Coppersmith 1994). All the 239 nodes resulted from MZ we treat as objects of recognition.

2.2.3 Pattern recognition of seismogenic nodes

The aim of pattern recognition analysis is to divide the whole set of the nodes "W" delineated in a region into two classes: class "D" (dangerous) containing the nodes where shallow earthquakes with magnitude $M \geq M_0$ may occur; class "N" (not dangerous) containing the nodes where only smaller earthquakes with $M < M_0$ may occur, where M_0 is magnitude of the target earthquakes for a study region (Gorshkov et al., 2003). The choice of M_0 depends upon the regional seismicity. In this work, we defined M_0 = 5.0 because events of this size regularly occur in northeast Egypt and expose the real threat for population and economy.

The classification of nodes into "D" and "N" is performed by the pattern recognition algorithm CORA-3 with learning (Gelfand et al., 1972, 1976; Gorshkov et al., 2003) using a set of parameters based on available geomorphic, geological, and geophysical data. Each node is associated with the vector of topographic, geological and geophysical parameters describing nodes. Parameters used in this work are presented in Table 2.2.

2.2.3.1 Selection of learning sets

Classification of the entire set of the nodes into seismogenic (class D) and non-seismogenic ones (class N) for M5+ is performed by the pattern recognition algorithm CORA-3. At the learning step each node was arbitrarily assigned to one of the following three sets:

- Set D_0 composed of 37 nodes hosting instrumental and historical events M5+.
- Set N_0 consisting of 134 nodes, in the vicinities of which there are neither any recorded events M5+ nor smaller earthquakes with M = 4.00-4.99.
- Set X includes 68 nodes marked by smaller recorded earthquakes with M = 4.0-4.99. The set X is not employed by CORA-3 for selecting the characteristic traits, but at the recognition stage, each node from X is assigned either to D or N classes. The assignment of each node to one of the learning sets is shown in Fig. 2.30.

2.2.3.2 *Parameters used for recognition*

In this work, the parameters listed in Table 2.3 are used, which have been successfully used for recognizing seismogenic nodes in other regions studied (e.g., Gorshkov et al., 2003). The parameter values were measured within circles of radius 20km around points of lineament intersections using topographic, geological, and gravity maps, as well as the MZ map of northeast Egypt (Fig. 2.29).

Table 2.3 introduces five types of parameters, including the morphometric, morphological, geological, gravity ones and those related to the lineament-and-block geometry. The morphometric and morphological parameters as well as the parameter Q (the portion of the node area covered by soft Quaternary sediments) reflect the long-term tectonic effects of uplift and subsidence and characterize the contrast and intensity of vertical tectonic movements indirectly. The parameters describing the lineament-and-block geometry and the hierarchy of the block-structure characterize the complexity of the media in the vicinity of the nodes. The gravity parameters characterize the heterogeneity of the upper crust beneath the nodes.

Since CORA-3 operates with the binary vectors, before its application, the actual values of the parameters were converted into a vector of binary components with the help of discretization and coding procedures (Gorshkov et al. 2003). The discretization was performed with a prior splitting of the nodes into sets $\mathbf{D_0}$ and $\mathbf{N_0}$ by dividing the interval of variation for each parameter into two (“small” and “large”) or three (“small”, “medium”, and “large”)

subintervals by applying one or two threshold values. The thresholds of discretization are given in Table 2.3.

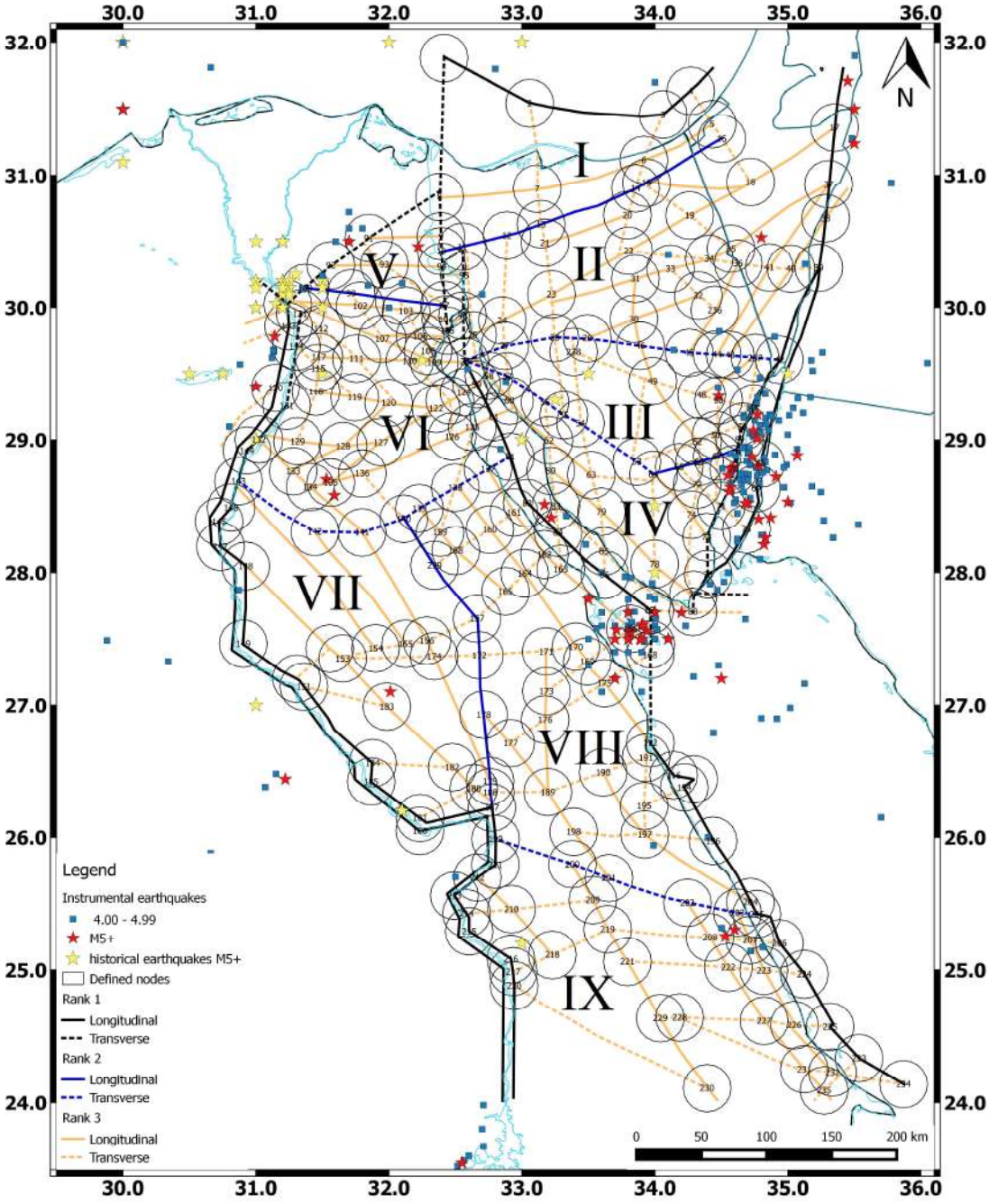

Fig. 2.29: MZ map of northeast Egypt and earthquakes M4+.

Black lines: lineaments of the first rank; Blue lines: lineaments of the second rank; Orange lines: lineaments of the third rank. Continuous lines: longitudinal lineaments; Dashed lines: transverse lineaments. Red stars: instrumental earthquakes M5+; Blue square: instrumental earthquakes M = 4.0-4.99; Yellow Stars: historical events M5+.

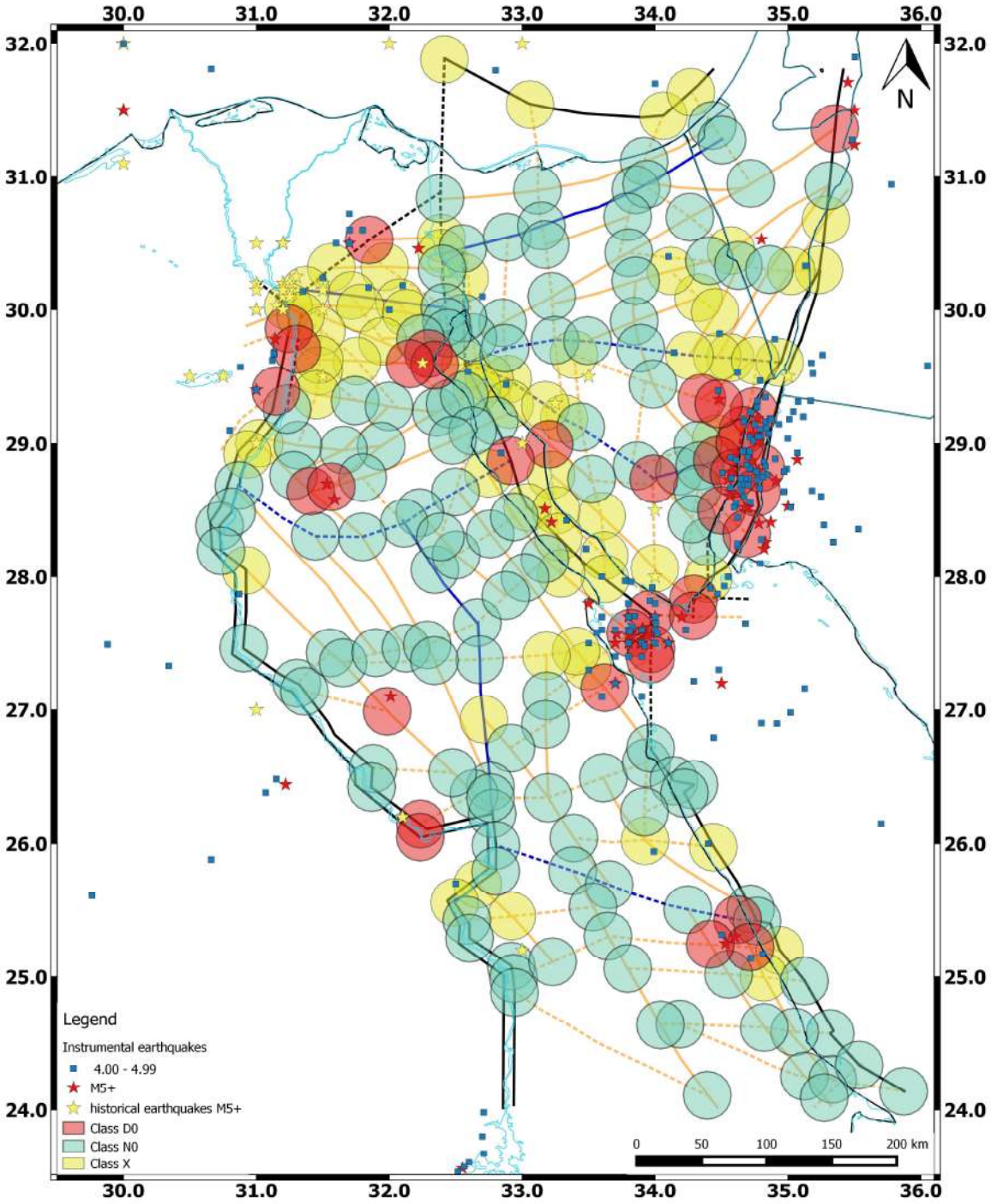

Fig. 2.30: Learning sets.

Class D_0 (Red Circles) includes nodes (37 nodes) hosting instrumental and historical events M5+. Class N_0 (Green Circles) includes nodes (134 nodes), in the vicinities of which there are neither recorded events of M5+ nor smaller earthquakes with M = 4.00-4.99. Class X (Yellow Circles) includes nodes (68), in the vicinities of which there are recorded earthquakes with M = 4.00-4.99.

2.2.4 ***Recognition results***

At the recognition stage CORA-3 assigned each node to class **D** or to class **N** in accordance with the decision rule defined at the learning stage (Table 2.3). The decision rule includes twelve **D** traits and ten **N** traits (Table 2.3) that discriminate **D** nodes from **N** ones. The resulting classification of the nodes is shown in Fig. 2.31. Out of the 239 considered nodes 108 ones are recognized as class **D**, 67 of them did not show earthquakes with M5+ till now (which are marked with Orange color in Fig. 2.31) and 131 are recognized as class **N**. Most of the nodes recognized as D, where no earthquakes with M5+ happen till now, are located along the Nile Valley, Western coast of the Red Sea, Gulfs of Aqaba and Suez and along the Suez Canal region.

2.2.5 ***Control experiments***

The stability of the resulting classification of the nodes shown in Fig. 2.31 was examined by the control tests (Gvishiani et al., 1988; Gorshkov et al., 2003) that allow evaluating the sensitivity of the resulting classification to the changes in the learning sets and in the vector of parameters. In the course of experiments, we have excluded nodes one after another from the learning sets D_0 and N_0 and run the CORA-3 to obtain experimental classifications. During the following test, the parameters composing the decision rule (Table 2.4) were also excluded in turn from the recognition procedure. After that, we have compared the experimental classifications with the resulting one displayed in Fig. 2.31. In the experimental classifications, maximum 10% of the nodes changed their belonging to **D** or **N** classes with respect to the resulting classification. According to Gvishiani et al. (1988), such insignificant changes in the resulting classification indicate its sufficient stability.

As shown in Fig. 2.31, the recognized 108 D nodes concentrate mainly along the large active fault zones marked by high ranks lineaments. Most earthquakes M = 4.0-4.99 fall in the recognized nodes, suggesting that most of the tectonically active areas were identified by pattern recognition. At the same time, some large areas like North Sinai (megablock II), the interiors of the Eastern Desert (inner parts of megablocks VI, VII, and IX) reveal lower seismic potential: most nodes within these areas were recognized N.

The characteristic traits of D and N nodes (Table 2.4) provide information on geological-geophysical features of D and N nodes. Out of 15 parameters (Table 2.3) employed for recognition, twelve ones formed the decision rule discriminating D nodes from N ones. The assemblage of the characteristic traits given in Table 2.4 indicates that more contrasting

topography and more complex structure of D nodes discriminate them from N nodes. Specifically, the characteristic traits of D nodes presented in Table 2.4 indicate the contrasting neotectonic movements, evidenced by "large" values of dH/L (> 21.5) and by the contrast topography at such nodes. The contrasting topography typical for D nodes is evidenced by the following combinations of landforms within D nodes: mountain/plain, mountain/plateau, and mountain/mountain. In addition, the features of **D** nodes point to an intense fracturing of the crust, as suggested by the "large" number of lineaments forming a node (NL > 2). On the contrary, N nodes are characterized by non-contrasting topography evidenced by such combinations of landforms as plateau/plain, plateau, and plain. N nodes are also characterized by "small" values of the relief energy (dH/L $\leq$ 21.5) suggesting weaker intensity of neotectonic movements as compared with D nodes.

Table 2.3: Parameters used for pattern recognition and thresholds of their discretization.

Parameters	**Thresholds of discretization**
A)Morphometric parameters	
Maximum topographic altitude, *m* (Hmax)	425 800
Minimum topographic altitude, *m* (Hmin)	-5 150
Relief energy, *m* (ΔH) (Hmax - Hmin)	400 700
Distance between the points Hmax and Hmin, *km* (L)	27
Slope, (ΔH/L)	21.5
B) Geological parameters	
Portion of the node area covered by soft (quaternary) sediments, % ,(Q)	1.8
C) Lineaments-and-blocks geometry	
The highest rank of lineament in a node, (HR)	2
Number of lineaments forming a node, (NL)	2
Distance to the nearest 1st rank lineament, *km*, (D1)	30
Distance to the nearest 2nd rank lineament, *km*, (D2)	46
Distance to the nearest node, *km*, (Dn)	22
D) Morphological parameter (Mor)	
This parameter is equal to one of the following six values in accord with the morphology within each node: 1 – mountain and plain (m/p) 2 – mountain and plateau (m/pt) 3 – mountain and mountain (m/m) 4 – plateau and plain (pt/p) 5 – plateau only (pt) 6 - plain only (p)	
E) Gravity parameters	
Maximum value of Bouguer anomaly, mGal ,(Bmax)	17 47
Minimum value of Bouguer anomaly, mGal, (Bmin)	-18
Difference between Bmax and Bmin, mGal ,(ΔB)	37 67

Two intermediate earthquakes have just occurred after the presentation of this work at two international conferences (Hassan et al., 2016; Gorshkov et al., 2016) at nodes that have been defined as D i.e., the Gulf of Aqaba, 16 May, 2016, M5 and another along Suez-Cairo district, 21 January, 2017 M4.3 (plotted with green diamond symbol in Fig. 2.31). This fact and the positive results of the control tests proof the reasonability of the results obtained.

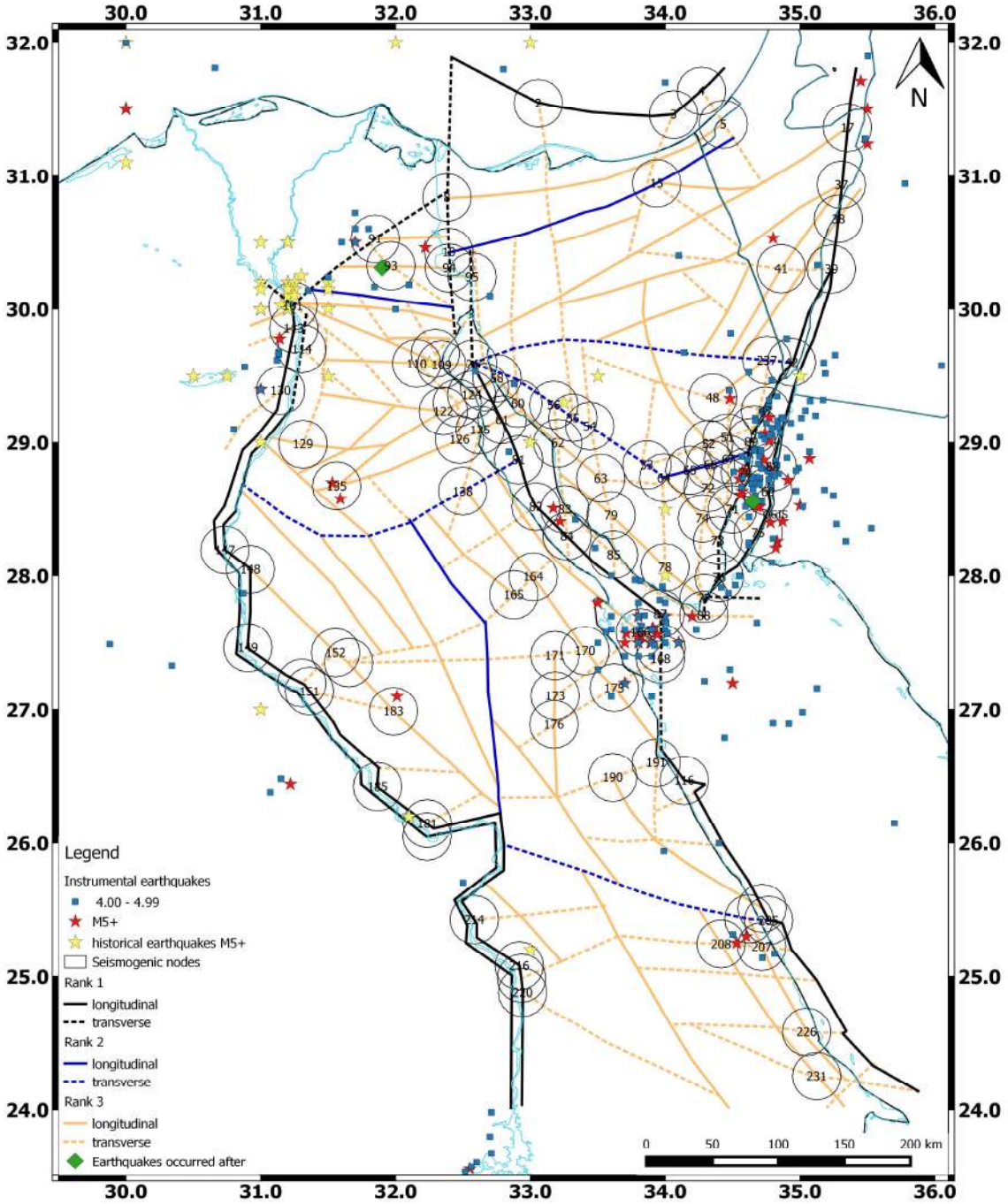

Fig. 2.31: Seismogenic nodes capable of generating earthquakes M5+.

Table 2.4: Characteristic traits of D and N nodes (the decision rule)

	Parameters *(see Table 2.3 for explanation)*											
Trait №	**Hmin M**	**dH m**	**L Km**	**dH/L**	**Q %**	**HR**	**NL**	**D1 Km**	**D2 Km**	**Dn Km**	**Mor**	**Bmax Mgl**
Characteristic traits of D nodes												
1	≤-5									>22		>47
2						1 or 2			> 46			> 47
3							>2	≤ 30				>47
4		>700										≤ 17
5	> 150										1-4	≤ 17
6				>21.5			>2					≤ 17
7			>27	>21.5							1-4	
8	≤-5	≤400									1-4	
9		≤400		>21.5							4-6	
10						1 or 2			> 46		1-3	
11								≤ 30	≤ 46		1-3	
12			≤ 27			3		≤ 30				
Characteristic traits of N nodes												
1											4-6	17-47
2		≤400									4-6	>17
3	>-5										4-6	>17
4		≤700					2					>17
5					≤ 1.8							>17
6				≤ 21.5								>17
7	>-5	≤700										>17
8		400-700									4-6	
9		≤700						>30		> 22		
10	>-5			≤ 21.5					≤ 46			

The results obtained provide information for long-term seismic hazard assessment on the potential earthquake sources in north-east Egypt. The recognition performed, pinpoints a number of D nodes where moderate events have not been recorded to date that could provide additional information and incorporation of this information with the seismogenic zones can better improve the result of seismic hazard assessment than using the seismogenic model alone.

The recognition performed pinpoints a number of D nodes where moderate events have not yet been recorded to date. Fig. 2.32 displays that most of the delineated nodes have occurred within the seismotectonic zones defined in section 2.1, while few nodes occurred in the areas which did not show up a strong magnitude until now.

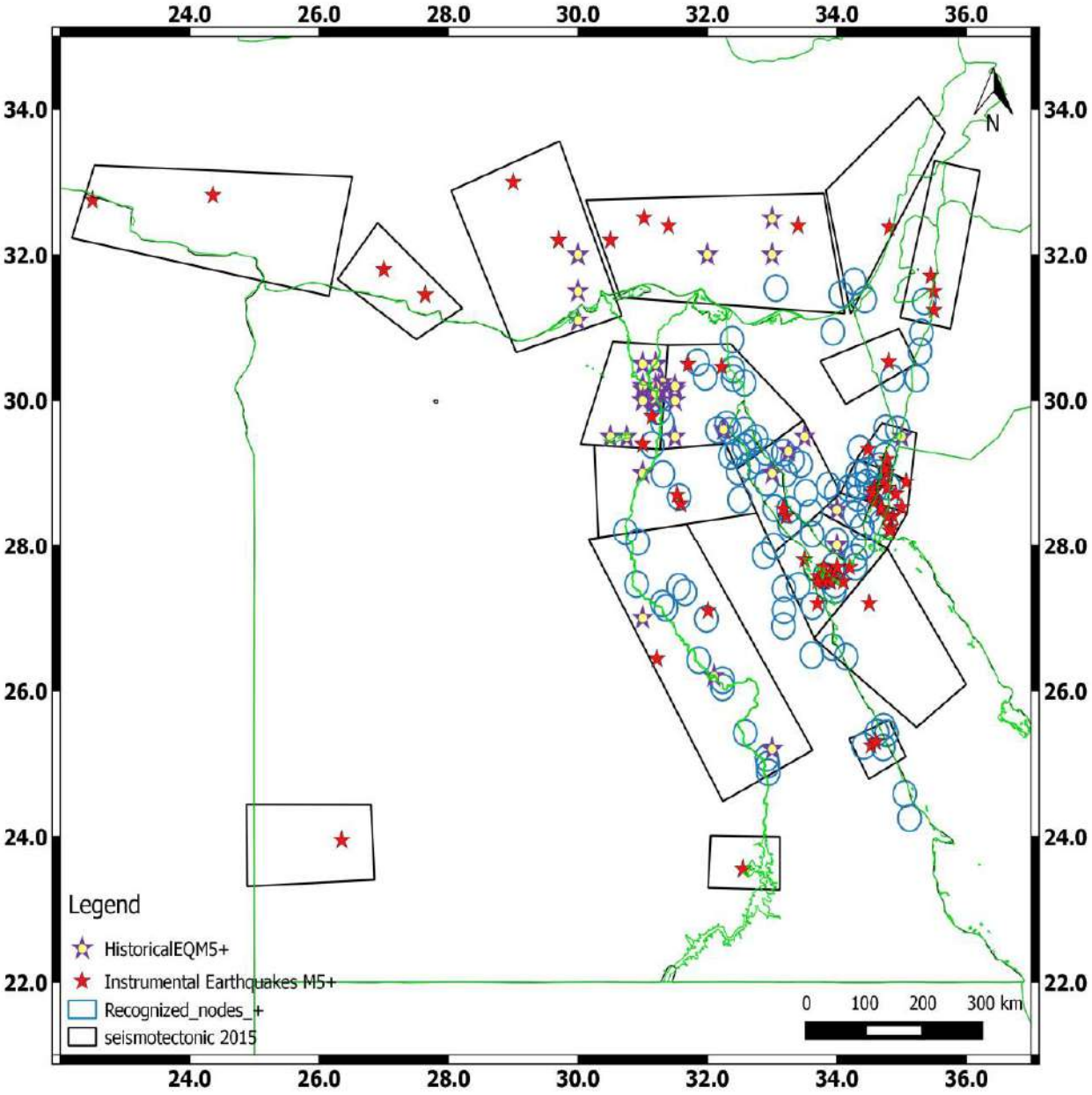

Fig. 2.32: Defined seismogenic nodes and zones for Egypt.

The seismogenic zones and nodes delineated in this Chapter will be used in the computation of seismic hazard maps (PGD, PGV, and PGA) for Egypt within the framework of the NDSHA approach. The inclusion of seismogenic nodes is crucial as well in site-specific seismic hazard assessment for the site of interest, since they can contribute strong effects if they happened in the future. We expect that the incorporation of seismogenic nodes information in seismic hazard computation may improve the performance of the resulting maps for the studied region, especially for the sites of rare or no seismic activity so far. Some of the recognized D nodes can give more knowledge about seismic risk affecting the sites of critical structures such as water power plants and dams, as well as large metropolitan areas.

Chapter 3

Neo-Deterministic Seismic Hazard Assessment for Egypt

3.1 Introduction

Prediction of earthquake ground motion parameters (e.g., displacement, velocity, and acceleration) can be made using empirical or physics-based approaches or a combination of them (i.e., hybrid methods) (Douglas and Aochi, 2008).

Empirical approaches for earthquake ground motion prediction are based upon the statistical regression of the available strong motion database, which necessitates dealing jointly with different earthquake sources, travel paths, and local site conditions. In fact, these approaches should be limited to the regions where the data itself is collected and where seismic sources, propagation paths, and site conditions are similar. In fact, most of the GMPEs used in the prediction of earthquake ground motion for Egypt both probabilistic (PSHA) and deterministic (DSHA) seismic hazard assessments have been developed for other regions. Thus many authors (e.g., Mohamed et al., 2012; EzzElarab et al., 2016; Gaber et al., 2017) have "imported GMPEs", because of the lack of strong motion database sufficient to construct an empirical relationship for Egypt or to explore and evaluate a suitable GMPE. Most, if not all of these seismic hazard studies - PSHA and DSHA for Egypt - have incorporated many different GMPEs from regions of tectonic setting somehow similar to the present-day tectonic setting of Egypt but they did not consider at all the possible effect of the propagation path that definitely is quite variable from path to path as shown in Chapter 1. There is no consensus on just one, or on a set of GMPE(s), that should be used. The choice of suitable GMPE(s) always depends on the mapmaker's preference and most of the studies have used more than one GMPE with different

weighting values with the aim of taking into account possible epistemic uncertainties. Moreover, the adoption of such equations is bound to lead to the disruption of the tensor character in the predicted earthquake ground motion.

In addition, the existing PSHA studies in Egypt supply the horizontal component of the ground motion only, relying on the untested assumption that the amplitude of the vertical component of strong motion can be defined as a fraction of the horizontal one. The vertical component generally could be less than the horizontal components, but this is not necessarily true for high-frequency ground motion in the near-source condition (Reiter, 1991; Shrestha, 2009). Actually, the directivity, propagation effect, and local site condition may combine and produce a dominant vertical component (e.g., Gazli, Uzbeksitan 1976 M6.8; Nahanni, Canada 1985 M6.8; Chi-Chi, Taiwan 1999 M7.6) and that is why it is essential to reliably estimate the vertical component of the ground motion as well.

Seismic time histories are of great importance for structural and technical engineers willing to design a new structure and/or evaluate the seismic performance of the existing built environment, and for investigating the liquefaction potential at a given site. The employment of hybrid methods (see Douglas and Aochi, 2008 and the references therein) that use the physical understanding of earthquake rupture, the knowledge of propagation properties of seismic waves and the available strong motion data is, in principle, naturally more preferable than using one method alone. Although, these methods still suffer from certain endemic shortcomings which are adequately described by Douglas and Aochi (2008).

The third class of methods employs numerical modeling codes based upon the physical description of earthquake rupture process and seismic wave propagation to predict the ground motion parameters reliably. The ground motion parameters from the potential seismic sources can be estimated with a high degree of reliability by the NDSHA approach (see Panza et al., 2001; Panza et al., 2012; Magrin et al., 2016 and the references therein). NDSHA stands for scenario-based methods for seismic hazard analysis, where realistic synthetic time series are used to construct earthquake scenarios. NDSHA is best suited to compute the ground motion parameters at 1 and 10 Hz cut-off frequencies for a set of 1D structural models at an epicentral distance greater than the focal depth of the source at different spatial scales. Starting from the available knowledge about Earth's crustal model, seismic source model and earthquake catalog of the study area, it is possible to compute the synthetic seismograms realistically. The peak

values of the ground shaking i.e., acceleration (PGA), velocity (PGV) and displacement (PGD) or any other ground motion parameter relevant to seismic engineering, e.g., design ground acceleration (DGA) can be extracted from the computed time histories. In the framework of NDSHA procedure, the study region is covered by a regular grid (typically 0.2° × 0.2°). The earthquake sources are centered in the grid cells that fall within the adopted seismogenic zones, while the computation sites are placed at the nodes of the chosen grid. The NDSHA approach apply a smoothing procedure for the definition of earthquakes location and magnitude, M, to account for spatial uncertainty and source extension. After smoothing only the cells (earthquake sources) located within the seismogenic zones are retained. The smoothing process makes NDSHA robust and prevents it from the possible uncertainties in the earthquake catalog, which is required to be complete just for $M \geq 5$. A double-couple point source is placed at the center of each cell, with a representative focal mechanism which is consistent with the present-day dominant tectonic regime of the corresponding seismogenic zone. Source depth is taken into consideration as a function of magnitude. A thorough description of the NDSHA methodology can be found in Panza et al. (2001), and its updates and validations in Panza et al. (2012) and Magrin et al. (2016).

Also, NDSHA permits, if necessary, to account for earthquake recurrence rate (Peresan et al., 2013 and references therein). Peresan et al. (2013) have performed the characterization of the frequency-magnitude relation for earthquake activity in Italy according to the multi-scale seismicity model (Molchan et al., 1997; Kronrod, 2011); an estimated recurrence is associated to each modeled source. Since the recurrence of the source is associated to the related synthetic seismograms, coherently with the physical nature of the problem, we shall obtain two separate maps: one for the ground shaking, one for the corresponding recurrence. In fact, when two sites prone to earthquakes of similar magnitude, given that all the remaining conditions are the same, the ground shaking parameters for seismic design must be equal at the two sites, since the earthquake magnitude we have to defend against is the same independently from the sporadic recurrence of the earthquake. The flow chart that explains the NDSHA procedure for regional-scale analysis is shown in Fig. 3.1. The physics-based ground motion modeling is limited up to a frequency 10 Hz because the estimate of ground motion at higher frequencies requires a better knowledge about seismic source heterogeneity, physical properties of the rock/soil, and the attenuation parameters with a resolution realistically not available at the moment. This statement

is well in agreement with Aki`s (2003) conclusion: results about the source-controlled f_{max}, non-linear soil response and the studies of seismic attenuation from borehole data indicate that there is no need to consider frequencies higher than about 10Hz in the field of strong motion seismology.

In fact, the quality of the results obtained by physics-based ground motion modeling depends on the quality of the input data. The NDSHA approach allows for sensitivity analyses to evidence and addresses the uncertainties using different input data and varying levels of knowledge about seismic source model and structural models of the medium. The assessment and communication of the possible uncertainties associated with the ground motion computation may help the potential users to decide how much confidence to place on a seismic hazard map.

This Chapter provides an update for the seismic hazard maps available for Egypt that incorporate the results of recent studies, i.e., revised historical earthquake catalogs, MZ data, reviewed focal mechanism solutions, and lithospheric structure mechanical models and it represents a base for the next Chapter. Moreover, a sensitivity analysis based upon the different ground motion maps computed adopting different seismic source models, crustal structural data and using different mapmaker`s preconceptions (e.g., different seismotectonic models) is shown to assess the potential uncertainties in the computed ground computation adequately.

The following update and sensitivity studies are accomplished using NDSHA. The main characteristics of the different variants can be summarized as follows:

- adoption of an updated definition of seismic sources (seismicity and seismotectonic zones) and structural models;
- change of the Size-Scaled Point Source point (SSPS) model into the Size and Time-Scaled Point Source (STSPS) model;
- application of the results of MZ study obtained for the north-eastern part of Egypt;

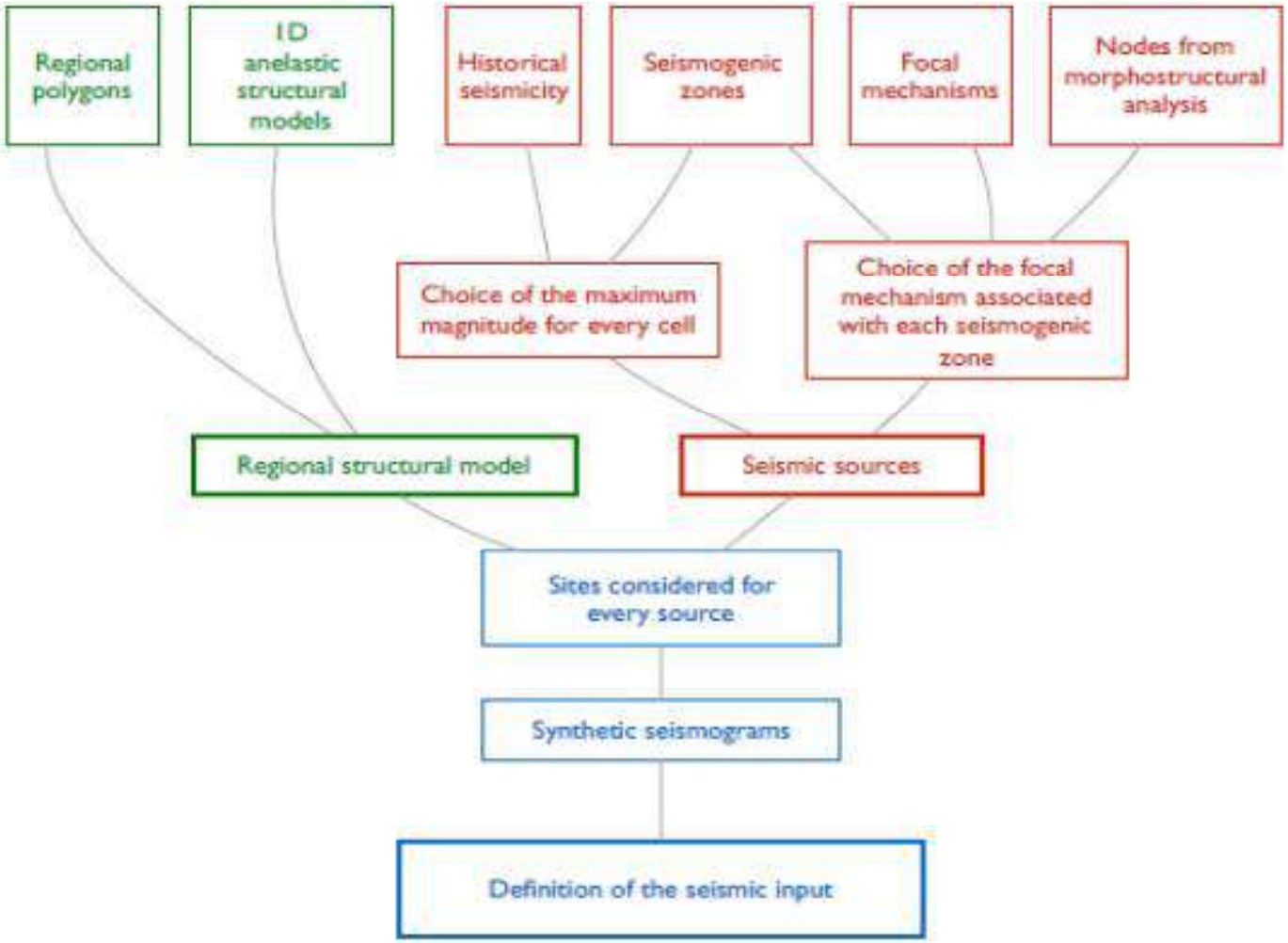

Fig. 3.1: Flow chart of the different steps in the NDSHA approach for the regional-scale analysis.

3.2 Computation of synthetic seismograms

3.2.1 Reference ground motion maps for sensitivity studies (Variant 1)

To test the influence of adopting different input parameters on the resulting ground motion scenarios, an initial configuration has to be set as the reference one. The reference ground motion maps for Egypt are obtained by NDSHA using the same input data used in the study by Mourabit et al. (2014) but limiting the computation to the Egyptian territory. The input data used in this variant are:

- (I) the earthquake catalog used in the calculation is extracted from the catalog being used in NDSHA for North Africa, which was compiled by Peresan et al. (2009) for North Africa region using earthquake data from national and international databanks (Mourabit et al., 2014 and the references therein) (Appendix A, Table 1) ;
- (II) the seismotectonic sources and the selected focal mechanisms are obtained by Mourabit et al. (2014); earthquake sources belonging to the same seismogenic zone share a representative focal mechanism associated with the zone itself (Appendix A, Table 2);
- (III) Five average layered anelastic bedrock models which have been defined for different areas in Egypt; these are the same structural models have been first proposed by El-Sayed et al. (2001) for the computation of the first NDSHA maps for Egypt. The earthquakes focal depth is assigned as a function of earthquake magnitude and is fixed at 10km for $M < 7$ and 15km for $M \geq 7$ in all the computations presented in this Chapter. The adoption of these shallow depth values is validated by the fact that the strong ground motion is generally generated by shallow sources in many active areas around the world, as indicated by Vaccari et al. (1990). The mean of estimated focal depths for earthquakes in Egypt is a range from 10 to 20km as deduced from the statistical analysis of the earthquake catalog used in this study (see the appendix A, Table 1) which is consistent with the assigned depth magnitude thresholds. The use of magnitude dependent depth has been done to account for the magnitude–depth relationship demonstrated in the statistical properties of the earthquake occurrences (Caputo et al., 1973; Molchan et al., 1997).

The synthetic seismograms are computed for 1 Hz cut-off frequency at the nodes of a grid 0.2°×0.2°. The computation at 1Hz is acceptable since it does not need much detailed information about the vertical variation in mechanical properties of the structural structures being used. The 1Hz cut-off frequency is capable of simulating the dominant part of seismic wave`s displacements and velocities, but it is not

adequate for accelerations as indicated by Panza et al. (1999). To obtain reliable acceleration values, it is necessary to extend the modeling results to higher frequencies (i.e., 10Hz in our case) and this can be readily done by extending the response spectrum at frequencies higher than 1Hz, using any appropriate design response spectrum (for details see Panza et al., 2001). The resulting values at period T=0s are called design ground acceleration (DGA).

A designed response spectrum defines the normalized elastic response spectrum of the ground motion for different rock/soil types (i.e., A, B, C and D; they are assigned based on shear-wave velocity), considering a certain percentage of damping. In the following computations, the Egyptian Code of Practice-201 (ECP-201, 2011) has been employed in all the executions to compute the ground motion acceleration at higher frequencies, which is defined for 5% critical damping.

In Variant 1, the point source approximation is adopted. In the point source approximation (this approximately is valid when the receiver is at distances greater than the source dimensions) the synthetic seismograms are scaled with magnitude using the relatively simple spectral scaling curves of Gusev (1983), with zero phases. The Gusev source scaling curves that reasonably represents seismic source data at a global scale are suitable for the shallow events and successfully tested against the observations (roughly speaking h <20km) by Boore (1986)); for more in depth events other scaling laws should be used (e.g., Gusev et al., 2002).

The seismograms are computed based on the point source approximation with $M_0 = 10^{20}$dynecm. The scalar seismic moment of each source is obtained using the equation:

$$\log(M_0) = 1.5\,M + 16.05$$

where M is the earthquake magnitude. For the scaling, each seismogram is Fourier-transformed then its amplitude spectrum is multiplied by the curve corresponding to the proper M_0, obtained by bilinear interpolation from the curves reported by Aki (1987) which are based on the source scaling laws of Gusev (1983). In the computations done by Mourabit et al. (2014), the magnitude-distance thresholds were fixed at 150km regardless of the size of the earthquake. In all the NDSHA computations discussed from now on, the magnitude-distance limits of 150, 200, 400 and 800km, for the magnitude of 5, 6, 7 and 8, have been adopted, respectively. The choice of the maximum distance between the source and the receiver for different magnitude thresholds is based on our insight on the available

intensity data for Egypt that illustrate the capability of far seismic sources to cause different levels of damage at distant sites. The ability of far-field sources to impact Egypt may be due to the strong magnitude they can produce and low attenuation of the propagation path, local site effects, and poor building design and construction quality or a combination of them. The need to increase the magnitude-distance threshold is clearly illustrated in Fig. 3.2, which shows that the intensity VI (MSK) from 12 September 1955 M_w = 6.8 (continental margin of Egypt) and 31 March 1969, M_w = 6.9 (the entrance of the Gulf of Suez) earthquakes were felt at distances > 20 km. Intensity VI level is chosen since it represents the boundary between the intensity with minor damage (V) and the one with significant damage (VI).

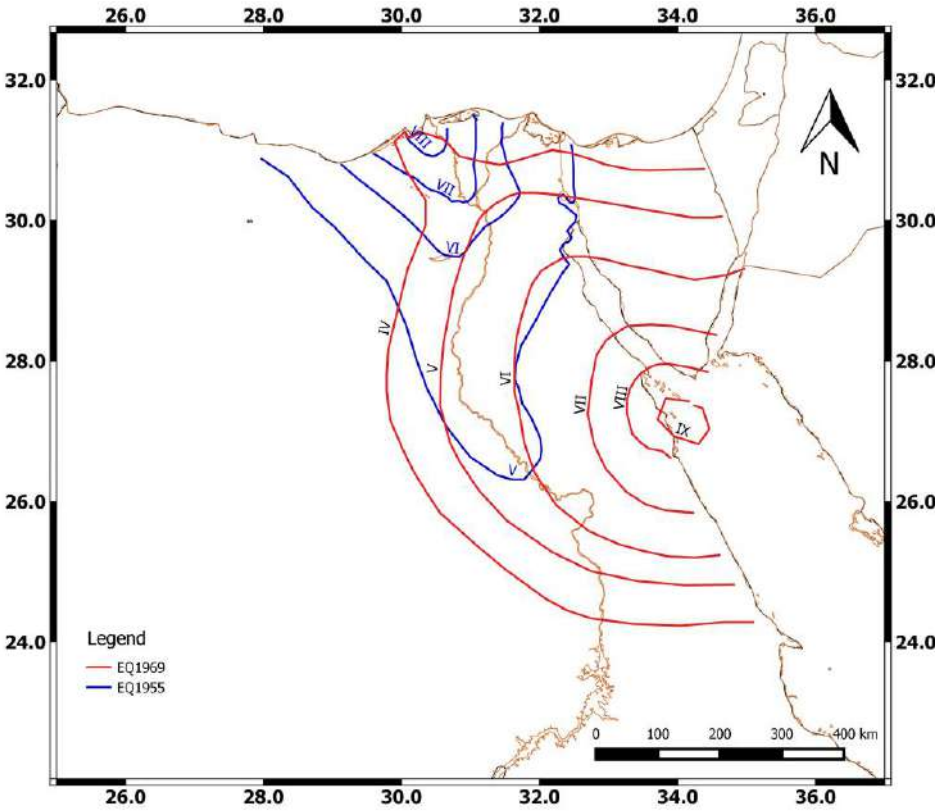

Fig. 3.2: Intensity distribution for the 12 September 1955 M_w = 6.8 (Continental margin) and the 31 March 1969 M_w= 6.9 (Entrance of Gulf of Suez) earthquakes.

In furtherance of computing the reference maps for applying the sensitivity analysis, the synthetic seismograms for the vertical and the two horizontal components are calculated, their peak values are extracted, then mapped. The default output of the computation includes the peak values of vertical components as well the peak values of the horizontal component, defined by the vector sum of the radial (P-

SV, Rayleigh modes) and transverse (SH Love modes) components computed at each receiver inside the given structural models.

3.2.2 Updated seismic sources and structural models (Variant 2)

In the updated version of ground motion maps for Egypt, we have revised and updated all input data relative to the reference variant, i.e., earthquake catalog, seismotectonic zones with their representative focal mechanisms and structural models. The release of a new data and data quality control studies, which have been carried out during the last decade (e.g., Abu El-Nader, 2010; Badawy et al., 2010), has motivated the following updates:

Earthquake catalog: The earthquake catalog used by NDSHA package requires the availability, as complete as possible, only for earthquakes with M5+, which are capable of generating a significant ground motion. The starting data set is the earthquake catalog of North Africa, used in the computation of the reference maps (Variant 1), and updated with a proper comparison with the other available historical or instrumental earthquake catalogs from national (e.g., Abu El-Nader, 2010; Abou Elenean, 2009; Badawy et al., 2010; and international sources (e.g., European Mediterranean Seismological Center (EMSC) http://www.emsc-csem.org/; International Seismological Center (ISC) bulletins http://www.isc.ac.uk/iscbulletin/search/). All this information has been used to compile a uniform and, as much as possible, complete earthquake catalog (smoothed seismicity is shown in Fig. 3.3 (a)). The pre-instrumental earthquake catalog (64 events M5+) is taken from the revised and quality controlled catalog of Badawy et al. (2010). The instrumental earthquake catalog (69 events M5+) is compiled using all available national (either published or unpublished) and international catalogs and existing publications about the seismicity and source mechanisms (e.g., Kebeasy et al., 1981; Abdel-Fattah, 2005; Abu El-Nader, 2010; Abdel Rahaman et al., 2008; Hussein et al., 2008). In the updated catalog (Table 1 in Appendix A), we assigned the moment magnitude (M_w) scale for earthquakes with $M \geq 6$ and M_b for the earthquakes with $5 \leq M < 6$, in order to avoid magnitude saturation problem. Different magnitude values on the same magnitude scale are often assigned for the same earthquake by various authors (in the study case the variation in magnitude is ranging from 0.1 to 0.6, well in agreement with global studies e.g., Musson (2012), therefore in Variant 2

we adopted the maximum between them, to be more conservative. In other words, in Variant 5, the seismogenic nodes defined by MZ capable of generating M5+ have been identified, and M5 is adopted for all the nodes in the seismic hazard computation.

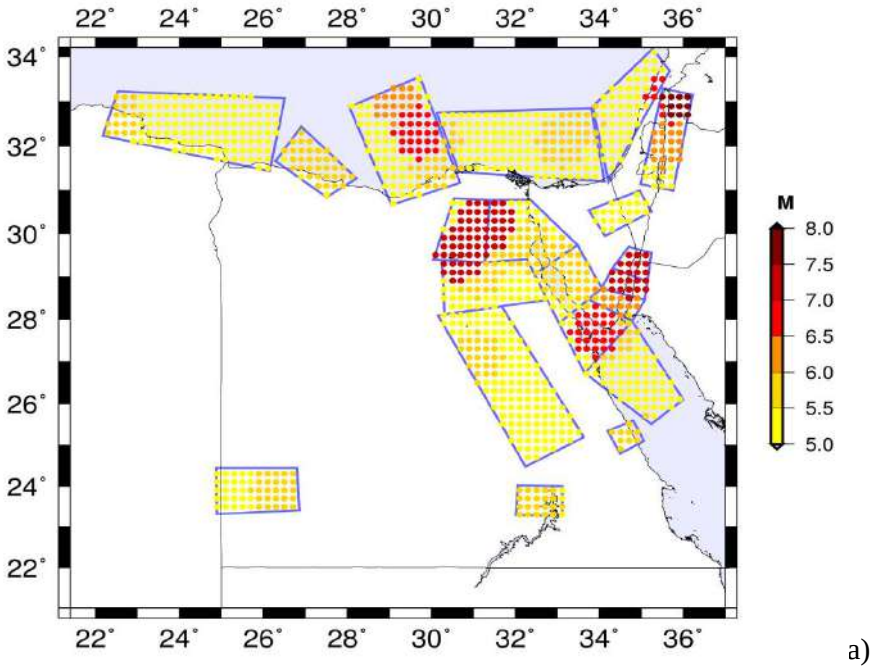

a)

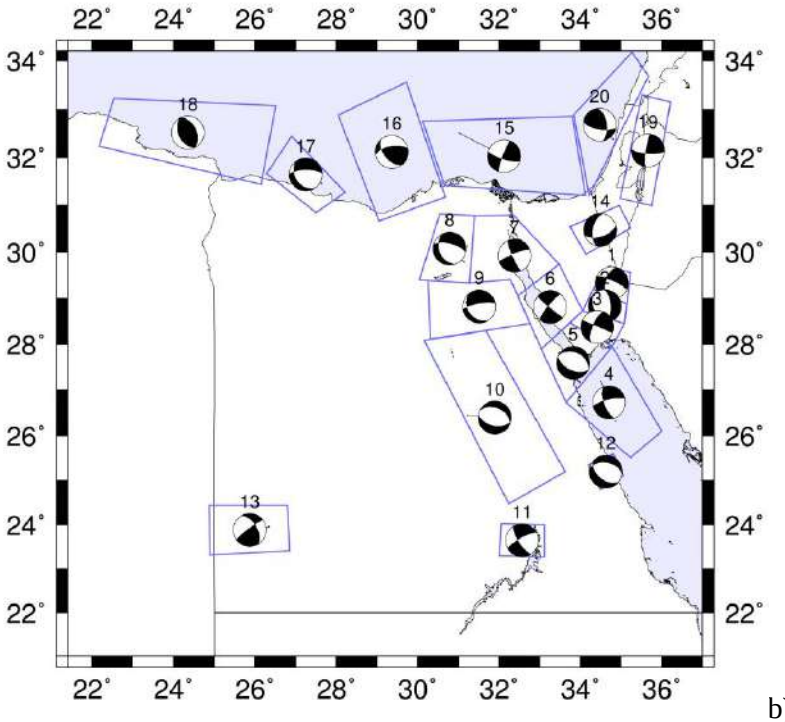

b)

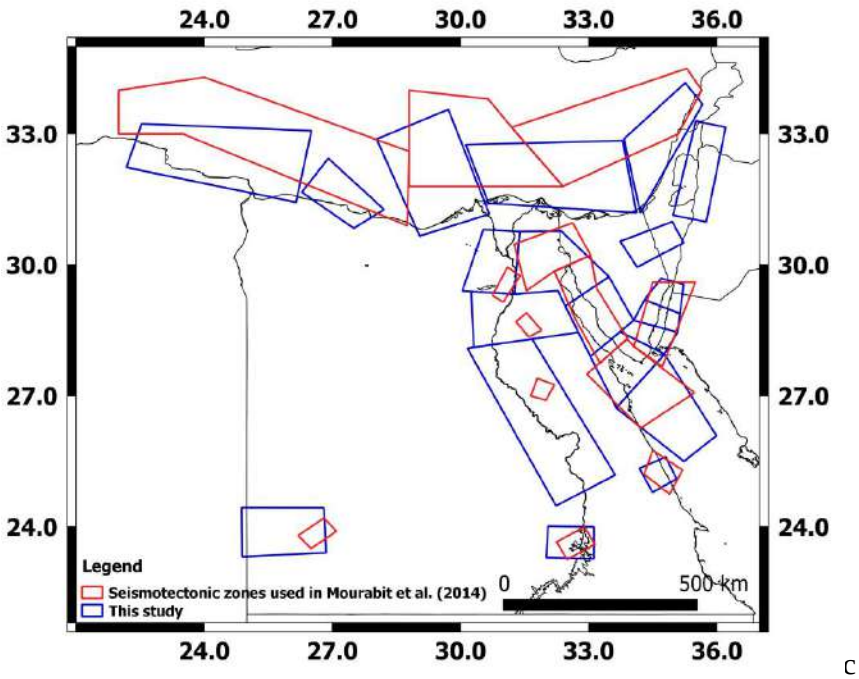

c

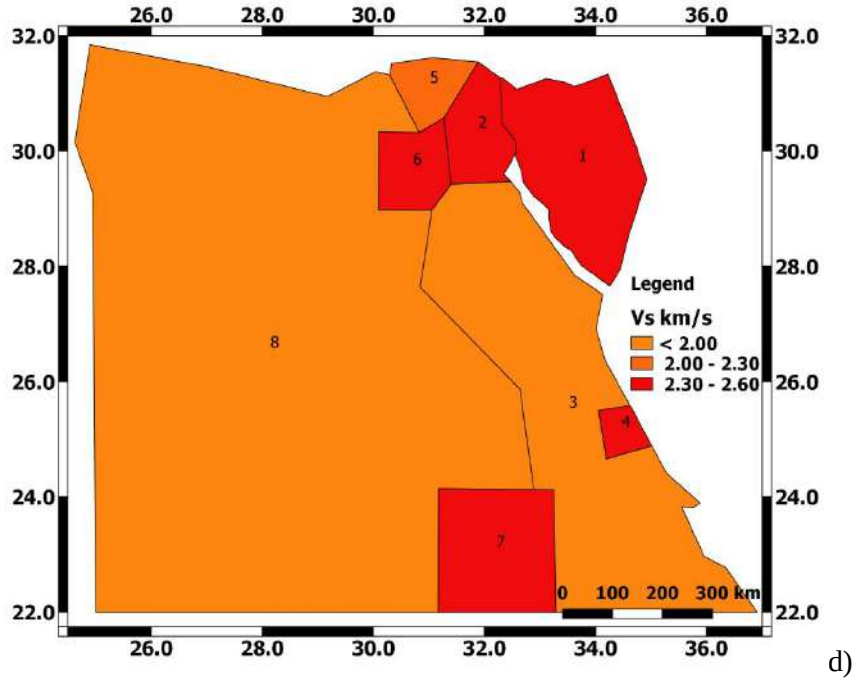

d)

Fig. 3.3: a) Smoothed magnitude within the seismogenic zones developed in this computation; b) Updated seismotectonic zones and representative focal mechanisms for Egypt; c) Difference in the geometry, orientation and covered areas by the Mourabit et al. (2014) seismotectonic model and the model used in Variant 2 developed in this study (Chapter 2); d) Thickness and V_S for the uppermost layer of the updated structural model used in Variant 2.

Seismotectonic zones: Twenty zones have been defined in Chapter 2 (Fig. 3.3 (b)) based on the available information: historical earthquake record, refined focal mechanism solutions (based on quality control criteria), stress tensor data, surface

geological, geophysical studies, geomorphologic investigations, bathymetry data, surface faults, GPS data, crustal structure, and other related studies (e.g., Said, 1990; Abou Elenean, 2007; Abou Elenean, 2010; Deif et al., 2011) then used in Variant 2. The comparison between the configuration of the seismotectonic model used in Mourabit et al. (2014) "Variant 1" and the model developed in this study in Chapter 2 is shown in Fig. 3.3 (c). The representative focal mechanism for each zone is selected based on the best solution of the largest event that occurred in the zone; using the focal solution catalog of Abu El-Nader (2010) (see Table 2 in Appendix A).

Structural model: Eight average anelastic structural polygons are delineated based on all the available crustal structure data from seismic reflection and gravity surveys and on the velocity models adopted by Egyptian National Seismological Network (ENSN), NRIAG for earthquake location in Egypt (e.g., Makris et al., 1979; Marzouk, 1988; El-Hady et al., 2004). The properties of the uppermost layers are compiled from different detailed studies (e.g., Makris et al., 1979; Marzouk, 1988; El-Hady et al., 2004) and a reference structure is used for deeper earth`s structure. The S-wave velocity and the thickness of the uppermost layer of each regional structure are shown in Fig. 3.3(d).

The synthetic seismograms have been computed at 1Hz cut-off frequency and the seismic sources within the seismogenic zones are treated as Size Scaled Point Sources (SSPSs) (Parvez et al., 2011). The ground motion parameters have been computed for the vertical and horizontal components then the maximum value at each site is extracted and plotted as a map of peak ground motion. Using the same default parameters (maximum source-receiver distance for different magnitude thresholds and event depth-magnitude thresholds, 1Hz cut-off and SSPS approximation) adopted in the computation of Variant 1, the PGD, PGV and DGA value at each site are computed and mapped as shown in Fig. 3.4 (a), (b) and (c), respectively. To measure and present the scatter in the computed ground motion due to change in the input of the two variants, it is possible to consider the difference between the resulting ground motion maps and to represent it with either upward (if the difference is positive) or downward triangles (if the difference is negative) with a color scale (different colors refer to the absolute value of the difference). A similar procedure can be made considering the ratios between Variant 2 and the reference Variant 1. To recognize significant differences between the two different Variants, as in Panza et al. (2012), we use the fact that the change in macroseismic intensity by one unit corresponds to

two factors of DGA, as implied by Cancani (1904); the same rule can be assumed for PGVs and PGDs (Panza et al., 1997). The sites where there is a change in the ground motion parameter of at least one intensity level (corresponding to about a factor of 2 in the peak value) are plotted as upward or downward triangles depending on the sign of the change. Let us assume that we have two maps, A and B, and at each node i, j of the adopted grid the ratio can be computed $R_{i,j} = A_{i,j}/B_{i,j}$ as shown in Fig. 3.5 (b, d, and f). The result of the ratio $R_{i,j}$ is visualized by an upward triangle if the result is ≥ 1, while the value $1/ R_{i,j}$ is visualized with a downward triangle if the result is < 1.

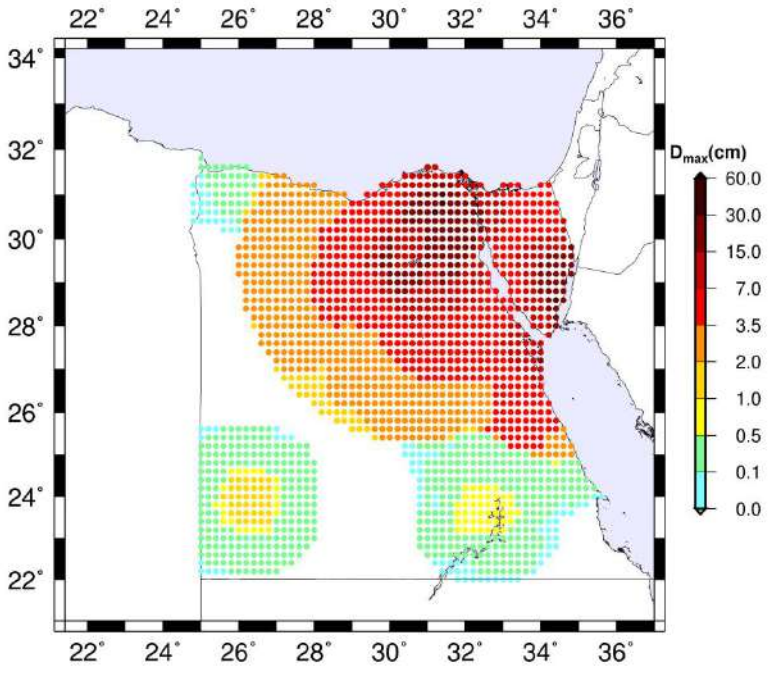

a)

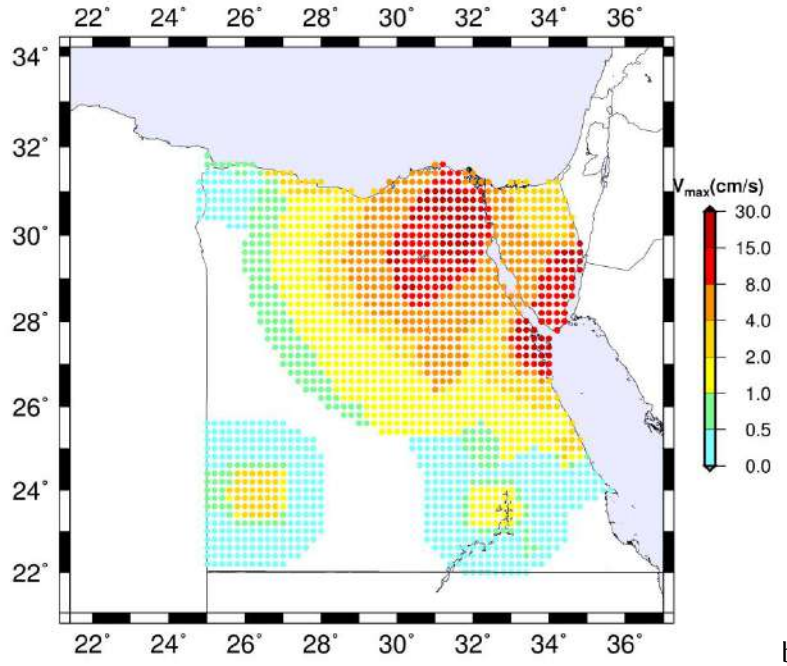

b)

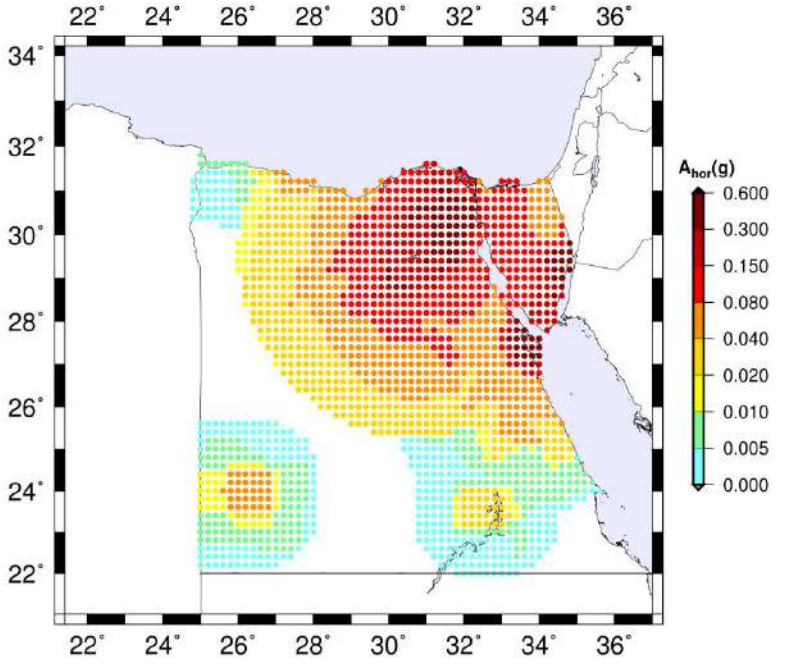

c)

Fig.3.4: a) Peak ground displacement (D_{max}) map (Variant 2); b) Peak ground velocity (V_{max}) map (Variant 2); c) Maximum horizontal acceleration (A_{hor}) map (Variant 2).

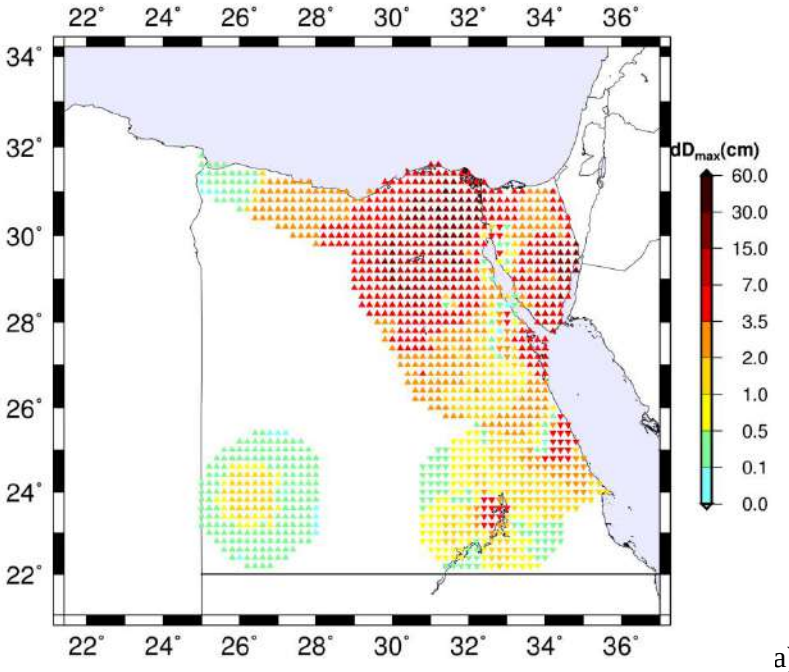
22° 24° 26° 28° 30° 32° 34° 36°
34° 32° 30° 28° 26° 24° 22°
dDmax(cm)
60.0
30.0
15.0
7.0
3.5
2.0
1.0
0.5
0.1
0.0

a)

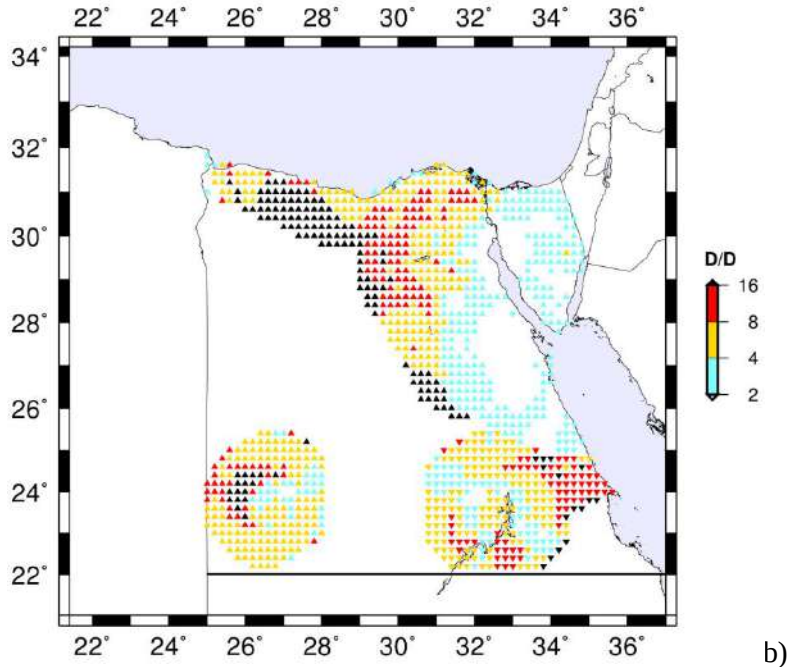
22° 24° 26° 28° 30° 32° 34° 36°
34° 32° 30° 28° 26° 24° 22°
D/D
16
8
4
2

b)

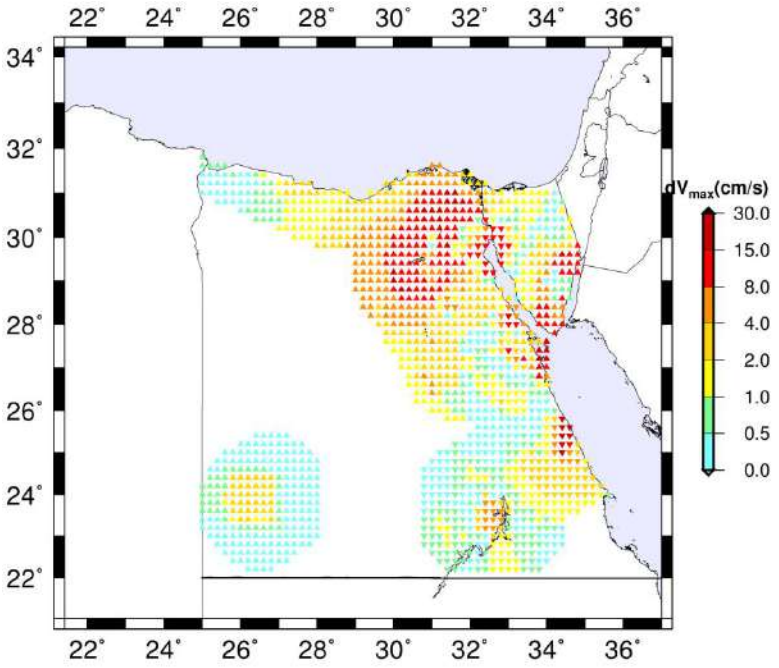
22° 24° 26° 28° 30° 32° 34° 36°
34° 32° 30° 28° 26° 24° 22°
dV$_{max}$(cm/s)
30.0
15.0
8.0
4.0
2.0
1.0
0.5
0.0

c)

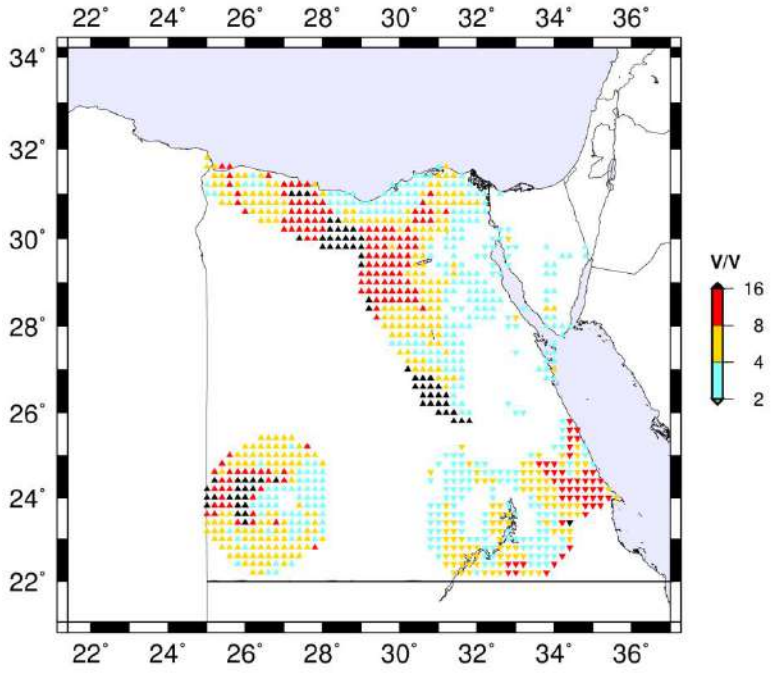
22° 24° 26° 28° 30° 32° 34° 36°
34° 32° 30° 28° 26° 24° 22°
V/V
16
8
4
2

d)

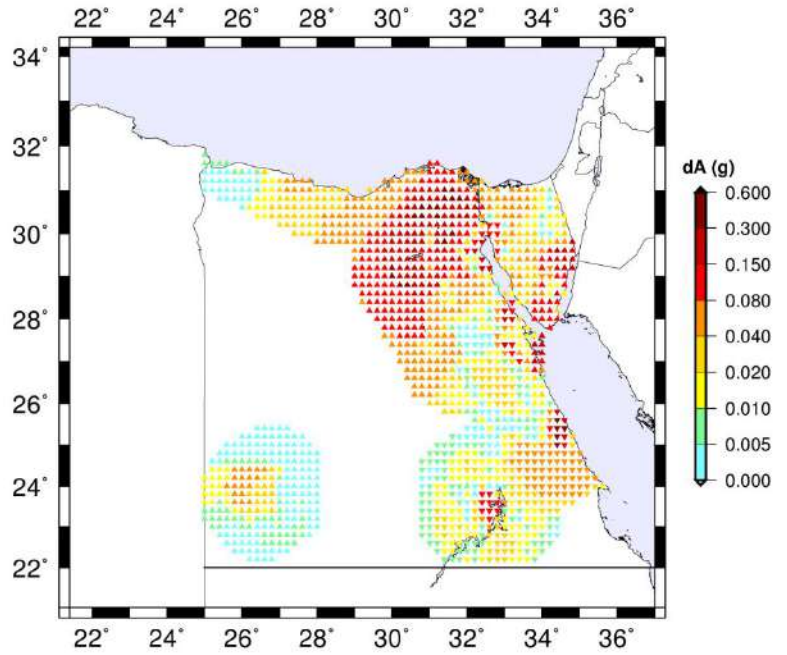

e)

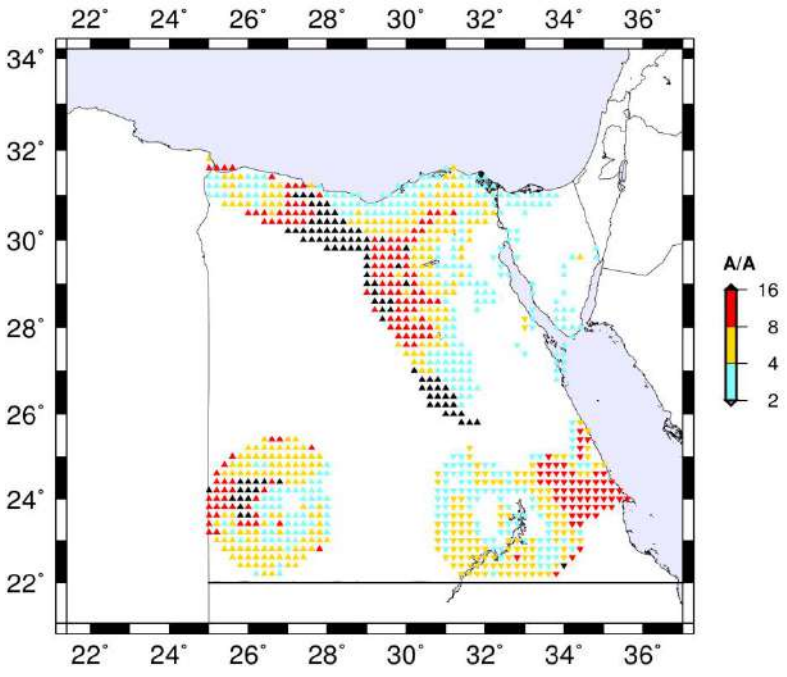

f)

Fig. 3.5: a) Difference between PGDs from Variants 2 and 1, respectively (dD_{max} = Variant 2-Variant 1); b) Ratio between PGDs from Variants 2 and 1, respectively (D/D = Variant 2/Variant 1); c) Difference in PGVs from Variants 2 and 1, respectively (dV_{max}= Variant 2-Variant 1); d) Ratio between PGVs from Variants 2 and 1, respectively (V/V = Variant 2/Variant 1); e) Difference between DGAs from Variants 2 and 1, respectively (dA = Variant 2-Variant 1); f) Ratio between DGAs from Variants 2 and 1, respectively (A/A = Variant 2/Variant 1).

Here, in order to present and measure the scatter in the computed ground motion between different variants we offer both visualization ways in order to have general (maps of the ratios) and detailed (maps of differences) insights on the

scattering in the resulting ground motion values, since using the ratio alone could cause many details to be hidden. The comparison between the two configurations evidently show that the dominant change in the obtained ground motion parameters is an increase of hazard (marked by an upward triangle, and graduated color characterizes of the magnitude of the change) that can be attributed to inclusion of new sources, the change in the configuration of seismotectonic zones (Fig. 3.3 (c)) and their representative focal mechanisms, and the update of the earthquakes parameters (magnitude and location). The sites showing a decrease in the computed ground motion values (marked by downward triangles) could be related to the change in the updated structural model (Fig. 3.3 (c)) (increase in the seismic velocity of bedrocks), the removal of the events with poor quality for the updated catalog, the change in the configuration of seismogenic zones and the use of different representative focal solutions.

An example of the increase in the ground motion is evident in Nile Delta and Cairo, which can be related to the increase, in Variant 2 relative to the reference run, in the adopted magnitudes estimated from intensity data from the updated historical catalog, while the increase around the Gulf of Aqaba can be well due to the presence of new events in the updated catalog (Variant 2) which may be missed or unrecognized in the reference configuration (Variant 1) (see Fig. 3.5 (a, b, c, d, e, and f)). In fact, any magnitude estimation based only on the epicentral intensity, I_0, can be subject to high uncertainty due to the possible influence of many factors, like hypocentral depth, quality of construction, attenuation and local site conditions, which can strongly influence (increase/decrease) the observed intensity value.

The correction for the possible local effect of Nile's sediments on the intensity data has never been explicitly addressed in any of the available macroseismic studies, so special care is needed when relying on such data. In order to substantiate the magnitude estimate, derived from epicentral intensity using the equation of Maamoun (1979),

$$M = 0.7\ I_0 + 2.7 \log h - 3.0$$

where, I_0 is the epicentral intensity on the MSK scale and h is the hypocentral depth, we compute the magnitude from the observed epicentral intensity (I_0) for some recent strong earthquakes for which both intensity data and seismograms are available, e.g., 1992 M_w = 5.9 with I_0 = VIII and 1969 M_w = 6.9 with I_0 = IX earthquakes. The estimated magnitudes turn out to be 6.1 and 6.6 for the 1992 and 1995 earthquakes,

respectively using the observed hypocentral depth. The difference in magnitude values due to the perturbation of hypocentral depth with fixed incremental value (5 km) above and below the observed one for the mentioned above earthquakes is ranging between ±0.2 to 0.3, a value comparable with one standard deviation (σ) of global instrumental estimates of magnitude (Musson, 2012). The largest change in the ground motion values (Fig. 3.5 (a, b, c, d, e, and f)) (marked by black upward and downward triangles) can be seen in west, south-east, south-west and north-west Egypt, particularly at the maximum source-receiver distance considered for different magnitudes thresholds, and this may be due to the change in the seismogenic zones dimensions and orientations. In the areas showing a varying level of decrement, i.e., Abu-Dabbab and Aswan, the change (marked with downward triangles) could be attributed to the removal of some historical events evaluated as of scarce quality in the work of Badawy et al. (2010), which represents the last update for the historical catalog in Egypt. These events are 997, M5.5, and 1887, M6.9, earthquakes for Abu-Dabbab and 1854 M6.4 earthquake in Aswan.

3.2.3 Size and Time Scaled Point Source Model (STSPS) (Variant 3)

In Variants 1 and 2, the earthquake sources have been modeled with the SSPS approximation. In Variant 3, the STSPS source representation described by Parvez et al. (2011) is used with the same input data used in Variant 2 (i.e., only the source model is changed). Therefore, in Variant 3 the earthquake sources are realistically modeled and include source rupture process (i.e., directivity, rupture velocity and slip distribution). In such a way we investigate the influence of adopting different source models on the resulting ground motions. The STSPS is a mixture of extended and point source models, computed with the ***PULSYN06*** algorithm (Gusev, 2011; Magrin et al., 2016), which provides a broadband kinematic source model. The extended source (ES) model is described in terms of a grid of sub point-sources (shortly sub-sources) and the time functions of each sub-source are summed together to obtain an equivalent single representative source of the entire space and time structure of the ES. The considered earthquake source model has a neutral directivity (90°), unilateral rupture style and only one realization of the rupture process.

As described by Panza et al. (2012), the adoption of the STSPS model in the ground motion computation leads, in general, to an increase in the duration and to a decrease in the amplitudes of generated signal, relative to the point source model used

in Variant 2. The duration of seismic wave train is a crucial factor for the damaging potential, particularly at relatively large epicentral distances, where the dispersion of surface waves produces, as a rule, relatively long durations.

The STSPS approximation is adopted starting from this variant and the next ones (Variants 3, 4 and 5). The comparison between maps of the peak ground motion parameters obtained using SSPS, and STSPS models show, as expected, a general decrease, but with varying absolute value, all over Egypt, with the exception of few sites (Fig. 3.6 (a, b, c, d, e, and f)).

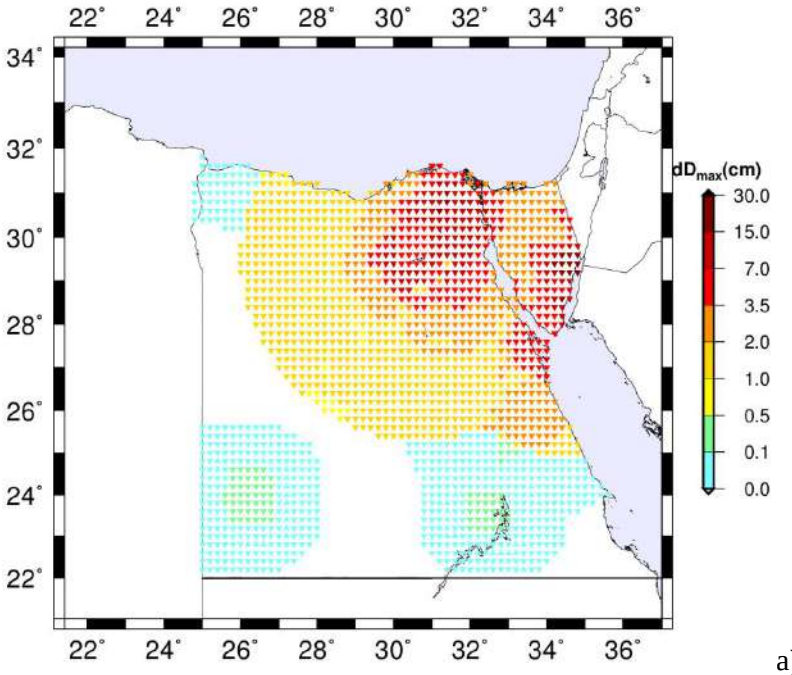

a)

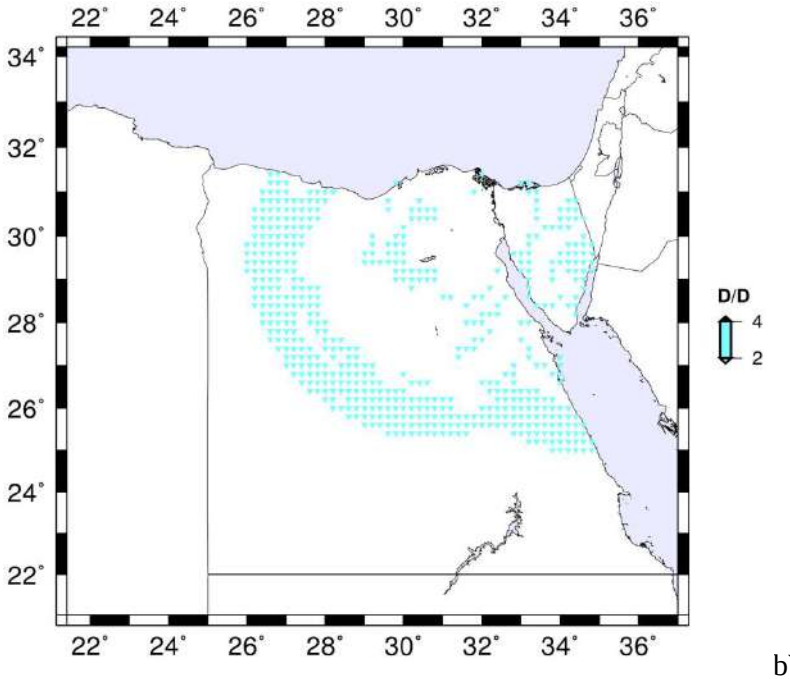
22° 24° 26° 28° 30° 32° 34° 36°
34° 32° 30° 28° 26° 24° 22°
D/D
4
2

b)

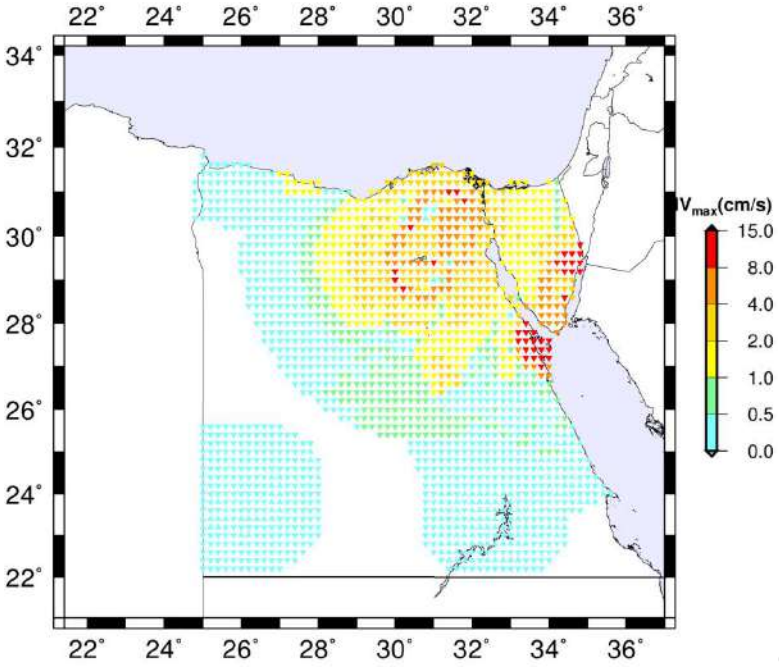
22° 24° 26° 28° 30° 32° 34° 36°
34° 32° 30° 28° 26° 24° 22°
V_{max}(cm/s)
15.0
8.0
4.0
2.0
1.0
0.5
0.0

c)

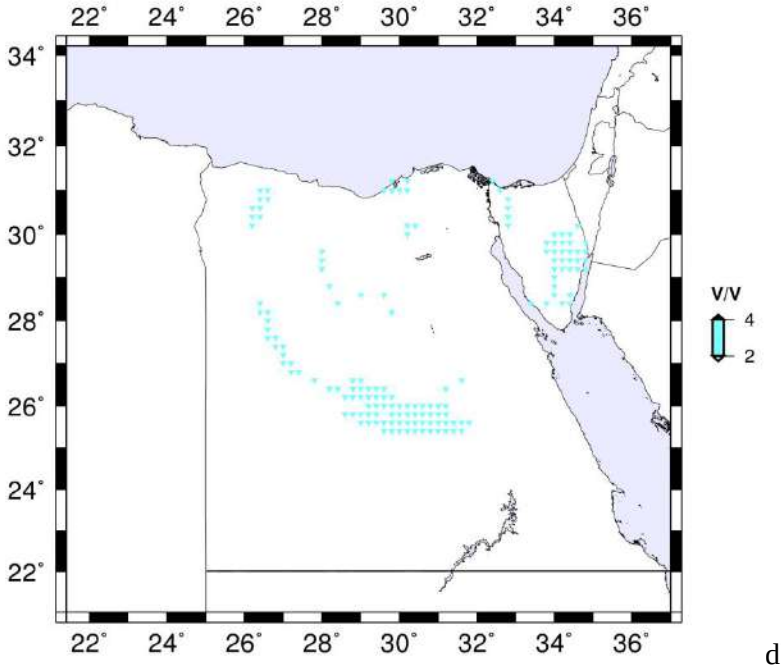
22° 24° 26° 28° 30° 32° 34° 36°
34° 32° 30° 28° 26° 24° 22°
V/V
4
2

d)

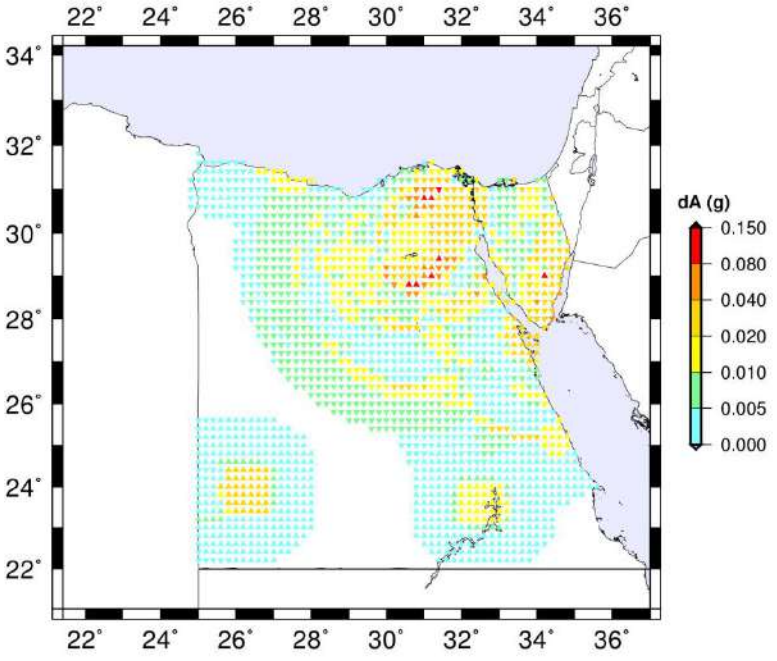
22° 24° 26° 28° 30° 32° 34° 36°
34° 32° 30° 28° 26° 24° 22°
dA (g)
0.150
0.080
0.040
0.020
0.010
0.005
0.000

e)

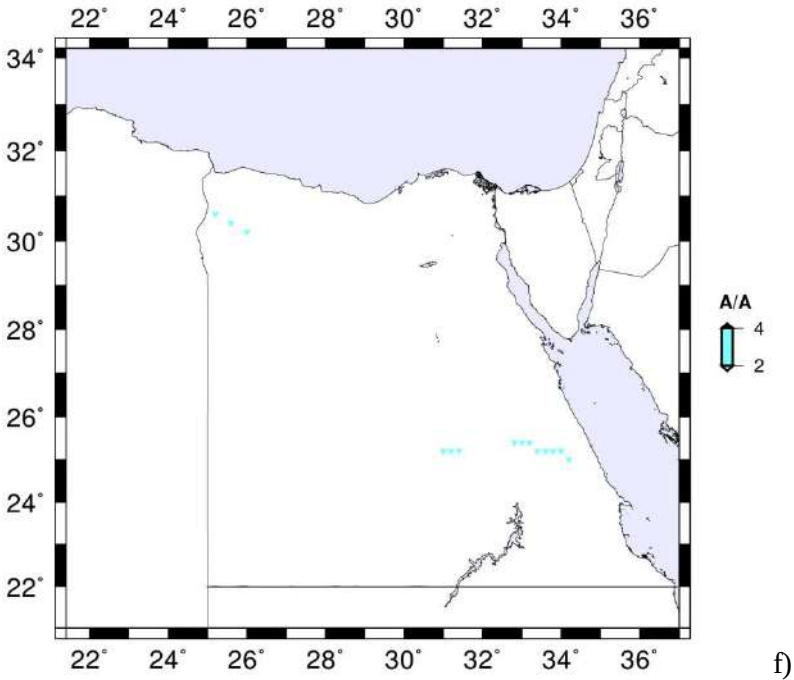

f)

Fig. 3.6: a) Difference in the PGD values from the Variants 3 and 2, respectively (dD_{max} = Variant 3 - Variant 2); b) Ratio between the PGD values from the Variants 3 and 2, respectively (D/D=Variant 3 / Variant 2); c) Difference in the PGV values from the Variants 3 and 2, respectively (dV_{max} = Variant 3 - Variant 2); d) Ratio between the PGV values from the Variants 3 and 2, respectively (V/V = Variant 3 / Variant 2); e) Difference in the DGA values from the Variants 3 and 2, respectively (dA = Variant 3 - Variant 2); f) Ratio between the DGA values from the Variants 3 and 2, respectively (A/A = Variant 3/ Variant 2).

3.2.4 *Change of the seismotectonic zones model (Variant 4)*

In this section, we describe the sensitivity test performed adopting an updated version of the seismogenic zones to investigate the effects of using different expertise, knowledge and of involving micro-earthquakes in the zones definition. The main idea for using the seismogenic zones, with different minimum magnitude, comes from the fact that we do not know if the geologic forces which cause the micro-earthquakes in the past and present can generate a strong earthquake and cover a broad spectrum of preconceptions instead of using a single model. Here, the last updated version of seismogenic zones for Egypt developed by Sawires et al. (2015) is used. In this section, twenty-eight seismotectonic sources are used to cover the areas where the seismic activity (Fig. 3.7 (a)) shows minor changes in the representative focal mechanisms. Fig. 3.7 (b) shows the superposition of the seismotectonic zones used in Variants 2 and 3 and those used in Variant 4.

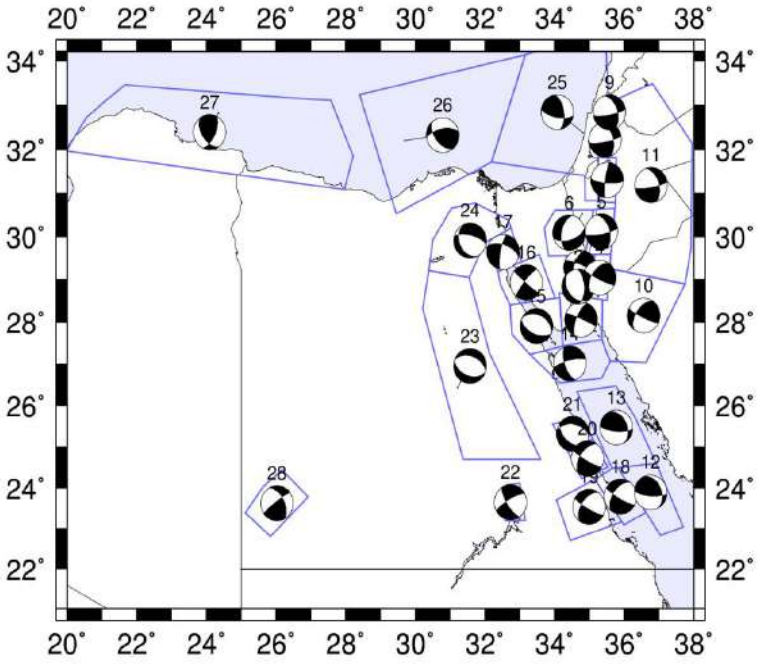

a)

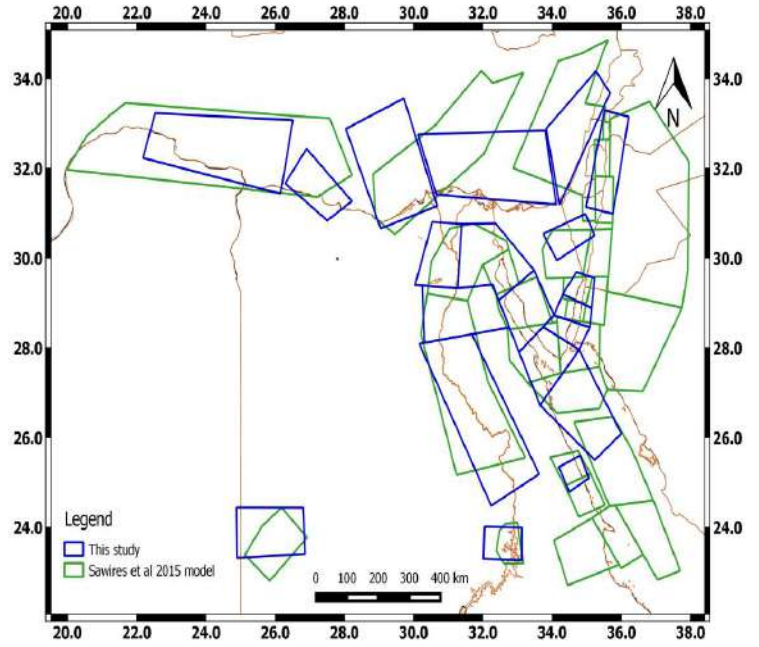

b)

Fig. 3.7: a) Seismotectonic zones and the selected focal mechanisms as delineated by Sawires et al. (2015) and adopted in Variant 4; b) Difference in the geometry, orientation and covered areas by the Sawires et al. (2015) seismotectonic model and the model used in Variant 3.

In NDSHA, if the zones do not show a magnitude M5+, the magnitude 5 is assumed. The comparison between the results obtained with Variant 4 and the results from Variant 3 is shown in Fig. 3.8 (a, b, c, d, e, and f). The maps of differences and ratios clearly demonstrate the influence, on the obtained ground motion parameters, of

changes in a) the seismotectonic zones configuration (i.e., geometry and orientation) relative to smoothed seismicity; b) the definition of new seismogenic zones in comparison with the model that has been used in Variant 3; c) the choice of the representative focal mechanisms for each zone. The downward triangles (difference < 0 or ratio < 1) reflect the smaller extent of the seismotectonic area of Variant 4 with respect to that of Variant 3, while the upward triangles represent (difference > 0 or ratio > 1) either new areas covered by the new seismotectonic model (Variant 4) relative to the one adopted in the last computation of Variant 3 or/and the newly defined seismotectonic zones, introduced in the Variant 4, that cover an area much larger than the one used in Variant 3, e.g., southeastern part of the Eastern Desert of Egypt (see also the map of the overlap between the two seismotectonic models adopted in Variants 4 and 3 shown in Fig. 3.7 (b)).

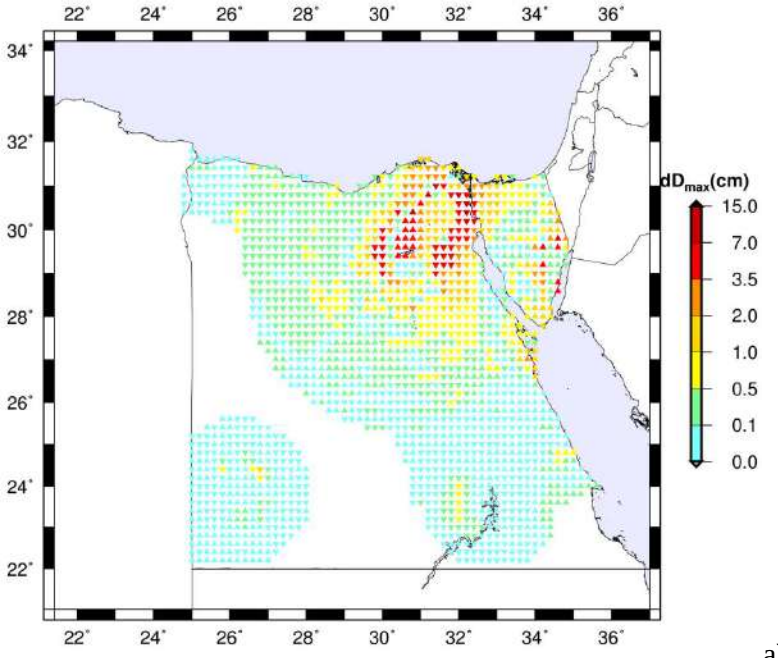

a)

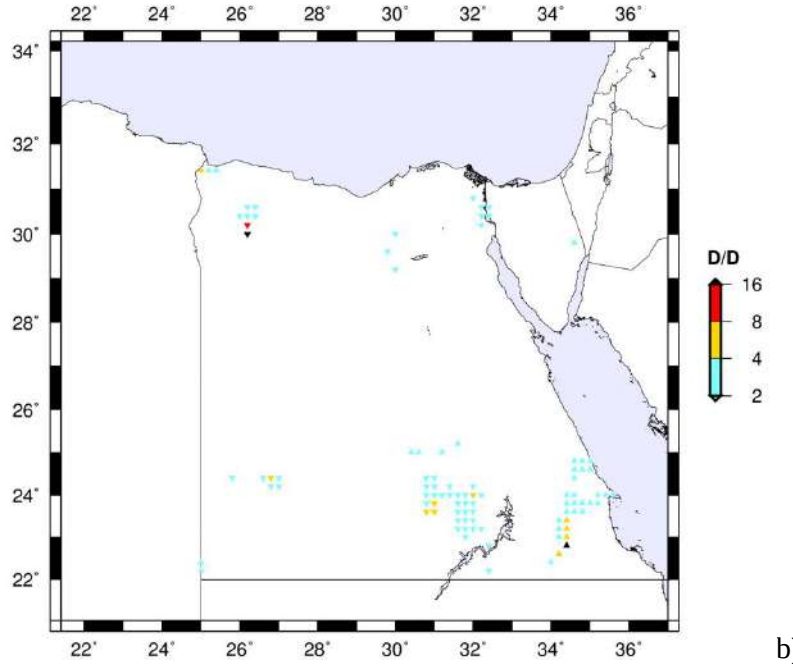
22° 24° 26° 28° 30° 32° 34° 36°
34° 32° 30° 28° 26° 24° 22°
D/D
16
8
4
2

b)

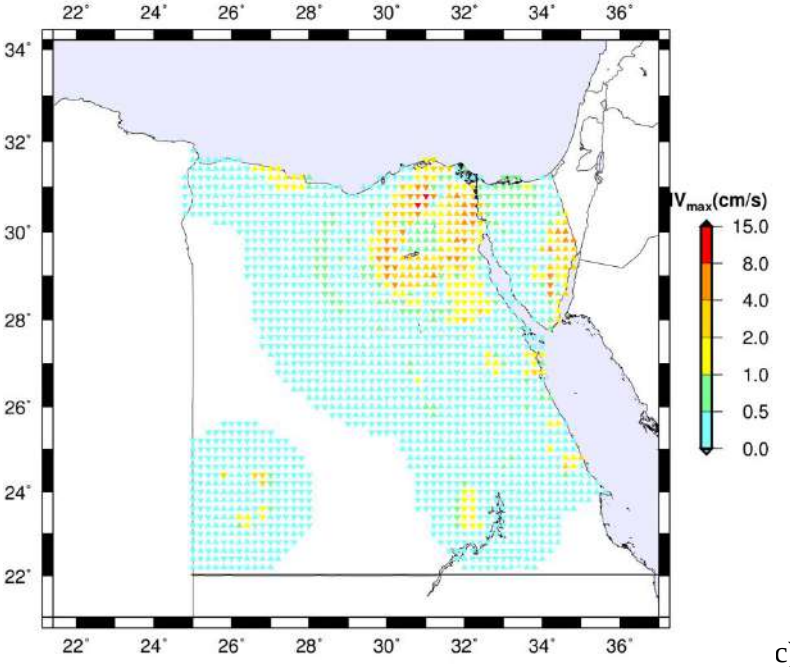
22° 24° 26° 28° 30° 32° 34° 36°
34° 32° 30° 28° 26° 24° 22°
V_{max}(cm/s)
15.0
8.0
4.0
2.0
1.0
0.5
0.0

c)

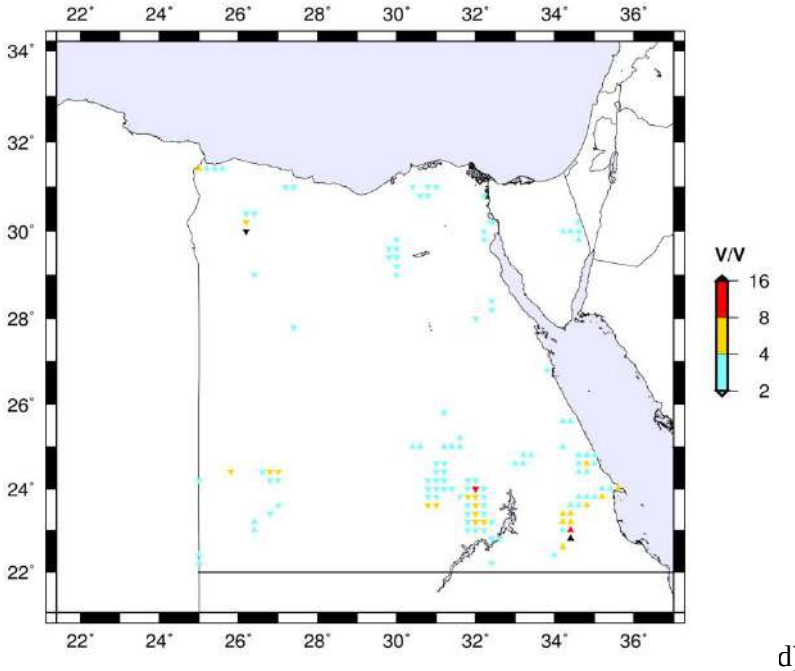
22° 24° 26° 28° 30° 32° 34° 36°
34° 32° 30° 28° 26° 24° 22°
V/V
16
8
4
2

d)

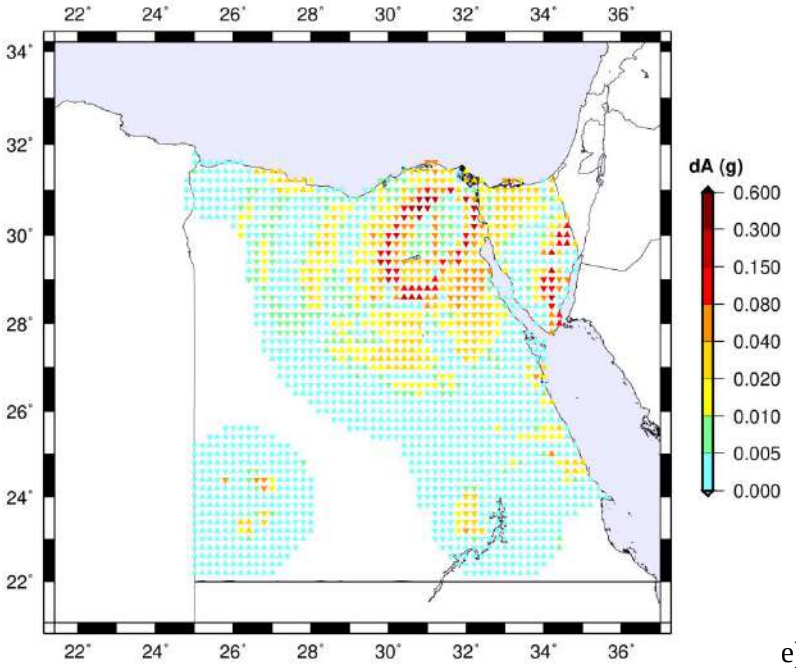
22° 24° 26° 28° 30° 32° 34° 36°
34° 32° 30° 28° 26° 24° 22°
dA (g)
0.600
0.300
0.150
0.080
0.040
0.020
0.010
0.005
0.000

e)

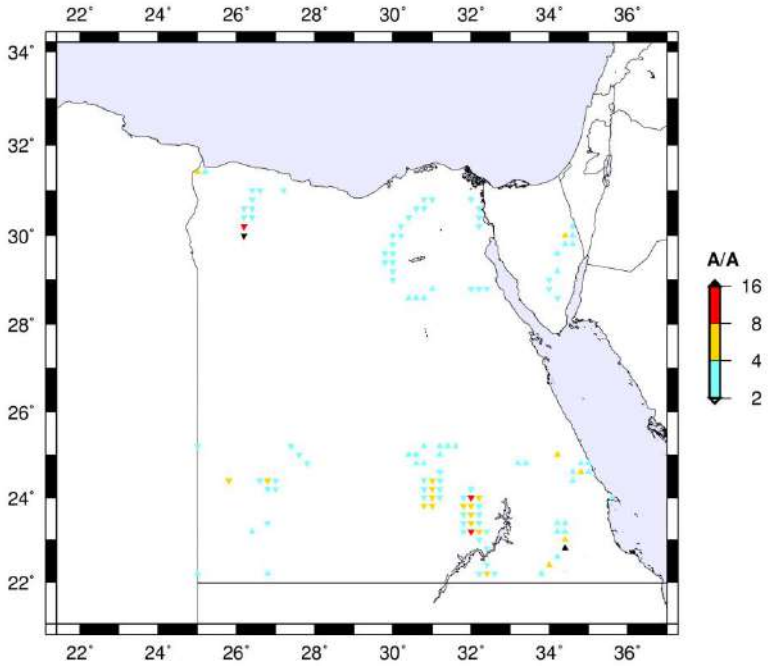

f)

Fig. 3.8: a) Difference in PGD values due to change in seismotectonic zones used in Variants 4 and 3 (dD_{max} = Variant 4 - Variant 3); b) Ratio between PGD values at different sites due to the change in seismotectonic zones used in Variants 4 and 3 (D/D = Variant 4/Variant 3); c) Difference in PGV values due to change in seismotectonic zones used in Variants 4 and 3 (dV_{max} = Variant 4 - Variant 3); d) Ratio between PGV values at different sites due to changes in seismotectonic zones used in Variants 4 and 3 (V/V = Variant 4/Variant 3); e) Difference in DGA values due to change in seismotectonic zones used in Variants 4 and 3 (dA = Variant 4-Variant 3); f) Ratio between DGA values at different sites due to changes in seismotectonic zones used in Variants 4 and 3 (A/A = Variant 4/Variant 3).

3.2.5 *Inclusion of the seismogenic nodes (Variant 5)*

The seismogenic zones adopted in the previous computations cover only the areas marked by past earthquake activity, as evidenced by available historical and instrumental earthquake catalogs. For the areas where the seismicity is not well understood, it is essential to rely on information from other relevant studies. Among these studies, the formalized identification of seismogenic prone sites (seismogenic zones) using MZ and pattern recognition (e.g., Gorshkov et al., 2003; Keilis-Borok and Soloviev, (2013) are particularly useful; Peresan et al., 2014). The result from MZ can be easily incorporated in the seismic hazard computation by the NDSHA.

Seismogenic nodes capable of earthquakes with $M \geq 5.0$ have been identified for the north-east part of Egypt using MZ and pattern recognition (Fig. 3.9) in Chapter 2. The study region includes the Sinai Peninsula and the northern part of the Eastern Desert between the Nile River, and the Red Sea, and exhibits moderate and rare strong seismicity.

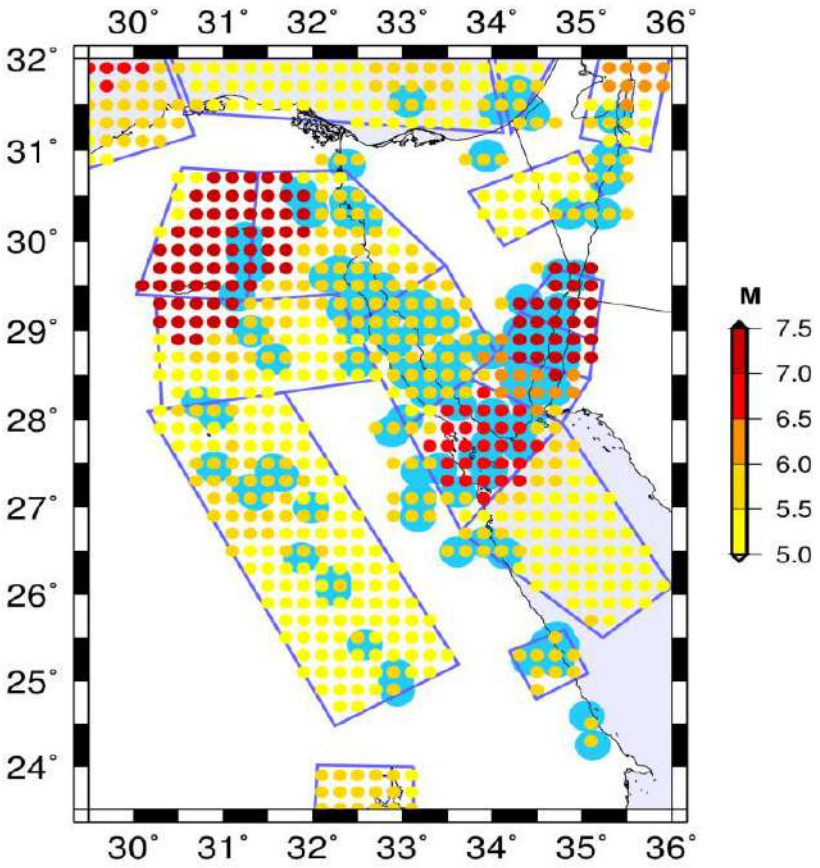

Fig. 3.9: Smoothed magnitude and nodes used in Variant 5.

Here, in addition to the seismogenic nodes, the same input data as in Variant 3 is used. The change in the obtained results is assessed using the maps of differences and ratios between Variant 5 and Variant 3. Focusing on the north-eastern part of Egypt, where seismogenic nodes have been identified, the comparison (difference and ratio) shows a varying increase in the ground motion peak values marked by an upward triangle as shown in Fig. 3.10 (a, b, c, d, e, and f). This change is relatively large in the south of the Sinai Peninsula, along the Nile Valley, along with the Red Sea coast of south-east Egypt, and to a minor extent around the Gulf of Suez and Cairo metropolitan area.

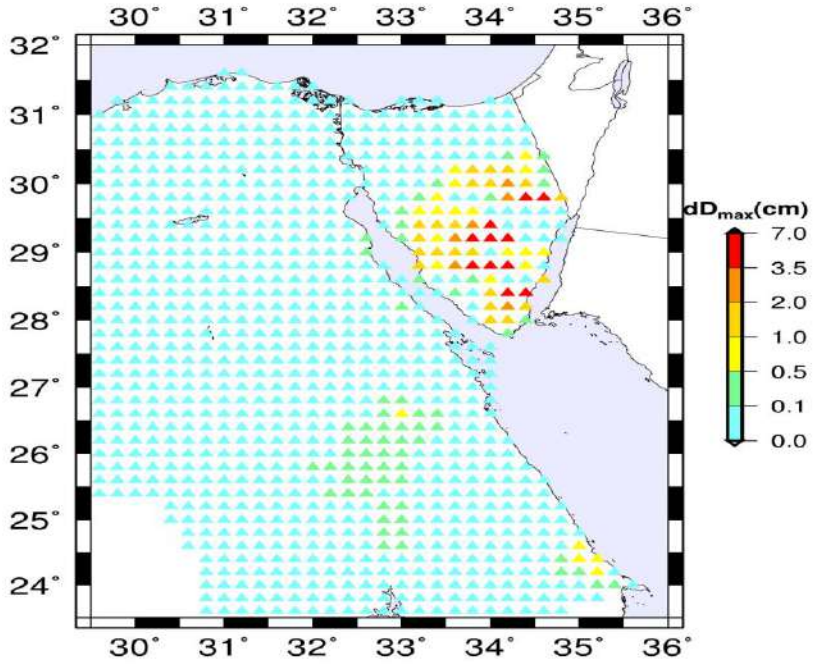
30° 31° 32° 33° 34° 35° 36°
32° 31° 30° 29° 28° 27° 26° 25° 24°
dDmax(cm)
7.0
3.5
2.0
1.0
0.5
0.1
0.0

a)

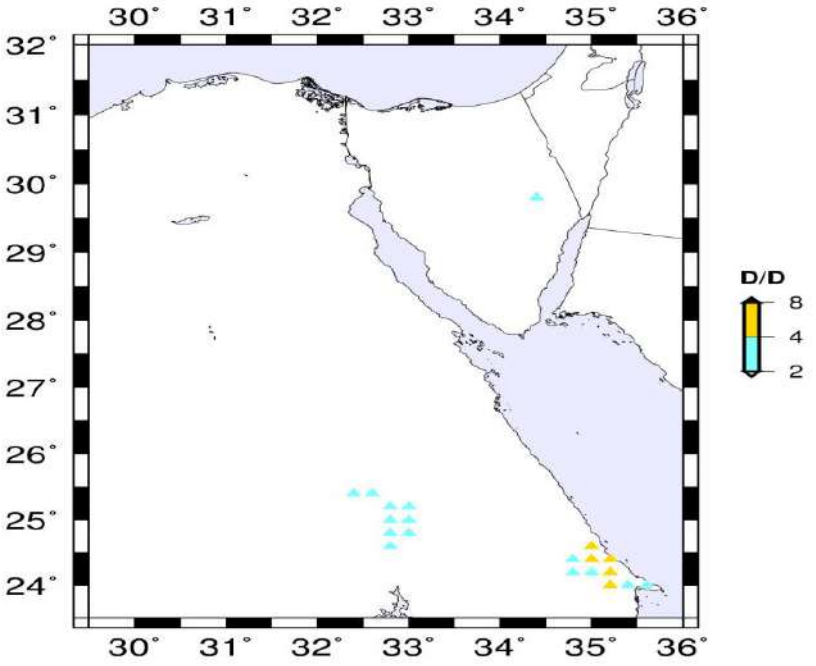
30° 31° 32° 33° 34° 35° 36°
32° 31° 30° 29° 28° 27° 26° 25° 24°
D/D
8
4
2

b)

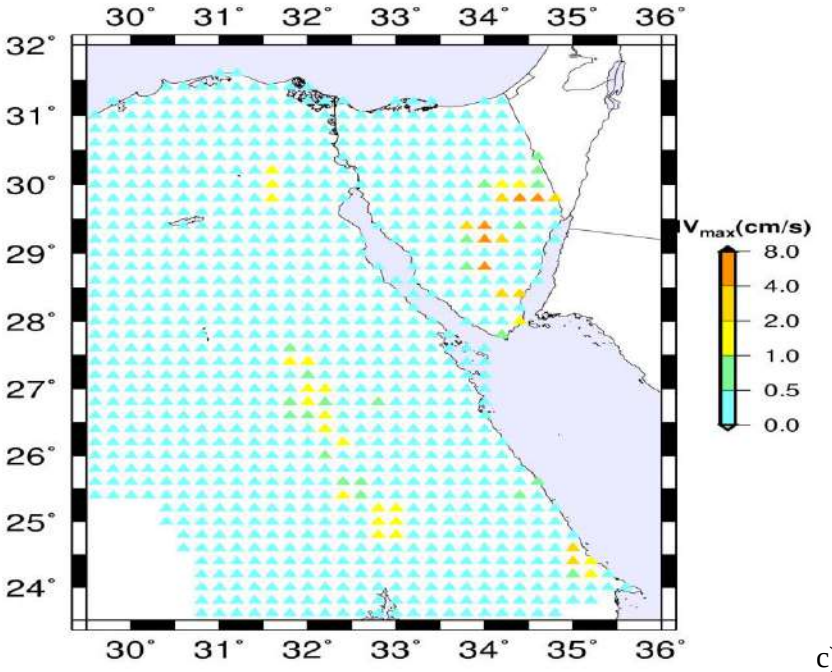
30° 31° 32° 33° 34° 35° 36°
32° 31° 30° 29° 28° 27° 26° 25° 24°
V_{max}(cm/s)
8.0
4.0
2.0
1.0
0.5
0.0

c)

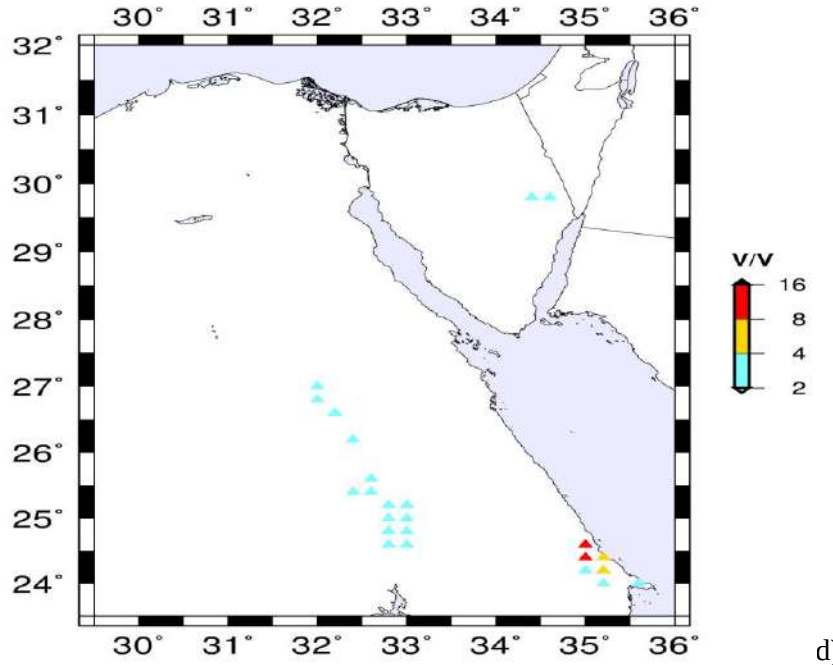
30° 31° 32° 33° 34° 35° 36°
32° 31° 30° 29° 28° 27° 26° 25° 24°
V/V
16
8
4
2

d)

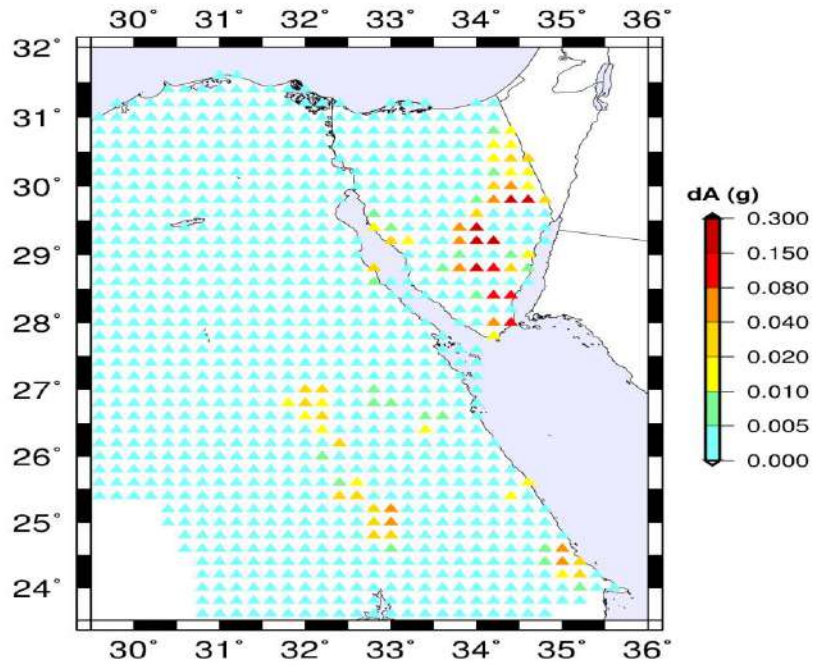

e)

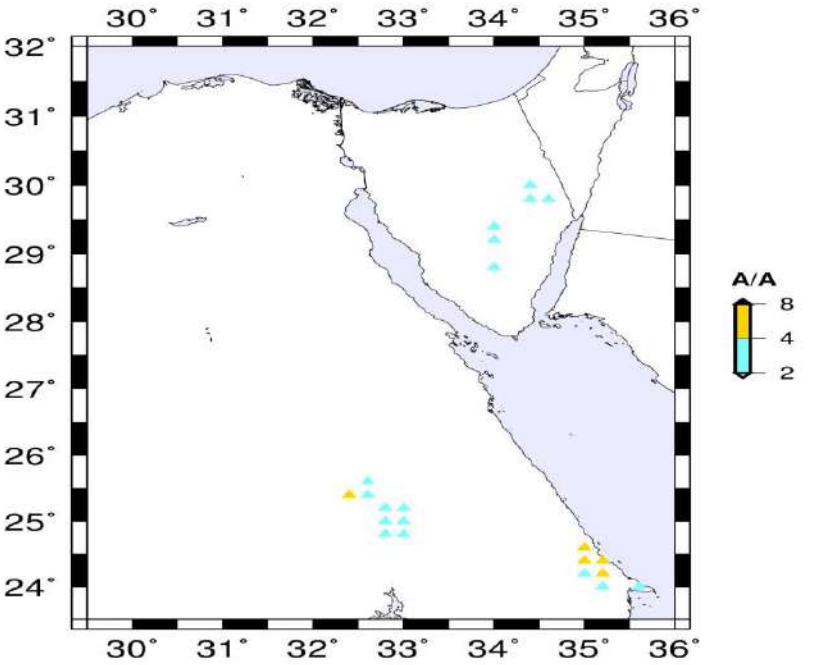

f)

Fig. 3.10: a) Difference in PGD values at different sites between Variant 5 (with seismogenic nodes) and Variant 3 (without seismogenic nodes) (dD_{max} = Variant 5 - Variant 3); b) Ratio between PGD values at different sites between Variant 5 and Variant 3 (D/D = Variant 5 / Variant 3); c) Difference in PGV values at different sites between Variant 5 and Variant 3 (dV_{max} = Variant 5 - Variant 3); d) Ratio between PGV values at different sites between Variant 5 and Variant 3 (V/V = Variant 5 / Variant 3); e) Difference in DGA values at different sites between Variant 5 and Variant 3 (dA = Variant 5 - Variant 3); f) Ratio between DGA values at different sites between Variant 5 and Variant 3 (A/A = Variant 5 / Variant 3).

This Chapter illustrates the influence of adopting new information about earthquake activity, different source models and a wide range of preconceptions on

the computed seismic hazard maps for Egypt to provide potential users with an adequate wide spectrum of choices and to reliably assess and communicate the possible uncertainty. The updated seismic hazard maps for Egypt that incorporated all available information are presented in Fig. 3.11 (a, b and c).

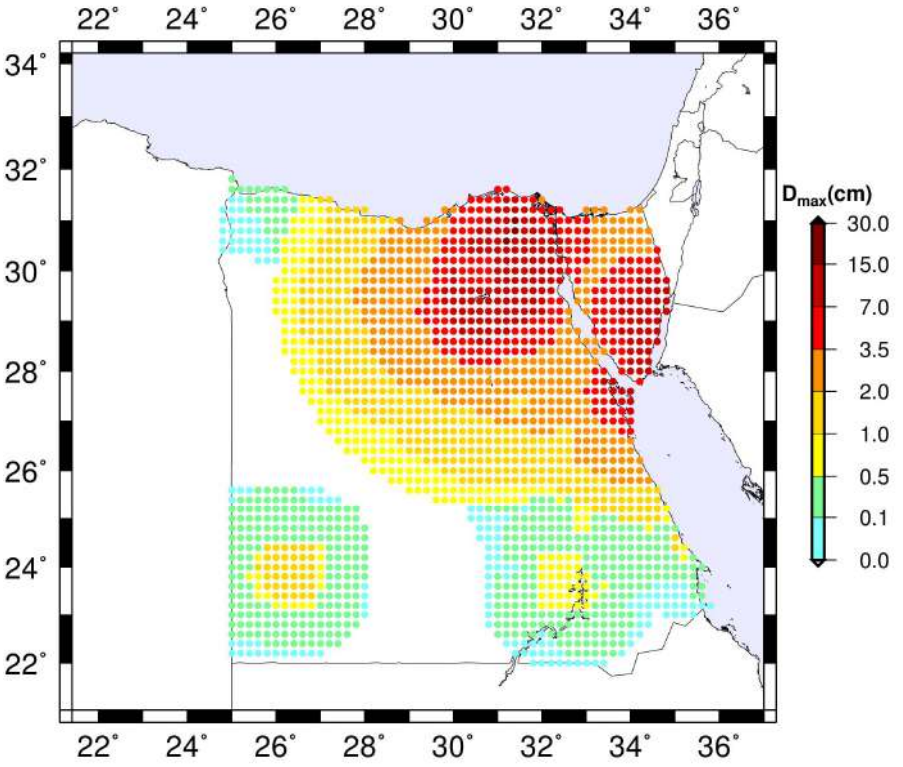

a)

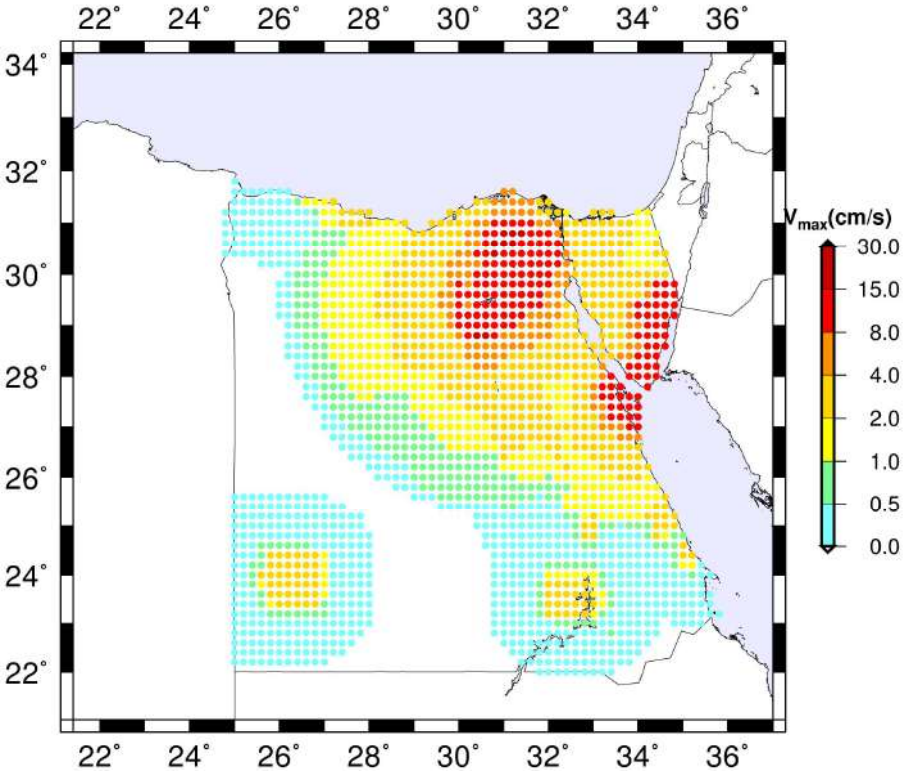

b)

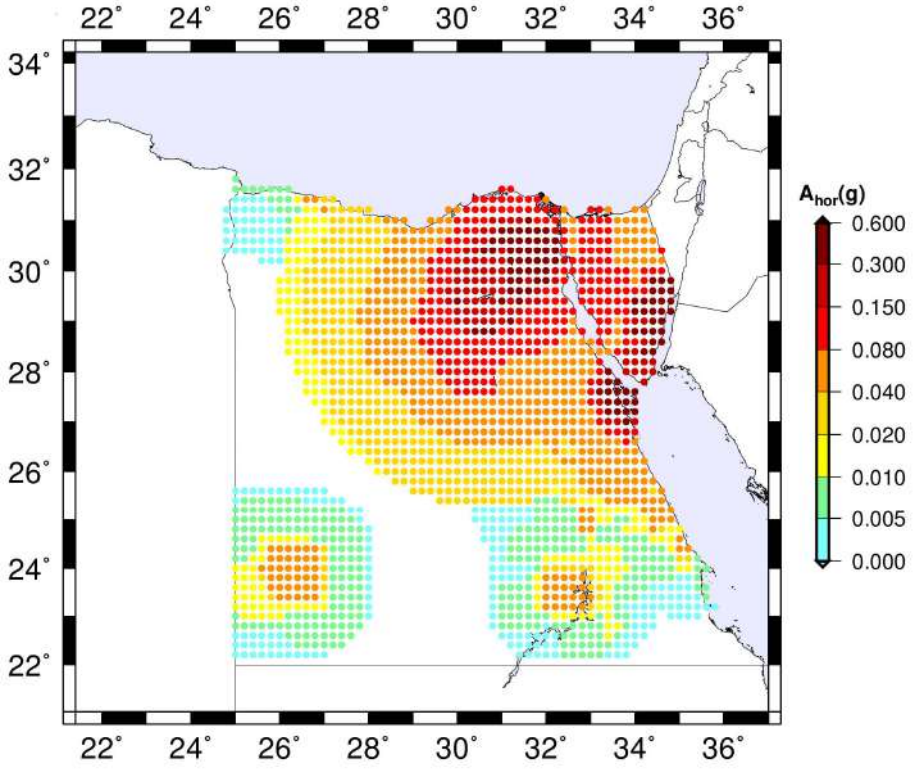

c)

Fig. 3.11: a) Peak ground displacement (D_{max}) map (Variant 5); b) Peak ground velocity (V_{max}) map (Variant 5); c) Maximum horizontal acceleration (A_{hor}) map (Variant 5).

A single map cannot supply useful enough answers to all the problems posed by adequate seismic risk assessment. The NDSHA approach provides a big database of synthetic seismograms for each configuration, particularly crucial for the regions that suffer from endemic lack of strong motion time histories. The synthetic seismograms can be computed with a cut-off frequency as large as 10Hz for a set of laterally non-varying structural models, where the fault finiteness is duly taken into account by size and time scaled point source (STSPS) model (Parvez et al., 2011), computed with ***PULSYN06*** algorithm (Gusev, 2011, Magrin et al., 2016) that provides a broadband kinematic source model.

NDSHA estimates the earthquake ground motions as a tensor product (of earthquake source tensor with the Greens function for the medium) and it avoids using an approximate scalar quantity implied in the GMPEs and/or attenuation relationships (Panza et al., 2014).

Magrin et al. (2016) have compared the results of national scale NDSHA modeling for the Italian region at 10Hz cut-off, based on the relevant available knowledge, with observations (e.g., peak ground motion values) and existing GMPE in order to test the NDSHA modeling procedure. They conclude that the adoption of a new set of scaling laws of source spectra produces acceptable results in terms of PGV and spectral acceleration (SA). The synthetic PGA and SA at higher frequency attenuate faster than the observed ones; this could be the effect of complex attenuation factors and this problem will be addressed in a forthcoming Chapter.

NDSHA aims to supply an envelope value, in other words, hat indicated by NDSHA it is necessary to measure the variance. If it turns a value that should not be exceeded, therefore it is immediately falsifiable and verifiable: if an earthquake occurs with a magnitude larger than that indicated by NDSHA, it is necessary to measure the variance. If it turns out to be larger than the multiple of standard deviation used to define MCE, for instance (Dominique and Andre, 2000) equal to the maximum observed magnitude plus $2\sigma=0.5$, then maps are immediately falsified; similarly if the peak values (e.g., PGA) recorded at the bedrock at the occurrence of an earthquake after the compilation of NDSHA maps exceed, within error limits, those given in the same maps. When used, the cut-off frequency of 1Hz, is not imposed by a technical limitation of the computational algorithm (Panza et al., 2012; Magrin et al., 2016) but is a cautious choice, entirely consistent with the resolution and present-day knowledge of the physical properties of the rock/soil and the

attenuation parameters available for the studied region. In the computation, to reliably estimate the DGA from SA at 1Hz, we used the shape of the design code of Egypt to extend the modeling results at a frequency higher than 1 Hz following the scheme of Panza et al. (2001). The computation at 10 Hz cut-off frequency is the primary focus of the ongoing work at the local scale, for selected areas in Egypt.

The results obtained in this Chapter represent a database toward detailed and comprehensive ground motion modeling in historic Cairo area which is the primary focus of Chapter 4. The Fig. 3.12 (a, b, and c) shows the sources that contribute the peak ground motion values at the sites where synthetic seismograms have been computed. These maps are used in Chapter 4 in order to define the earthquake scenarios to be considered for detailed local site investigation or parametric studies (e.g., effects of considering more rupture process (slip distribution and rupture velocity) realizations and of change in focal mechanisms). Parametric studies are crucial to identify the parameters (e.g., fault configuration, focal depth) that could cause the maximum ground motion at the site (or MCE). In fact, the use of the parameters that characterize the MHE proved to be inadequate (Cultrera et al., 2010).

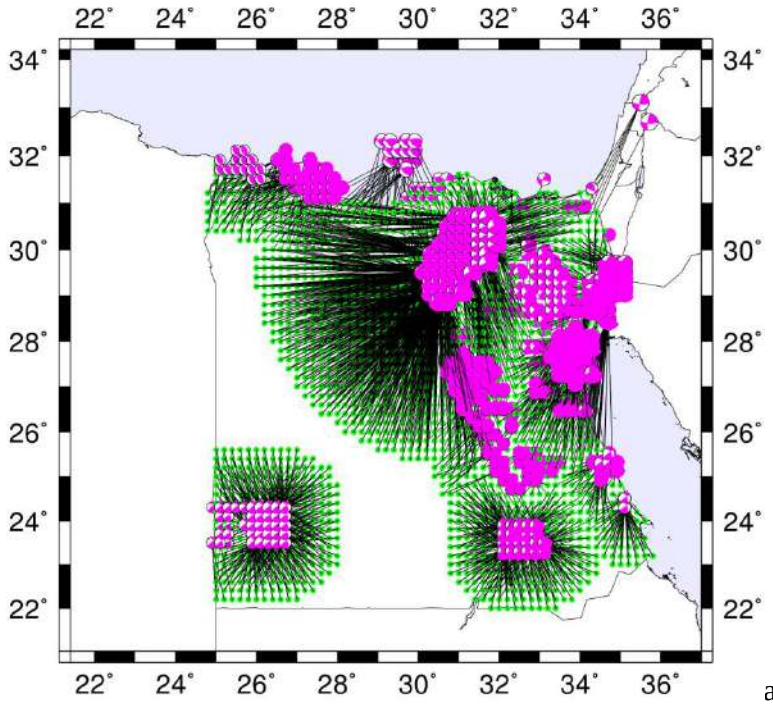

a)

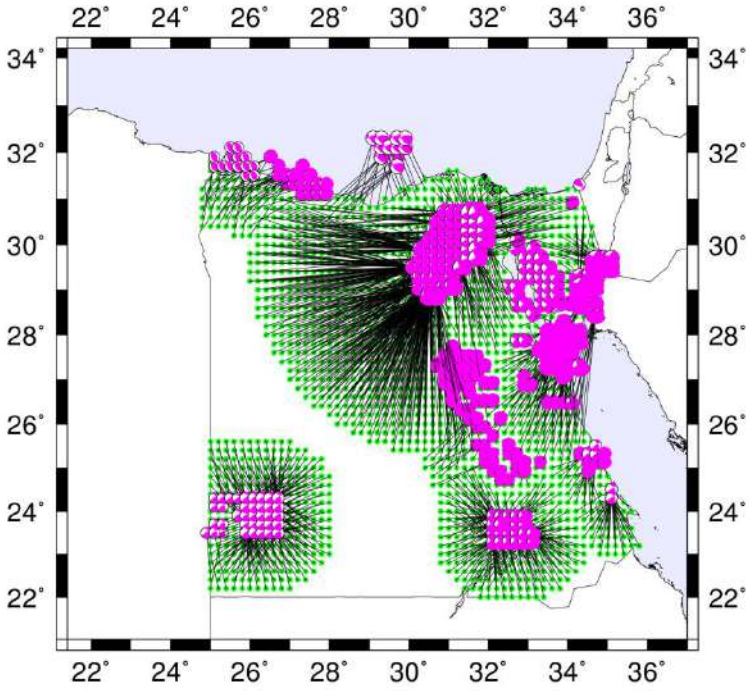

b)

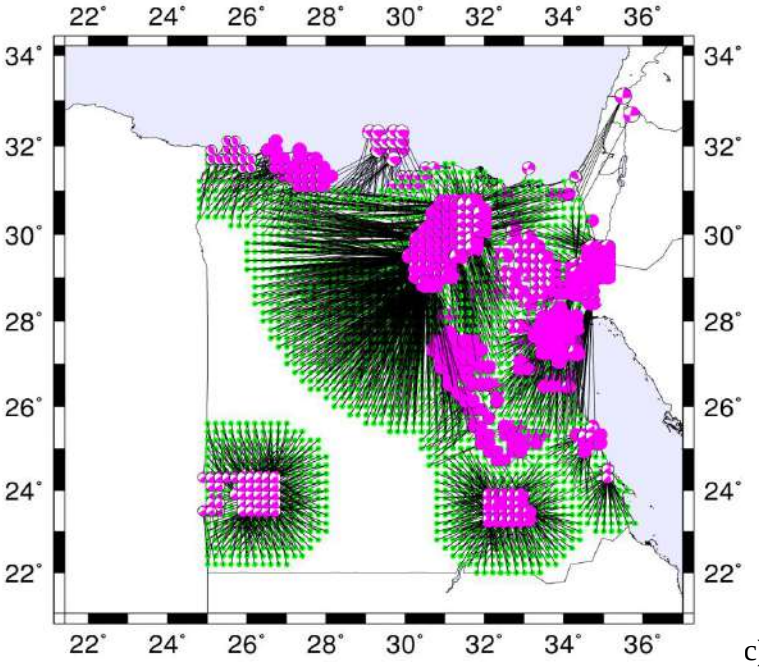

c)

Fig. 3.12: Sources which contribute to the peak values i.e., a) displacements; b) velocity; c) acceleration; at each site.

Chapter 4

Site-Specific Ground Motion Modeling for Historical Cairo

4.1 Introduction

Cairo is Egypt's capital and largest city, with its metropolitan area populated by more than 10 million inhabitants. The city of Cairo is culturally complex and stratified witnessing different historical periods throughout its long history. It comprises many cultural heritage sites of different ages and represents an open museum with ancient Egyptian, Greco-Roman, Coptic and Islamic monuments. The history of the city dates back to the foundation of the ancient Egyptian city of Ayn Shams or Heliopolis, the oldest of the ancient capitals. Cairo city, in its current form, dates back to the Islamic conquest of Egypt by Amr ibn al-Aas in 641.

Historic Cairo is located east of the modern city and a metropolis that contains the remnants of Fatimid Cairo in addition to Fustat, al-Askar, and al-Qatta'I, which were capitals before al-Qahira (Cairo). It comprises many archaeological sites such as the Hanging Church, one of the oldest churches in Egypt and the mosque of Amr ibn al-Aas, the oldest mosque in Africa and many other residential, administrative, and public service buildings in addition to many mosques, madrasas, hammams and fountains that are registered as UNESCO World Cultural Heritage. The redundancy of historical monuments belonging to different cultures and eras has made the historic Cairo the destination of many tourists who are interested in the history of Egypt. Many monuments of historic Cairo are now suffering from severe deterioration due to the effect of several factors (e.g., groundwater, poor building condition, inadequate seismic resistance, lack of maintenance, protection, and preservation policies). These factors can combine together and form irreparable and challenging situation for some monuments that made them very vulnerable to even intermediate seismic hazard.

On 12 October 1992, an earthquake with M_w = 5.9 occurred near Dahshur, Egypt (about 20 km southwest Cairo), as reported by the U.S. Geological Survey

(USGS) and National Earthquake Information Center (NEIC). This earthquake was felt throughout most of Egypt, as far south as Aswan, Egypt, (670km). The maximum observed intensity was VIII on Modified Mercalli Intensity scale (MMI) (Fig. 4.1) and the epicenter coordinates of this event, its basic characteristics, and the fault orientation of the earthquake are presented in Table 4.1. More than 500 people killed, 6,500 injured, and 8,300 buildings had damaged or destroyed due to this earthquake.

According to Sykora et al. (1993), about 212 monuments in Cairo were reportedly damaged. The distance from the epicenter of the 1992 Dahshur earthquake to the historic Coptic and Islamic districts in Cairo city, known as "Historic Cairo," ranges from 13 to 30km. Although this earthquake was of intermediate size, strong impacts were observed in Cairo. In fact, the observed damages could be due to a combination of different factors besides the earthquake ground motion: 1) proximity of the earthquake epicenter to Cairo city; 2) propagation effects; 3) site amplification; 4) high vulnerability of buildings. The intensity map of the 1992 earthquake (Fig. 4.1) compiled by Thenhaus et al. (1993) shows an intensity between VI and VII on the for the historic district of Cairo. Therefore, it is essential to study the site-effects to better investigate the behavior of monumental structures during the earthquake loading by defining the levels of seismic action for which no harm may result and to propose some retrofitting policies, for the case when these levels are exceeded.

The recently occurred large earthquakes worldwide have evidenced the profound effects the site conditions on the spatial distribution of earthquake damages (e.g., September 19, 2017, 7.1 Puebla, Mexico earthquake). Ambraseys (2001) has studied the decay of intensity with a distance of earthquakes (after 1900) originating in the southern part of the Aegean, offshore Egypt and the Eastern Mediterranean regions (originated in the Hellenic arc with epicentral distances ranging between 300-1200km) on Lower Egypt region. He concluded that the resultant ground shaking from large earthquakes (~ 5.5+), of shallow to intermediate focal depth, are capable of causing some concern and occasionally some damage in the region of North Egypt (e.g., Mediterranean earthquakes of February 17, 1810, 7.5M and September 12, 1955, 6.1M_w). In contrary, earthquakes of similar magnitudes occurred along the Gulfs of Suez and Aqaba and the Red Sea (1969, Shedwan earthquake, 6.9M_w and 1995, Aqaba earthquake, 7.2M_w) had also been felt in the North Egypt region but no significant damage was observed. The comparison between the two sources indicates that the Mediterranean earthquakes attenuate less to the south than respect to the north

producing damages in North Egypt, while earthquakes originate at the eastern side of the country are encountering a high attenuation along their path due to the presence of the Red Sea Mountain Ranges. Also, the comparison reveals that the direction from which the waves are coming in combination with the geometry of subsurface structures and local site conditions can yield strong ground motion in the North Egypt region; if this is the case for far-field earthquakes, we may expect stronger effects from local earthquakes of even smaller size.

Moreover, the presence of a loose low-velocity layer of mound structure at the top of the Nile sediments underneath Cairo area beside the reasons mentioned above are the main motive for carrying out detailed and accurate assessment of site-effects, which is the primary target of this Chapter. Thus, the proper site-specific analysis (SSA) that takes into account the ingredients that influence site amplification (e.g., resonance, surface and subsurface topography, the geometry of the sedimentary layers, wave conversions) is due in order to compute the reliable seismic input at the site of the interest. The SSA in role will help the engineers in studying the dynamic response of the built structure then finding and selecting the proper mitigation. Moreover, the results from SSA are essential for reducing the possible socio-economic losses in the study area from future earthquakes.

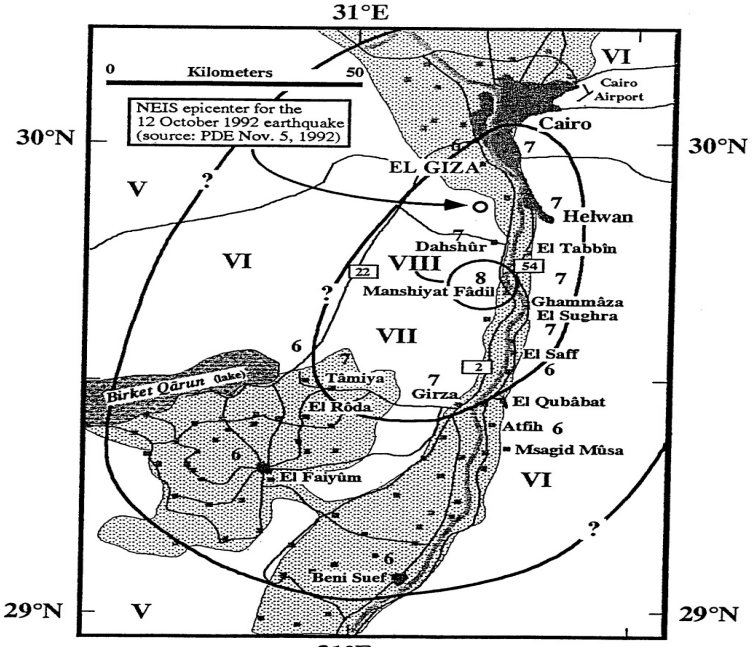

Fig. 4.1: Intensity map of October 12, 1992 Dahshur earthquake, after Thenhaus et al. (1993).

Few noise-based studies have shed light on seismic site-response in Cairo (e.g., Gamal, 2009). In fact, noise-based methods (e.g., H/V) alone cannot adequately provide an accurate estimation of the ground motion modification. An alternative techniques, which are based on the scenario-based approaches that overcome the limitation of using the empirical methods only, is required in order to accurately define the amplification patterns (site-effects) in urban areas. This is crucial for the finding and selection of the reasonable mitigation measures for historical Cairo area, that requires a detailed investigation of the local site conditions and the realistic assessment of their possible effects. El-Sayed et al. (2004) and Kebeasy and Husebye (2003) have studied the site-effects for specific sites that are located south Cairo using the scenario-based approach and they conclude that the loose sediments of the Nile Valley and the Nile Delta can strongly amplify the seismic ground motion from far and near-field earthquakes. Therefore, the pre-event strong ground motion modeling in a megacity like Cairo is essential and indispensable for reducing the potential socio-economic impacts from future earthquakes.

This Chapter aims to provide a specific focus on the site characterization for the historic Cairo area which hosts a large number of invaluable value heritage buildings, through the detailed ground motion modeling for site effects using scenario-based detailed ground motion modeling. The results obtained in this Chapter represent an essential and forward step toward the proper assessment of dynamic behavior under earthquake action, which in turn might lead to preservation and risk reduction for the existing cultural heritage structures by combining both scientific and engineering knowledge. Moreover, the obtained results could be useful for residential buildings in the historic Cairo area, as well.

4.2 Geology and seismicity of Cairo area

Cairo area stretches along both sides of the Nile River at about 20km south of the location where the river divides into the Rosetta and Damietta branches. The city entirely lies on the floodplain of the Nile River with a width of about 12km from Mokattam hills on the southeast to the pyramids plateau on the west. The surface geology of the city consists some formations that represent different geologic age are (Fig. 4.2). The oldest rocks are exposed in Abu Roash and Pyramids of Gizeh and belong to the Cretaceous period. Eocene formation, composed of limestone, outcrops in the Mokattam hills in the east and Pyramids plateau in the west. The Oligocene in

the area is represented by two different facies: sands and gravels of the Gebel Ahmer type and Basalt flow. The Miocene is composed of marine sediments, made up of sandy limestone and sands enriched with fossils, outcrops in northeast Cairo area. Finally, the Pliocene marine deposits, exposed south of the Sphinx ditch, are represented by marls and sandy limestone beds. The detailed description of the surface geology of the city is discussed in Said (1975), Shata (1988), Said (1990) and Said (2012).

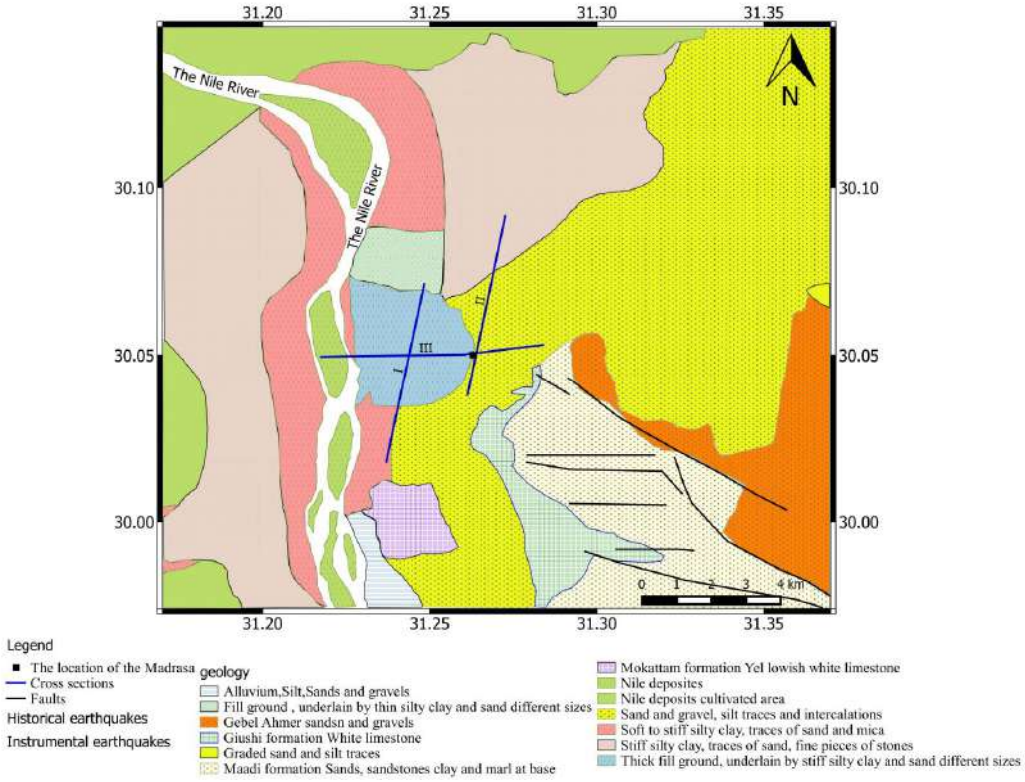

Fig. 4.2: Surface geology and seismicity of the study area combined with the location of the considered profiles.

The landscape of areas around Cairo (east and west) is profoundly affected by different fault systems (EGSMA, 1981; Said, 1990) and the most predominant ones are those of EW (Mediterranean trend) and NW - SE (Claysmic trend) trends; these trends are reported on both surface and subsurface of Cairo area. The faults are mainly normal, with steep planes, and form a portion of a graben and horst complex (Shata, 1988). Minor folding associated with faulting is identified in Gebel Mokattam and east Heliopolis areas. In Abu Roash the dominant geologic structure is folding which is a part of the Syrian arc system, a system of folds crossing the unstable shelf area of northern Egypt (Shata, 1988). Said (1981) has shown that the basin, having a

depth of about 2.5km, was fault-bounded and it was subsequently eroded by the Eonile in late Miocene.

The spatial distribution of earthquakes in Egypt shows that most of the seismic activities are concentrated in the northern part of Egypt. The seismicity map of the region, which is shown in Fig. 4.3, demonstrate that the Cairo area is surrounded by some of active seismic sources, i.e., Dahshur and the Cairo-Suez district sources. The available records for the historical earthquake in northern Egypt go back for 4,000 years ago with differing completeness levels; the first documented earthquake is believed to occur around 2200 B.C (Kebeasy and Maamoun, 1981). The history of felt earthquake motions at Cairo indicates that moderate, or higher, levels of shaking occur rather infrequently.

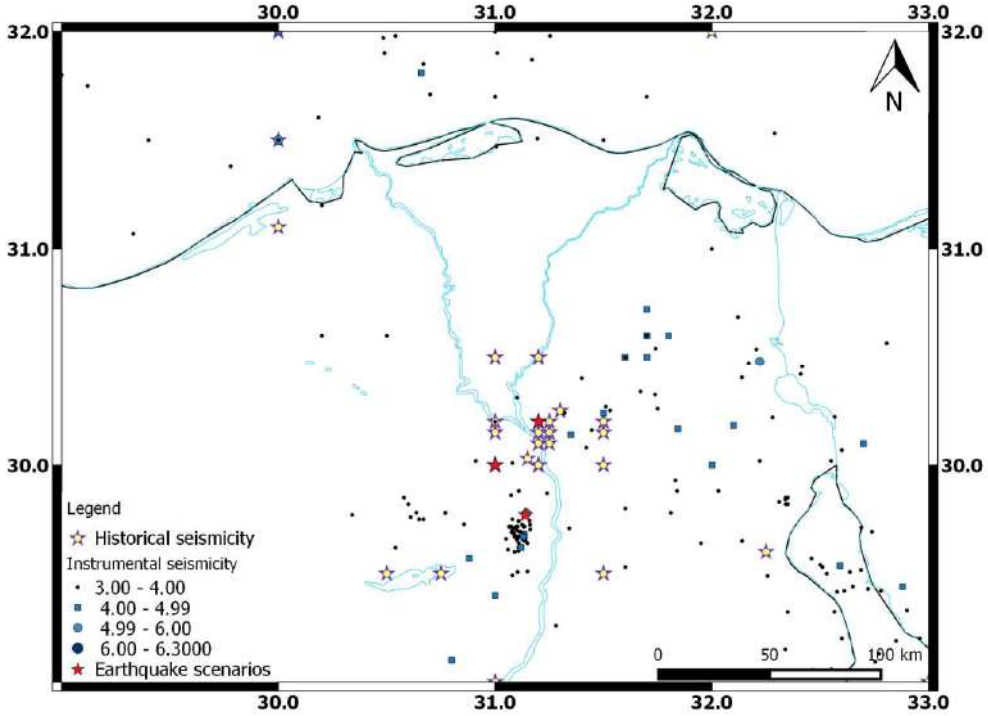

Fig. 4.3: Seismicity and considered earthquake scenarios of the study area.

In fact, the available historical reports about earthquake impacts in the Cairo area are long in time and varying in details and are exhibiting the strong earthquake impacts in the past and the recent times. The available understanding about the location of the seismic sources which are responsible for the damage being experienced is pointing to near and far-field sources (e.g., Dahshur seismic source, Eastern Mediterranean, and the Dead Sea fault system).

4.3 Site-specific seismic hazard assessment

Earthquake (weak or strong events) based seismic zonation/microzonation for a specific area can be performed throughout empirical seismic methods. This need a vast dataset of strong motion records from all the potential earthquake sources in the vicinity of the site of interest. Also, for the characterization of site-effect the realistic modeling of the ground motion scenarios developed from the physical knowledge of seismic waves generation and propagation can be used. In some circumstances, the use of empirical methods for a given site is not possible, because of the endemic lack of ground motion records for the region of interest. Correspondingly, the usage of the seismic noise measurements methods to infer the site resonance is challenging for areas of a dense population such as historical Cairo and they may not fully reveal the tensor nature and of earthquake ground motion and the amplification pattern of the site. Since, the available database is not yet adequate for seismic microzonation and needs more time to be suitable enough, a preventive tool, i.e., NDSHA, applied at local scale, is ready to be used before the occurrence of strong earthquakes in the future. This could help in reducing the risks from the impending earthquakes (see Panza et al., 2001; Panza et al., 2012; Magrin et al., 2016 and the references therein).

In Chapter 3, a set of seismic hazard maps computed within the framework of NDSHA procedure are provided at a national scale that effectively accommodated any new information to calculate the ground shaking maps adequately. The current Chapter represents an extension for Chapter 3 since it uses the same earthquake scenarios responsible for the peak ground motion parameters at the study area, which is predefined in the previous Chapter.

To compute the seismic input (realistic synthetic time histories) needed in the engineering analysis of relevant structures, e.g., infrastructures, historical and critical buildings further investigations should be performed taking into account the source effects and local soil conditions,

In this Chapter, the map of the seismic sources (Fig. 4.4) that contribute to peak ground motion values at historic Cairo area sites obtained using the NDSHA approach (Hassan et al., 2017b) is used for the definition of the earthquake scenarios that could affect a given site. This is needed to be considered for the detailed SSA studies to investigate the modification of the ground motion parameters due to the source, propagation medium, and the possible local site conditions.

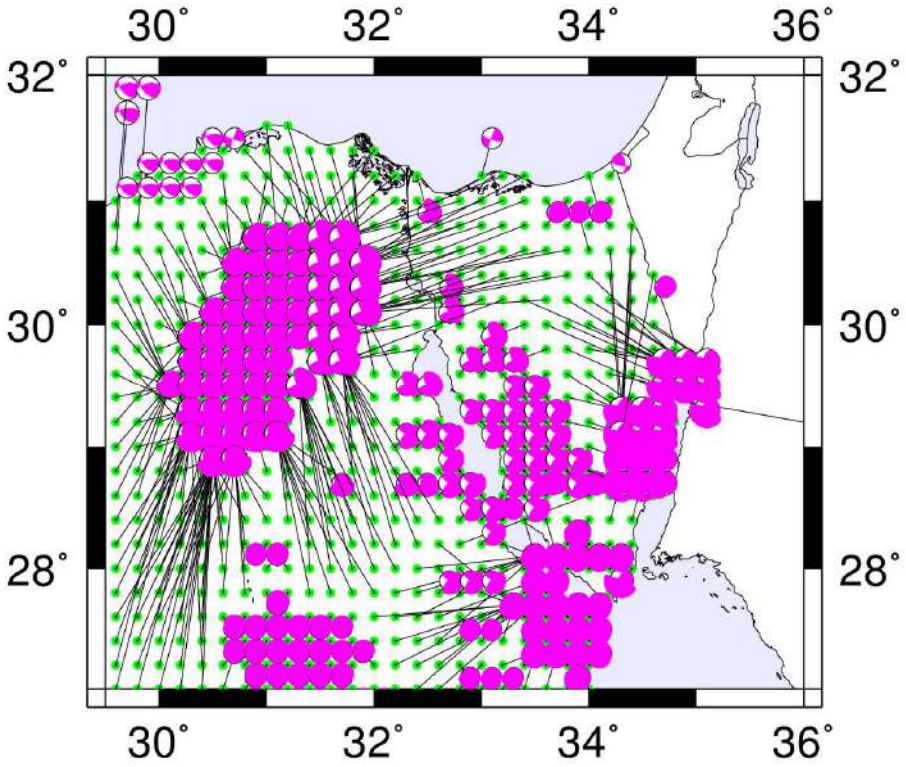

Fig. 4.4: Earthquake sources that contribute to the peak ground acceleration for north-east Egypt. Green dots indicate the sites; purple balls represent the earthquake scenarios.

The available surface and subsurface geological, geophysical, seismological, MZ, and seismotectonic data for a specific site can be used to realistically generate the synthetic seismograms from all the possible seismic sources that could affect the site of interest (Panza et al., 2001)), as illustrated by the scheme in Fig. 4.5. A hybrid technique (Fäh et al., 1993; Panza et al., 2001) that combines both modal summation (MS) and finite differences (FD) techniques (Fig. 4.6), is used to simulate the ground motion induced in laterally heterogeneous structural models at the selected sites.

This approach has been successfully applied for microzonation purpose using the NDSHA approach in several urban areas around the world, e.g., Rome (Fäh et al., 1993), (Beijing (Sun et al., 1998), Naples (Nunziata et al., 2000), Delhi (Parvez et al., 2004), Sofia (Slavov et al., 2004). Each of the two modeling methods, i.e., MS and FD, is applied in the part of the structural model where it works most efficiently:

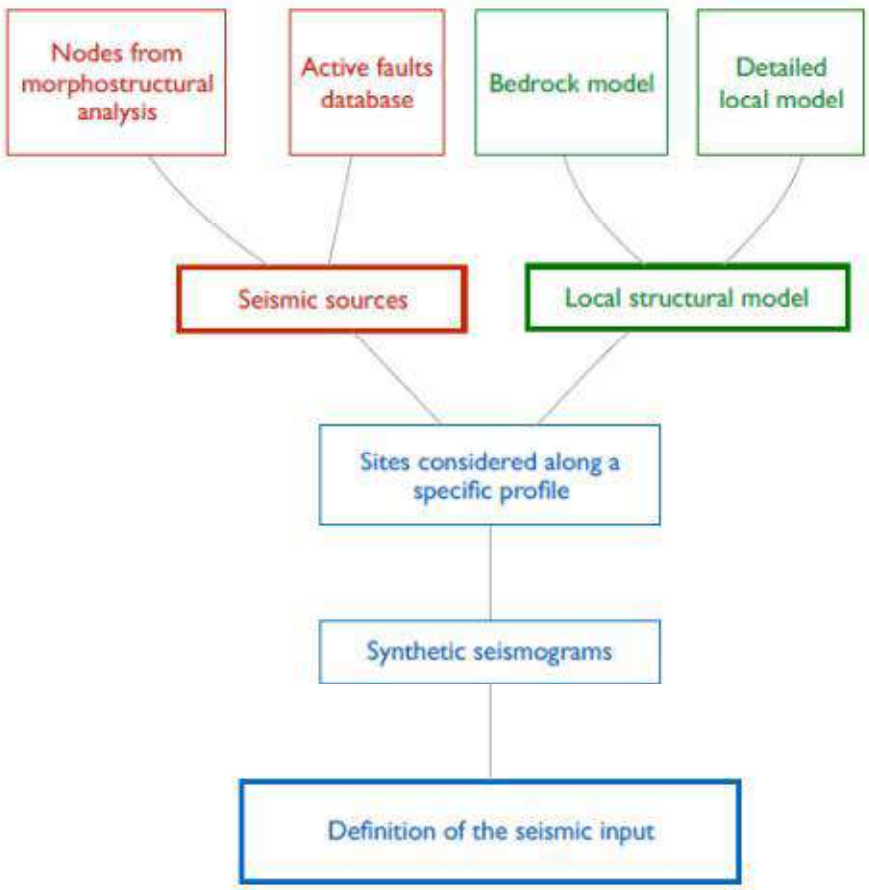

Fig. 4.5: Flow chart of the Neo-deterministic for seismic hazard assessment at the local scale.

The MS technique is applied to simulate wave propagation from the source to the sedimentary basin of interest (profiles of the lateral heterogeneity), while the FD method is used to propagate the incoming wavefield in the laterally heterogeneous part of the structural model that contains the sedimentary basin. The way from the seismic source position to the local heterogeneous structure of interest is approximated by a structure composed of laterally homogeneous layers (1D). The coupling of the two methods is carried out by introducing the resulting time histories obtained with the MS into the FD computations, used to model wave propagation in the laterally heterogeneous part of the model. For the application of the FD technique, the local structure is discretized into a mesh, whose step has to be small enough so that there are at least ten points per wavelength.

Ground motion amplification patterns are obtained according to the scheme shown in Fig 4.7. At each site along the profile, two seismograms are computed for each component of motion, and their response spectra (RS): RS_{1D} for the reference

bedrock model and RS_{2D} for the laterally heterogeneous 2D model. The ratio RS_{2D}/RS_{1D} (RSR 2D/1D) at that site provides the amplification expected at different frequencies due to the characteristics of the local structure. The procedure is repeated for all the sites along the profile so that the general amplification pattern is obtained by contouring the distribution of amplification value along the profile as a function of frequency and distance along the profile.

It worth mention, that the following computations are linear. The linearity between stress and strain is no longer valid for higher acceleration values. Due to nonlinearity, the shear wave velocity decreases with stress increase, which in role lead to more energy loss. As a consequence, the resonance frequency of the soil can be shifted to lower frequencies and also can lead to lower amplification at higher frequencies.

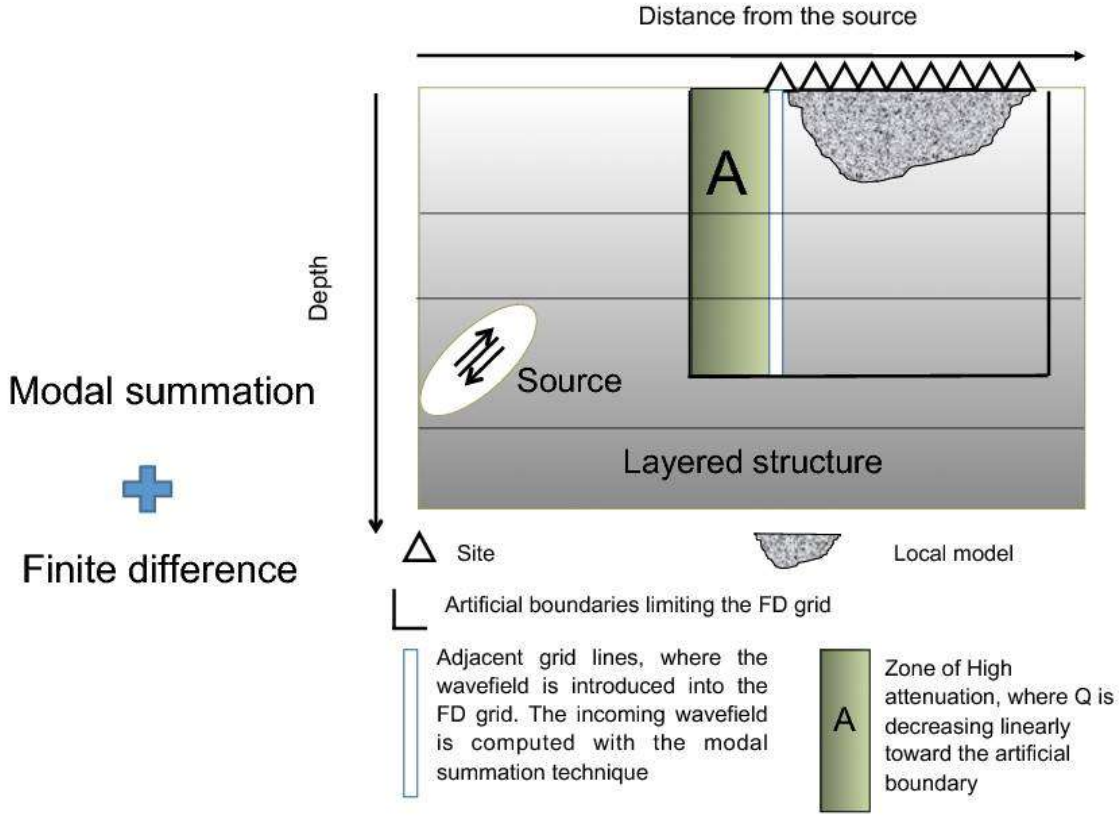

Fig. 4.6: Scheme of the hybrid technique.

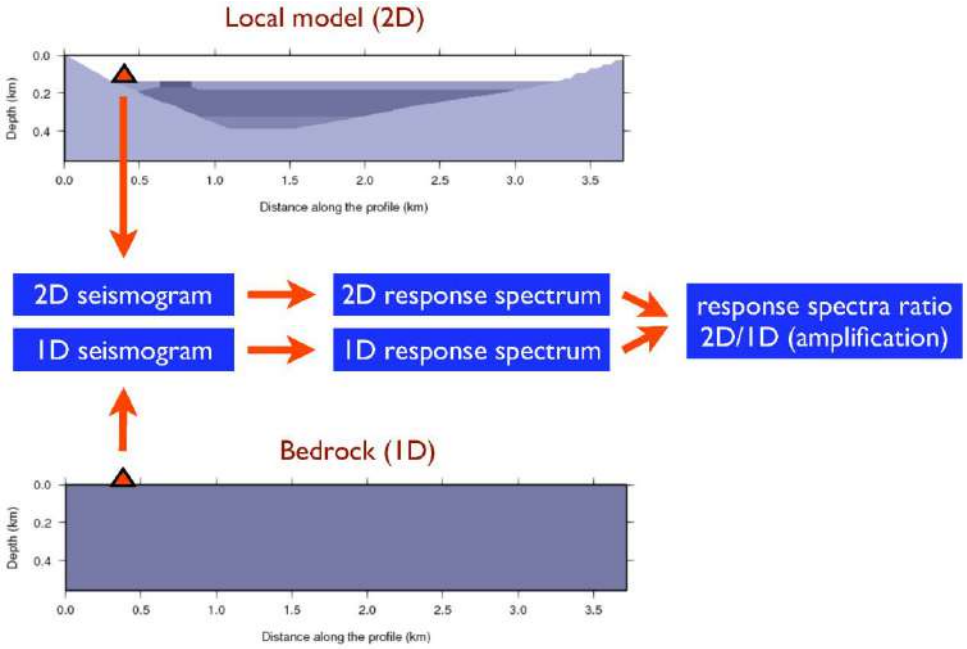

Fig. 4.7: Scheme for the estimation of site responses pattern along a profile.

4.4 Earthquake scenarios

In this Chapter, synthetic seismograms are computed up to 8Hz cut-off, using a point source represented by a double-couple of forces placed at the hypocenter. Besides the hypocentral depth and the magnitude, the other seismic source parameters are reported in Table 4.1. The considered scenarios comprise one instrumental and two historical ones. October 12, 1992, is one of the adopted seismic sources in the modeling of NS cross-sections (I and II, Fig. 4.2), and could help in the validation of the results obtained through the comparison of the obtained ground motion parameters at the free field with the observed intensity. The other two nearby events to the area of historic Cairo of interest are labeled as 857 (this event is assumed in the modeling along the EW cross-sections) and 950 with M~ 6.5-7.0, according to the revised historical earthquake catalog of Badawy et al. (2010).

Parametric studies are crucial in identifying the earthquake parameters that could cause the maximum ground motion at a given site. Romanelli and Vaccari (1999) and Lokmer et al. (2002) showed that the focal mechanism of earthquake scenario could play a crucial role in the modification of seismic ground motion at a given site, sometimes dominating the effects of the local structure itself. This can be done considering several rupture process realizations for each earthquake scenario, different focal depths and fault orientations and taking envelopes of averages and of

upper extremes or any other representative value of the parameters describing the hazard itself, extracted from the synthetic signals, which can be calibrated against the available records if any. The adoption of the average, percentiles or the maximum of ground motion parameters can be decided by the engineers, based on the target performance level for the structure of interest. Besides the hypocentral depth and the magnitude, the other seismic source parameters are reported in Table 1.

Table 4.1: Parameters of scenario earthquakes adopted in this study compiled from the study of Abu El-Nader (2010).

Scenarios		**Location**		**Magnitude**	**Focal depth (km)**	**Focal mechanism**			**Cross-sections**	**Place of the Source**	**Epicentral distance (km)**
No	Date	Lat	Lon			Strike°	Dip°	Rake°			
1	12 October 1992	29.74	31.63	5.9	20	285	66	-117	I (NS)	South	26
									II (NS)	South	30
2	25 July 950	30.20	31.20	6.5 - 7.0	15	136	42	-75	I (NS)	North	20
									II (NS)	North	15
3	April 857	30.00	31.00	6.5 - 7.0	15	136	42	-75	III (EW)	West	22

4.5 Cross-sections along the area of historic Cairo

There can be significant differences in local site conditions from one location to another due to variations in geological formations, thickness, properties of soil/rock layers, depth of bedrock, water table elevation and surface and underground topography. These variations can have significant effects on the characteristics of earthquake motions on the ground surface.

The laterally heterogeneous profiles of the local site conditions have been composed using data from the literature (Fig. 4.9). Detailed 2D subsurface soil cross-sections representing the site conditions beneath most of the monuments have been introduced by Said (1975), based on data of 217 shallow boreholes, which are used for building the local 2D model needed for the site-specific ground motion modeling. These cross-sections are composed of fill overlying silty clay with thick sand and gravel layers beneath varying vertically and horizontally in the studied area. The average depth of the profiles developed by Said (1975) is about 60m below the MSL, and then they have been further extended below, to approximate the bedrock depth

(~120 m), based on the study of Toni (2012). The details of the physical properties of the profiles are adopted after Toni (2012). The quality factors for P- and S-waves for different soil types are taken using standard compilations. A Pleistocene-age plastic clay unit is believed to underlay the entire alluvial valley (Said, 1975). This unit outcrops on the eastern margin of the valley. General descriptions of soil from top comprising the alluvium are described hereinafter.

a) Fill:

Most of the Cairo city is built on a layer of fill material made up of builders rubbish or refuse heap either from the remains of old buildings that had decayed or fallen then trodden down. Canals, remnant river channels, and ponds that are found on maps from the 14th century have been filled with the materials mentioned above (Said, 1975). This layer varies strongly in the thickness from one location to another and ranging from a few meters to 40m with an average of 15m. The shear wave velocity (Vs) for this layer is low and ranging between 170 to 270m/s.

b) Holocene Clay-Silt member:

This unit contains the modern mud of the Nile and its thickness is distributed uniformly and varying from 8 to 10m in the most of available boreholes for the Cairo area. The mud is dark gray to brown and contains clay and sandy clay (for more details see Said, 1975). The measured Vs for this layer is ranging between 415 to 460 m/s.

c) Pleistocene Graded sand-Gravel member:

This member has been recognized almost in all the available wells in the city. The content of this layer may be coincident with the exposed gravel layer on both east and west banks of the Nile River. The isopach contour map of this layer shows that the layer thickness increases northward with a maximum recorded thickness of 90m in the Zaitun basin, while the minimum thickness has been encountered in the boreholes at the eastern side of the Nile River (Said 1975). The Vs of this layer is ranging between 500 to 750m/s.

d) Plastic clay layer:

This layer made up of two units, the upper unit consists of silts and clays and the lower unit consists of clays with brackish water micro-fossils. This layer lies at about 100m depth in Cairo, forming the base for the valley sediments and overlies the Oligocene gravel and sand of Gebel Ahmar type. The thickness of this layer is ranging from few of meters to 90m. Plastic clays may exist at shallow depths in some

locations and could shrink and swell in volume if the groundwater begins to fluctuate significantly. In the historical Cairo area, this unit is ranging from 20 to 40m in thickness.

4.6 Site-specific ground motion modeling for historic Cairo

The computation of synthetic seismograms for a medium with localized lateral heterogeneities is performed using the MS-FD hybrid technique to investigate the effects of propagation path and local effects on the wavefield. The seismic wavefield is computed first in the laterally non-varying structural model with the MS technique, here we employed a regional bedrock model from the study of El-Khrepy (2008) (Fig. 4.8), and then it is introduced into the laterally heterogeneous local models which have been composed using data from Said (1975), and numerically propagated in using the FD approach. In SH wavefield computation, the displacements are used as inputs for the FD, while for the P-SV wavefield, the velocities time histories are employed. The testing procedure is based on the comparison between the synthetic seismograms computed at the same sites along the profile of the regional bedrock model, using MS and FD methods.

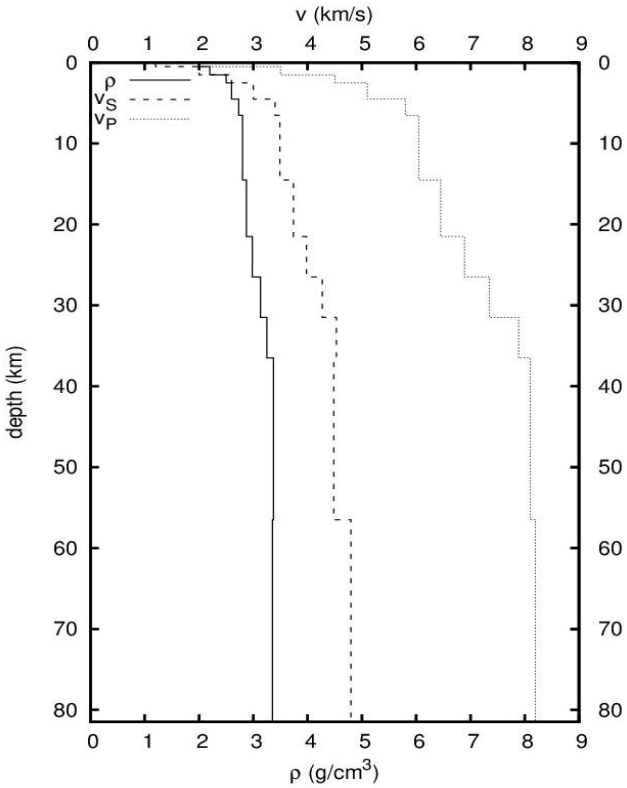

Fig. 4.8: Reference bedrock model for the Cairo area.

4.6.1 Ground shaking for the local models I and II (NS cross-sections): Scenarios 1 and 2

For the modeling of ground motion along NS (named I and II) cross-sections, we have chosen the October 12, 1992 "Scenario 1" (MMI = VIII, $M_w = 5.9$) and 950 "Scenario 2" (MMI = IX, M ~ 6.5-7.0) event as earthquake scenarios, Table 4.1. Three components synthetic seismograms and amplification maps for Scenario 1 along the local models I and II are shown in Figs. 4.9 and 4.10, respectively. The synthetic seismograms have been computed using the hybrid approach for an array of sites regularly spaced (60m) along the NS cross-sections (I and II) which cross along the historic Cairo area. Fig. 4.9 (a, b) show the three-component synthetic accelerograms calculated for Scenario 1 (southern source) along the cross-sections I and II, respectively. These figures clearly show the amplification effect and reflect well the geometry, local heterogeneity, and the subsurface topography of the cross-section models adopted in the computation. Peak acceleration (AMAX) of 38.5gal (12 Oct 1992 earthquake $M_w = 5.9$) is estimated in the transverse component of cross-section I at distance of 31.7km from the source. For cross-section II AMAX of 69.8 gal is obtained in the radial component at 30.3km epicentral distance.

The three-component synthetic accelerograms calculated for the cross-sections I and II for the Scenario 2 (northern source) are shown in Fig. 4.11 (a and b, respectively). AMAX of 1259 gal and 838gal are estimated in the radial component of Profiles I and II, at distances of 22.3 and 15.3km from the source, respectively. The obtained values are larger than the ones from Scenario 1 and they express a severe seismic hazard, as can be expected from the Scenario 2 of magnitude between M ~ 6.5-7.0 which is the MCE, i.e., the maximum historical earthquake $+2\sigma = 0.5$ (sigma is the standard deviation of magnitude estimation at the global scale).

The response spectra ratios (RSR), which are the RS computed from the synthetic signals computed for the local profiles normalized by RS computed from synthetic signals for the regional bedrock model, is another critical parameter for engineering purposes. The RSR patterns as a function of frequency along the NS cross-sections I and II are shown, for the three components of acceleration, in Fig. 4.10 (a and b, respectively) for Scenario 1 and Fig. 4.12 (a and b, respectively) for Scenario 2.

For Scenario 1, the maximum amplification obtained along Profile I is about 4 on the vertical component at frequencies between 5.5 and 6.5 Hz and epicentral

distance of about 27km from the source, while the maximum amplification along Profile II from the same scenario is about 4 at frequencies between 4.5 and 6Hz for the radial component at epicentral distance of 30km from the source. The sites along the Profile II (east historical Cairo) are less affected by amplification which indicates that the Profile II is less affected by lateral heterogeneities than Profile I.

For Scenario 2 (Fig. 4.12), the maximum amplification along Profile I is obtained on the vertical component which is larger than Scenario 1 in the size is about 5 at frequencies between 3.5Hz and 4.5Hz at 20.5km approximately from the source, while for Profile II the maximum amplification from the same scenario is about 3 at frequencies between 5Hz and 6.5Hz for the radial component at distance of 21km from the source. As in the case of Scenario 1, sites along the Profile II are less affected by amplification because it has less lateral heterogeneity than Profile II. The comparison between the RSR patterns for Scenarios 1 and 2, computed along Profiles I and II, explain that the differences in the amplification patterns along the same profile but different scenarios are could be due to change in earthquake size, propagation path and the incident angle of wavefield. This reflects the fact that that the site effects which may be not persistent when earthquake source changes (Molchan et al., 2011), especially in the Nile Delta and Valley, and can have a significant impact on the polarization in the horizontal plane (also defined amplification/de-amplification) of seismic waves and on ground failure or soil liquefaction as pinpointed by El-Sayed et al. 2004.

4.6.2 Ground shaking for the local model III (EW): Scenario 3

Three components synthetic accelerograms have been computed with the hybrid method for an array of sites along the Profile III (EW) for Scenario 3 and they are shown in Fig. 4.13 (a). Peak acceleration of 571gal (Fig. 4.13 a) is estimated in the radial component of Profile III at an epicentral distance of about 26.3km from the source.

The distribution of RSR versus frequency and position along Profile III is shown for the three components in Fig. 4.13 (b). The maximum amplification is about five obtained for the vertical component at a frequency between 3.5Hz and 5Hz. The transverse and radial components show fewer amplification patterns of about three at a frequency range from 2Hz to 4Hz.

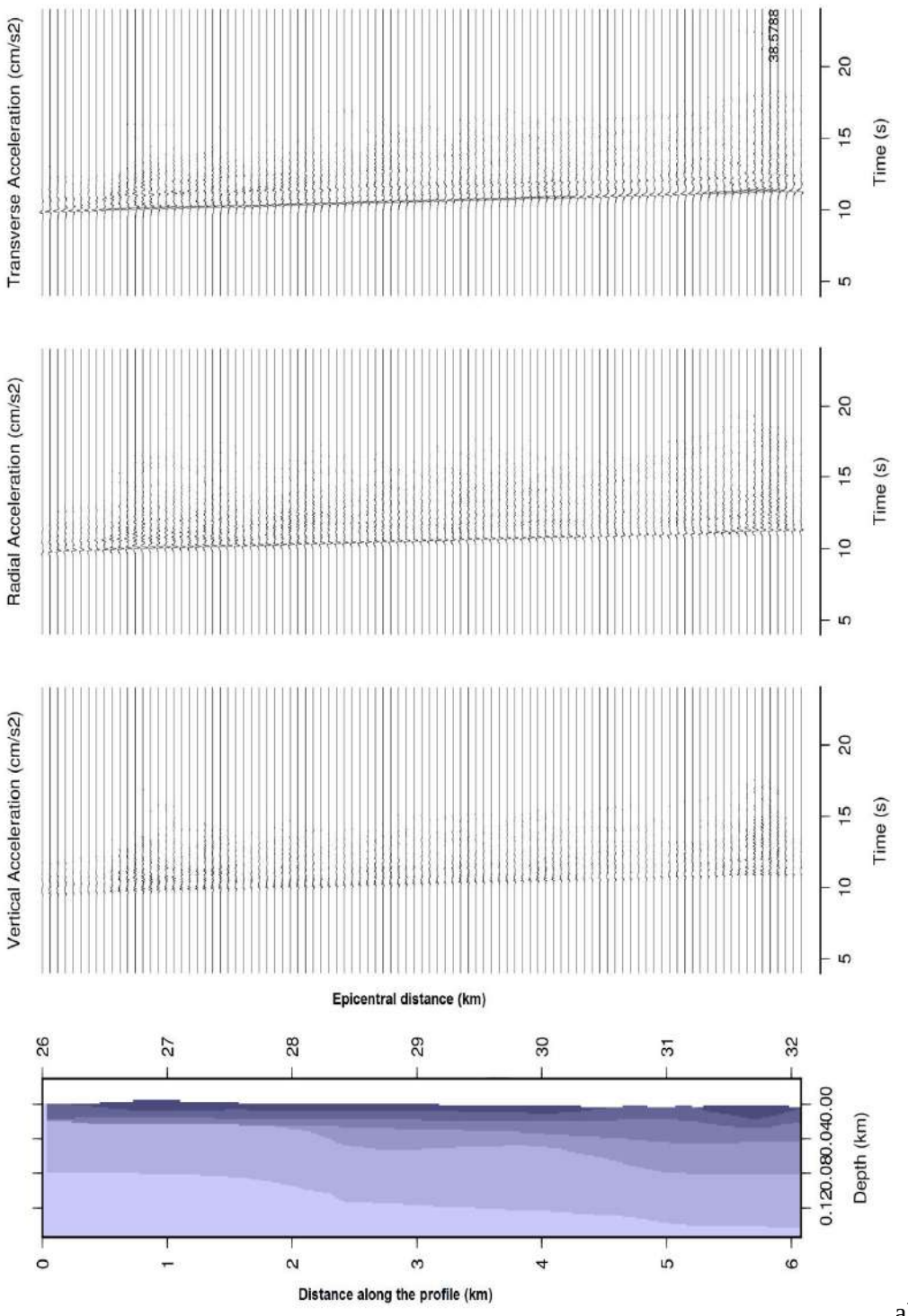
Transverse Acceleration (cm/s2)
38.5788
Time (s)
Radial Acceleration (cm/s2)
Time (s)
Vertical Acceleration (cm/s2)
Time (s)
Epicentral distance (km)
Depth (km)
Distance along the profile (km)

a)

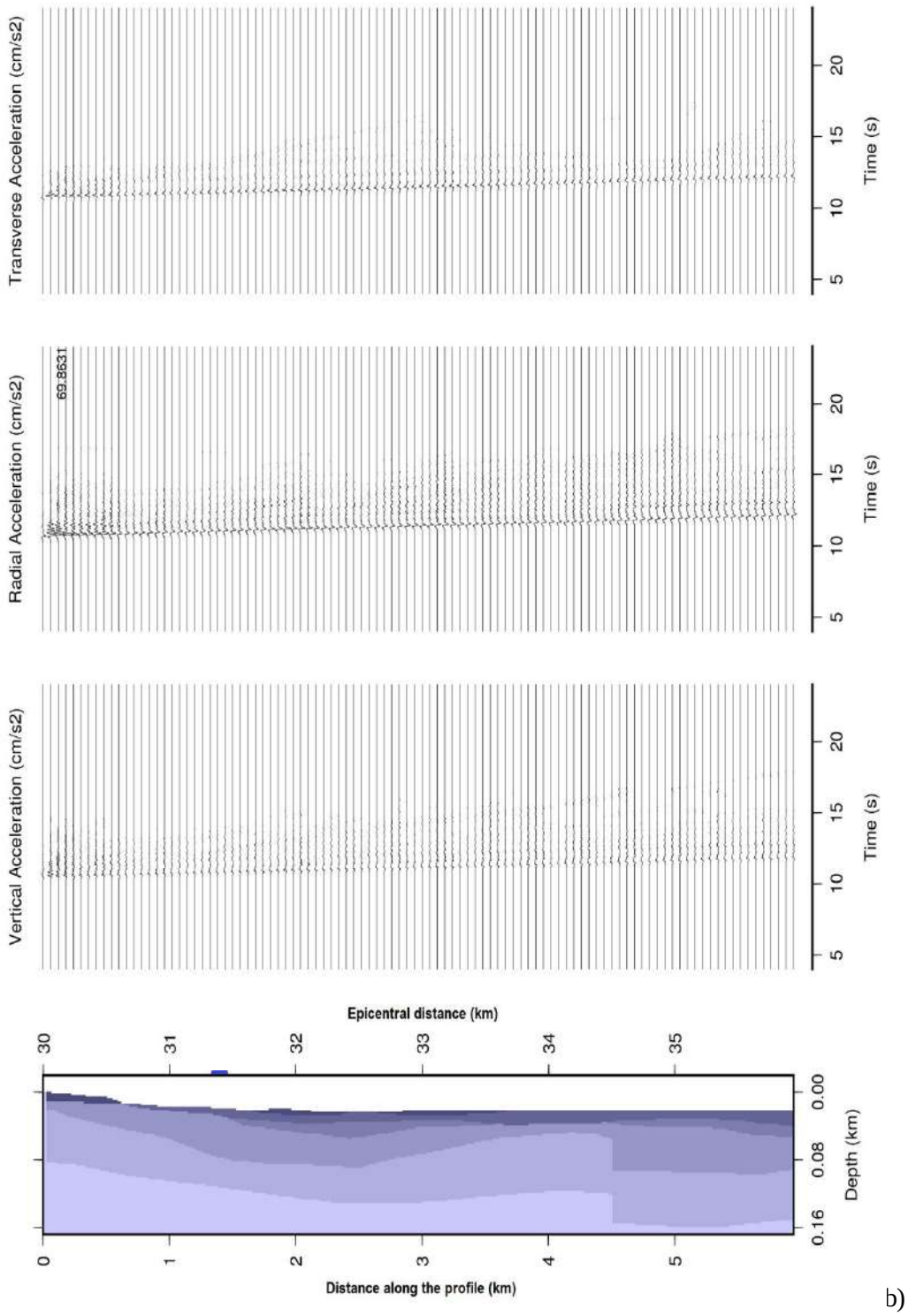

Fig. 4.9: The NS profiles I (a) and II (b) and corresponding synthetic seismograms computed for Scenario 1 (southern source).

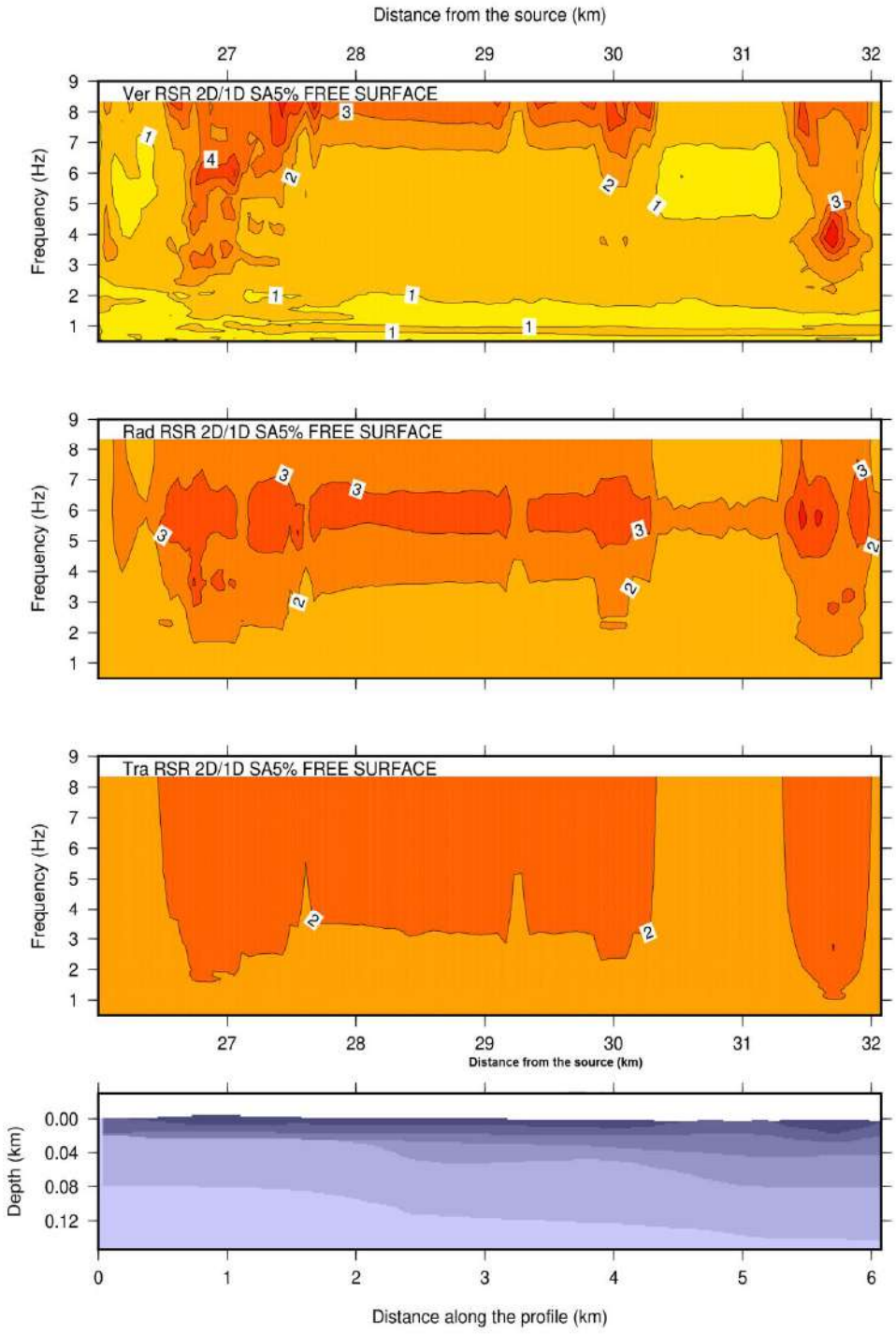
Distance from the source (km)
Ver RSR 2D/1D SA5% FREE SURFACE
Rad RSR 2D/1D SA5% FREE SURFACE
Tra RSR 2D/1D SA5% FREE SURFACE
Frequency (Hz)
Depth (km)
Distance along the profile (km)

a)

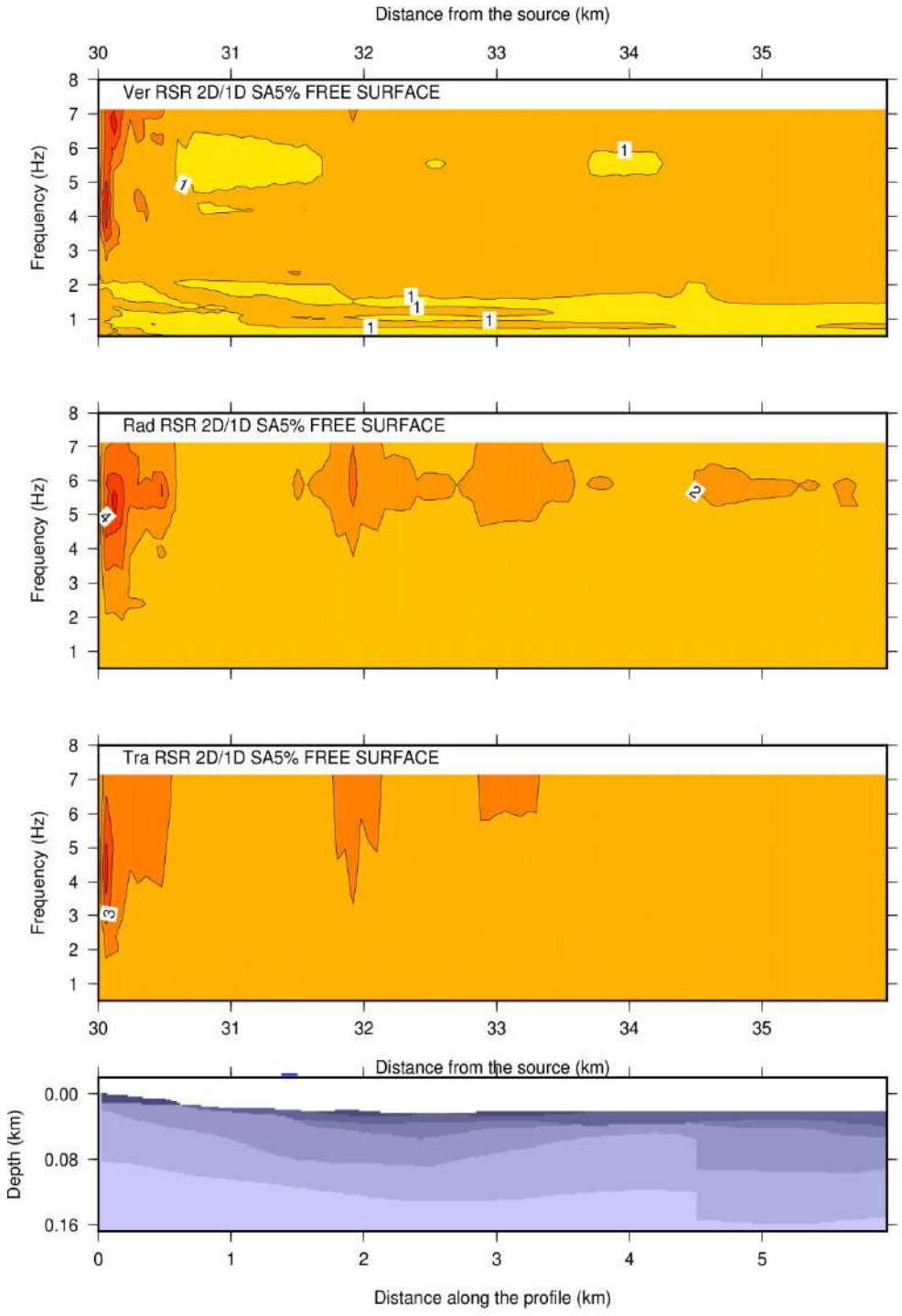

b)

Fig. 4.10: Amplification patterns (response spectra ratio (RSR) vs. frequency) for the three components of motion for the Profiles I and II (a, b, respectively) computed for Scenario 1.

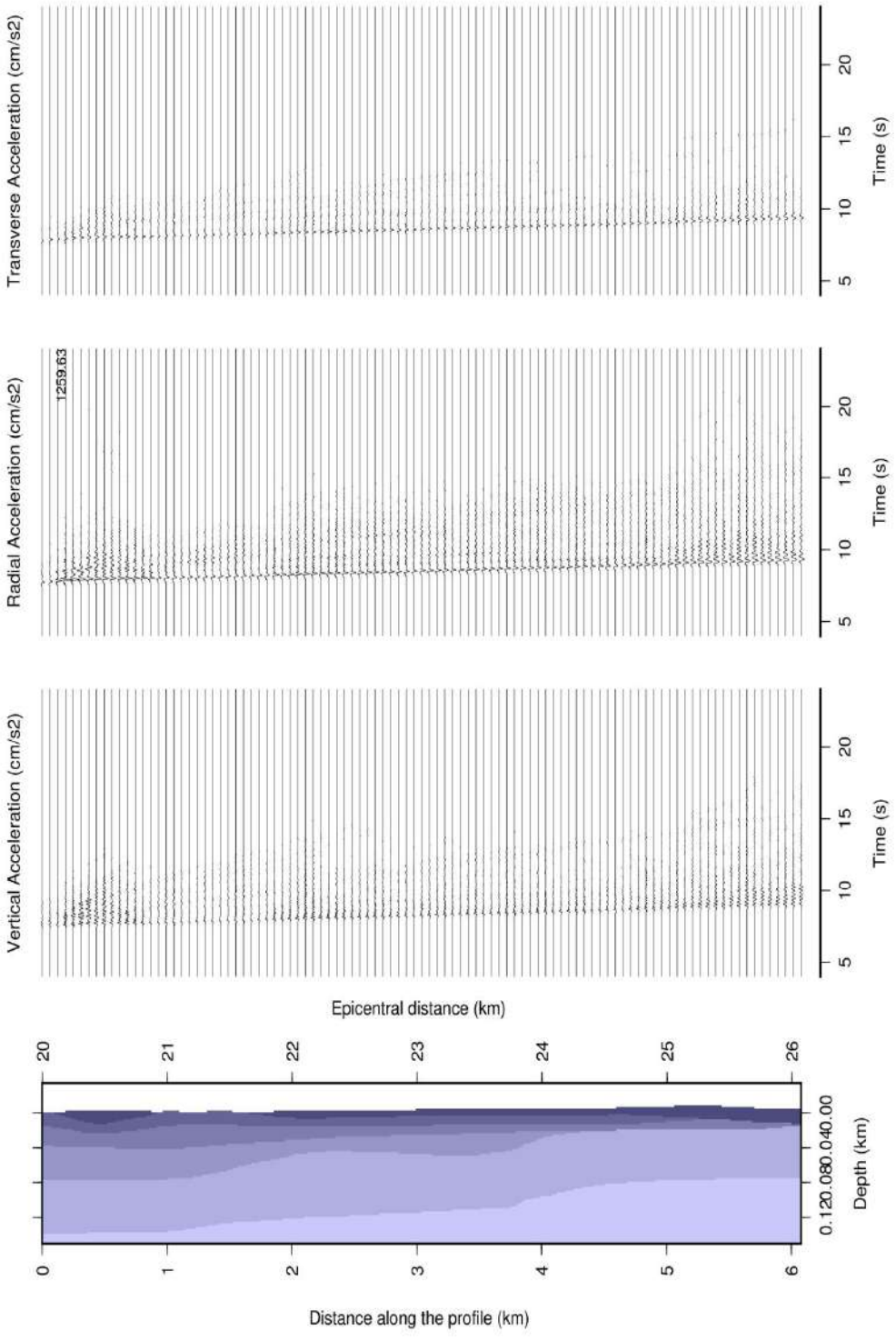
Transverse Acceleration (cm/s2)
Radial Acceleration (cm/s2)
1259.63
Vertical Acceleration (cm/s2)
Time (s)
Epicentral distance (km)
Depth (km)
Distance along the profile (km)

a)

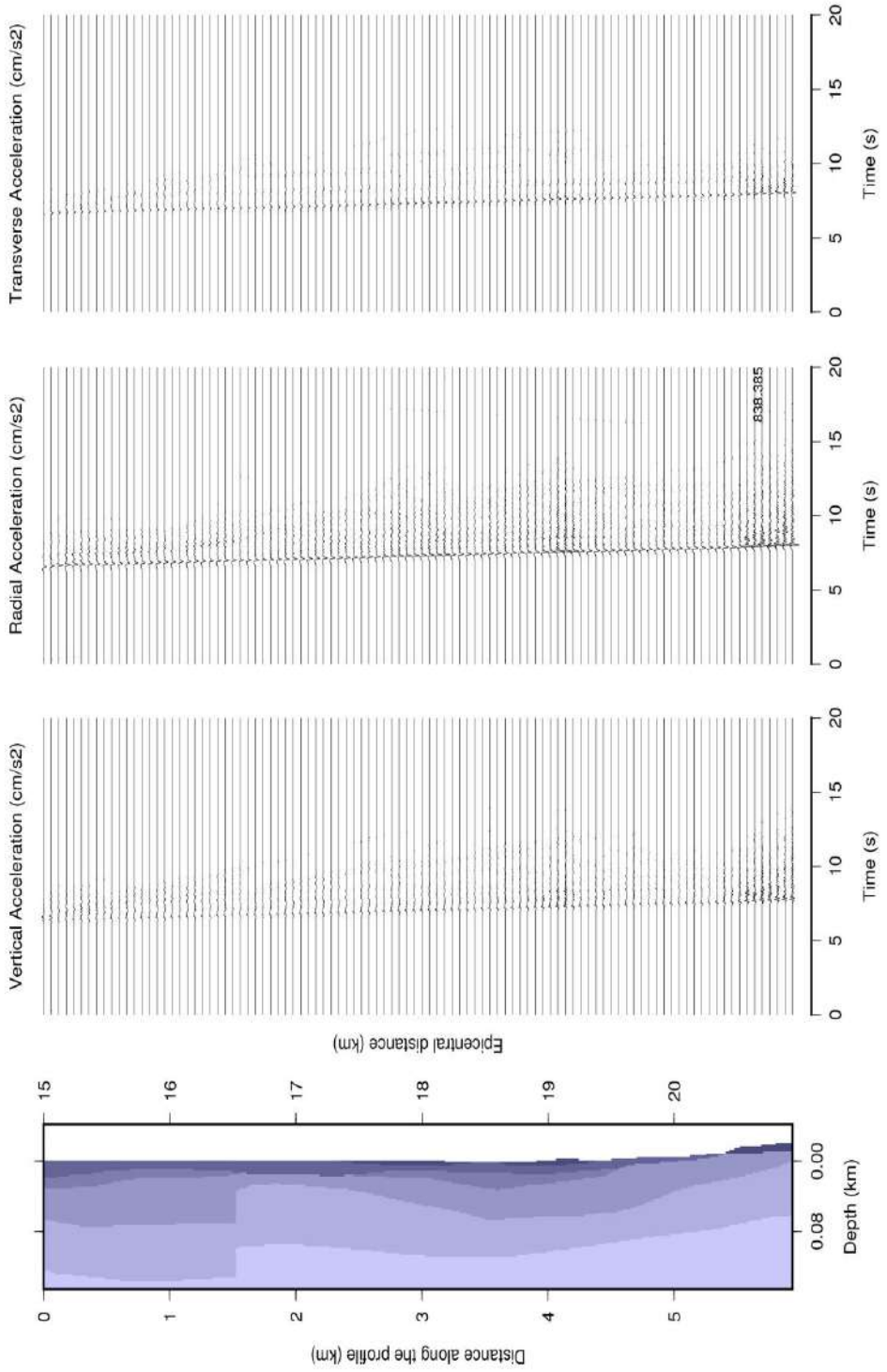

b)

Fig. 4.11: The NS profiles I (a) and II (b), respectively and corresponding synthetic seismograms computed for Scenario 2 (northern scenario).

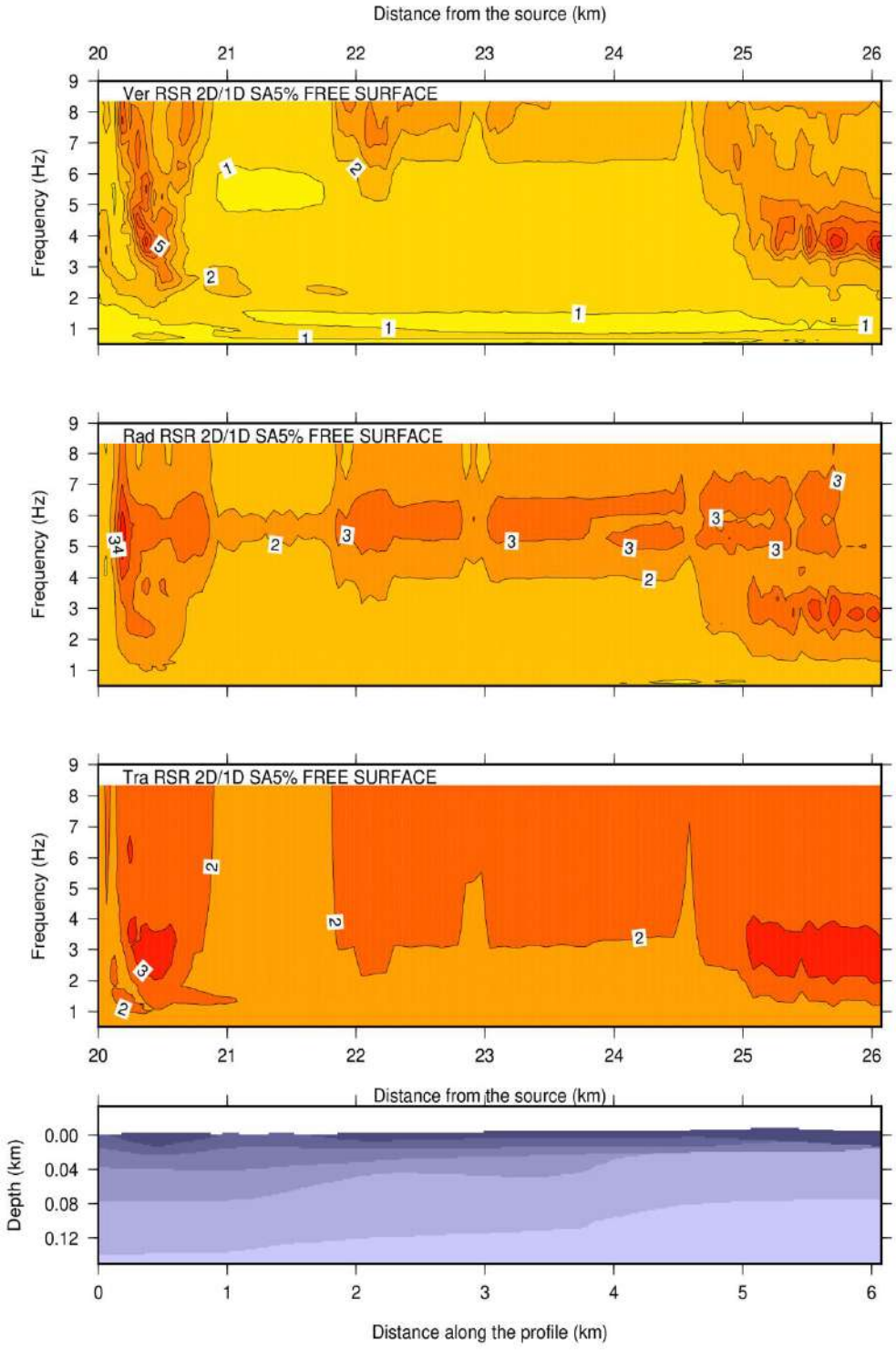
Distance from the source (km)
Ver RSR 2D/1D SA5% FREE SURFACE
Rad RSR 2D/1D SA5% FREE SURFACE
Tra RSR 2D/1D SA5% FREE SURFACE
Frequency (Hz)
Depth (km)
Distance along the profile (km)

a)

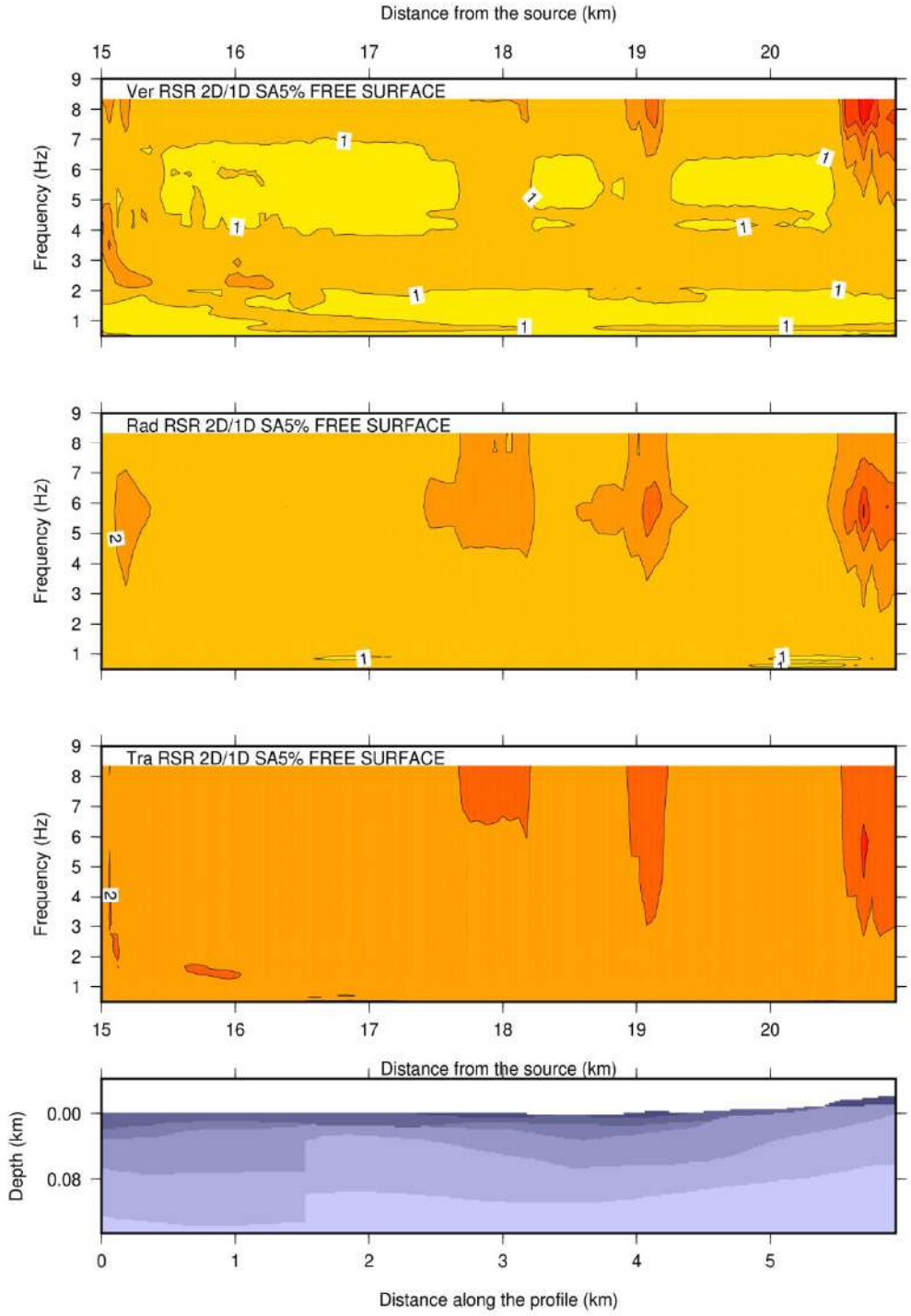

b)

Fig. 4.12: Amplification patterns (response spectra ratio (RSR) vs. frequency) for the three components of motion for the Profiles I and II (a and b, respectively) computed for Scenario 2 (northern source).

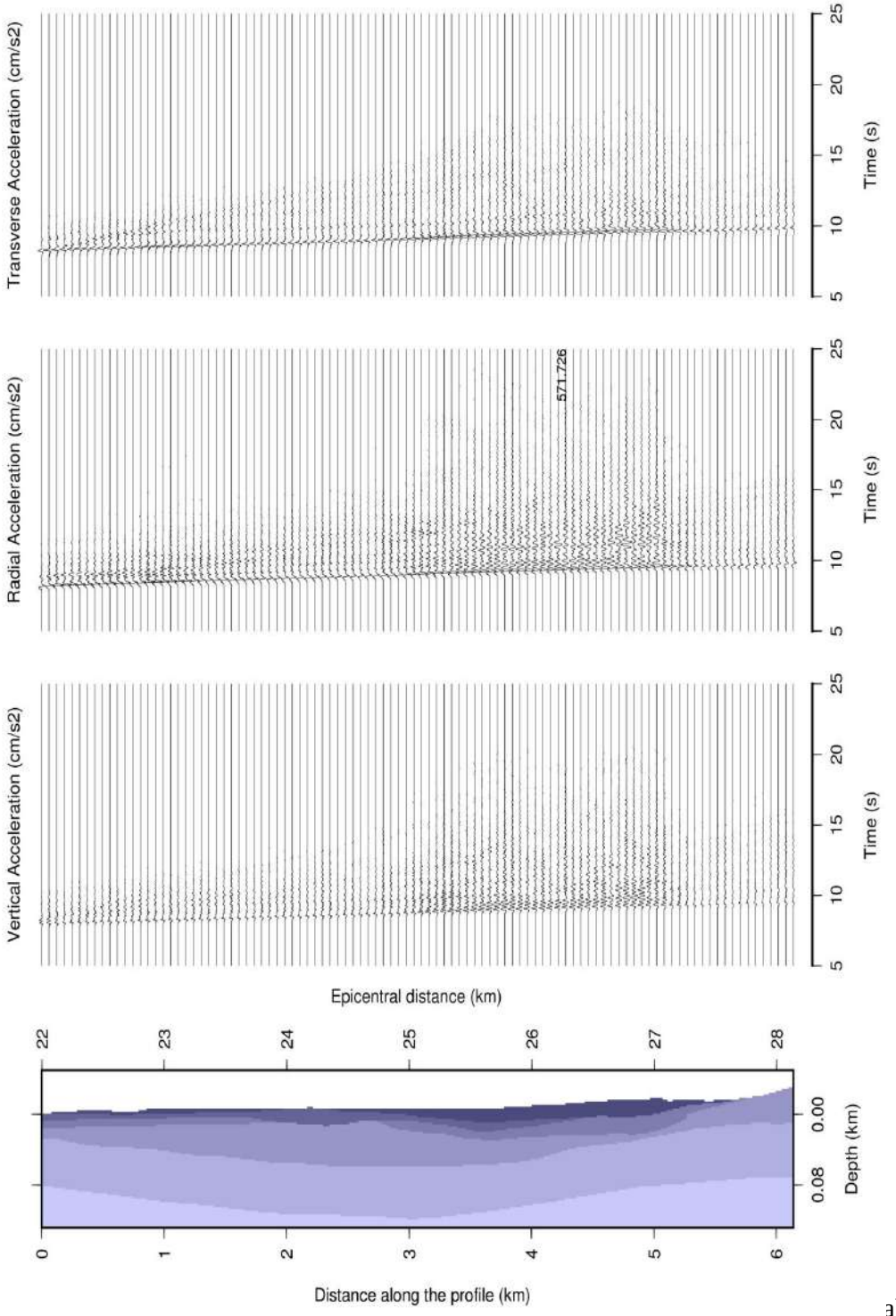
Transverse Acceleration (cm/s2)
Radial Acceleration (cm/s2)
571.726
Vertical Acceleration (cm/s2)
Time (s)
Epicentral distance (km)
Depth (km)
Distance along the profile (km)

a)

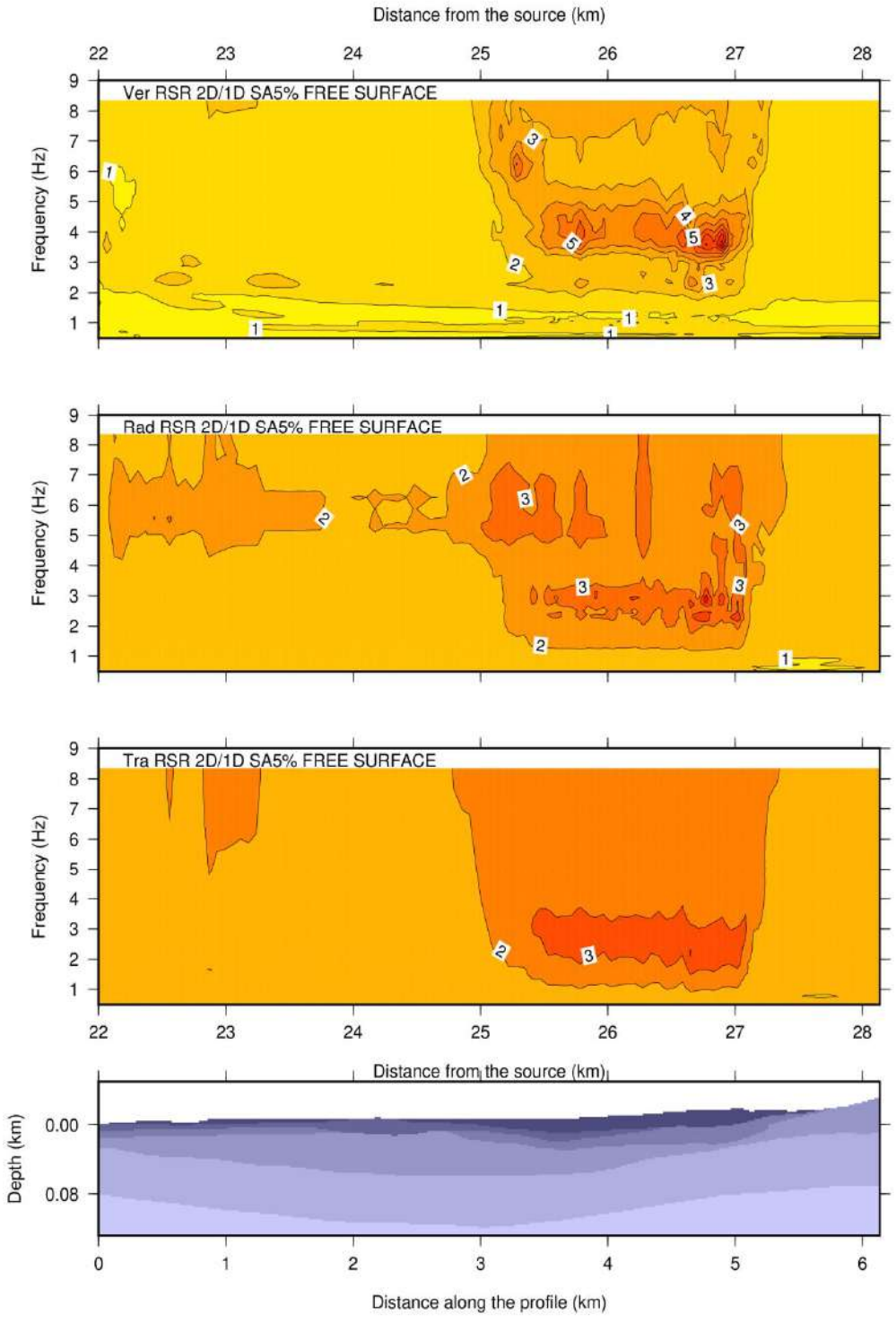

b)

Fig. 4.13: Synthetic seismograms (a) and amplification pattern (response spectra ratio (RSR) vs. frequency) (b) for the three components of motion for the Profile III computed for Scenario 3 (western source).

4.7 Discussion

The nature of observed damage from October 12, 1992, Dahshur earthquake indicates a significant amplification of earthquake ground motion probably occurred due to the alluvial deposits of the Nile Valley in and around Cairo (El-Sayed et al., 2004; Kebeasy and Husebye, 2003). This Chapter aims to provide a specific focus on the possible site-effects for the area of historic Cairo, which contains a large number of cultural heritage buildings, through the detailed ground motion modeling using the hybrid approach. A hybrid approach that combines both MS and FD techniques, is used to model the ground motion induced in laterally heterogeneous structural models at the selected sites using different earthquake scenarios.

The synthetic accelerograms are computed first in the laterally non-varying structural model with the MS and FS techniques, here we employed a regional bedrock model from the study of El-Khrepy (2008), and then it is introduced into the laterally heterogeneous Profiles I, II, and III, which have been composed using borehole data from Said (1975) and fieldwork, and numerically propagated in using the FD approach.

The scenarios being used are the earthquakes of 1992 and two historical ones. The main idea behind adopting modeling of Scenario1, although its moderate size, is to validate the obtained results through the rough comparison between the estimated ground motion parameters with the real observed damage. The general amplification pattern is obtained by contouring the distribution of amplification value along the profile as a function of frequency and space. The seismic wavefield has been computed with the hybrid method at all sites along both cross-sections with a regular spacing of 60m up to 8Hz cut-off, using initially a point source represented by a double-couple of forces placed at the hypocenter.

For the modeling of ground motion along NS (named I and II) cross-sections, we have chosen the October 12, 1992 “Scenario 1” (MMI = VIII, M_w = 5.9) and 950 “Scenario 2” (MMI = IX, M = 6.5-7.0) earthquakes as earthquake scenarios while for the Profile III, we have selected the earthquake of April 857 (Scenario 3) which is located west of the profile. The global amplification pattern over the study area is ranging between 2 and 5 and occurs at a frequency range 1.0 - 7.0Hz.

The Figs 4.10, 4.12, and 4.13 manifest the effect of subsurface geometry of the adopted profiles on the correspondent amplification patterns which indicate that sites where there are steeper edges in the geometry subsurface profiles being used, higher amplifications have appeared. Fig. 4.14 shows the RS for a group of selected sites spaced 3km from each other along profiles I, II, and III computed by adopting the earthquake scenarios 1, 2, and 3 as shown in Table 4.1.

The reported damage and the small distance between heavily damaged structures and intact ones in Cairo after October 12, 1992, Dahshur earthquakes indicate the capability of local site conditions to largely amplify the seismic ground motion and variability of the vulnerability of existing buildings. The fill layer of varying thickness distributed underneath most of the historic buildings in Cairo, which is composed of rubbish or refuse heap either from the remains of old buildings that had decayed or fallen then trodden down, is the main responsible for the amplification. According to the earthquake damage report of Japanese Expert Team in 1993, the one- and two-story adobe dwellings performed poorly during the earthquake and were the primary cause of the more than 500 earthquake fatalities. The occurrence of damage to the low rise buildings proves that the amplification may happen at a higher frequency range which fit well with the obtained results of this work.

The results obtained in this work may represent an important and forward step toward the proper assessment of dynamic behavior under earthquake action, preservation and risk reduction for the existing cultural heritage structures by providing both scientific and engineering knowledge. Moreover, the obtained results from ground motion modeling could be useful for land use and urban planning, retrofitting of existing buildings, construction of new buildings, and upgrading infrastructures in the historic Cairo area, as well.

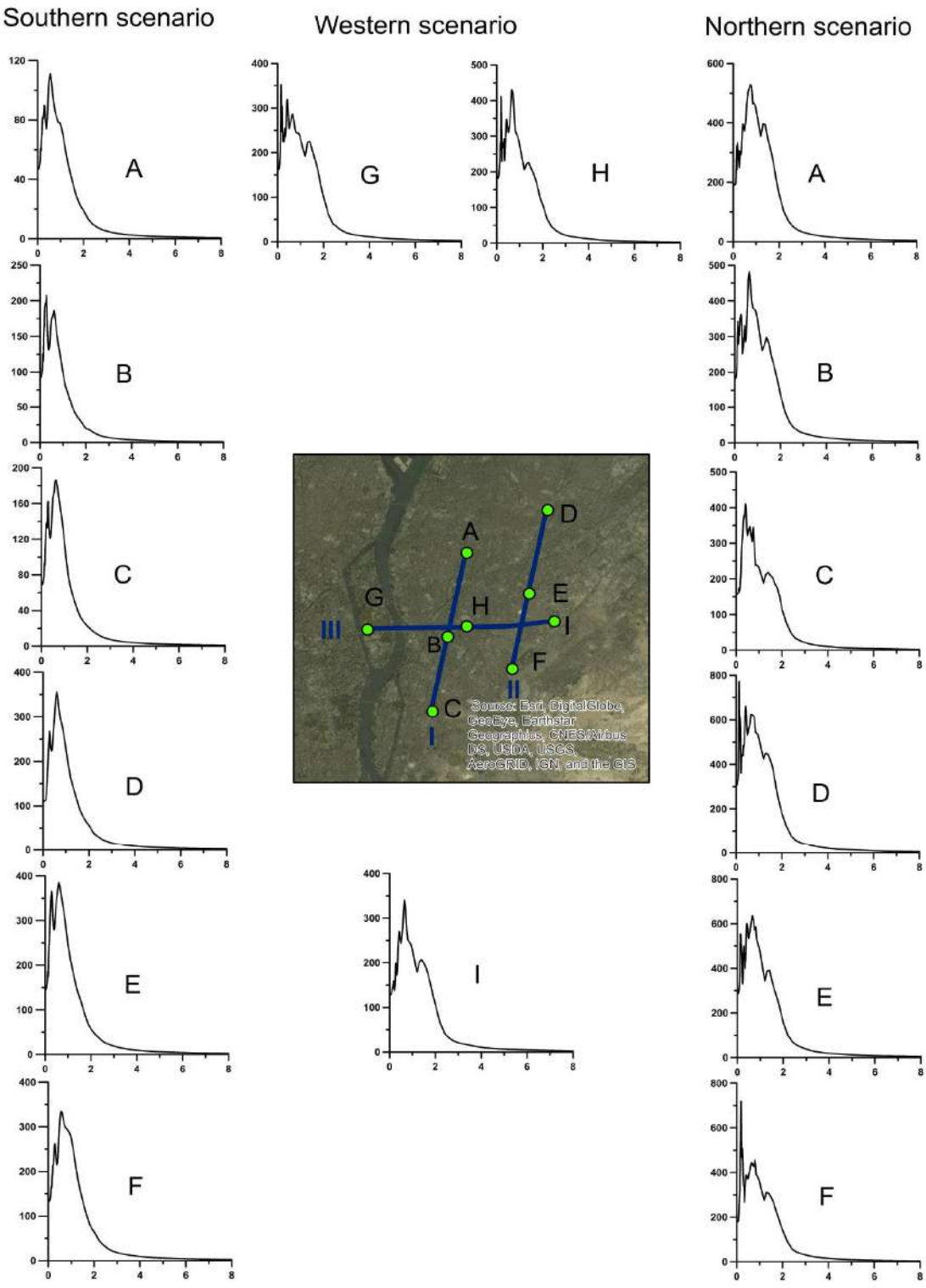

Fig. 4.14: RS for some selected sites along the adopted cross-sections I, II, and III computed for the Scenarios 1 (Left side), 2 (Right side), and 3 (Middle).

Chapter 5

Seismic Assessment for a Cultural Heritage Structure in Historical Cairo Considering the Scenario-Based Approach

5.1 Introduction

By virtue of its location at the confluence of both the Mediterranean basin and the continents of Africa and Asia, Egypt has been known for its history and geography. Egypt has inherited from multicultural heritage (e.g., Pharaohs, Greco-Coptic, and Islamic monuments) well known for its diversity and richness at the global level. This heritage, which is a symbol of identity and an essential element of our memory, holds our shared principles and values and can be transferred to future generations if we take action to protect it. Cultural heritage is a unique wealth, requiring particular attention such as security, management, restoration, and preservation from all kinds of impacts brought about by natural or human-made. Conservation of cultural heritage involves protection, maintenance, and restorations using intervention strategies that prove effective in maintaining a particular property in a condition as close to the original one and for as long as possible.

Historic Cairo is World Cultural Heritage Site (WHC) with its famous mosques, madrasas, hammams, and fountains. Although these buildings were built in periods goes back to more than ten centuries many of them have survived consequent seismic loads with no or minor damage; others have suffered severe or complete damage So, for finding and selection of proper mitigation strategy for cultural heritage buildings, a detailed site-specific seismic hazard assessment and understanding of the dynamical behavior of such structure during earthquake action should be taken into account. Actually, in the preservation of historical monuments against the seismic action expected, it’s well known that each monument has its own characters, so different requirements are needed, due to several factors related to the

building itself, the site, the expected ground motion level and its relation with the surroundings. It is worth mention that the protection objectives developed for ordinary buildings are not directly applicable in the case of heritage buildings since they do not address the cultural importance for them.

In Chapter 3, updated NDSHA maps for Egypt at national scale have been computed then deeply discussed, where the seismic sources are defined from the available information about the spatial distribution of large size earthquakes, taking into account the seismic history (revised historical and instrumental earthquake catalogs), seismotectonic (seismogenic zones) and morphostructural zonation (seismogenic nodes available only for Northeastern part of Egypt where our structure of interest is situated).

In Chapter 4, a detailed linear site-specific ground motion modeling that incorporates the source, propagation and site effects has been accomplished for historical Cairo area, where the minaret is located, in order to reliably compute the ground motion parameters.

In this Chapter, we define the seismic input (RS and time histories) for the proper evaluation of the dynamic response of the minaret of the Madrasa the Princess Tatar al-Higaziya (Fig. 5.1). The detailed site-specific ground motion modeling for historical Cairo has been accomplished and described in Chapter 4. At the site of the minaret, we provide the Maximum Credible Seismic Input (MCSI) (Fasan et al., 2017) to be used for the assessment of the dynamic behavior of the minaret, obtained by joining both scientific and engineering knowledge in order to understand the performance of this monument under the possible earthquake action. The results could help in finding the proper mitigation measures for thin invaluable value minaret and could represent a step toward the risk reduction and management for this historic structure. It is worth mentioning that, for historical buildings and monuments, i.e., when considering very long time intervals (since we do not want to lose our cultural heritage), the use of standard seismic hazard estimates of is really questionable (Romanelli and Vaccari, 2015).

The Madrasa (meaning school in Arabic), of princess Tatar al-Higaziya, was constructed in two stages. First, the mausoleum was built in 1348 as an extension to princess Tatar's house, then after thirteen years the palace and the mausoleum was converted into the madrasa (Williams, 2008). The Madrasa complex consists of a mausoleum, minaret, and an ablutions court, and is one of few schools endowed by a

woman in Cairo. The school was built and endowed for educating orphan children and for uplifting the daily prayers, as well as serving as a public library. A clear sketch of the school layout, three-dimensional views, and a recent photo of the minaret are illustrated in Fig. 5.1. The school has been restored several times, in 1895, 1980-1982, and most recently by the Egyptian government. The minaret is one of the most significant elements of the school, consisting of a 24.16m vertical shaft above the ground level, and it lacks an upper tier (Mayer & Abteilung, 2007). The ground plan of the minaret is squared, with a width of 3.45m up to a height of 11m, after which there is a transition to an octagonal plan, which is further emphasized through the use of beveled corners. A detailed numerical model of the minaret is established in SAP2000 (CSI, 2016), while linear elastic analysis is conducted under the earthquake loading.

This minaret has been through studied by Imam (2001) after 1992 Cairo, earthquake in the framework of the UNESCO project for the restoration of historic Cairo. In that study, the performance of the minarets under earthquake loading was examined. But this study was lacking important seismological and entering details. In the modeling, a simplified shaft model that ignores some critical structural elements without justifications was considered. Additionally, the excitation records used in the study was merely the 475 years return period elastic response spectra of the Egyptian Building code which is not logic as the building age is already beyond that period. This has triggered the importance to reevaluate the dynamic response of the minaret using realistic seismic input and modern modeling techniques.

Several previous studies have introduced the numerical modeling and dynamic analysis of historical minarets under earthquake loading. For example, El-Attar et al. (2005) proposed a seismic protection technique for a historic limestone masonry minaret built between the year 1348 and 1960 A.D in historic Cairo. The minaret in their study was built one year after the minaret reviewed in this study, with the same construction techniques and limestone material properties. Moreover, they considered a linear elastic finite element model in SAP2000 for the minaret, while the modal analysis results were evaluated and compared with ambient vibration test results. Sezen et al. (2008) have investigated the dynamic analysis and assessment of reinforced concrete (RC) cylinder minaret constructed in Turkey. They developed four finite element models in SAP2000 representing the same minaret while ignoring various structural components in each model such as openings, balconies, and interior

spiral stairs, to arise a simplified numerical modeling approach for similar cylindrical RC minarets. They concluded that ignoring modeling the spiral stairs slightly influenced the modal analysis and modal participation factor, while it significantly reduced the stresses in the minaret.

In the view of the forementioned studies, we constructed our model considering all openings, balcony, and geometrical transitions while ignoring the spiral stairs conservative estimation. Oliveira et al. 2012 have performed a series of in situ ambient variation tests on eleven old minarets in Turkey, and they conducted linear numerical dynamic modeling of seven of the selected minarets in SAP2000. They suggested several retrofit techniques be considered to correct the observed deficiencies in the minarets, such as applying exterior steel ring(s) to increase the outer walls confinement or installing wire-mesh or carbon fiber on the inner side of the outer walls to increase their resistance.

This work is divided into two main tasks. The first task deals with the estimation of the seismic input needed for the seismic assessment of the minaret using information about the earthquake scenarios that may affect the minaret and local site conditions beneath. While the second task focuses on assessing the dynamic modeling and behavior of the minaret under seismic loading. Moreover, the results of this work could be important for the risk reduction of heritage structures from strong earthquakes in the future, especially for those constructed during the same time period and having similar structural systems and components.

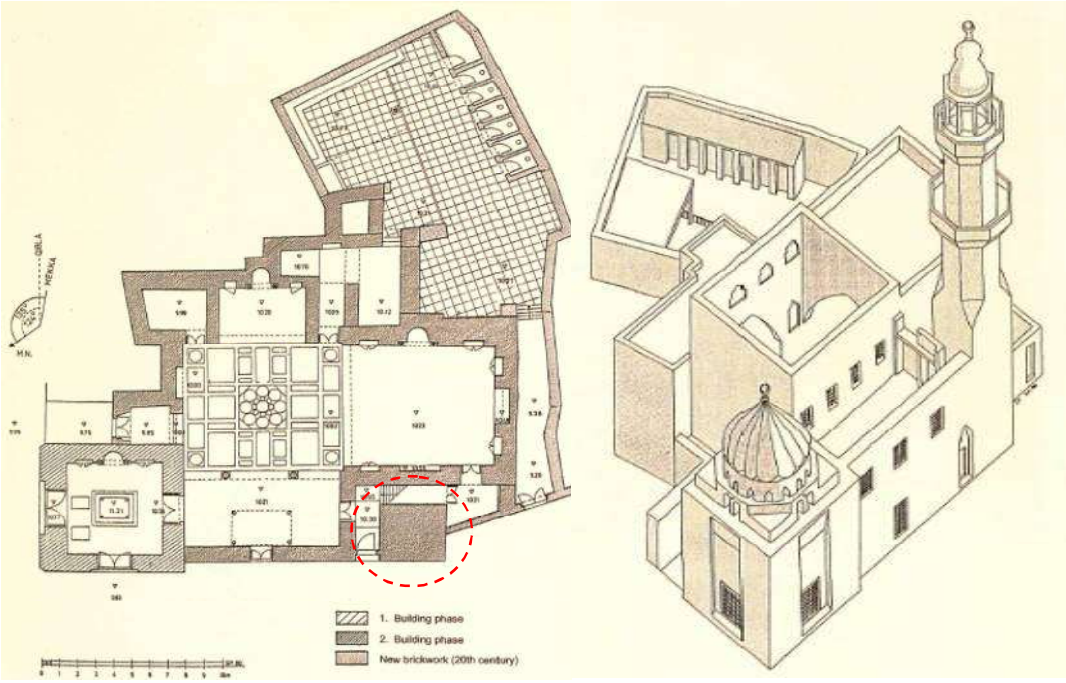

(a) (b)

(c)

Fig.5.1: Madrasa of the princess Tatar al-Higaziya: (a) layout; (b) three-dimensional view; (c) recent photo of the minaret.

5.2 Comparison between PSHA and NDSHA for Cairo area

In Chapter 1, the drawbacks, limitations, and performance of standard PSHA studies in Egypt have been briefly revised and discussed. The revision has shown that

most of those studies are based on the traditional probabilistic approach, and the PGA values on the hazard maps are exceeded by earthquakes occurred after their publication. The failure of those maps is evidenced by testing the PGA values converted from observed intensity against the predicted ground motion before the occurrence of an earthquake.

The PGA values obtained for Cairo by a recently published PSHA study, which is done by Sawires et al. (2016) for two different return periods of 475 and 975 are 0.08-0.16g and 0.16-0.24g (Fig. 5.2), respectively, while PGA obtained from the recent NDSHA work for Egypt as shown in Chapter 3 (Fig. 3.11) is ranging between 0.15-0.4g. If we compare these values obtained by the two methods, we can notice that the estimate of PSHA associated with return periods of 475 and 975 years, appears to be lower than the NDSHA estimates.

In spite of the poor performances and basic shortcomings of existing PSHA studies available for Egypt, the Egyptian building code stills rely upon maps from those studies. To overcome the limits of design procedures based upon PSHA seismic input (Fasan et al., 2015; Rugarli, 2014; Indirli et al., 2013), it is necessary to resort to a new seismic design strategy based upon the NDSHA definition of the seismic input in Egypt. Given the mentioned PSHA limits, NDSHA represents a scenario-based approach for seismic hazard assessment at different geographic scales, providing realistic time histories from which it is possible to retrieve peak values for ground displacement, velocity, and acceleration in correspondence to earthquake scenarios. As we have discussed in Chapter 3, the NDSHA permits the integration of the available information provided by the most updated seismological, geological, geophysical and geotechnical databases for the site of interest. It also allows advanced physical modeling techniques and provides strong ground motion parameters (seismic input) based on the seismic waves propagation modeling at different scales, i.e., regional, national, local and site-specific (Panza et al., 2012 and references therein). An example of the NDSHA approach at a local scale for the City of Valparaiso is given in the framework of the “MAR VASTO” Project (see Indirli et al., 2011).

The reliable evaluation of the seismic input at the sites of cultural heritage buildings is a crucial factor for real conservation. For cultural heritage, the concept of return period is of little value. Therefore, the traditional PSHA should be replaced by more effective NDSHA, already well developed and widely applied; it provides

scenario-based approaches, removing PSHA ambiguities (Indirli et al., 2006; Indirli et al., 2009; Indirli et al., 2013).

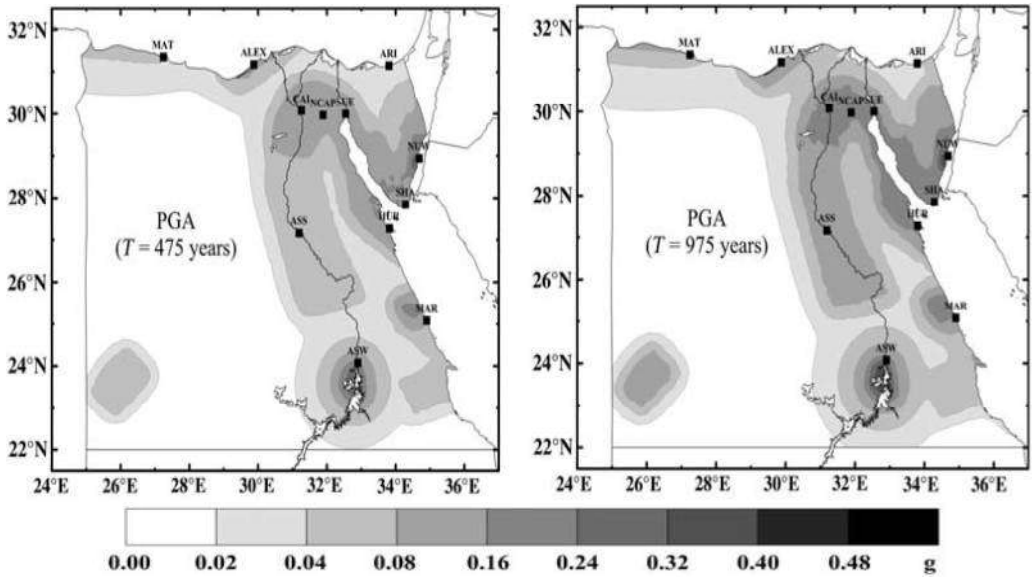

Fig. 5.2: Seismic hazard maps (for rock-site conditions) depicting mean peak ground acceleration (PGA), for return periods of 475 and 975 years after Sawires et al. (2016).

5.3 Computation of MCSI

Using the NDSHA approach, Fasan et al. (2015, 2017) proposed a procedure to define a level of seismic input, i.e., Maximum Credible Seismic Input and hereinafter (MCSI) to be used for engineering analysis. Its named "Maximum Credible" is because it aims to provide a reliable estimate of the "upper-bound ground motion" (RS or a set of accelerograms) that could occur at a site. While its named "Seismic Input" is because the output from this procedure can be adopted directly by engineers for the designation and retrofitting of buildings without carrying out any additional steps, e.g., scaling or filtering.

The MCSI (Fig. 5.3) can be computed directly from physics-based broadband simulations of the seismic process Fasan (2017). The sets of MCSI spectrum compatible accelerograms can be found looking directly into the simulations at 5% damping. The seismic input can be defined for a given site in the NDSHA framework by carrying out the analysis at two levels of detail. The first, called Regional-Scale Analysis (RSA) provides the MCSI as a RS at the bedrock ($MCSI_{BD}$). It is computed using a large number of the possible sources with different source model realizations and laterally non-varying crustal models. Furthermore, a RSA allows for the identification of the earthquake sources that form the highest hazard at the bedrock.

The $MCSI_{BD}$ spectrum can be carried out, firstly, for selecting the most hazardous source(s) at each period on the base of the median spectral acceleration of the simulations from every source, which is very similar to the de-aggregation procedure in PSHA.

The second one is called Site Specific Analysis (SSA), takes the source, path, and site effects into account, providing a Site Specific seismic input ($MCSI_{SS}$), to be used in the engineering analysis of relevant structures, such as historical and critical buildings. The SSA consists of a detailed site-specific analysis, which takes into account the site structural heterogeneities, (whether topographical or due to the presence of soft-sedimentary soils) by adding a local FD model. In a SSA, the wavefield generated by the MS technique is introduced into the 2D model that defines the local laterally heterogeneous area, and it is propagated according to the FD scheme, which is described briefly in Chapter 4.

With the MCSI procedure, there is no need for filtering by magnitudes, distances or site classifications, as done with original records since the accelerograms are all representative of the same site (site-specific). Moreover, there is no need to scale the accelerograms to match the target spectra linearly. This procedure repeats what is usually done with original records, replacing them with synthetic ones and the Uniform Hazard Spectrum (UHS) prescribed by the codes within the $MCSI_{SS}$ response spectra as suggested by Fasan (2017).

As we have explained above, the MCSI spectrum is a type of UHS, which is built by selecting the most hazardous source at each period on the base of the median spectral acceleration of the simulations from every source, which is very similar to the de-aggregation procedure in PSHA methods. Then, at each period a reference value is selected for the MCSI of the simulated spectral acceleration for the source that governs that specific period. MCSI envelopes uncertainty by means of a wide range of NDSHA simulations rather than quantifying them probabilistically, it can be defined either as a response spectrum or as a set of accelerograms, and it is free from arbitrary choices like a reference average life and probability of exceedance. The adoption of the average, percentiles or the maximum of ground motion parameters can be decided by the engineers, based on the target performance level for the structure of interest.

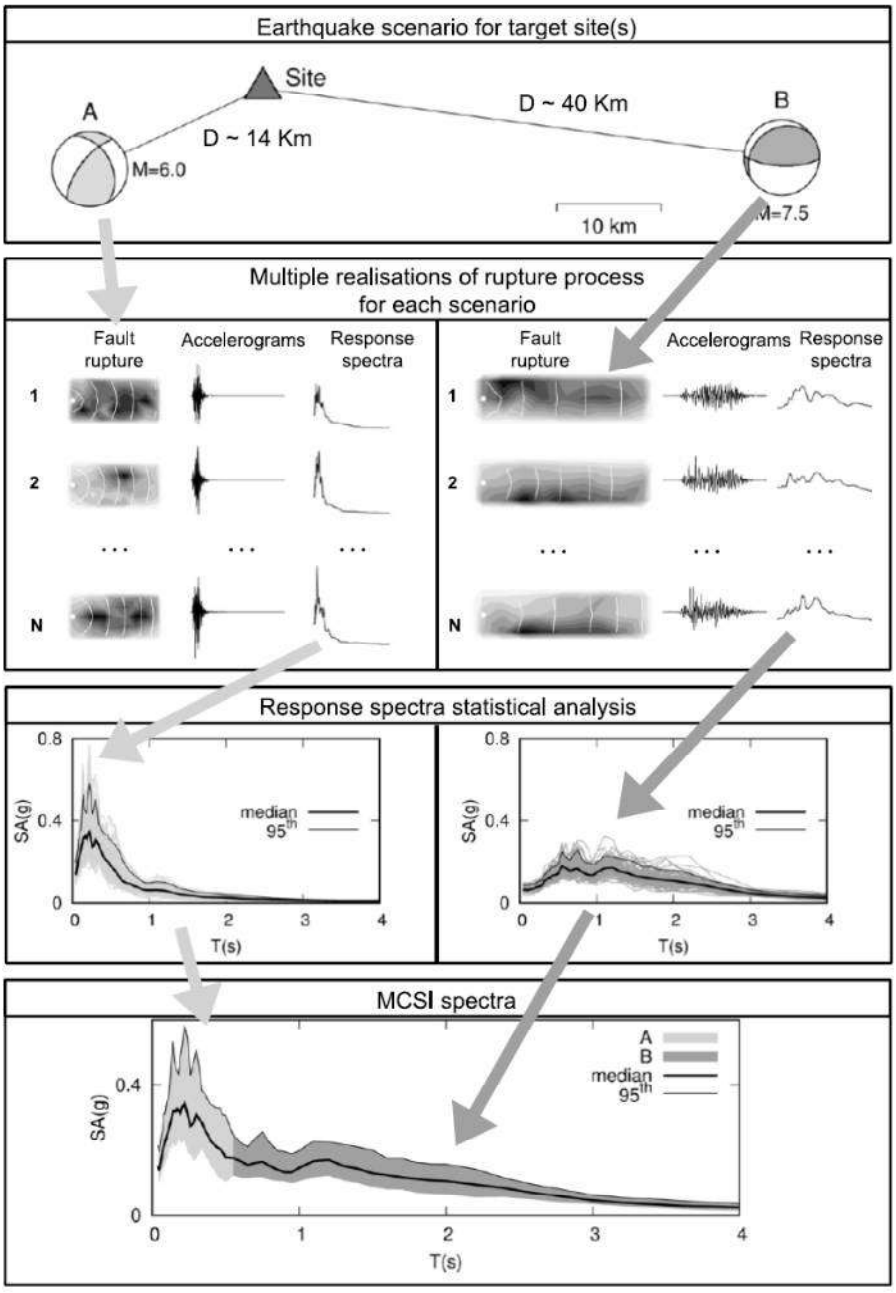

Fig. 5.3: Description of the MCSI definition procedure modified after Fasan et al. (2015).

5.3.1 Computation of $MCSI_{SS}$ spectra at the minaret site

To identify the earthquake scenarios that control the ground shaking at the site of the minaret, we carried out the MCSI at bedrock using the last updated computation of Chapter 3. The $MCSI_{SS}$ has been computed at the minaret site using NDSHA approach, which takes into account the site structural heterogeneities and the source rupture process. Three earthquake scenarios, which are shown in Table 5.1,

have been used to compute the $MCSI_{SS}$ at minaret site. The controlling events, for the range of periods from 0 to 4 seconds, have been found to be magnitude 5.9 - 7.0 earthquakes at a distance between 20km to 26km, north and west (Fig. 5.4) of the minaret. In this study, we have incorporated the scenario of the 1992 Cairo earthquake located at ~30km south of the Madrasa, although it is not contributing in the MCSI for our site. The computed response spectra for this event will be used to validate the model of the minaret in section 5.3.1 since the field visit and thorough inspection of the minaret structure did not find any cracks and the fact that the minaret was affected by the 1992 Cairo earthquake without any reported damage or cracks (Mayer & Abteilung, 2007).

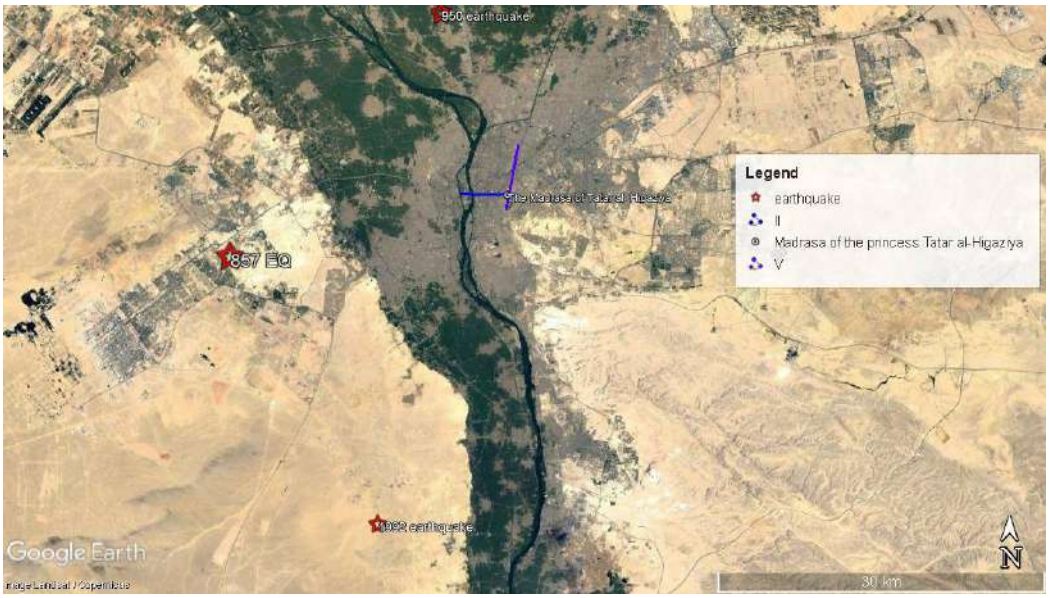

Fig. 5.4: Location of the Madrasa (pin) at the cross point between the two profiles and the adopted earthquake scenarios marked with red stars.

Synthetic seismograms have been computed with a 10Hz frequency cut-off adopting a double-couple of forces placed at the hypocenters as a seismic source representation. Besides the hypocentral depth and the magnitude, other parameters related to the rupture process at the sources have been considered (Hussein et al., 2013). During its millennial history, many earthquakes had occurred around Cairo causing damage to the built environment and human losses (e.g., Badawy et al., (2010); Ambraseys et al., 2005). For the scenarios definition, we have considered the events of October 12, 1992 (MMI = VIII, M_w = 5.9), July 25, 950 (MMI = IX, M = 6.5 - 7.0) and April 875 (MMI=XI, M = 6.5 - 7.0). Thus, the earthquake scenarios

comprise one instrumental and two historical earthquakes. The October 12, 1992, and July 25, 950 earthquakes were used as seismic sources in the modeling of the NS cross-sections which are located south and north to the cross-section, respectively (Fig. 5.3), while the April 857 was used as earthquake scenarios in the modeling of the EW cross-section. Detailed information about the source parameters for the scenarios used in the numerical modeling are given in Table 5.1.

Table 5.1: Seismological parameters for the scenario earthquakes selected for this study.

Scenarios		Location		Magnitude	Focal depth (km)	Focal mechanism			Epicentral distance (km)
No	Year	Lat	Lon			Strike°	Dip°	Rake°	
1	12 October 1992	29.74	31.63	5.9	10	285	66	-117	26
2	25 July 950	30.20	31.20	6.5 - 7.0	10	136	42	-75	20
3	April 857	30.00	31.00	6.5 - 7.0	10	136	42	-75	22

The stochastic nature of the seismic rupture process is taken into account with large numbers of fault rupture models "realizations" (i.e., 300) generated for each source; this number has been found as suitable to stabilize the solution at the percentiles of interest (Fasan et al., 2017).

Local site conditions differ from one location to another due to variations in geological formations, thickness and properties of soil and rock layers, depth of bedrock and water table, and surface and subsurface topography. These variations can cause significant effects on the characteristics of earthquake ground motions at the Earth's surface. In order to take into account the effects of soil and topographic characteristics on both the three components of the earthquake ground motion and to investigate the effect of the change in the propagation path and subsurface focusing geometry of the profiles two laterally heterogeneous profiles aligned along NS and EW directions. These profiles express the local conditions beneath the minaret of the madrasa (Fig. 5.5 a, b, respectively), have been realized using data from literature and fieldwork. Detailed 2D subsurface soil cross-sections representing the site conditions beneath most of the monuments have been introduced by Said (1975), based on the data of 217 shallow boreholes. These cross-sections are composed of fill overlying silty clay with thick sand and gravel layers beneath varying vertically and horizontally in the studied area (Fig 5.5 a and b). The average depth of the profiles developed by Said (1975) is about 80m below the MSL, and then they have been further extended

below, to approximate the bedrock depth (~120m), based on the study of Toni (2012). The details of the physical properties of the profiles are taken from Toni (2012), while the quality factors for P- and S-waves for different soil types are taken from slandered compilations. A Pleistocene-age plastic clay unit is believed to underlay the entire alluvial valley (Said 1975). This unit outcrops on the eastern margin of the valley. General descriptions of the foundation soils in the studied area are described in Said (1975).

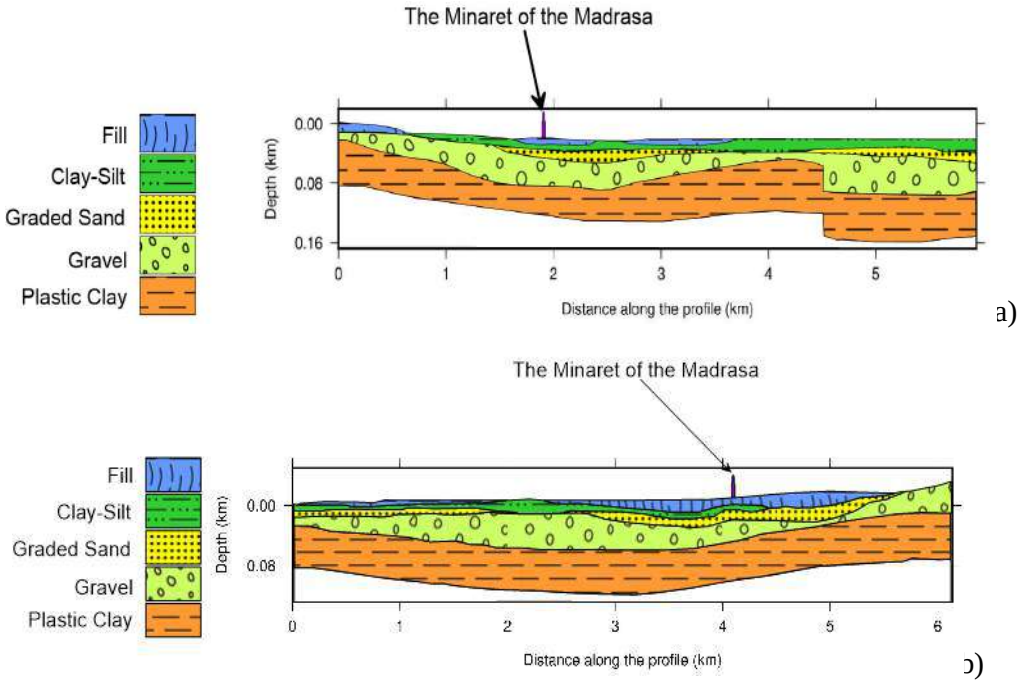

Fig. 5.5: Two laterally heterogeneous profiles go through EW (a) and NS (b) directions compiled from boreholes data and express the local conditions at the location of the minaret.

Fig. 5.6 (a and b) shows the $MCSI_{BD}$ and $MCSI_{SS}$ (values of the 50th, 84th and 95th percentiles) compared with the elastic spectra from the Egyptian building code (ECP-201 2011) (Type 1 is devoted for the whole country and Type 2 for the coastal zone along the Mediterranean) for different return periods and different site conditions, i.e., bedrock and soil site of type B according the site classification given by the code. The peak ground acceleration for two return periods (i.e., 475 and 2475) were used to scale the elastic response spectra defined by the Egyptian building code, the PGA value for 475 year spectra is adopted after the Egyptian building code (ECP-201 2011) (PGA=0.15g), while the PGA for 2475 return period (PGA=0.25g) is taken from a recent study done by Gaber et al. (2018). The comparison indicates that the $MCSI_{BD}$ and $MCSI_{SS}$ values are generally higher than those given by the building

code except for periods less than 0.2s, where the elastic response spectra exceed the MCSI. Also, Fig. 5.6 (a) indicates that the difference between $MCSI_{BD}$ and the elastic response spectra at bedrock (Types 1 and 2) for the 2475 year return period is relatively small while the difference between $MCSI_{SS}$ and response spectra at soil B site becomes large, as shown by Fig.5.6 (b), when the site effects are considered, this pinpoints that the current recommendations and practice dictated by the building code in order to account for the site effects by simply applying a site coefficient or factor based on the site classification (average shear wave velocity) is inadequate for the studied case. Also, one has to keep in mind that the scenarios that form the MCSI happened a long time before the Minaret construction that may be the reason behind the difference between the two inputs, since the PSHA approach largely depends on the completeness of the earthquake catalog which is complete only for a relatively short period (few decades) for the studied area.

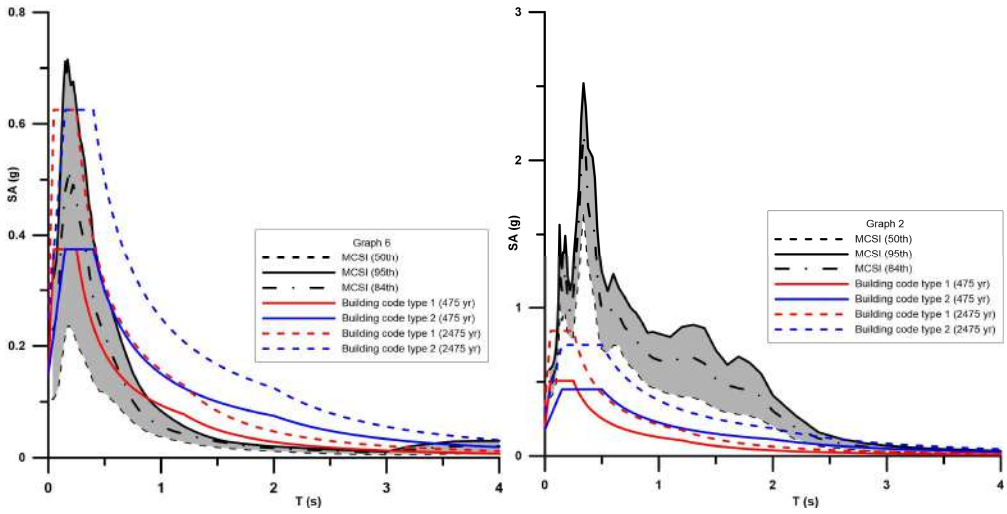

Fig. 5.6: a) $MCSI_{BD}$ for the values of the 50, 84 and 95th percentiles, compared to the building code (Type 1 and Type 2) for two different return periods (475 and 2475 years). $MCSI_{ss}$ for the values of the 50, 84 and 95th percentiles, compared to the building code (Type 1 and Type 2) for two return periods (475 and 2475 years) adopting recommended site coefficient. Shaded area represents the range between the 50 and the 95th percentiles.

5.3.2 Selection of RS and time histories

The MCSI spectrum represents a useful and conservative tool for response spectrum analyses and could be recommended for the designation of new structures, though it might be less suited to the selection of accelerograms that can be used for dynamic analysis for existing buildings and structures. A fast and effective method of

selection could be to directly use all the accelerograms, whose number depends on the number of rupture realizations, rupture style, and directivity angles, for every scenario that contribute to the MCSI spectrum. However, this could be impractical due to the huge amount of time histories, which will need long computational times and significant analysis efforts.

Since our second aim of this Chapter is evaluating the dynamic behavior of an already existing historical minaret, there is a need to find another approach for the proper selection of response spectra and time histories. A different approach can be used to select the target accelerograms, limiting at the structural periods of interest. For example, the period of the fundamental mode of the building, as defined by a "Conditional" Maximum Credible Seismic Input (C-MCSI), as proposed by Fasan (2017). The concept is very similar to what is called Conditional Mean Spectrum (CMS), proposed by Baker and Cornell in (2006) as a more realistic alternative to the UHS (Baker, 2011; Baker and Cornell, 2006).

C-MCSI response spectrum can simply be defined by considering the spectral accelerations with the most hazardous source at the period of interest and selecting only the restricted range of simulations, giving the highest values of spectral acceleration at that specific period.

Fig 5.7 shows the C-$MCSI_{SS}$, and the $MCSI_{SS}$ computed for the site of the minaret, which is set equal to the value of the 50^{th} percentile and compared to the building code (Type 1 and 2) after considering site-effects Fig. 5.8 shows the 50^{th} C-MCSI and 1992 Cairo earthquake response spectra computed using NDSHA at 5% damping at the site of the minaret then they will be used to analyze the seismic response for the minaret structure in the next section. C-MCSI is calculated by selecting the simulation that has a median spectral acceleration corresponding to the 50^{th} percentile at the period of interest and then choosing the median values of these simulations at each period. It worth to mention that, C-MCSI accounts for the spectral shape of the most dangerous scenario at the period of interest of the minaret Moreover, Fig 5.7 indicates that both 50^{th} C-MCSISS and MCSISS spectra largely exceed the elastic response spectra defined by the building code (Type 1 and 2) for return periods of 475 and 2475 years.

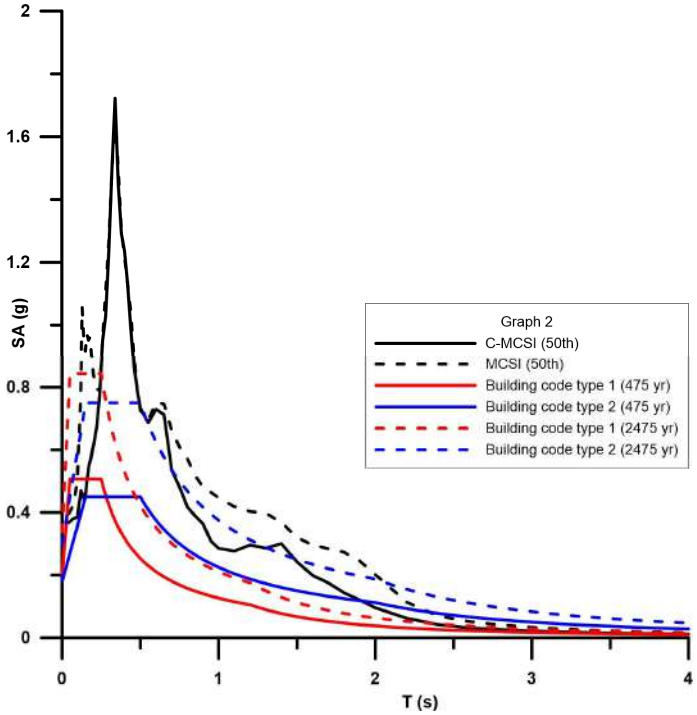

Fig. 5.7: The MCSI and C-MCSI are set equal to the value of the 50th percentile and compared to the building code (Type 1 and Type 2) after considering site-effects.

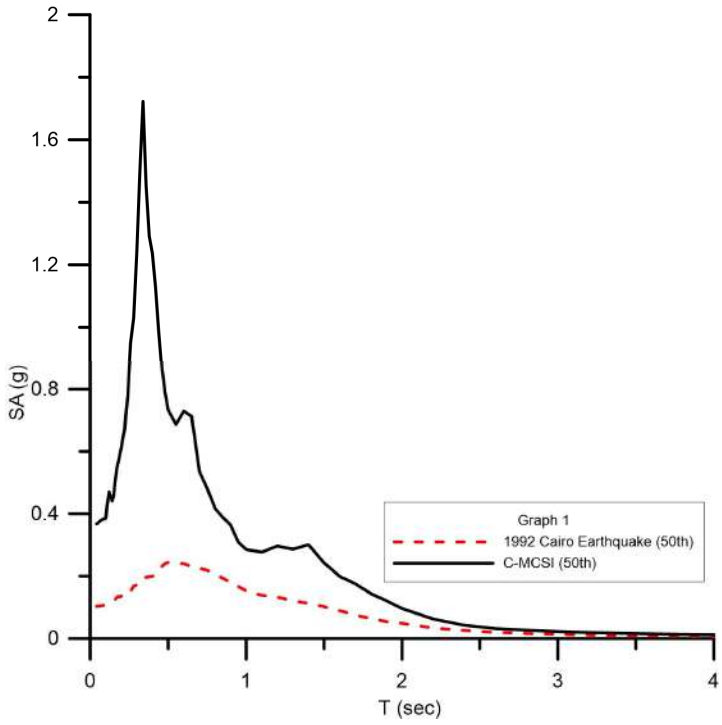

Fig. 5.8: C-MCSI and 1992 Cairo earthquake response spectra at 5% damping.

The selection, therefore, of the accelerograms for structural analysis become immediate, since it simply consists in retrieving the simulations used to define the C-MCSI. Since the standard number of realizations of the source rupture process is 300, the number of simulations used to define the C-$MCSI_{SS}$ is the median 31 (realization no 135-165 after arranging them in ascending order). If a larger number of accelerograms is needed for special purposes (i.e., defining the distribution of some Engineering Demand Parameters (EDP)), it is necessary to increase the number of realizations of the rupture process. On the contrary, to perform a smaller number of structural analyses (e.g., seven, as suggested by building codes), a subset of these accelerograms that has a spectrum compatible with C-MCSI should be used. In our case, we have chosen the median 7 realizations with 3 components, i.e., 21 accelerograms. The seven selected C-$MCSI_{SS}$ time histories in EW and NS directions at the site of the minaret and their corresponding response spectra of the ground motion components 50^{th} C-$MCSI_{SS}$ and 5% damping are plotted in Fig. 5. (a) and (b)**.** Once the accelerograms are selected, they can be considered as a seismic input to the engineering model of the building.

5.4 Minaret Modeling

The minaret consists of a 24.16m vertical shaft of cut stone above the ground level. The ground plan of the minaret is squared with a side of 3.45 m up to a height of 11 m, after which there is a transition to an octagonal plan, further emphasized by beveled corners. There are two tiers of balconies with stone parapets, accessed by an internal stone spiral staircase. The shaft changes in its cross-section from a square base to an octagon prism followed by a smaller octagon prism. A cylindrical shaft that contains the inner spiral staircase extends from 7.2 m above the ground to the crest of the minaret. The minaret dimensions and geometry is illustrated in Fig. 5.10.

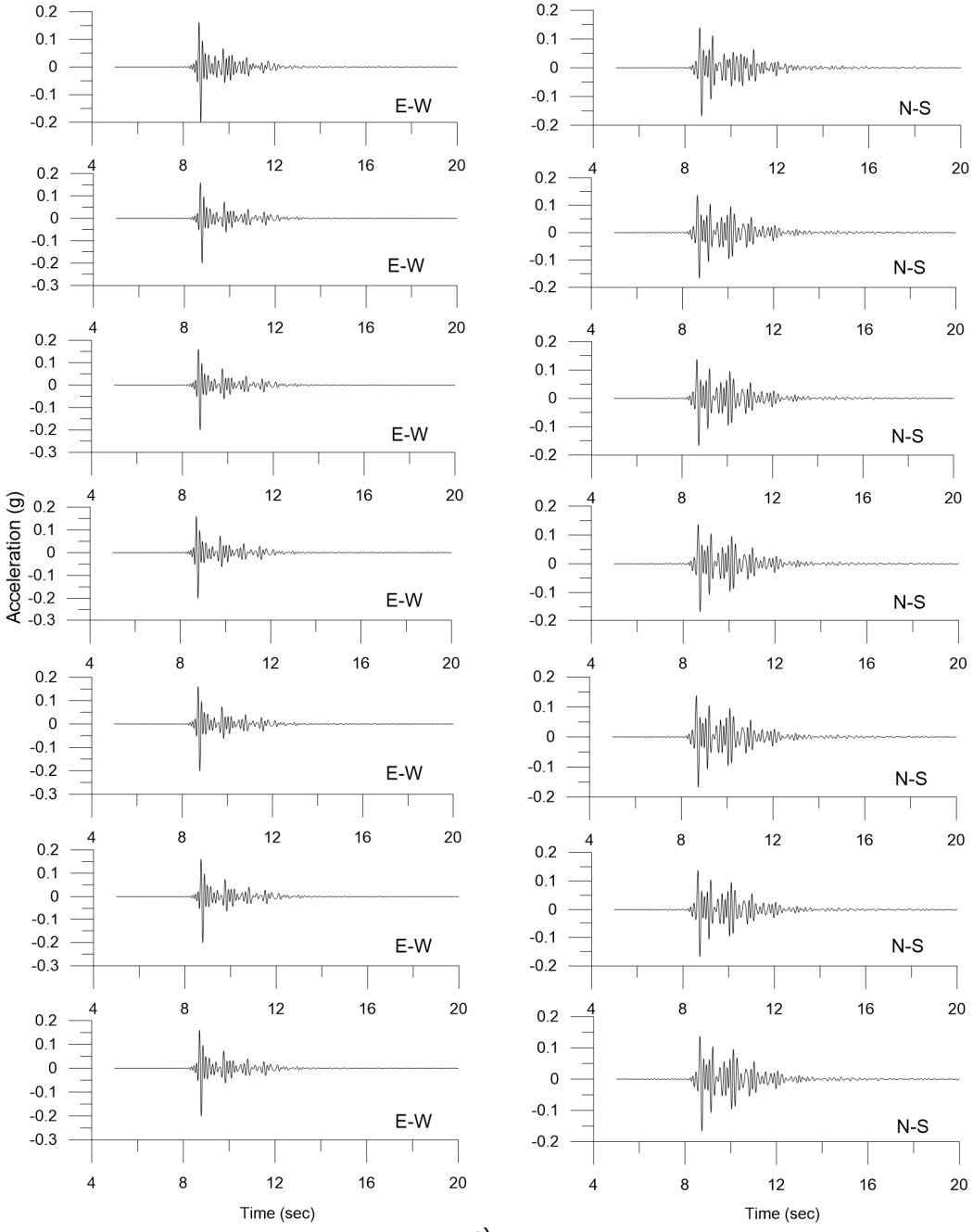

a)

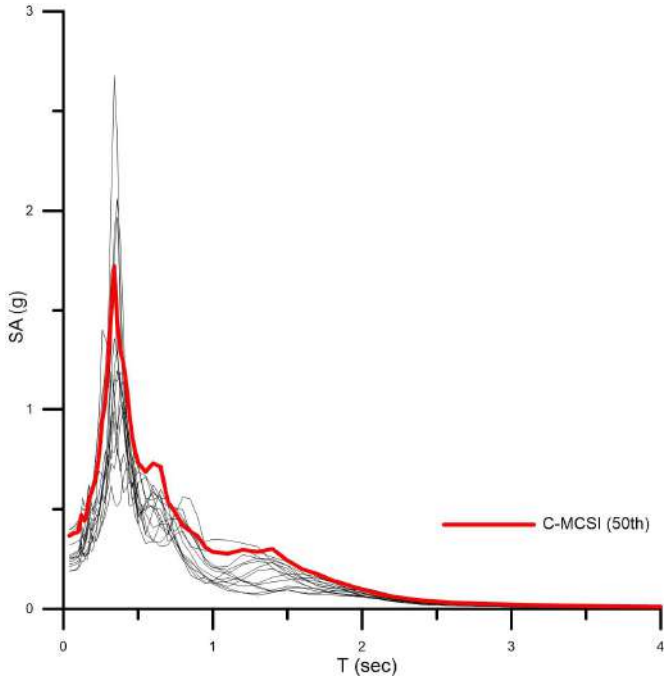

b)

Fig. 5.9: a)The seven selected (on the median) C-MCSI time histories in EW and NS directions at the site of the minaret and their corresponding; b)50th C-MCSI and response spectra of the ground motion components at 5% damping.

A previous study performed by Imam (2001) on the structural condition of the Madrasa and its buildings was conducted in 2001 as part of the national historic Cairo project. The study yielded a report affirmed that the minaret is structurally separated from the rest of the Madrasa with a vertical gap or separator which may pose a pounding potential between the adjacent structures due to the horizontal vibration of the minaret. Moreover, five stone cone samples from three different parts of the Madrasa were extracted by Imam (2001) to define the different values of the mechanical properties of the limestone used in the construction. The report found that the un-cracked stone samples have a specific weight of 2.08t/m^3, a compressive strength of 27.47MPa, a tensile strength of 5.4MPa, and elastic Young modulus of 25.497GPa. Therefore, the numerical modeling of the minaret in this study is conducted considering a structurally separated minaret with the aforementioned material properties of the limestone blocks.

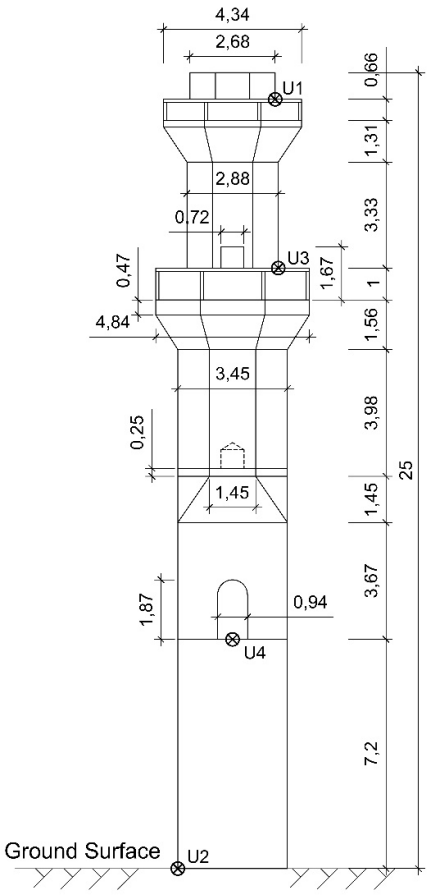

Fig. 5.10: Minaret geometry and instrumentation (Un) locations ***(all dimensions are in m).***

The minaret was visually and physically inspected to investigate cracking and construction materials condition. Correspondingly, ambient vibration measurements by deploying seismic instruments at different locations inside the minaret body were conducted. The ambient vibration was introduced to evaluate the modal frequencies of the generated finite element model of the minaret. After very precise inspection, no visible cracks were detected in the minaret body, around the different openings, or near the joints. Therefore, un-cracked limestone material properties are considered in the minaret modeling with values stated previously.

5.4.1 Ambient Vibrations Analysis

The ambient vibration measurements was significant for the calibration of the dynamic behavior of the minaret numerical model. Four tri-axial accelerometers with range of +/- 4g were installed at different heights on the minaret to record the ambient

vibration response of the minaret. The locations of the sensors are illustrated in Fig. 5.10. The McSIES-MT NEO data acquisition instrument for microtremors measurement and vibration monitoring is considered for the ambient vibration response analysis. The first sensor (U1) was placed at the top balcony at the height of 24.16m from the ground level, while the second sensor (U2) was placed at ground level. In addition, the third sensor (U3) was placed at the first balcony at height of 18.86m. The fourth sensor (U4) was placed at the minaret entrance at the height of 7.20m.

The ambient vibration recording lasted for 60 minutes, with a recording sampling frequency of 100Hz. Post-processing of the acceleration measurements with baseline correction and high-pass filter has been considered. A fourth-order Butterworth high-pass filter was applied, and the corner frequency for the selected filter is calculated as (Sayed et al., 2015):

$$f_c = \frac{1}{T\left[\frac{H_0}{1-H_0^2}\right]^{\frac{1}{2n}}}$$

Where, f_c is the corner frequency, n is the high-pass filter order, T is the acceleration recording time, and H_0 is the filter amplitude threshold that is selected as 0.02. The waveforms and power spectra at the top balcony (U1) are depicted through Figure 5.11 and 5.12, respectively, for the three orthogonal directions at the same recording point. Post-processing the different minaret measurement points indicates that the fundamental period of the minaret is approximately 0.5s. The ambient vibration results are correlated with the finite element model results in the following section.

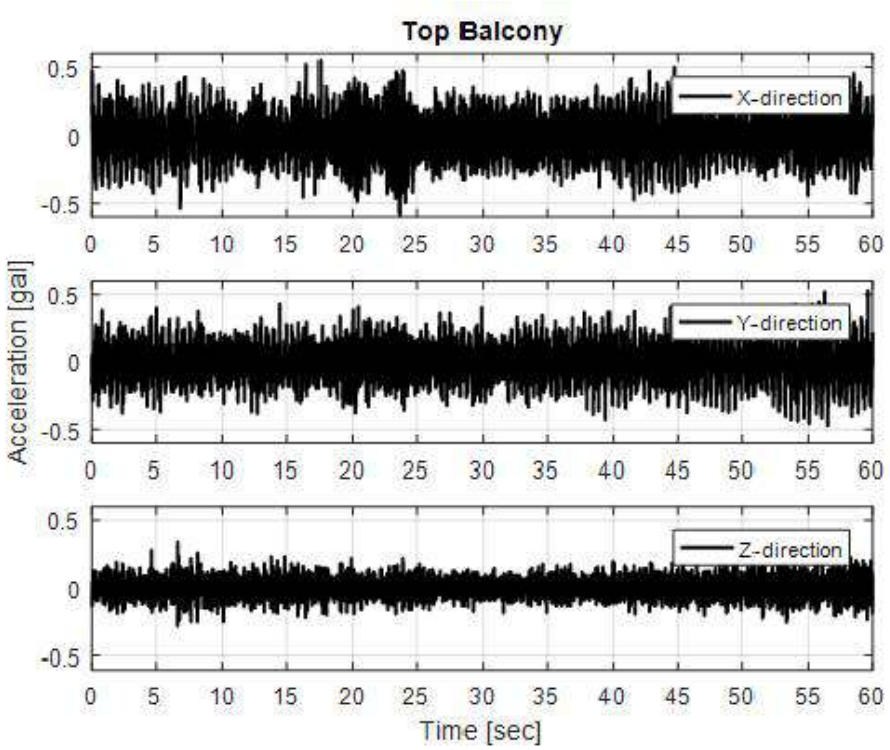

Fig.5.11: Ambient noise time series, for all directions, at the top balcony measurement point (U1).

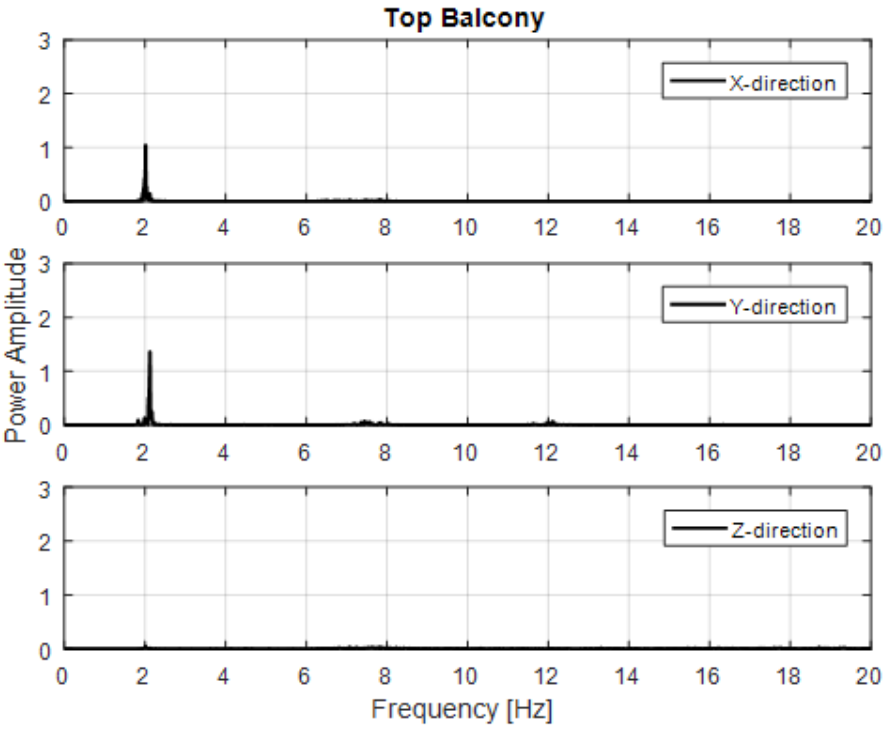

Fig. 5.12: Power spectra of the time histories, for all directions, at top balcony measurement point (U1).

5.4.2 Numerical Model

The numerical model of the minaret was modeled in SAP2000 (CSI, 2016). A linear elastic analysis is conducted for the minaret since no cracks were observed after the minaret inspection. The minaret base and shaft are modeled using eight-node solid elements, while the balcony posts are modeled as frame elements with square cross-section of 0.13m×0.13m, the balcony walls are modeled as shell elements with thickness of 0.13m. All the cross-sectional variation and openings in the minaret were accurately simulated in the model. The spiral stair was not modeled in this study for conservative modeling, since ignoring modeling the spiral stairs slightly influenced the modal analysis and reduced the stresses in the minaret (Sezen et al., 2008). Mesh sensitivity analysis is conducted to the minaret to produce a modal analysis close to the ambient vibration analysis. Following the minaret model discretization, the finite element model consists of 80,849 nodes, 64,355 solid elements, 16 frame elements, and 16 area elements. The total weight of the minaret is calculated as 4412.90KN.

The soil behavior beneath the minaret base is modeled as linear springs with a specified modulus of subgrade reaction. The soil modulus subgrade reaction was calculated using (Vesic, 1961) as:

$$K_s = \frac{0.65E_s}{B(1-\upsilon_s^2)} \sqrt[12]{\frac{E_s B^4}{E_f I_f}} \quad (2)$$

where, K_s is the soil modulus subgrade reaction, E_s is the soil Young's modulus, B is the foundation width, υ_s is soil Poisson ratio, E_f and I_f are the foundation Young modulus and moment of inertia, respectively. The soil properties beneath the minaret foundation are taken from the Chapter 4 with density of 1.5t/m^3, shear wave velocity of 180m/s, and the Poisson ratio of 0.30, while the calculated soil Young modulus is 74.77MPa. Moreover, the properties of the minaret foundation are considered as B of 3.45m, E_f of 25.497GPa and I_f of 11.805m^4. The calculated soil modulus subgrade reaction is 11.71N/mm^3. The modal analysis results and the comparison between the ambient vibration results and the numerical model with a modulus of subgrade reaction are illustrated in Table 5.2.

. The difference between the period obtained from the noise measurements and the FEM, which is about 12% only, could be attributed to the uncertainty in empirical equation used to estimate the subgraded soil reaction, the absence of accurate measurements for soil properties and the presence of micro cracks and local

deteriorations that cannot be tackled by the FEM model. Moreover, looking at the power spectrum for the different components of the noise measurements in Figure 5.12, the estimated natural period is ranging between 1.8-2.1Hz which is very close to the period for the FEM model (i.e., 2.29Hz). The numerical model of the minaret in SAP2000 is shown in Fig. 5.13. The results indicate that employing a soil modulus subgrade reaction of K_s=11.71N/mm^3 produces a fundamental time periods close to that from the ambient vibration. Therefore, all further analyses are investigated considering soil modulus subgrade reaction stiffness of K_s=11.71N/mm^3.

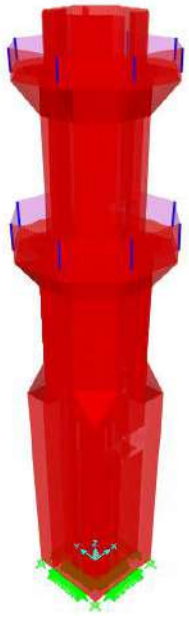

Fig. 5.13. Detailed finite element model of the minaret.

Table 5.2. Modal analysis results of the measured ambient vibration and finite element model with soil subgrade reaction and fixed base conditions.

Mode	Frequency (Hz)			Mode description
	Ambient Vibration	FEM with fixed base	FEM with soil modulus subgrade reaction	
1	1.8-2.1	5.59	2.29	(x direction)
2	2.1-2.4	5.72	2.42	(y direction)
3	-	-	2.80	(z direction)
4	14.7-15.6	21.69	16.87	(x direction)
5	15.7-17.7	40.07	17.11	(y direction)

The normalized horizontal displacement extracted from the ambient vibration and the modal analysis of the FEM model along the minaret height is plotted in Fig. 5.14. The normalized displacement of the ambient vibration analysis represents the peak displacements from the different sensor locations at the minaret, particularly

sensors U1, U3, and U4. Moreover, the normalized displacement of the modal analysis of the FEM stands for the lateral displacement in the x-direction of Mode 1 and the y-direction of Mode 2. Since the governing mode description of Mode 1 is the motion in x direction, while Mode 2 is in the y-direction (Table 5.2). The good general agreement between the normalized displacement of the FEM model and the ambient measurements is observed except at the geometry transition zones above the base, and the balcony slabs due to lack of measurements at these points owing to the impracticality of installing a sensor at them. Moreover, the FEM results gave a reasonable good estimate of the minaret lateral deformation since it adapts the precise geometry, sections, openings, and stiffness variation along the minaret height, while the ambient vibration plot is simply representing the linear piecewise connection between the limited available measurements (3 points) points. In addition, the disagreement between the results may also be attributed to the numerical model deficiency in simulating the minor deterioration in the actual limestone bricks or fill material. The previous results exhibit the significance of the field measurements for such structures on tuning and evaluating the finite element model.

The limestone bricks mechanical properties selected for the numerical modeling of the minaret yields to a compressive and tensile strength of 27.47MPa and 5.40MPa, respectively, as previously mentioned. The principal positive (tensile) and negative (compressive) stresses are investigated noting that by definition the principal stresses are oriented such that the associated shearing stress is zero. The principal stresses usage as a failure criterion is allowed and restricted to brittle materials such as limestone. The peak principal stresses analysis due the gravity loading cases is illustrated in Fig. 5.15. The results show that the peak principle compressive stresses are -1.02MPa, and the peak tensile stresses are 0.227MPa, for the three orthogonal principal stress tensor σ_{11}, σ_{22}, and σ_{33}. In details, the peak principle compressive and tensile stresses are -0.208, -0.209, -1.02, and 0.227, 0.177, 0.131MPa for stress σ_{11}, σ_{22}, and σ_{33}, respectively. The principal stresses results are acceptable within material stress limits used in the minaret construction, and they indicate that the minaret can withstand its weight with no cracking.

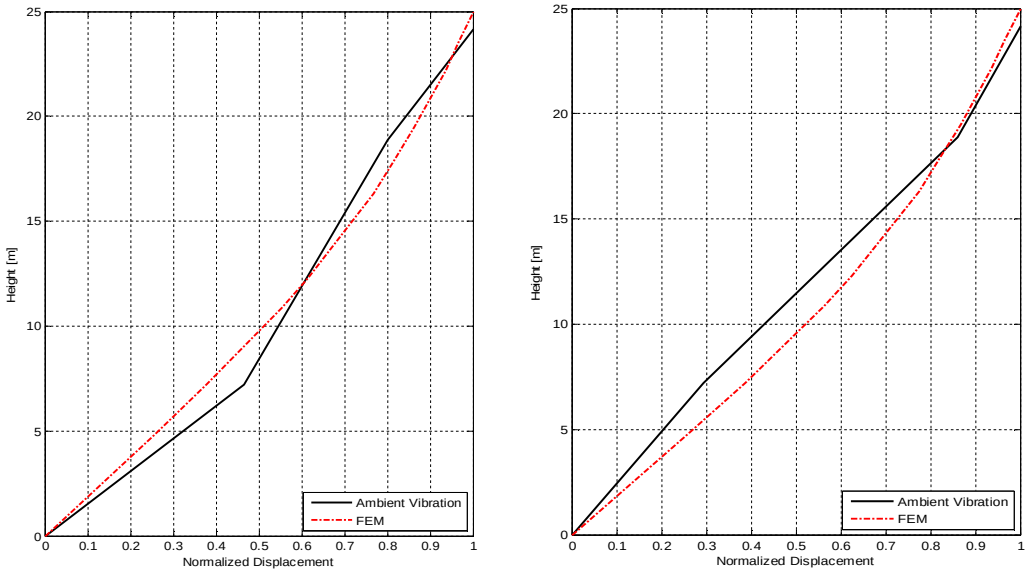

Fig. 5.14: Normalized horizontal displacement of the FEM model and the ambient vibration measurement points in X-direction (mode 1) and in Y-direction (mode 2).

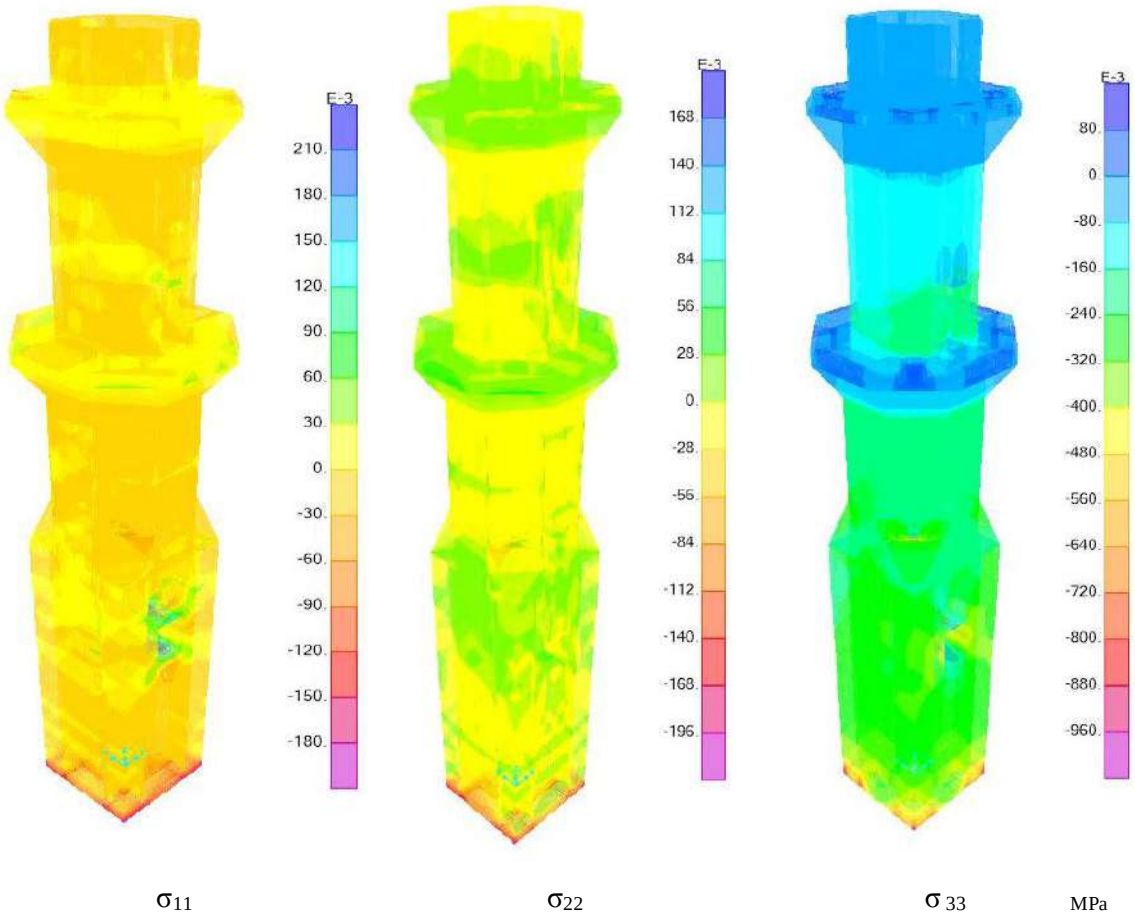

Fig. 5.15: Principal stresses on the minaret body due to gravity loading.

5.4.3 Earthquake Response Spectrum Analysis

In this section, the linear-dynamic response spectrum analysis is conducted to draw the maximum stresses on the minaret body taking into consideration the gravity load due to the self-weight of the minaret. Two response spectrum analysis cases are investigated: the 1992 Cairo earthquake and the C-MCSI response spectra.

5.4.3.1 1992 Cairo Earthquake Spectrum

The 1992 Cairo earthquake case is selected to determine the accuracy of the numerical model in detecting the minaret response, since the minaret has survived the Cairo earthquake with neither damages nor cracks. Moreover, the acceleration response spectrum of the 1992 Cairo earthquake obtained from the MCSI analysis is investigated, since there are no known ground motion records for the event near the site of interest. Therefore, the 50^{th} percentile response spectrum of the 1992 Cairo earthquake is used to conduct the response spectrum analysis for the minaret model in both horizontal directions. The principal stresses results are plotted in Fig. 5.16, and they show that compressive stresses are always under the allowable compressive strength with peak values of -0.206, -0.205, -1.00MPa for σ_{11}, σ_{22} and σ_{33}, respectively. On the other hand, the tensile stresses are large but not enough to exceed the tensile strength, as the peak recorded principle tensile stress tensor was 2.14, 1.39, 5.13MPa in the minaret body for σ_{11}, σ_{22}, and σ_{33}, respectively. As expected, the numerical model introduced an acceptable behavior of the minaret under the Cairo earthquake response spectrum through producing undamaging peak tensile and compressive stresses along the minaret, especially at the transition zone or near the openings.

5.4.3.2 C-MCSI Spectrum

The calculated C-MCSI at 50^{th} percentile spectrum is applied at the minaret base in both horizontal directions. The principal stresses results are depicted in Fig. 5.17 and they show that the minaret would suffer significant tensile stresses exceeding the limestone tensile strength, which denotes enormous cracking and even crushing in the minaret, particularly at the base and at the transition zone right above the base. The peak tensile and compressive stresses are 4.63, 4.94, 8.91MPa and -0.20, -0.19, -0.93MPa, respectively. This level of tensile stresses predicts severe damage or even

collapse of the minaret under the C-MCSI response spectrum. The previous results demonstrated that the tensile stress concentrations took place at the end of the transition zone between the square base and the hexagon shaft, where the reduction of the minaret cross-sectional area occurs.

The peak horizontal displacement along the minaret height under the 1992 Cairo and C-MCSI$_{SS}$ response spectra action is illustrated in Fig. 5.18. The results show that C-MCSI response spectrum developed higher lateral displacement along the minaret height. Furthermore, the peak lateral displacement under the C-MCSI$_{SS}$ spectrum is about 70.80mm and 72.80mm in x and y-direction, respectively, compared with 15.30mm and 13.0mm under the 1992 Cairo response spectrum in x and y direction, respectively.

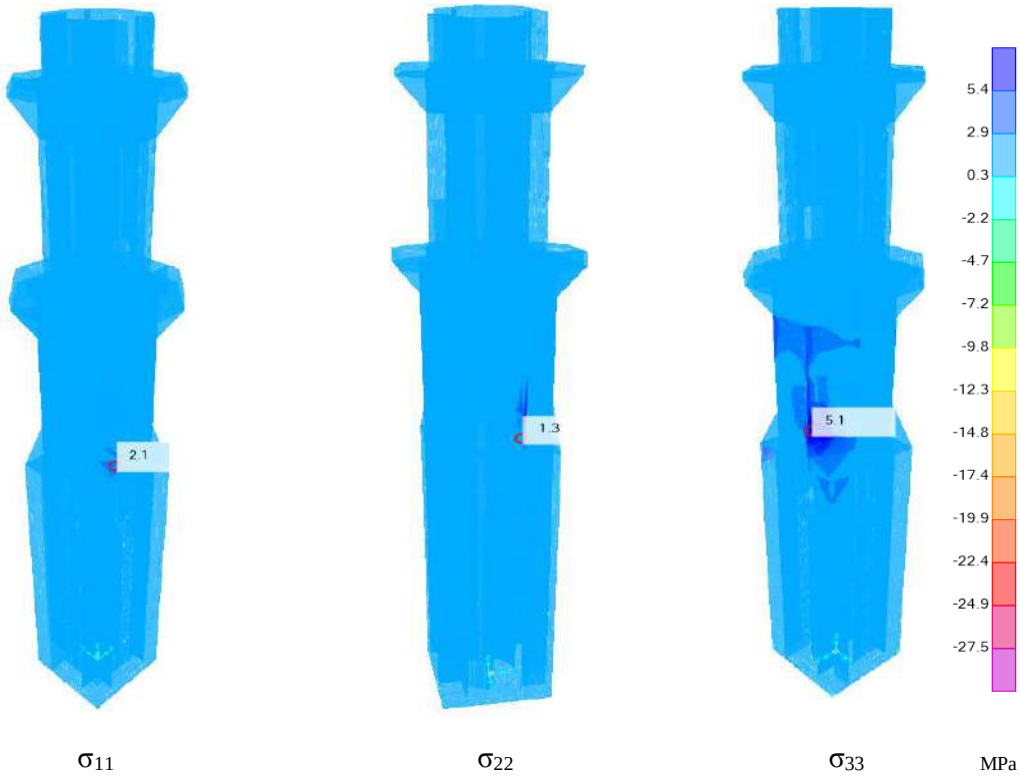

Fig.5.16: Compressive and tensile principal stresses on the minaret body under the 1992 Cairo earthquake response spectrum. The upper and lower values of the legend are set to equal the compressive and tensile strengths of the limestone brick used in the minaret model.

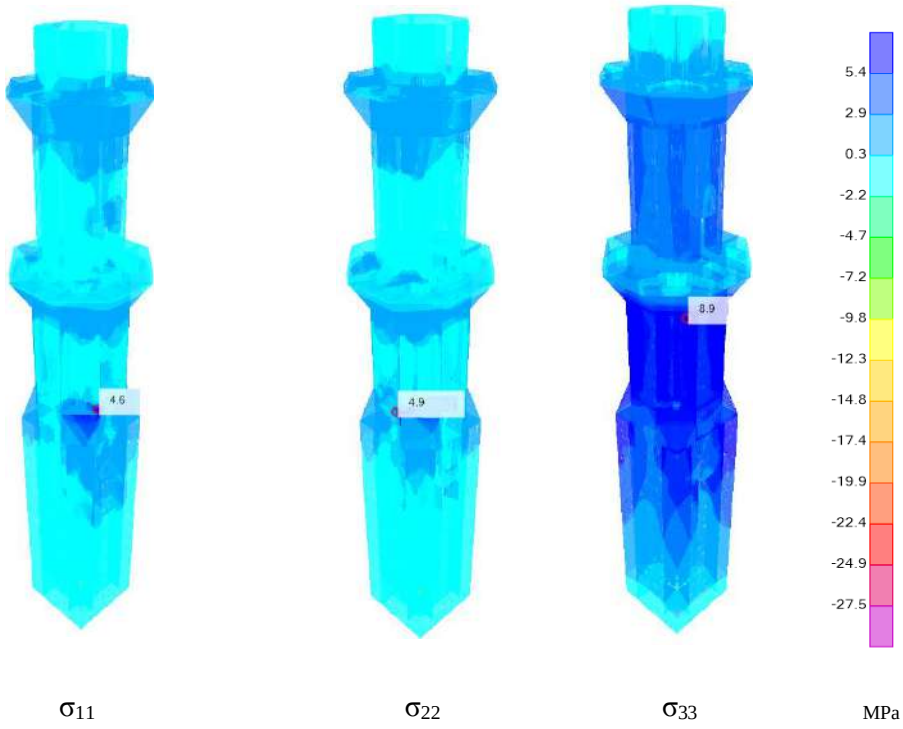

σ_{11} σ_{22} σ_{33} MPa

Fig. 5.17: Compressive and tensile principal stresses on the minaret body under C-MCSI response spectrum. The upper and lower values of the legend are set to equal the compressive and tensile strengths of the limestone brick used in the minaret model.

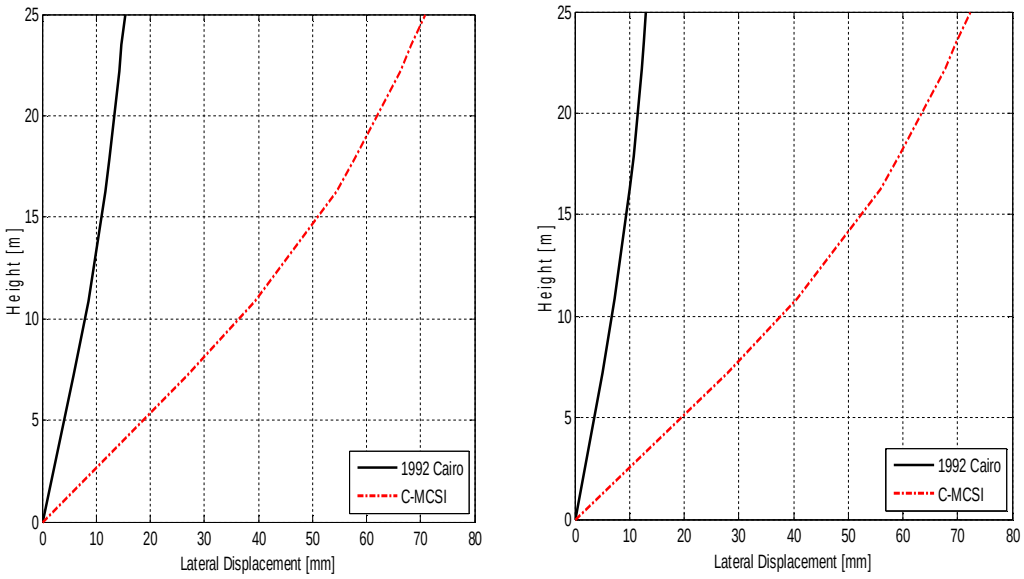

X direction Y direction

Fig. 5.18: Maximum horizontal displacement along the minaret in X-direction (left panel) and Y-direction (right panel) height under the 1992 Cairo and C-MCSI response spectra.

5.4.4 Time History Analysis

The seven pairs of accelerograms selected in section 5.3.2 are considered for conducting the time history analysis of the minaret. The peak lateral displacements at the transition zone and at the top of the minaret in X- and Y-directions are illustrated in Table 5.3; their fluctuation between the two orthogonal directions is mainly due to the difference between the ground motions components (NS or EW) assigned for each direction. However, it is worth mentioning that a slight difference exists in the peak displacement between the X- and Y-direction due to the geometry irregularity (i.e., openings, imperfect symmetry, etc.) as seen in the C-MCSI$_{SS}$ response spectrum results shown in Table 5.3, although identical response spectrum is applied in the X- and Y-direction at the minaret base.

The floor response spectra for 5% damping have been computed at the top of the minaret using time history analysis as shown in Fig.5.19, where the mean of the seven response spectra is also depicted for both orthogonal directions. The spectral responses at the top of the minaret (base of the mabkhara or cap), which describes a specific shape of the minaret finial, are here studied since the mabkhara is always considered the weakest part of the minaret i.e., more likely to collapse during ground shaking. The minaret cap (currently are not in place) already experienced damage and complete failure earlier as noticed comparing Fig.5.1 (b) and (c) (Mayer and Abteilung, 2007). Thus, the time histories analysis has been made at the top of the minaret (base of the cap or mabkhara) which it could be needed in case of the future restoration of this part since it is not currently in place. Substantial amplification occurs in the response spectra with peak ground acceleration (PGA) of 1.37g and 1.28g, in X- and Y-direction, respectively.

Table 5.3: Maximum horizontal displacement at the transition zone and at top of the minaret subject to time history analysis.

Measured point	Maximum horizontal displacement [mm]			
	Top		Transition zone	
Direction	X-dir	Y-dir	X-dir	Y-dir
Seven ground motion pairs	51.41	39.80	31.57	24.76
	63.49	54.65	39.04	33.93
	59.72	54.91	36.82	34.31
	60.20	44.37	37.17	27.75
	64.10	49.53	39.46	30.85
	59.07	31.14	36.35	19.38
	57.51	52.00	35.47	32.39
Mean	59.36	46.63	36.55	29.05
C-MCSI RS	70.80	72.80	43.70	45.20

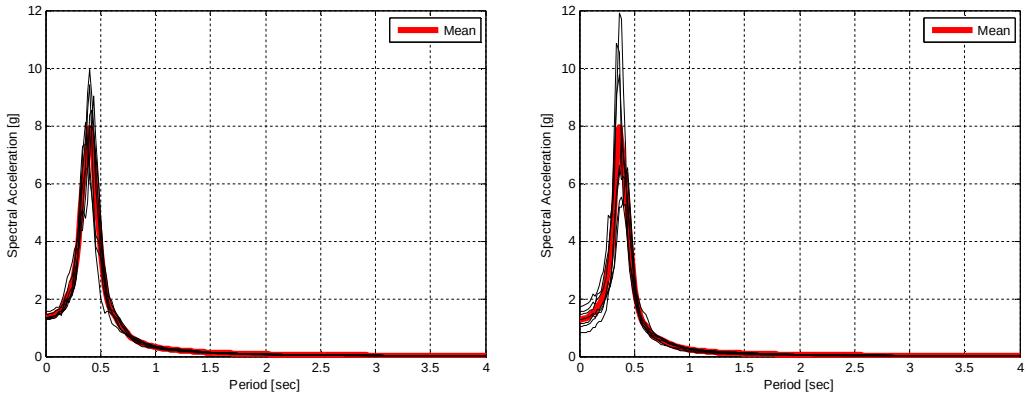

X-Direction Y-Direction

Fig.5.19: Acceleration response spectra at the top of the minaret, for 5% damping, in X-direction (left panel) and Y-direction (right panel)

Conclusions

We must accept, and adopt as reliable, the seismic hazard maps which fit well with what had been actually recorded (e.g., macroseismic intensity) and those that are based upon correct and tested theory, physical assumptions and methodology; then we have to try to improve them when new data or theoretical developments become available. In addition, the adoption of any hazard map should be done with a full understanding of its limitations and its relations to other steps in seismic engineering and risk analysis.

The main aim of this work is the computation of ground motion parameters at national and site-specific scales using the NDSHA approach, which is well suited for the computation of synthetic seismograms using information about earthquake scenarios and structural model. The results of this study are ready to be implemented in land use and urban planning and to be considered or adopted in the ongoing sustainable development in Egypt in order to reduce the possible socio-economic impacts from future earthquakes. Also, this work has provided the seismic input at a cultural heritage site and then used to evaluate its seismic response.

The author of this thesis think that in order to maximize the effectiveness and usefulness of seismic hazard analysis, at any scale of interest, the analyst should understand the needs of end users; therefore we tried to involve such understanding in the following work.

As a first step, we performed a detailed review for the seismic hazard studies accomplished at different geographic scales in Egypt, in order to evaluate the performance of the existing maps and to find out their shortcomings and limitations, if any. To do that, we properly collected and tested the existing SHA maps, computed at different scales, against the available observations and physical assumptions, data quality, and methodology and finally, we have proposed some suggestions and comments that could be considered before new seismic hazard maps can be produced, and then adopted, for the benefit of the society.

One of the main findings is that, as it is the case of global studies, although the many lessons learned through the time, most of the seismic hazard maps for Egypt and nearby regions failed to predict the ground motion parameters, as it is evidenced by merely comparing the expected ground motion parameters by different studies with macroseismic intensities. The failure may be due to the fact that, in order to identify the location and characteristics of seismotectonic sources for Egypt, only seismological observations (about 118 years) have been considered. While paleoseismological and MZ investigations or similar studies that are suitable to identify seismotectonic sources that may be active over a time scale that is larger than the instrumental database time span have been ignored or unappreciated. It is worth to mention that, the available seismological data for Egypt is not sufficient for sophisticated testing, but the result of the current testing cannot be overlooked.

In spite of the poor performances and fundamental shortcomings of the existing PSHA studies available for Egypt, the current seismic design strategy as well as the building code and its updates, still, rely upon seismic hazard maps obtained by those studies. To overcome the limits of design procedures based upon PSHA seismic input (Fasan et al., 2015; Rugarli, 2014), it is necessary to resort to a new seismic design strategy based upon the NDSHA definition of the seismic input in Egypt.

Taking into account the recommendations and suggestions developed in Chapter 1, we updated the seismotectonic model of Egypt. About 20 seismogenic zones that may produce significant ground shaking in Egypt were defined using all the available information from different disciplines. Most of these zones are aligned along well known and clearly defined active trends and faults, while a few of them exhibit sporadic seismic activity due to inadequate knowledge about their sources, so far. Developing an updated seismotectonic model of Egypt was motivated by the released of new information and it may subjects to future modification when new data will be available. In this work, the seismotectonic zones marked by strong earthquake M5+ have been identified. This condition could guarantee reliable identification of seismogenic zones not influenced by non-tectonic events (e.g., quarry blasts) which are common in some areas in Egypt. We used magnitude values between 3 and 5 to define reliably the zones borders. Since, the boundary between seismotectonic zones is not sharp as it appears; the reason behind the fuzziness of the boundary between defined seismogenic zones could be due to the possible uncertainty involved in the seismotectonic model definition and characterization. This uncertainty could be due to inadequate knowledge about

earthquake rupture process, active faults, lack of correlation between seismicity and active structures, and the errors in the earthquake catalogs. Then, for areas that did not show earthquake M5+, we used pattern recognition analysis for the identification of seismogenic nodes (earthquake prone sites), which represent a complementary and crucial step particularly for regions of low seismicity and long recurrence interval of strong earthquakes like Egypt.

A responsible seismic hazard assessment requires the incorporation of both results (i.e., defined seismogenic zones and nodes) since the results obtained can provide information for long-term seismic hazard assessment on the potential earthquake sources (i.e., in north-east Egypt). The recognition performed pinpoints some of dangerous nodes, where moderate events have not been recorded untill now. The incorporation of both seismogenic zones and nodes data together in seismic hazard computation may improve the performance of the resulting maps in the study region, especially for the sites that did not show any seismic activity, so far.

An update of the seismic hazard maps available for Egypt that incorporates recent studies, such as reviewed historical earthquake catalogs, morphostructural zonation data, revised focal mechanism solutions, and mechanical models of the lithospheric structure was performed (Chapter 3) and ready to be used. This is done in the framework of the NDSHA approach that may effectively accommodate any reliable new data to adequately compute the ground shaking parameters (i.e., PGA, PGV and PGD). Furthermore, with a set of relevant scenario earthquakes, it provides a large dataset of synthetic seismograms, particularly crucial for the areas that suffer from the endemic lack of useful strong motion time histories such as Egypt, setting the base towards detailed and comprehensive seismic microzonation studies.

Then, a sensitivity analysis based on the different ground motion maps computed adopting different (a) earthquake source process models, (b) crust structural models, and (c) mapmaker's preconceptions (e.g., different seismotectonic models), is provided in Chapter 3. The maps of difference and ratio between various ground motion maps computed for different variants are shown then discussed, in order to explore the influence of using multiple models as input data. This work provides the potential users with an adequate spectrum of choices and reliably assesses and communicates the possible uncertainties. Also, the results obtained in Chapter 3 represent a database toward detailed and comprehensive ground motion modeling for a given site. The update and the sensitivity analysis of seismic hazard maps have been

published as Hassan et al., (2017b). The structural anelastic models are an essential input in SHA computation using scenario-based approaches and have a profound effect on the resultant ground motion parameters. All of the existing models are simple and have not a uniform resolution (i.e., 1D average structural model), and the need for the revision of the crustal models is obvious, taking into account all the crustal studies available for different regions of the Egyptian territory and eventually, to plan new studies of uniform spatial resolution where crucially necessary.

A site-specific ground motion modeling study is accomplished for the area of historic Cairo, which contains a large number of cultural heritage, residential and infrastructure buildings, in order to figure out the possible modification in the wave field due to path effect and local conditions (Chapter 4). The results were used for seismic input computation in Chapter 5. We have made a detailed linear ground motion modeling and characterization of site-effects using a hybrid approach that combines both MS and FD techniques, to model the ground motion induced in laterally heterogeneous structural models at the selected sites using different earthquake scenarios. The synthetic accelerograms have been computed with a regular spacing of 60 meters up to 8 Hz cut-off, first in the laterally non-varying structural model with the MS and FS techniques. We have employed a regional bedrock model from the study of El-Khrepy (2008), and then it is introduced into the laterally heterogeneous Profiles I, II, and III, which have been composed using borehole data from Said (1975) and fieldwork, and numerically propagated by the FD approach. The scenarios being used are the earthquakes of 1992 and two historical ones (Chapter 4). For the modeling of ground motion along NS (named I and II) cross-sections, we have chosen the October 12, 1992 “Scenario 1” (MMI = VIII, M_w 5.9) and 950 “Scenario 2” (MMI = IX, M ~ 6.5 - 7.0) earthquakes as earthquake scenarios while for the Profile III we have selected the earthquake of April 857 (Scenario 3) which is located west of the profile. The global amplification pattern over the study area is ranging between 2 and 5 and occurs at a frequency range 1.0 - 7.0Hz.

The results obtained in the site-specific analysis represent an important and forward step toward the proper assessment of the dynamical behavior of buildings under earthquake action, preservation, and risk reduction for the existing cultural heritage structures by combining both scientific and engineering knowledge. Moreover, the obtained results from ground motion modeling could be useful for retrofitting of

existing buildings, construction of new buildings, and upgrading the infrastructure in historic Cairo area, as well.

Finally, in Chapter 5, we provided the seismic input (RS and time histories) for the proper evaluation of the dynamic performance of the minaret of the Madrasa the Princess Tatar al-Higaziya, which by role could help in proposing conservation strategy against the seismic action for this priceless value structure. We provided the $MCSI_{SS}$ and C-$MCSI_{SS}$ acceleration response spectra at the site of the minaret, to be used for the assessment of the dynamic behavior of the minaret, by joining both seismological and engineering knowledge in order to study the behavior of this monument under earthquake action. Three earthquake scenarios that comprise one instrumental and two historic earthquakes are adopted to model the ground motion and to compute the seismic input at the site of the minaret using NDSHA approach. The 1992 and 950 earthquakes have been used as seismic sources in the modeling of the NS cross-sections that go under the minaret, which are located south and north, respectively, respect to the cross-sections, while the 857 earthquake scenario has been used as earthquake scenarios in the modeling of the EW cross-section. The existence of the small vertical separation gap between the minaret and the wall of the Madrasa may pose a pounding potential between the adjoining structures due to the horizontal vibration of the minaret. This threat will be covered in the future of work of the Madrasa.

A detailed numerical model for the minaret was achieved, accompanied with the installation of vibration sensors for its calibration. A visual inspection was performed to summarize the construction materials and elements in the minaret body and to investigate the minaret cracking status. Two seismic analysis types were conducted for the minaret numerical model namely, the linear-dynamic response spectrum analysis and the time history analysis. The response spectrum analysis was selected to replicate the 1992 Cairo earthquake excitation scenario since no close records of the earthquake were preserved. The numerical model adequately captured the minaret response without performing in signs of cracking or damage which matches with the real behavior of the minaret during the 1992 earthquake. The response spectrum analysis was also adopted for the proposed C-$MCSI_{SS}$ spectrum. A careful assessment of the seismic excitation on the historic minaret, through conducting dynamical analysis using the C-$MCSI_{SS}$ response spectrum and time history analyses, predicts severe damage to the minaret. The analysis under the C-

$MCSI_{SS}$ predicts significant lateral displacements at the top of the minaret and excessive tensile stress concentration, particularly at the geometric transition zone between the squared base and the hexagon shaft.

Finally, since the minaret is expected to suffer severe damage against the anticipated scenario of earthquake shaking, a vital protection plan is recommended for the minaret to avoid any future damage or collapse. Stitching the walls with pre-stressed rebar or reinforcement of the inner side of the walls with incorporated steel are pervasive ways for restoring and protecting historic monuments and structures. In addition, skins of reinforced concrete coating or fiber-reinforced plastic (FRP) on the outer side of the walls may be beneficial in enhancing the tensile strength of the walls and hence improve the minaret performance against the anticipated strong earthquake scenario.

Recommendations

1. It is urgently necessary to carry out or launch new paleoseismological investigations for the active areas in Egypt, in order to figure out the real earthquake potentiality and to reduce the problem of the incompleteness of the earthquake catalog.
2. The structural anelastic models are an important input in SHA computation using scenario-based approaches and have a profound effect on the resultant ground motion parameters. All of the existing models are too simple, and the need for the revision of the crustal models is obvious, taking into account all the crustal studies available for different regions of Egyptian territory and, eventually, to plan new studies where crucially necessary.
3. A detailed and comprehensive seismic microzonation using all the possible approaches is due for the effective earthquake risk reduction in Cairo.
4. Seismic vulnerability assessment study for ancient minarets of Cairo is essential and due in order to protect these priceless value historical monuments against the possible earthquake action.
5. The extension of this work to include non-linear site response is important to compute reliably the seismic input.

References

Abdel Rahaman, M., Tealeb, A., Mohamed, A., Deif, A., Abou Elenean, K., & El-Hadidy, M. S. (2008, October). Seismotectonic zones at Sinai and its surrounding. In First Arab Conference on Astronomy and Geophysics.

Abdel-Fattah, R. (2005). Seismotectonics of Sinai Peninsula, Egypt and their implications for seismic hazard evaluation. PhD Thesis Faculty of Science, Geology Department, Mansoura University, Egypt.

Abdel-Fattah, R. (1999). Seismotectonic studies on the Gulf of Suez region, Egypt. M. Sc. Thesis , Mansoura Univ., Faculty of Science, Geol. Dept.

Abdel-Monem S., Rayan A., Saleh A., Mekkawi M., and Mahmoud S. (2009). Deformation analysis deduced from Geophysical and GPS data for Greater Cairo-Egypt. NRIAG Journal of Geophysics Special Issue, PP. 653-680.

Abdel-Monem, S., Abou-Aly, N., Mahmoud, S., Shereif, R., Saleh, M., Khalil., H., Hassib, G.H., and Rayan, A. (2011). GPS measurements of current crustal movements along the Gulf of Suez. NRIAG Journal, Special Issue, PP 45-66.

Abou Elenean, K. (1997). Seismotectonics of Egypt in relation to the Mediterranean and Red Sea tectonics. Ph.D. thesis. Ain Shams University, Egypt.

Abou Elenean, K. (2010). Seismotectonics studies of El-Dabaa and its surroundings, personal communication.

Abou Elenean, K. (2007). Focal Mechanism of Small and Moderate Size Earthquakes Recorded by the Egyptian National Seismic Network (ENSN), Egypt. NRIAG Journal of Geophysics, 6 (1) 119-153.

Abou Elenean, K. (2009). Unpublished earthquake catalog for Egypt.

Abou ELenean, K., and Deif, A. (2001). Seismic Zoning of Egypt. Unpublished Work. NRIAG, Egypt.

Abou Elenean, K. M. and Deif, A. G. (2003). Seismological Aspects and Source Parameters of Beni Suef Earthquake on 11 October 1999, Bull. Fac. Sci., Cairo Univ., 70, pp. 120–142.

Abou Elenean, K. M., Hussein, H. M., Abu El-Ata, A. S., & Ibrahim, E. M. (2000). Seismological aspects of the Cairo earthquake, 12th October 1992.

Abou Elenean, K. M., and Hussein, H. M. (2007). Source mechanism and source parameters of May 28, 1998 earthquake, Egypt, J. Seismol. 11, 259–274.

Abou Elenean, K. M., and Hussein, H. M. (2008). The October 11, 1999 and November 08, 2006 Beni Suef Earthquakes, Egypt. Pure appl. geophys. 165, 1391–1410.

Abrahamson, N. A., & Silva, W. J. (1997). Empirical response spectral attenuation relations for shallow crustal earthquakes. Seismological research letters, 68(1), 94-127. http://dx.doi.org/10.1785/gssrl.68.1.94.

Abu El-Nader, E. F. (2010). Seismotectonic of Northern Egypt in view of an Updated Earthquake Catalog. Ph.D. Thesis, geology dep., Mansoura, University.

Abu El-Nader, I. A., El Gabry, M. N., Hussein, H. M., Hassan, H. M., & Elshrkawy, A. (2013). Source characteristics of the Egyptian Continental margin earthquake, 19 October 2012. Seismological Research Letters, 84(6), 1062-1065.

Ahmed, K. A., Sobaih, M., & Kebeasy, R. M. (1992). Sensitivity analysis of uncertainty in estimating seismic hazard for Egypt. Egyptian Journal of Earthquake Engineering, 2. 10 pages.

Aki, K. (1987). Strong motion seismology. In M.O . Erdik and M.N. Toksoz, editors, Strong ground motion seismology, number 204 in NATO ASI Series, Series C: Mathematical and Physical Sciences. Springer.

Aki, K. (2003). A perspective on the history of strong motion seismology. Physics of the Earth 454 and Planetary Interiors 137:5–11. http://dx.doi.org/10.1016/S0031-9201(03)00004-9.

Aki, K., & Richards, P. G. (2002). Quantitative seismology: second Edition, University Science Books, p279-282.

Alexeevskaya, M. A., Gabrielov, A. M., Gvishiani, A. D., Gelfand, I. M., Rantsamn, E.Ya. (1977). Formal morphostructural zoning of mountain territories. Journal of Geophysics 43: 227-233.

Ambraseys, N. (2009). Earthquakes in the Mediterranean and Middle East: a multidisciplinary study of seismicity up to 1900. Cambridge University Press.

Ambraseys, N. N. (1971). Value of historical records of earthquakes. Nature, 232: 375-379.

Ambraseys, N. N. (2001). Far-field effects of Eastern Mediterranean earthquakes in Lower Egypt. Journal of Seismology, 5(2), 263-268.

Ambraseys, N. N., & Bommer, J. J. (1991a). The attenuation of ground accelerations in Europe. Earthquake Engineering & Structural Dynamics, 20(12), 1179-1202.

Ambraseys, N. N., & Douglas, J. (2000). Reappraisal of the effect of vertical ground motions on response. Civil and Environmental Engineering Department Imperial College.

Ambraseys, N. N., Melville, C. P., & Adams, R. D. (2005). The seismicity of Egypt, Arabia and the Red Sea: a historical review. Cambridge University Press.

Ambraseys, N. N., Simpson, K. U., & Bommer, J. J. (1996). Prediction of horizontal response spectra in Europe. Earthquake Engineering & Structural Dynamics, 25(4), 371-400.

Aptikaev, F., & Kopnichev, J. (1980). Correlation between seismic vibration parameters and type of faulting. In of: Proceedings of Seventh World Conference on Earthquake Engineering (Vol. 1, pp. 107-110).

Atkinson, G. M., & Boore, D. M. (1995). Ground-motion relations for eastern North America. Bulletin of the Seismological Society of America, 85(1), 17-30.

Atkinson, G. M., & Boore, D. M. (1997). Some comparisons between recent ground-motion relations. Seismological Research Letters, 68(1), 24-40. http://dx.doi.org/10.1785/gssrl.68.1.24.

Atkinson, G. M., & Goda, K. (2011). Effects of seismicity models and new ground-motion prediction equations on seismic hazard assessment for four Canadian cities. Bulletin of the Seismological Society of America, 101(1), 176-189.

El-Attar, A. G., Saleh, A. M., & Zaghw, A. H. (2005). Conservation of a slender historical Mamluk-style minaret by passive control techniques. Structural Control and Health Monitoring, 12(2), 157-177.

Badawy, A. (1998). Earthquake hazard analysis in northern Egypt. Acta Geodaetica et Geophysica Hungarica, 33(2-4), 341-357. http://dx.doi.org/10.1007/BF03325544.

Badawy, A. (2001). Status of the crustal stress in Egypt as inferred from earthquake focal mechanisms and borehole breakouts. Tectonophysics, 343(1), 49-61.

Badawy, A., ElGabry, M., Girgis, M. (2010). Historical seismicity of Egypt. In: A Study for Previous Catalogues Producing Revised Weighted Catalogue the Second Arab Conference for Astronomy and Geophysics, Egypt.

Baker, J. W., Cornell, A. C. (2006a). Spectral shape, epsilon and record selection. Earthquake Engineering & Structural Dynamics 35, 1077–1095. doi:10.1002/eqe.571.

Baker, J.W. (2011). Conditional mean spectrum: Tool for ground motion selection. Journal of Structural Engineering 137, 322–331. doi:10.1061/(ASCE)ST.1943-541X.0000215.

Bartov, Y., Steinitz, G., Eyal, M., Eyal, Y. (1980). Sinistral movement along the Gulf of Aqaba-its age and relation to the opening of the Red Sea. Nature 285, 220–221.

Ben-Avraham, Z. (1985). Structural framework of the gulf of Elat (Aqab), northern Red Sea. Journal of Geophysical Research: Solid Earth, 90(B1), 703-726.

Ben-Avraham, Z., Almagor, G., and Garfunkel, Z., (1979). Sediments and structure of the Gulf of Elat (Aqaba)- Northern Red Sea. Sediment, Geol. 23, pp. 239–267.

Bertero, V. V., & Uang, C. M. (1992). Issues and future directions in the use of an energy approach for seismic resistant design of structures. Nonlinear seismic analysis and design of reinforced concrete buildings, 3-22.

Bolt, B. A., & Abrahamson, N. A. (1982). New attenuation relations for peak and expected accelerations of strong ground motion. Bulletin of the Seismological Society of America, 72(6A), 2307-2322.

Bommer, J. J., & Abrahamson, N. A. (2006). Why do modern probabilistic seismic-hazard analyses often lead to increased hazard estimates?. Bulletin of the Seismological Society of America, 96(6), 1967-1977.

Boore, D. M. (1986). Short-period P-and S-wave radiation from large earthquakes: implications for spectral scaling relations. Bulletin of the Seismological Society of America, 76(1), 43-64.

Boore, D. M., Joyner, W. B., & Fumal, T. E. (1997). Equations for estimating horizontal response spectra and peak acceleration from western North American earthquakes: a summary of recent work. Seismological research letters, 68(1), 128-153. http://dx.doi.org/10.1785/gssrl.68.1.128.

Bosworth, W. (1985). Geometry of propagating continental rifts. Nature, 316, 625-627.

Campbell, K. W. (1981). Ground motion model for the central United States based on near-source acceleration data. In " Proc. Earthquake & Earthquake Eng.: The Eastern U. S.". (Vol. 1, pp. 213-232).

Campbell, K. W., & Bozorgnia, Y. (2003). Updated near-source ground-motion (attenuation) relations for the horizontal and vertical components of peak ground acceleration and acceleration response spectra. Bulletin of the Seismological Society of America, 93(1), 314-331. http://dx.doi.org/10.1785/0120020029.

Campbell, K. W., & Bozorgnia, Y. (2008). NGA ground motion model for the geometric mean horizontal component of PGA, PGV, PGD and 5% damped linear

elastic response spectra for periods ranging from 0.01 to 10 s. Earthquake Spectra, 24(1), 139-171. http://dx.doi.org/10.1193/1.2857546.

Cancani, A. (1904). Sur l'emploi d'une double échelle sismique des intensités, empirique et absolue. Gerlands Beitr Geophys, 2, 281-283.

Caputo, M., Keilis-Borok, V., Kronrod, T., Molchan, G., Panza, G.F., Piva, A., Podgaezkaya, V. and Postpischl, D., (1973). Models of earthquake occurrence and isoseismals in Italy. Ann. Geof., 26, pp. 421-444.

Casciati, S., & Borja, R. I. (2004). Dynamic FE analysis of South Memnon Colossus including 3D soil–foundation–structure interaction. Computers & structures, 82(20), 1719-1736.

Cisternas A, Godefroy P, Gvishiani A, Gorshkov A, Kossobokov V, Lambert M, Rantsman E, Sallantin J, Saldano H, Soloviev A, Weber C (1985). A dual approach to recognition of earthquake prone areas in the Western Alps. Annale Geophysicae 3(2): 249-270.

Cochran J. R., Martinez F., Steckler M. S., and Hobart M. A. (1986). Conrad Deep: a new northern Red Sea Deep. Origin and implications for continental rifting. Earth and Planetary Science Letters 78, 18-32.

Cochran, J.R. (1983). A model for the development of the Red Sea. Amer. Assoc. Petrol. Geol. Bull., 67, 41–69.

Cochron, J.R. (2005). The northern Red Sea: nucleation of an oceanic spreading center within a continental rift. Geochemistry Geophysics Geosystems, 6, Q03006, doi: 10.1029/2004GC000826.

Colletta, B., Le Quellec, P., Letouzey, J., and Moretti, I. (1988). Longitudinal evolution of the Suez rift structure (Egypt). Tectonophysics, 153, 221-233.

Crouse, C. B. (1991). Ground-motion attenuation equations for earthquakes on the Cascadia subduction zone. Earthquake spectra, 7(2), 201-236. http://dx.doi.org/10.1193/1.1585626.

CSI, (2016). SAP2000: Integrated finite element analysis and design of structures basic analysis reference manual, Berkeley, California (USA), Computers and Structures Inc.

Cultrera, G., Cirella, A., Spagnuolo, E., Herrero, A., Tinti, E., & Pacor, F. (2010). Variability of kinematic source parameters and its implication on the choice of the design scenario. Bulletin of the Seismological Society of America, 100(3), 941-953. doi: 10.1785/0120090044.

Davies, F. B. (1984). Strain analysis of wrench faults and collision tectonics of the Arabian-Nubia shield. Journal of Geology, 82, 37-53.

Decanini, L. D., & Mollaioli, F. (1998). Formulation of elastic earthquake input energy spectra. Earthquake engineering & structural dynamics, 27(12), 1503-1522. http://dx.doi.org/10.1002/(SICI)1096-9845(199812)27:12<1503::AID-EQE797>3.0.CO;2-A.

Deif, A. (1998). Seismic hazard assessment in and around Egypt in relation to plate tectonics (Unpublished doctoral thesis). Ain Shams University, Cairo, Egypt. 244 pages.

Deif, A., & Tealeb, A. (2001). Deterministic seismic hazard assessment for Toshka and High Dam projects. Bull Natl Res Inst Astron Geophy (B), 233-263.

Deif, A., Elenean, K. A., El Hadidy, M., Tealeb, A., & Mohamed, A. (2009a). Probabilistic seismic hazard maps for Sinai Peninsula, Egypt. Journal of Geophysics and Engineering, 6(3), 288. http://dx.doi.org/10.1088/1742-2132/6/3/008.

Deif, A., Elenean, K. A., El Hadidy, M., Tealeb, A., & Mohamed, A. (2009b). Probabilistic seismic hazard maps for Sinai Peninsula, Egypt. Journal of Geophysics and Engineering, 6(3), 288.

Deif, A., Hamed, H., Ibrahim, H. A., Elenean, K. A., & El-Amin, E. (2011). Seismic hazard assessment in Aswan, Egypt. Journal of Geophysics and Engineering, 8(4), 531. http://dx.doi.org/10.1088/1742-2132/8/4/006.

Deif, A., Khalil, A. E. (2003). Preliminary assessment and interpretation of seismic hazard at Sphinx Pyramid plateau, Giza, Jour.Petrol.Min.Eng.pp.39-51.

Deif, A., Nofal, H., & Elenean, K. A. (2009a). Extended deterministic seismic hazard assessment for the Aswan High Dam, Egypt, with emphasis on associated uncertainty. Journal of Geophysics and Engineering, 6(3), 250. http://dx.doi.org/10.1088/1742-2132/6/3/004.

DeMets, C., R.G. Gordon, D.F. Argus and S. Stein, (1990). Current plate motions, Geophys. J. Int., 101:425-478.

DeMets, C., R.G. Gordon, D.F. Argus and S. Stein, (1994). Effects of recent revisions to the geomagnetic reversal time scale on estimates of current plate motions, Geophys. Res. Lett., 12, 2191-2194.

Dixon, T. H., Stern, R. J., and Hussein, I. M., (1987). Control of Red Sea rift geometry by Precambrian structures. Tectonics, 6, 551-57l.

Dominique, P., & Andre, E. (2000). Probabilistic seismic hazard map on the French national territory. In Proceedings of the 12th World Conference on Earthquake Engineering.

Douglas, J., & Aochi, H. (2008). A survey of techniques for predicting earthquake ground motions for engineering purposes. Surveys in geophysics, 29(3), 187-220. doi:10.1007/s10712-008-9046-y.

Egyptian Code of Practice-201 (ECP-201) (2011). Egyptian Code of Practice No. 201 for calculating loads and forces in structural work and masonry, National Research Center for Housing and Building, Ministry Housing, Utilities and Urban Planning, Cairo.

Egyptian General Survey and Mining Authority (EGSMA) (2004). Topographic Maps of Egypt 1:1000000 and 1:500000.

Egyptian Geological Survey and Mining Authority (EGSMA) (1993). A preliminary report on the Dahshur earthquake, 12 October, 1992.

Egyptian Geological Survey and Mining Authority "EGSMA" (1981). Geologic Map of Egypt 1:2000000.

Egyptian Geological Survey and Mining Authority "EGSMA" (2009). Tectonic Maps of Egypt 1:500000.

El-Adham, K. A., & El-Hemamy, S. T. (2006). Modelling of seismic hazard for the El-Dabaa area, Egypt. Bulletin of Engineering Geology and the Environment, 65(3), 273-279. http://dx.doi.org/10.1007/s10064-005-0028-8.

El-Fiky, G. S. (2000). Crustal strains in the Eastern Mediterranean and Middle East as derived from GPS observations. Bull. Earthq. Res. Inst. Univ. Tokyo Vol. 75 / pp. 105-125.

El-Fiky, G. (2005). GPS-derived velocity and crustal strain field in the Suez–Sinai area, Egypt. Bulletin of the Earthquake Research Institute of the University of Tokyo, 80, 73-86.

ElGabry, M. N., Panza, G. F., Badawy, A. A., & Korrat, I. M. (2013). Imaging a relic of complex tectonics: the lithosphere-asthenosphere structure in the Eastern Mediterranean. Terra Nova, 25(2), 102-109.

El-Hady, S. M., Khalil, A. E., and Hosney, A. (2004). 1-D Velocity structure in Northwest of Aswan Lake, Egypt deduced from travel time data. J. Appl. Geophs., Vol. 3, No.1. P.55-62.

El-Hefnawy, M., Deif, A., El-Hemamy, S. T., & Gomaa, N. M. (2006). Probabilistic assessment of earthquake hazard in Sinai in relation to the seismicity in the eastern Mediterranean region. Bulletin of Engineering Geology and the Environment, 65(3), 309-319. http://dx.doi.org/10.1007/s10064-006-0044-3.

El-Khashab, H. M. A., Hassib, G. H., Ibrahim, E., and Dessoky, M. M., (1991). Seismicity and composite focal mechanism for microearthquakes in Kalabsha area west of Aswan Lake and their tectonic implication, J. of Geodynamics, Vol. 14, 87-104.

El-Khrepy, S. (2008). Detailed Study of the Seismic Waves Velocity and Attenuation Models Using Local Earthquakes in the Northeastern Part of Egypt. Ph.D. Thesis, Mansoura Univ., Egypt.

Elmahdy, S. I., & Mohamed, M. M. (2016). Mapping of tecto-lineaments and investigate their association with earthquakes in Egypt: a hybrid approach using remote sensing data. Geomatics, Natural Hazards and Risk, 7(2), 600-619.

Elmahdy, S. I., Mohamed, M. M. (2014b). Automatic detection of near surface geological and hydrological features and investigating their influence on groundwater accumulation and salinity in southwest Egypt using remote sensing and GIS. Geocarto Int. 30:132_144.

El-Sayed, A. (1996). Seismic Hazard of Egypt. Ph.D. Thesis, Seismological Department Uppsala University, Sweden.

El-Sayed, A., Vaccari, F., & Panza, G. F. (2001). Deterministic seismic hazard in Egypt. Geophysical Journal International, 144(3), 555-567. http://dx.doi.org/10.1046/j.1365-246x.2001.01372.x.

El-Sayed, A., Vaccari, F., & Panza, G. F. (2004). The Nile Valley of Egypt: a major active graben that magnifies seismic waves. pure and applied geophysics, 161(5-6), 983-1002. doi:10.1007/s00024-003-2504-z.

Eppelbaum, L.V., Katz, Y.I., (2015). Eastern Mediterranean: Combined geologicalegeophysical zonation and paleogeodynamics of the Mesozoic and Cenozoic structuralsedimentation stages. Marine and Petroleum Geology 65 (2015) 198e216 http://dx.doi.org/10.1016/j.marpetgeo.2015.04.008

Eyal, M., Eyal, Y., Bartov, Y., Steinitz, G. (1981). The tectonic development of the western margin of the Gulf of Elat (Aqaba) rift. Tectonophysics 80, 39–66.

Ezzelarab, M., Shokry, M. M. F., Mohamed, A. M. E., Helal, A. M. A., Mohamed, A. A., & El-Hadidy, M. S. (2016). Evaluation of seismic hazard at the northwestern part

of Egypt. Journal of African Earth Sciences, 113, 114-125. http://dx.doi.org/10.1016/j.jafrearsci.2015.10.017.

Fäh, D., Iodice, C., Suhadolc, P., & Panza, G. F. (1993). A new method for the realistic estimation of seismic ground motion in megacities: the case of Rome. Earthquake Spectra, 9(4), 643-668.

Fasan, M., Amadio, C., Noè, S., Panza, G., Magrin, A., Romanelli, F., & Vaccari, F. (2015). A new design strategy based on a deterministic definition of the seismic input to overcome the limits of design procedures based on probabilistic approaches. In XVI ANIDIS Conference, L'Aquila, Italy. arXiv preprint arXiv:1509.09119.

Fasan. M., Magrin. A., Amadio. C., Panza. G.F., Romanelli. F., Vaccari. F., Noè. S. (2017). A possible revision of the current seismic design process to overcome the limitations of standard probabilistic seismic input definition. 16th World Conference on Earthquake, 16WCEE 2017, Paper N° 1893.

Fasan, M. (2017). Advanced seismological and engineering analysis for structural seismic design. PhD thesis, Trieste University – Italy.

Fat-Helbary, R. E., & Ohta, Y. (1996). Assessment of seismic hazard in Aswan Area, Egypt. Conference paper. 11 WCEE: Eleventh World Conference on Earthquake Engineering, Acapulco, Mexico, June 23-28, 1996, paper (No. 136). http://www.iitk.ac.in/nicee/wcee/article/11_136.PDF.

Fat-Helbary, R., & Ohta, Y. (1994b). Attenuation models of seismic intensity and peak ground acceleration in Egypt. In Proceedings of the first Cairo earthquake engineering symposium, Cairo (pp. 55-70).

Förste C., Bruinsma S.L., Abrikosov O., Lemoine J.-M., Marty J.C., Flechtner F., Balmino G., Barthelmes, F., Biancale, R. (2015). EIGEN-6C4 The latest combined global gravity field model including GOCE data up to degree and order 2190 of GFZ Potsdam and GRGS Toulouse; http://dx.doi.org/10.5880/icgem.2015.1.

Gaber, H., El-Hadidy, M. & Badawy, A. Pure Appl. Geophys. (2018). Up-to-date Probabilistic Earthquake Hazard Maps for Egypt https://doi.org/10.1007/s00024-018-1854-5

Gamal, M. A. (2009). Using microtremors for microseismic zonation in Cairo's crowded, urban areas. Journal of Seismology, 13(1), 13-30.

Garfunkel, Z. and Bartov, Y. (1977). The tectonics of the Suez Rift. Isr. Geol. Surv. Bull., 71, 1-44.

Garfunkel, Z., (1981). Internal structure of the Dead Sea leaky transform (rift) in relation to plate kinematics. Tectonophysics, 80, 81-108.

Gaulier, J., Le Pichon, X., Lyberis, N., Avedik, F., Geli, L., and Moretti, I. (1988). Seismic study of the crust of the northern Red Sea and Gulf of Suez. Tectonophysics, 153, 55-88.

Gelfand I, Guberman Sh, Izvekova M, Keilis-Borok V, Rantsman E (1972). Criteria of high seismicity, determined by pattern recognition. Tectonophysics 13: 415-422.

Gelfand I, Guberman Sh, Keilis-Borok V, Knopoff L, Press F, Rantsman E, Rotwain I, Sadovsky A (1976). Pattern recognition applied to earthquake epicentres in California. Physics of the Earth and Planet Interiors 11: 227-283.

Geller, R. J., Mulargia, F., & Stark, P. B. (2015). Why We Need a New Paradigm of Earthquake Occurrence. Subduction Dynamics: From Mantle Flow to Mega Disasters, 211, 183.

Girdler RW, McConnell DA, (1994). The 1990 to 1991 Sudan earthquake sequence and the extent of the East African Rift System. Science 264; 67–70.

Gitterman, Y. (1999, March). Seismic response estimation from strong motion records in Israel. Unpublished internal report. Prepared for the Ministry of National Infrastructures and Earth Science Research Administration. Report No: 570/88/98, 36 pages.

Gorshkov A., Kuznetsov I., Panza G., and Soloviev A. (2000). Identification of future earthquake sources in the Carpatho-Balkan orogenic belt using morphostuctural criteria. PAGEOPH, 157, 79-95.

Gorshkov A.I., Panza G.F., Soloviev A.A., Aoudia A. (2002). Morphostructural zonation and preliminary recognition of seismogenic nodes around the Adria margin in peninsular Italy and Sicily, JSEE: Spring 2002, Vol.4, No.1, 1-24.

Gorshkov AI, Kossobokov V, Soloviev AA (2003). Recognition of earthquake prone areas. In: Keilis-Bork V, Soloviev AA (eds) Nonlinear Dynamics of the Lithosphere and Earthquake Prediction. Springer, Heidelberg: 235-320.

Gorshkov A.I., Panza G.F., Soloviev A.A., Aoudia A. (2004). Identification of seismogenic nodes in the Alps and Dinarides Bolletino della Societa Geologica Italiana, 123, 3-18.

Gorshkov, A.I., Kossobokov V.G., Rantsman E.Ya., and Soloviev A.A. (2005). Recognition of earthquake-prone areas: Validity of results obtained from 1972 to

2000. In Editor D.K.Chowdhury, Computational Seismology and Geodynamics, Vol.7, AGU, Washington DC, pp. 37-44.

Gorshkov, A.I., Panza, G.F., Soloviev, A.A., Aoudia, A., Peresan, A. (2009). Delineation of the geometry of the nodes in the Alps-Dinarides hinge zone and recognition of seismogenic nodes (M ≥ 6.0). Terra Nova, doi: 10.1111/j.1365-3121.2009.00879.x

Gorshkov A.I., Soloviev A.A., Jiménez M.J., García-Fernández M., and Panza G.F. (2010). Recognition of earthquake-prone areas (M ≥ 5.0) in the Iberian Peninsula. Rendiconti Lincei - Scienze Fisiche e Naturali, 21(2), 131-162. doi:10.1007/s12210-010-0075-3

Gorshkov A., Hassan H. M., Novikova O. (2016). Seismogenic nodes defined in north-east Egypt by the pattern recognition approach. 35th General Assembly of the European Seismological Commission. September 2016, Trieste, Italy (http://meetingorganizer.copernicus.org/ESC2016/oral_program/22633)

Gorshkov, A., Kossobokov, V., & Soloviev, A. (2003). Recognition of earthquake-prone areas. In Nonlinear Dynamics of the Lithosphere and Earthquake Prediction (pp. 239-310). Springer, Berlin, Heidelberg.

Gorshkov, A.I., Kossobokov V.G., Rantsman E.Ya., and Soloviev A.A. (2005). Recognition of earthquake-prone areas: Validity of results obtained from 1972 to 2000. In Editor D.K.Chowdhury, Computational Seismology and Geodynamics, Vol.7, AGU, Washington DC, pp. 37-44.

Gorshkov A.I., Panza G.F., Soloviev A.A., Aoudia A. (2002). Morphostructural zonation and preliminary recognition of seismogenic nodes around the Adria margin in peninsular Italy and Sicily, JSEE: Spring 2002, Vol.4, No.1, 1-24.

Gorshkov A.I., Soloviev A.A., Jiménez M.J., García-Fernández M., and Panza G.F. (2010). Recognition of earthquake-prone areas (M ≥ 5.0) in the Iberian Peninsula. Rendiconti Lincei - Scienze Fisiche e Naturali, 21(2), 131-162. doi:10.1007/s12210-010-0075-3

Guennoc, P., Pautot, G., & Coutelle, A. (1988). Surficial structures of the northern Red Sea axial valley from 23 N to 28 N: time and space evolution of neo-oceanic structures. Tectonophysics, 153(1-4), 1-23.

Gusev, A. A. (1983). Descriptive statistical model of earthquake source radiation and its application to an estimation of short-period strong motion.Geophysical Journal International, 74(3), 787-808. doi: 10.1111/j.1365-246X.1983.tb01904.x.

Gusev, A. A. (2011). Broadband kinematic stochastic simulation of an earthquake source: a refined procedure for application in seismic hazard studies. Pure and Applied Geophysics, 168(1-2), 155-200. doi:10.1007/s00024-010-0156-3.

Gusev, A., Radulian, M., Rizescu, M., & Panza, G. F. (2002). Source scaling of intermediate-depth Vrancea earthquakes. Geophysical Journal International,151(3), 879-889. doi: 10.1046/j.1365-246X.2002.01816.x.

Gutenberg, B., & Richter, C. F. (1956). Earthquake magnitude, intensity, energy, and acceleration (second paper). Bulletin of the seismological society of America, 46(2), 105-145.

Gvishiani A, Gorshkov A, Kossobokov V, Cisternas A, Philip H, Weber C (1987). Identification of Seismically Dangerous Zones in the Pyrenees. Annales Geophysicae 5 B(6): 681-690.

Gvishiani A, Gorshkov A, Rantsman E, Cisternas A, Soloviev A (1988). Identification of earthquake-prone-areas in the regions of moderate seismicity. Nauka, Moscow, 175 p. [in Russian].

Gvishiani, A., & Soloviev, A. (1980). On the Concentration of the Major Earthquakes Around the Intersections of Morphostructural Lineaments in South America, in Methods and Algorithms for Interpretation of Seismological Data. Edited by VI Keilis-Borok and AL Levshuin, 46-50.

Hall, J., and Ben-Avraham, Z. (1978). New bathymetric map of the Gulf of Elat (Aqaba), paper presented at the Tenth International Congress on Sedimentology, 1, 285, International Assoc. of Sedimentologists, Jerusalem.

Hassan, H. M., Gorshkov, A., Novikova, O. V. (2016, April). Recognition of seismogenic nodes (M > 5.0) in north-east of Egypt. The African Seismological Commission 1st general Assembly, Luxor, Egypt.

Hassan, H. M., Panza, G. F., Romanelli, F., & ElGabry, M. N. (2017a). Insight on seismic hazard studies for Egypt. Engineering Geology.

Hassan, H. M., Romanelli, F., Panza, G. F., ElGabry, M. N., & Magrin, A. (2017b). Update and sensitivity analysis of the neo-deterministic seismic hazard assessment for Egypt. Engineering Geology, 218, 77-89.

Hassan, M.Y., Issawi, B., and Zaghloul, E.A. (1978), Geology of the area east of Beni Suef, Eastern Desert, Egypt, Annals Geolog. Surv. Egypt VIII, 129–162.

Hu, Y. X., Liu, S. C., & Dong, W. (1996). Earthquake engineering. CRC Press.

Hudnut, K. W., Seeber, L., Pacheo, J., (1989). Cross-fault triggering in the November 1987 Superstition Hills earthquake sequence, Southern California. Geophysical Research Letters 16: 199–202.

Hussein, H. M., Elenean, K. A., Marzouk, I. A., Korrat, I. M., El-Nader, I. A., Ghazala, H., & ElGabry, M. N. (2013). Present-day tectonic stress regime in Egypt and surrounding area based on inversion of earthquake focal mechanisms. Journal of African Earth Sciences, 81, 1-15.

Hussein, H. M., Elenean, K. A., Marzouk, I. A., Peresan, A., Korrat, I. M., El-Nader, E. A., ... & El-Gabry, M. N. (2008). Integration and magnitude homogenization of the Egyptian earthquake catalog. Natural hazards, 47(3), 525-546. doi:10.1007/s11069-008-9237-3.

Hussein, H.M., Marzouk, I., Moustafa, A.R. and Hurukawa, N. (2006). Preliminary seismicity and focal mechanisms in the southern Gulf of Suez: Agust 1994 through December 1997, J. Afr. Earth Sci., 45, 48-60.

Hussein, I. M., & Abd-Allah, A. M. A. (2001). Tectonic evolution of the northeastern part of the African continental margin, Egypt. Journal of African Earth Sciences, 33(1), 49-68.

Ibrahim, E. M., & Hattori, S. (1982). Seismic risk maps for Egypt and vicinity. Helwan Inst Astronom Geophys, 2(Series B), 183-207.

Imam, H. F. (2001). Technical study on the structural condition of the Tatar al-Higaziya Madrasa and minaret (monument#36). Historic Cairo Project, Stage 3, Group 3. Cairo, Egypt.

Indirli, M., Carpani, B., Panza, G., Romanelli, F., & Spadoni, B. (2006). Damage evaluation and rehabilitation of the Montorio medieval tower after the September 14th, 2003 earthquake (No. IC--2006/144). Abdus Salam International Centre for Theoretical Physics.

Indirli, M. (2009). Organization of a Geographic Information System (GIS) database on natural hazards and structural vulnerability for the historic center of San Giuliano di Puglia (Italy) and the city of Valparaiso (Chile). International Journal of Architectural Heritage, 3(4), 276-315.

Indirli, M., Razafindrakoto, H., Romanelli, F., Puglisi, C., Lanzoni, L., Milani, E., ... & Apablaza, S. (2011). Hazard evaluation in Valparaiso: the MAR VASTO Project. Pure and applied geophysics, 168(3-4), 543-582.

Indirli, M., S. Kouris, L. A., Formisano, A., Borg, R. P., & Mazzolani, F. M. (2013). Seismic damage assessment of unreinforced masonry structures after the abruzzo 2009 earthquake: The case study of the historical centers of L'Aquila and Castelvecchio Subequo. International Journal of Architectural Heritage, 7(5), 536-578.

Japanese Expert Team, (1993). Report of Japan Disaster Relief Team on the earthquake in Arab Republic of Egypt of October 12 , 1992, p. 77.

Jestin, F., Huchon, P., & Gaulier, J. M. (1994). The Somalia plate and the East African Rift System: present-day kinematics. Geophysical Journal International, 116(3), 637-654.

Joyner, W. B., & Boore, D. M. (1981). Peak horizontal acceleration and velocity from strong-motion records including records from the 1979 Imperial Valley, California, earthquake. Bulletin of the Seismological Society of America, 71(6), 2011-2038.

Kasahara, K. (1981). Earthquake Mechanics. Cambridge University Press, Cambridge.

Kebeasy, R. M. and Maamoun, M. (1981). Seismicity and Earthquake Risk of the Proposed Site of Shoubra al-Khaimah Electric Power Station. Bull.. Int'l Inst. Seismol. And Earthquake Energy. Vol 19, pp 21-33.

Kebeasy, R. M., Maamoun, M., Albert, R. N. H., & Megahed, M. (1981). Earthquake activity and earthquake risk around Alexandria, Egypt. Bull Int Inst Seismol Earthq Eng, 19, 93-113.

Kebeasy, R., Maamoun, M., & Albert, R. (1981). Earthquake activity and earthquake risk around the Alexandria area in Egypt. Acta Geophys Pol, 29(1), 37-48.

Kebeasy, R.M. (1990). Seismicity. IN: The Geology of Egypt (R. Said, Ed.) A.A. Balkerma, Rotterdam, 1990, 51-59.

Kebeasy, T. R. M., & Husebye, E. S. (2003). A finite-difference approach for simulating ground responses in sedimentary basins: quantitative modelling of the Nile Valley, Egypt. Geophysical Journal International, 154(3), 913-924.

Keilis-Borok, V., & Soloviev, A. A. (Eds.). (2013). Nonlinear dynamics of the lithosphere and earthquake prediction. Springer Science & Business Media.

Kimata, F., Murakami, H., Hurukawa, N., and Tealeb, A. (1996). Coseismic displacements in Aqaba earthquake of 1995, Egypt (program and abstracts). The Seismology Society of Japan B42 no. 2.

Kimata, F., Tealeb, A., Murakami, H., Furukawa, N., Mahmoud, S., Khalil, H., ... & Hamdy, A. M. (1997). The Aqaba Eartquake of November 22, 1995 and Co-Seismic Deformation in Sinai Peninsula, Deduced from Repeated GPS Measurements. Acta Geodaetica et Geophysica Hungarica, 32(1-2), 53-71.

King, G., (1986). Speculations on the geometry of the initiation a termination processes of earthquake rupture and its relation to morphology and geological structure. Pure and Applied Geophysics 124: 567–583.

Klinger, Y., Rivera, L., Haessler, H., Maurin, J. C. (1999). Active faulting in the Gulf of Aqaba: new knowledge from the Mw 7.3 earthquake of 22 November 1995. Bull. Seismol. Soc. Am. 89, 1025–1036.

Klügel, J. U. (2005). Problems in the application of the SSHAC probability method for assessing earthquake hazards at Swiss nuclear power plants. Engineering Geology, 78(3), 285-307. http://dx.doi.org/10.1016/j.enggeo.2005.01.007.

Klügel, J. U. (2007a). Error inflation in probabilistic seismic hazard analysis. Engineering Geology, 90(3), 186-192. http://dx.doi.org/10.1016/j.enggeo.2007.01.003.

Klügel, J. U. (2007b). Comment on “Why do modern probabilistic seismic-hazard analyses often lead to increased hazard estimates?” by Julian J. Bommer and Norman A. Abrahamson. Bulletin of the Seismological Society of America, 97(6), 2198-2207. http://dx.doi.org/10.1785/0120070018.

Koch, M., Mather P. M. (1997). Lineament mapping for groundwater resource assessment: a comparison of digital synthetic aperture radar (SAR) imagery and stereoscopiclarge format camera (LFC) photographs in the red sea hills, Sudan. Int J Remote Sens. 27:4471-4493.

Kossobokov, V. G., & Nekrasova, A. K. (2012). Global seismic hazard assessment program maps are erroneous. Seismic instruments, 48(2), 162-170. http://dx.doi.org/10.3103/S0747923912020065.

Kronrod, T. (2011). Estimation of GR law parameters for strong earthquakes in Italy. Technical report, ICTP, Miramare, Trieste, Italy.

Le Pichon, X., and Francheteau, J. (1978). A plate-tectonic analysis of the Red Sea – Gulf of Aden area. Tectonophysics, 46, pp. 369–406.

Lokmer, I., Herak, M., Panza, G. F., & Vaccari, F. (2002). Amplification of strong ground motion in the city of Zagreb, Croatia, estimated by computation of synthetic seismograms. Soil Dynamics and Earthquake Engineering, 22(2), 105-113.

Maamoun, M. (1979). Observed intensity – epicentral distance relations in Egyptian earthquakes, Bull. of Helwan Obs. No. 184.

Maamoun, M., Megahed, A. and Allam, A. (1984). Seismicity of Egypt. HIAG Bull., IV (B), 109-160.

Magrin, A., Gusev, A. A., Romanelli, F., Vaccari, F., & Panza, G. F. (2016). Broadband NDSHA computations and earthquake ground motion observations for the Italian territory. International Journal of Earthquake and Impact Engineering, 1(1-2), 131-158.

Mahmoud S.M. (2002). Seismicity and GPS-derived crustal deformation in Egypt. Journal of Geodynamics 35, 333–352.

Mahmoud, S., Reilinger, R., McClusky, S., Vernant, P., & Tealeb, A. (2005). GPS evidence for northward motion of the Sinai Block: implications for E. Mediterranean tectonics. Earth and Planetary Science Letters, 238(1), 217-224. http://dx.doi.org/10.1016/j.epsl.2005.06.063.

Makris, J., Stofen, B., Vees, R., Allam, A., Maamoun, M., & Shehata, W. (1979). Deep seismic sounding in Egypt, Part I: The Mediterranean Sea between Crete, Sidi Barani, and the coastal area of Egypt. Unpublished report, National Research Institute of Astronomy and Geophysics, Helwan, Egypt.

Martinez, F., and Cochran, J. R. (1988). Structure and tectonics of the northern Red Sea: catching a continental margin between rifting and drifting. In: E. Bonatti (Editor), Zabargad Island and the Red Sea Rifting. Tectonophysics, 150, 1-32.

Marzouk, I. A. M. (1988). Study of crustal structure of Egypt deduced from deep seismic and gravity data. Universität Hamburg.

Marzouk, I. A., Khalil, A. E., and Maamoun, S. A. (2014). Delineation of Active Seismotectonic trends in Central Egypt. Helwan University Journal, Egypt.

Mayer, W., & Abteilung Kairo Deutsches Archäologisches Institut. (2007). A future for the past: restorations in Islamic Cairo; 1973-2004. von Zabern.

McClusky, S., Balassanian, S., Barka, A., Demir, C., Ergintav, S., Georgiev, I., ... & Kastens, K. (2000). Global Positioning System constraints on plate kinematics and dynamics in the eastern Mediterranean and Caucasus. Journal of Geophysical Research: Solid Earth, 105(B3), 5695-5719.

McGuire, R. K. (1978). FRISK: computer program for seismic risk analysis using faults as earthquake sources (No. 78-1007). US Geological Survey. http://pubs.usgs.gov/of/1978/1007/report.pdf.

McKenzie, D. P., & Morgan, W. J. (1969). Evolution of triple junctions. Nature, 224(5215), 125-133.

McKenzie, D. P., Davies, D., and Molnar, P. (1970). Plate tectonics of the Red Sea and East Africa. Nature, 226, 243-248.

Medvedev, S. V., & Sponheuer, W. (1969, January). Scale of seismic intensity. In Proc. IV World Conference of the Earthquake Engineering, Santiago, Chile, A-2 (pp. 143-153).

Meshref, W. M. (1990). Tectonic framework of Egypt. In: Said, R. (Editor), The Geology of Egypt. A. A. Balkema, Rotterdam Nertherlands, 1990.

Mohamed, A. E. E. A., El-Hadidy, M., Deif, A., & Elenean, K. A. (2012). Seismic hazard studies in Egypt. NRIAG Journal of Astronomy and Geophysics, 1(2), 119-140. http://dx.doi.org/10.1016/j.nrjag.2012.12.008.

Mohamed, A. E. E. A., El-Hadidy, M., Deif, A., & Elenean, K. A. (2012). Seismic hazard studies in Egypt. NRIAG Journal of Astronomy and Geophysics, 1(2), 119-140. http://dx.doi.org/10.1016/j.nrjag.2012.12.008.

Mohamed, A. M. S., Hosny, A., Abou-Aly, N., Saleh, M., & Rayan, A. (2013). Preliminary crustal deformation model deduced from GPS and earthquakes' data at Abu-Dabbab area, Eastern Desert, Egypt. NRIAG Journal of Astronomy and Geophysics, 2(1), 67-76.

Mohamed, H. H. (2007). Seismicity and seismotectonic of Idfu area, Northern Aswan, Egypt. Exploration Geophysics, Remote Sensing and Environment . XIV. 1-2.

Molchan, G., Kronrod, T., & Panza, G. F. (1997). Multi-scale seismicity model for seismic risk. Bulletin of the Seismological Society of America, 87(5), 1220-1229.

Molchan, G., Kronrod, T., & Panza, G. F. (2011). Hot/cold spots in Italian macroseismic data. Pure and applied geophysics, 168(3-4), 739-752. http://dx.doi.org/10.1007/s00024-010-0111-3.

Mourabit, T., Elenean, K. A., Ayadi, A., Benouar, D., Suleman, A. B., Bezzeghoud, M., ... & Hfaiedh, M. (2014). Neo-deterministic seismic hazard assessment in North Africa. Journal of seismology, 18(2), 301-318. http://dx.doi.org/10.1007/s10950-013-9375-2.

Moustafa, A. and Abd-Allah, A. (1992). Transfer zones with en echelon faulting at the northern end of the Suez rift, Tectonics, 11, 499-509.

Moustafa, A. M. (1976). Block faulting in the Gulf of Suez. Fifth E.G.,P.C. Exploration Seminar, Cairo, Egypt, 1-19.

Moustafa, A. R. (1988). Structural geology of Sierra Del Carmen, Trans-Pecos Texas, scale 1:48,000, Geol. Quad. Ser., map 54, Bur. of Econ. Geol., Univ. of Tex.

Moustafa, A. R. (1993). Structural characteristics and tectonic evolution of the east-margin blocks of the Suez Rift. Tectonophysics, **223,** 381–399.

Moustafa, A. R. (1997). Controls on the development and evolution of transfer zones: the influence of basement structure and sedimentary thickness in the Suez rift and Red Sea. J. of Struct. Geol. 19(6), 755-68.

Moustafa, A. R., (1996a). Internal structure and deformation of an accommodation zone in the northern part of Suez rift. J. Struct. Geol., 18, 93-107.

Moustafa, A. R., Yehia, M. A., and Abdel Tawab, S. (1985). Structural setting of the area east of Cairo, Maadi, and Helwan. MERC Ain Shams Univ., Sci. Res. Ser., 5: 40-64.

Moustafa, A.R. (2004). Geological maps and sections of Sinai Margin: Amer. Assoc. Petrol. Geol. data pages.

Musson, R. M. (2012). The effect of magnitude uncertainty on earthquake activity rates. Bulletin of the Seismological Society of America, 102(6), 2771-2775. doi: 10.1785/0120110224

Neev., D. (1975). Tectonic evolution of the Middle East and the Levantine basin (easternmost Mediterranean). Geology, 3, 683-686.

Badawy, A., ElGabry, M., Girgis, M. (2010). Historical seismicity of Egypt. In: A Study for Previous Catalogs Producing Revised Weighted Catalog. The Second Arab Conference for Astronomy and Geophysics, Egypt.

Nunziata, C., Costa, G., Marrara, F., and Panza, G. F. (2000), Validated Estimation of Response Spectra for the 1980 Irpinia Earthquake in the Eastern Area of Naples, Earthquake Spectra 16, 643–660.

Panza, G. F., Romanelli, F., & Vaccari, F. (2001). Seismic wave propagation in laterally heterogeneous anelastic media: theory and applications to seismic zonation. Advances in geophysics, 43, 1-95.

Panza G.F., Peresan A. and La Mura C. (2013). Seismic hazard and strong ground motion: an operational neo-deterministic approach from national to local scale.

Geophysics and Geochemistry, [Eds.UNESCO-EOLSS Joint Committee]. Encyclopedia of Life Support Systems (EOLSS), Developed under the Auspices of the UNESCO, Eolss Publishers, Oxford, UK.

Panza, G. F., & Suhadolc, P. (1987). Complete strong motion synthetics. Seismic strong motion synthetics, 4, 153-204.

Panza, G. F., Cazzaro, R., & Vaccari, F. (1997). Correlation between macroseismic intensities and seismic ground motion parameters.

Panza, G. F., Kossobovok, G. V., Peresan, A., & Nekrasova, A. (2014). Why are the standard probabilistic methods of estimating seismic hazard and risks too often wrong. Earthq Hazard Risk Disasters. doi: 10. 1016. B978-0-12-394848-9. 00012-2.

Panza, G. F., La Mura, C., Peresan, A., Romanelli, F., & Vaccari, F. (2012). Chapter three-seismic hazard scenarios as preventive tools for a disaster resilient society. Advances in geophysics, 53, 93-165.

Panza, G. F., Peresan, A., Magrin, A., Vaccari, F., Sabadini, R., Crippa, B., ... & Cannizzaro, L. (2013). The SISMA prototype system: integrating Geophysical Modeling and Earth Observation for time-dependent seismic hazard assessment. Natural hazards, 69(2), 1179-1198. http://dx.doi.org/10.1007/s11069-011-9981-7.

Panza, G. F., Romanelli, F., & Vaccari, F. (2001). Seismic wave propagation in laterally heterogeneous anelastic media: theory and applications to seismic zonation. Advances in geophysics, 43, 1-95.

Panza, G. F., Vaccari, F., & Cazzaro, R. (1999). Deterministic seismic hazard assessment. In Vrancea earthquakes: tectonics, hazard and risk mitigation(pp. 269-286). Springer Netherlands. http://dx.doi.org/10.1007/978-94-011-4748-4_25.

Panza, G.F., Romanelli, F., Vaccari, F. (2001). Seismic wave propagation in laterally heterogeneous anelastic media: theory and applications to seismic zonation. Advances in Geophysics, vol. 43. Academic Press, pp. 1–95.

Parvez, I. A., Romanelli, F., & Panza, G. F. (2011). Long period ground motion at bedrock level in Delhi city from Himalayan earthquake scenarios. Pure and applied geophysics, 168(3-4), 409-477. doi:10.1007/s00024-010-0162-5.

Parvez, I. A., Vaccari, F., & Panza, G. F. (2004). Site-specific microzonation study in Delhi metropolitan city by 2-D modelling of SH and P-SV waves. In Seismic Ground Motion in Large Urban Areas (pp. 1165-1184). Birkhäuser Basel.

Peresan, A., & Nekrasova, A. (2014). Why are the standard probabilistic methods of estimating seismic hazard and risks too often wrong. Earthquake Hazard, Risk and Disasters, 309.

Peresan, A., Gorshkov, A., Soloviev, A., & Panza, G. F. (2014). The contribution of pattern recognition of seismic and morphostructural data to seismic hazard assessment. arXiv preprint arXiv:1406.2932.

Peresan, A., Gorshkov, A., Soloviev, A., & Panza, G. F. (2014). The contribution of pattern recognition of seismic and morphostructural data to seismic hazard assessment. arXiv preprint arXiv:1406.2932. http://arxiv.org/abs/1406.2932v3.

Peresan, A., Harbi, A., Hussein, H. M., Ogwari, O. P., & Panza, G. F. (2009). Toward the compilation of a unified earthquake catalog for North Africa. IASPEI Assembly, 10-16.

Peresan, A., Magrin, A., Nekrasova, A., Kossobokov, V. G., & Panza, G. F. (2013, July). Earthquake recurrence and seismic hazard assessment: a comparative analysis over the Italian territory. In Proceedings of the ERES 2013 Conference. WIT transactions on the built environment (Vol. 132, pp. 23-34).

Petersen, M.D., Frankel, A.D., Harmsen, S.C., Mueller, C.S., Haller, K.M., Wheeler, R.L., Wesson, R.L., Zeng, Yuehua, Boyd, O.S., Perkins, D.M., Luco, Nicolas, Field, E.H., Wills, C.J., and Rukstales, K.S. (2008). Documentation for the 2008 update of the United States national seismic hazard maps: U.S. Geological Survey Open-File Report 2008–1128, 128 p.

Rantsman E. Ya. (1979). Sites of Earthquakes and Morphostructures of Mountain Countries. (Editorial Nauka, Moscow: 171 pp. [in Russian].

Refai, E., Riad, S., and Tealeb, A. (1973). The main tectonic trends of west Cairo area, HIAG Bull., No. 102.

Reiter, L. (1991). Earthquake Hazard Analysis. Columbia University Press, 1991.

Riad S., Ghalib M., El-Difrawy MA., Gamal M (2000). Probabilistic Seismic Hazard Assess- ment in Egypt. Annals of the Geological Survey of Egypt; 23: 851-881.

Riad, S., & Yousef, M. (1999). Earthquake hazard assessment in the southern part of the western desert of Egypt. Report submitted to the National Authority for Remote Sensing and Space Sciences. Center of Studies and Research for the South Valley Development Assuit University.

Riad, S., Ghalib, M., El-Difrawy, M. A., & Gamal, M. (2000). Probabilistic seismic hazard assessment in Egypt. Annals Geol. Surv. Egypt, 23, 851-881.

RIGW (Research Institute of Groundwater), (1997). Hydro-Geological Map of Luxor Area, Explanatory Notes: Research Institute of Groundwater: Kalioubia, Egypt, scale 1:100,000.

Romanelli, F., & Vaccari, F. (1999). Site response estimation and ground motion spectrum scenario in the Catania area. Journal of Seismology, 3(3), 311-326.

Romanelli, F., & Vaccari, F. (2015). Earthquake scenarios and seismic input for cultural heritage: applications to the cities of Rome and Florence. arXiv preprint arXiv:1511.02602.

Rugarli, P. (2014). Validazione strutturale. EPC.

Sabry, A.A., Agaiby, S.W., Mourad, S.A., Aly, T.M. (2001). Seismic hazard of Egypt with consideration to local geotechnical conditions. Paper from PhD thesis, faculty of Engineering, Cairo University.

Said, R. (1962). The Geology of Egypt, Elsevier, Amsterdam, the Netherlands, 377 pp.

Said, R. (1975). Subsurface Geology of Cairo Area. Memoire de L'Institue d'Egypte, Tome Soixante, Cairo, 70 pgs.

Said, R. (1981). The Geologic Evolution of the Nile River. Springer-Verlag, New York,

Said, R. (1990). The geology of Egypt: Rotterdam. Netherlands, Brookfield.

Said, R. (2012). The geological evolution of the River Nile. Springer Science & Business Media.

Salamon, A., Hofstetter, A., Garfunkel, Z., and Ron, H., (1996). Seismicity of the Eastern Mediterranean region: Perspective from the Sinai subplate. Tectonophysics, 263, 293-305.

Saleh, K. H. (2005). Active faulting and seismic hazard assessment of the north western desert, with contribution of geographic information system.Annals. Geol. Surv. Egypt, 28, 435-560.

Saleh, M. & Becker, M. (2013). A New Velocity Field from the Analysis of the Egyptian Permanent GPS Network (EPGN). Arabian Journal of Geosciences, 7, 4665-4682.

Saleh, M., & Becker, M. (2015). New constraints on the Nubia–Sinai–Dead Sea fault crustal motion. Tectonophysics, 651, 79-98.

Sawires, R., Peláez, J. A., Fat-Helbary, R. E., & Ibrahim, H. A. (2016a). A review of seismic hazard assessment studies and hazard description in the building codes for

Egypt. Acta Geodaetica et Geophysica, 51(2), 151-180. http://dx.doi.org/10.1007/s40328-015-0117-5.

Sawires, R., Peláez, J. A., Fat-Helbary, R. E., & Ibrahim, H. A. (2016b). Updated Probabilistic Seismic Hazard Values for Egypt. Bulletin of the Seismological Society of America. http://dx.doi.org/10.1785/0120150218.

Sawires, R., Peláez, J. A., Fat-Helbary, R. E., Ibrahim, H. A., & García-Hernández, M. T. (2015). An updated seismic source model for Egypt. Earthquake engineering—from engineering seismology to optimal seismic design of engineering structures. InTech, Croatia, 1-51.

Sawires, R., Peláez, J. A., Fat-Helbary, R. E., Ibrahim, H. A., & García-Hernández, M. T. (2015). An updated seismic source model for Egypt. Earthquake engineering from engineering seismology to optimal seismic design of engineering structures. InTech, Croatia, 1-51.

Sayed, M.A., Go, S., Cho, S.G. and Kim, D. (2015). "Seismic responses of base-isolated nuclear power plant considering spatially varying ground motions", Structural Engineering and Mechanics. 54(1): 169-188; doi: 10.12989/sem.2015.54.1.169

Schwartz, D. P., & Coppersmith, K. J. (1984). Fault behavior and characteristic earthquakes: Examples from the Wasatch and San Andreas fault zones.Journal of Geophysical Research: Solid Earth, 89(B7), 5681-5698. http://dx.doi.org/10.1029/JB089iB07p05681.

Seleem, T. A., & Aboulela, H. A. (2011). Seismicity and geologic structures indubitable in Wadi Hagul, north Eastern Desert, Egypt. International Journal of Geosciences, 2(01), 55.

Sezen, H., Acar, R., Dogangun, A., & Livaoglu, R. (2008). Dynamic analysis and seismic performance of reinforced concrete minarets. *Engineering Structures*, *30*(8), 2253-2264.

Shata, A. A. (1988). Geology of Cairo, Egypt. Environmental & Engineering Geoscience, 25(2), 149-183.

Shrestha, B. (2009, November). Vertical ground motions and its effect on engineering structures: a state-of-the-art review. In Proceeding of International Seminar on Hazard Management for Sustainable Development in Kathmandu, Nepal (pp. 29-30).

Slavov, S. l., Paskaleva, I., Vaccari, F., Kouteva, M., Panza, G. F. (2004), Deterministic earthquake scenarios for the City of Sofia, PAGEOPH 161, N5/6, 1221–1237.

Smith, J.G. (1965). Fundamental transcurrent faulting in northern Rocky Mountains, AAPG Bull., 49, 1398-1409.

Sobaih, M., Kebeasy, R.M., Ahmed, K.A. (1992). Development of seismic hazard maps for Egypt, International Journal of Earthquake Engineering, Vol. 2.

Soloviev A. A., Gvishiani A. D., Gorshkov A. I., Dobrovolsky M. N., Novikova O. V. (2014). Recognition of Earthquake-Prone Areas: Methodology and Analysis of the Results. Izvestiya, Physics of the Solid Earth, Vol. 50, No. 2, pp. 151–168 DOI: 10.1134/S1069351314020116.

Stein, S., Geller, R. J., & Liu, M. (2012). Why earthquake hazard maps often fail and what to do about it. Tectonophysics, 562, 1-25. http://dx.doi.org/10.1016/j.tecto.2012.06.047.

Sun, R., Vaccari, F., Marrara, F., and Panza, G. F. (1998), The Main Features of the Local Geological Conditions Can Explain the Macroseismic Intensity Caused in Xiji-Langfu (Beijing) by the MS = 7.7 TANGSHAN 1976 earthquake, Pure Appl. Geophys. 152, 507–521.

Sykes, L. R. (1967). Mechanism of earthquakes and nature of faulting on the mid-oceanic ridges. Journal of Geophysical Research, 72(8), 2131-2153.

Sykora, D., Look, D., Croci, G., & Karaesmen, E. (1993). Reconnaissance Report of Damage to Historic Monuments in Cairo, Egypt Following the October 12, 1992 Dahshur Earthquake. Army Engineering Waterways Experiment Station Vicksburg MS Geotechnical Lab.

Talwani, P., (1988). The intersection model for intraplate earthquakes. Seismological Research Letters 59: 305–310.

Thenhaus, P., Sharp, R., Celebi, M., Ibrahim, A-B., and Van de Pol, H. (1993). Reconnaissance Report on the 12 October 1992 Dahshur, Egypt, Earthquake, Open File Rpt 93-181, U.S. Geological Survey, Denver, CO.

Toni, M. (2012). Site Response ad seismic hazard assessment for the southern part of Cairo city, Egypt. Unpublished PhD thesis. Faculty of Science, Assiut University. 151 pages.

Vaccari, F., Suhadolc, P., & Panza, G. F. (1990). Irpinia, Italy, 1980 earthquake: waveform modelling of strong motion data. Geophysical Journal International, 101(3), 631-647. doi: 10.1111/j.1365-246X.1990.tb05575.

Vesic, A.B. (1961). Beams on elastic subgrade and Winkler's hypothesis, Proc. 5 th. Int. Conf. on Soil Mech. Found. Engrg., Paris, p.p. 845-50.

Wells, D. L., & Coppersmith, K. J. (1994). New empirical relationships among magnitude, rupture length, rupture width, rupture area, and surface displacement. Bulletin of the seismological Society of America, 84(4), 974-1002.

Williams, C. (2008). Islamic monuments in Cairo: the practical guide. American Univ in Cairo Press.

Woodward-Clyde Consultants (WWCC), (1985). Earthquake activity and stability evaluation for the Aswan High Dam, Unpublished report, High and Aswan Dam Authority, Ministry of Irrigation, Egypt.

Wyss, M., Nekrasova, A., & Kossobokov, V. (2012). Errors in expected human losses due to incorrect seismic hazard estimates. Natural hazards, 62(3), 927-935. doi:10.1007/s11069-012-0125-5.

Younes, A. I., Engelder, T. E., and Bosworth, W. (1998). Fracture distribution in faulted basement blocks, Gulf of Suez, Egypt. In: Coward, M. P., Daltaban, T. S., Johnson, H. (Eds.), Structural Geology and Reservoir Characterization. Geological Society of London Special Publication 127, 167-190.

Youngs, R. R., Chiou, S. J., Silva, W. J., & Humphrey, J. R. (1997). Strong ground motion attenuation relationships for subduction zone earthquakes.Seismological Research Letters, 68(1), 58-73. http://dx.doi.org/10.1785/gssrl.68.1.58.

Zhao, J. X., Zhang, J., Asano, A., Ohno, Y., Oouchi, T., Takahashi, T., ... & Fukushima, Y. (2006). Attenuation relations of strong ground motion in Japan using site classification based on predominant period. Bulletin of the Seismological Society of America, 96(3), 898-913. http://dx.doi.org/10.1785/01200501.

Appendix A

Table 1: Earthquake catalog for Egypt with magnitude ≥ 5 extends from 320 AD to 2016.

Year	Month	Day	hour	min	sec	Latitude	longitude	depth	M_{max}
320	0	0	0	0	0	31.5	30	33	5.9
554	10	14	0	0	0	32	30	33	5.9
857	4	0	0	0	0	30	31	30	7.0
885	22	0	0	0	0	30.1	31.2	30	7.2
912	0	0	0	0	0	30	31	30	5.2
935	10	4	0	0	0	30.5	31.2	30	7.0

950	7	25	0	0	0	30.2	31.2	30	7.0
951	9	15	0	0	0	32	30	30	5.3
1068	3	18	0	0	0	29.5	35	30	7.0
1091	2	12	0	0	0	28	34	30	5.9
1111	8	31	0	0	0	30.03	31.15	30	7.0
1202	5	20	0	0	0	33	36	30	7.0
1210	0	0	0	0	0	25.2	33	30	5.2
1259	6	6	0	0	0	30	31	30	6.6
1264	2	20	0	0	0	30	31	30	5.9
1299	1	8	0	0	0	29.5	30.5	30	7.0
1307	8	10	0	0	0	30.2	31	30	5.2
1313	2	27	0	0	0	30.5	31.2	30	5.2
1335	5	29	0	0	0	30	31	30	5.2
1347	12	8	0	0	0	30	31.2	30	5.2
1373	10	19	0	0	0	30.2	31.5	30	5.2
1385	9	19	0	0	0	30.5	31	30	5.2
1386	7	17	0	0	0	30.2	31.2	30	5.2
1422	1	28	0	0	0	30	31.2	30	5.2
1425	6	23	0	0	0	29.5	33.5	30	5.9
1433	12	14	0	0	0	30	31	30	5.2
1434	11	6	0	0	0	30	31.2	30	5.9
1455	3	5	0	0	0	30.5	31.2	30	5.2
1467	12	15	0	0	0	30	31	30	5.2
1476	11	1	0	0	0	30.2	31.2	30	5.2
1483	1	15	0	0	0	30.1	31.2	30	5.2
1486	10	11	0	0	0	30.5	31.2	30	5.2
1498	10	16	0	0	0	30	31.2	30	5.2
1502	11	17	0	0	0	30.15	31.25	30	5.9
1513	3	28	0	0	0	30	31.2	30	5.2
1523	4	4	0	0	0	30.25	31.3	30	5.2
1525	3	9	0	0	0	30.15	31.2	30	5.2
1527	7	14	0	0	0	30	31.2	30	5.2
1529	11	12	0	0	0	30.15	31.5	30	5.2
1532	7	10	0	0	0	30.2	31.25	30	5.2
1534	3	23	0	0	0	30.1	31.2	30	5.2
1537	0	0	0	0	0	32	32	30	5.2
1576	4	1	0	0	0	30	31.5	30	5.2
1588	4	7	0	0	0	29.5	31.5	30	5.2
1694	12	12	0	0	0	29	31	30	5.9
1698	10	2	0	0	0	32	30	30	5.2
1710	8	27	0	0	0	29.3	33.25	30	5.2
1754	10	18	0	0	0	29.6	32.25	30	5.9
1759	10	30	0	0	0	33.1	35.6	30	6.6
1778	6	22	0	0	0	26.2	32.1	30	5.2

1801	10	10	0	0	0	30	31.2	30	5.2
1814	6	27	0	0	0	29	33	30	5.9
1825	6	21	0	0	0	30.15	31	30	5.2
1839	0	0	0	0	0	28.5	34	30	5.9
1846	6	15	0	0	0	30	31	30	5.2
1847	8	7	0	0	0	29.5	30.75	30	7.0
1849	7	23	0	0	0	30.15	31.25	30	5.2
1850	10	27	0	0	0	27	31	30	5.9
1858	12	30	0	0	0	30	31.2	30	5.2
1865	4	11	0	0	0	31.1	30	30	5.2
1868	2	20	0	0	0	32	33	30	5.9
1873	1	12	0	0	0	32.5	33	30	5.2
1879	7	11	0	0	0	29	33	30	5.9
1886	11	17	0	0	0	30.15	31.2	30	5.2
1895	12	7	0	0	0	30.1	31.25	30	5.2
1900	3	6	17	58	0	33	29	30	6.2
1906	12	26	17	45	0	27.7	34	20	5.5
1906	12	26	11	4	30	27.7	34	20	5
1909	2	23	20	51	0	27.8	33.5	20	5
1920	10	1	2	10	0	29.4	31	29	5.8
1927	7	11	13	4	7	32	35.5	35	6.2
1936	6	13	3	20	0	32.75	22.5	30	5.6
1951	1	30	23	7	24	32.4	33.4	10	5.7
1951	5	28	14	16	21	31.8	27	33	5.6
1952	3	22	4	52	33	27.2	34.5	33	5
1954	10	28	13	39	1	32.4	31.4	30	5.4
1954	7	20	0	52	42	31.5	30	33	5.4
1955	11	12	5	32	14	25.3	34.6	33	5.6
1955	9	12	6	9	24	32.2	29.7	50	6.8
1956	12	18	17	53	0	31.5	35.5	10	5.2
1969	5	10	9	27	57	27.5	34.1	25	5
1969	3	31	21	44	0	27.5	33.89	40	5
1969	3	31	7	15	54	27.61	33.91	20	6.9
1969	3	24	11	54	14	27.5	33.9	16	5.2
1969	9	26	2	14	0	27.56	33.8	33	5.2
1969	3	24	12	50	51	27.5	33.8	13	5.3
1969	4	23	13	27	20	27.57	33.71	18	5
1969	5	10	9	27	57	27.5	34.1	25	5
1969	4	8	10	31	54	27.5	33.7	24	5.1
1970	10	8	2	34	0	27.2	33.7	10	5.1
1971	7	8	23	40	56	27.6	33.9	22	5
1972	1	12	8	15	44	27.55	33.82	22	5.2
1972	6	28	9	49	33	27.7	33.8	15	5.6
1974	4	29	20	4	37	30.5	31.7	12	5.2

1978	12	9	7	12	52	23.95	26.35	10	5.7
1979	4	23	13	1	0	31.24	35.5	10	5
1981	11	14	9	5	28	23.55	32.55	10	5.6
1982	2	3	13	46	5	29.19	34.77	24	5
1983	6	12	12	0	6	28.51	33.17	10	5.3
1984	8	24	6	2	29	32.38	34.81	28	5.3
1984	7	2	1	47	9	25.25	34.53	10	5.1
1984	8	24	6	22	3	32.76	35.04	30	5.1
1987	1	2	10	14	46	30.46	32.22	21	5
1987	6	2	10	14	46	32.2	30.5	15	5
1987	6	28	0	50	17	32.82	24.36	24	5.2
1992	10	12	13	9	56	29.78	31.14	21	5.9
1993	8	3	13	33	43	28.4	34.78	10	5
1993	8	3	13	12	18	28.52	34.68	10	5.2
1993	8	3	16	33	23	28.79	34.59	13	5.7
1993	8	3	12	54	6	28.78	34.57	10	5.4
1993	8	3	13	45	0	28.61	34.56	10	5.1
1993	8	3	12	43	5	28.73	34.55	10	6.1
1995	11	22	12	47	5	28.53	35	10	5.1
1995	11	22	4	15	26	29.07	34.74	18	7.3
1995	11	22	22	16	53	28.52	34.7	10	5.7
1995	11	23	18	7	17	29.33	34.48	10	5.7
1995	10	11	17	33	26	27.56	33.94	24	5
1996	2	21	4	59	51	28.8	34.78	10	5.1
1997	5	10	23	1	47	28.21	34.82	10	5.3
1997	3	8	6	0	5	27.7	34.2	1	5.5
1998	4	7	13	32	55	28.72	34.91	15	5
1998	12	14	20	48	46	26.44	31.22	16	5.4
1998	5	28	18	33	16	31.45	27.64	18	5.9
1999	10	5	5	4	34	28.88	35.07	15	5.6
1999	6	13	4	20	9	28.26	34.83	5	5.2
1999	10	28	15	39	17	30.53	34.8	16	5
1999	10	11	20	39	35	28.7	31.53	17	5
2000	12	25	1	58	56	28.41	34.87	11	5.2
2000	3	8	14	22	26	28.87	34.73	7	5.7
2000	8	3	14	22	25	28.64	34.57	10	5
2003	6	4	9	14	49	27.1	32.01	9	5.1
2004	2	11	8	15	6	31.71	35.45	26	5.1
2006	11	8	4	32	10	28.58	31.59	3	5.2
2012	10	19	3	35	12	32.51	31.02	10	5.2
2013	6	1	11	49	28	28.41	33.22	22	5
2015	6	27	15	34	2	29.01	34.77	10	5.5

Table 2: The representative focal mechanisms of seismotectonic zones adopted Chapter 3.

No	year	mo	dy	hr	min	sec	latitude	longitud	depth	Mmax	strike1	dip1	rake1	strike2	dip2	rake2	area
1A	1995	11	22	41	52	6	29.07	34.73	18	7.3	196	59	345	294	77	211	NAQABA
2A	1993	8	3	12	34	15	28.73	34.55	10	7.3	139	36	238	357	60	291	CAQABA
3A	1995	11	22	22	16	53	28.52	34.7	10	5.4	202	67	357	294	87	203	SAQABA
4A	1952	3	22	45	23	3	27.2	34.5	33	5	159	64	343	256	75	207	N.RED
5A	1969	3	31	71	55	4	27.61	33.91	20	6.9	113	53	269	294	37	271	SGSUEZ
6A	1983	6	12	12	0	6	28.51	33.17	10	6.9	129	86	350	219	83	185	CGSUEZ
7A	1987	1	2	10	14	46	30.46	32.22	21	5	248	80	190	156	80	350	C-S.DISTRICT
8A	1992	10	12	13	9	59	29.78	31.14	21	5.9	285	66	243	156	35	316	DAHSHUR
9A	1999	10	11	20	39	35	28.7	31.53	17	5	145	32	332	259	75	241	BANISUEIF
10	1998	12	14	9	52	7	26.44	31.22	16	5.4	294	41	279	102	50	262	YUT-SOHAG
11A	1981	11	14	90	52	7	23.55	32.55	33	5.6	146	72	345	241	7	198	ASWAN
12A	1978	12	9	71	25	2	23.95	26.35	10	5.7	234	82	143	343	54	11	G.KEBER
13A	1984	7	2	14	70	9	25.25	34.53	10	5.1	281	45	250	128	49	289	ABU-DABBAB
14A	1987	6	28	18	33	15	31.45	27.64	18	5.9	269	67	242	168	35	317	W-MARGIN
15A	1998	5	28	0	51	7	32.82	24.35	24	6	154	44	89	335	46	91	W2-MARGIN
16A	1955	9	12	6	9	24	32.2	29.7	20	6.8	259	61	46	141	50	141	C-MARGIN
17A	2012	10	19	33	51	2	32.51	31.02	10	5.2	108	75	173	199	84	16	E-MARGIN
18A	1999	10	28	15	39	17	30.53	34.8	15	5	71	56	312	204	33	205	SIANI
19A	1979	4	23	13	1	0	31.24	35.5	10	5	187	80	15	95	75	170	DSF
20A	1984	8	24	60	22	9	32.38	34.81	28	5	100	65	38	190	55	150	LEVANT-COAST